UTS UNIVERSITY OF TECHNOLOGY SYDNEY

Understanding the Function of SpoIIIL during Spore Development

by ODIKA CHIMEZIE PROGRESS

Thesis submitted in fulfilment of the requirements for the degree of

Doctor of Philosophy

under the supervision of A/Prof. Dr. Iain Duggin

University of Technology Sydney
Faculty of Science
Australian Institute for Microbiology and Infection (AIMI)

June 2023

Certificate of Original Authorship

I, **Odika Chimezie Progress,** declare that this thesis, is submitted in fulfilment of the requirements for the award of Doctor of Philosophy, in the Australian Institute for Microbiology and Infection (AIMI), Faculty of Science, at the University of Technology Sydney.

This thesis is wholly my own work unless otherwise referenced or acknowledged. In addition. I certify that all information sources and literature used are indicated in the thesis.

This document has not been submitted for qualifications at any other academic institution.

This research is supported by the Australian Government Research Training Program, Australian Research Council Discovery Project (DP190100793), and the University of Technology Sydney International Research Scholarship.

Signature: Production Note:
Signature removed prior to publication.

Date: 30/06/2023

Acknowledgement

I would like to sincerely thank:

Members and Alumni of the Rodrigues Lab: Christopher Rodrigues, for providing the opportunity to conduct this project in his laboratory, while he was based at UTS. Helena Chan, for her salient contributions to this project, helping me get to grips with certain lab techniques in the lab. Her data interpretation prowess is outstanding. Ahmed Mohamed for his quick wit and experience which always save the day whenever I run out of troubleshooting ideas. Johana Luhur, a smart, tireless, and hardworking colleague with a bright mind, and an exceptional tact in organizing, troubleshooting, and implementing experiments. Luhur was key to my smooth transitioning into the experimental aspects of this work. Salwa Souka for the construction of ten different *Bs* strains with 10 different point mutations in SpoIIIL ORF.

Members and Alumni of the Duggin and Söderström Labs: Iain Duggin who is also my principal supervisor for his close monitoring and follow up of both me and this work up until the submission of this thesis. His guidance, and his help towards the finalization of this work, and my final DSPIII seminar, is laudable. Bill Söderström, for suggestions and reagent supplementation. Some western blot results actually looked nicer when I borrowed anti-GFP antibodies from Bill. Yan Liao, Solenne Ithurbide, Dora Pittrich, Hannah Brown, Vinaya Shinde, Mathew Pittorino, Charlotte Abell-King, Ariana Costas, Lauren Ryan, Alaska Pokhrel, Johnathan Christianos, Connor McCloskey, for all the informative discussions we always had during our combined lab meetings.

Also, Neville Firth, a panel member of my supervisory team from the University of Sydney, for his very helpful contributions during my presentations.

Our beloved technical staff, Mercedes Ballesteros, Luke Beebe and Sarah Osvath for maintenance of decorum and safety in the UTS PC2 laboratories on Building 4, level 7, and making it possible for researchers to consistently obtain excellent and reproducible data every single time. Louise Cole, Christian Evenhuis, Amy Bottomley, and Elizabeth Peterson for maintenance of the microscopes in the Microbial Imaging Facility (MIF), multiple training

sessions on the different state-of-the-art microscopes, and softwares which increased my expertise and technical know-how in handling and getting the best out of the MIF at UTS.

The UTS Faculty of Science and AIMI for this scholarship as well as the opportunity to grow intellectually within the confines of its academic enclave. To every scholar or researcher, whether young or old, upcoming or established, with whom I ever discussed my project, and who offered valuable advice one way or the other, briefly or in detail. My hat is raised in humble salute.

My parents, my siblings, my friends, both far and wide, near and around, for all the encouragement, financial support, good memories, thoughtful words and sweet smiles. Much love!

God Almighty above all, for life, strength, health, and inspiration throughout this process.

Finally, I wouldn't dare fail to thank me, myself and I, for stepping up, and not giving up.

Statement of Contribution of Authors to the Chapters of this Thesis

Results Chapter 3: Dr. Chris Rodrigues and Dr. Helena Chan oversaw the stage 1 and stage 2 assessment documents from which this Chapter derives. But Helena and Chris were not involved in compiling, editing, or reading this chapter as it is, in this thesis. Dr. Chris Rodrigues, Odika Chimezie Progress, and Ms Salwa Souka planned the experiments to make the ten different single mutations (N4A, D5A, Y6A, K8A, T11A, R25A, P38A, F44A, G45A, and P48A) in SpoIIIL ORF found in section 3.3.6. Ms Salwa Souka constructed the ten different single mutations (N4A, D5A, Y6A, K8A, T11A, R25A, P38A, F44A, G45A, and P48A) in SpoIIIL ORF, and Salwa did the first biological replicate of the heat-kills and first biological replicate of the imaging data found in section 3.3.6. Although the imaging data done by Salwa is not in this thesis. Dr. Helena Chan has contributed to the work presented in this chapter, by doing the fluorescence microscopy imaging of MalF-GFP and SpoIIIL-GFP presented in Figure 3.3.5.

Results Chapter 4: This is to acknowledge that Chris Rodrigues, has contributed to the work presented in this chapter, by developing the Tn-seq screen on the SpoIIIL mutant and for providing all the Tn-seq data that was then used to identify potential hits in the *spoIIIL* mutant background.

Results Chapter 5: This is to acknowledge that all the experimental work contained in this chapter was solely done by Odika Chimezie Progress.

General Discussion Chapter 6: This is to acknowledge that the table and illustrative schematics contained in the general discussion chapter was solely organized and drawn up by Odika Chimezie Progress.

ABSTRACT

Sporulation in *Bacillus subtilis* is an alternative developmental pathway that encompasses several complex cellular events involving hundreds of genes many of which have poorly understood functions. During sporulation, a very interesting and highly-conserved protein complex called the SpoIIIA-SpoIIQ (A-Q) complex believed to aid the maturation of the forespore by functioning as a specialized secretion system contributes to spore shape, as well as the transcription potential of the spore. A lot of questions surround the A-Q complex, including what roles its different components play in its overall function.

The focus of this project was to unravel the functions of SpoIIIL, a recently discovered 59 amino acids, 9.6kDA protein, transcribed during sporulation under the control of σ^F, and is believed to be a component of the A-Q complex from the forespore compartment. In doing so, this project will contribute to new knowledge surrounding sporulation that could potentially provide broadly-relevant insight into the creation of strategies for controlling spore-forming pathogens.

Here, we report that SpoIIIL is required for spore shape, functions in the monitoring, regulation, and signalling of cortex assembly, and is unlikely a component of the SpoIIIA-SpoIIQ complex. We propose that SpoIIIL ensures the timely activation of σ^G in order to make sure that all necessary σ^G-dependent resources required for the normal process of cortex assembly such as SpoIVB activation, pro-σ^K processing, activation of the cortex PG synthases SpoVD/E, upregulation of the Mur genes as well as increased precursor synthesis will occur or be supplied right on time, to avoid any cortex assembly anomaly. And that the precipitation of SpoIIIL from the forespore inner membrane where it is uniformly localized prior to the commencement of cortex assembly, into the forespore cytoplasm where it looks like intriguing patchy-like structures as the result of a SpoIVB-mediated proteolytic event, is the prime indicating signal for the assembly of the cortex. Also, SpoIIIL although predicted to contain a patch of hydrophobic residues at the C-terminus, is not surface exposed.

This work revealed that the proper localization of SpoIIIL depends on SpoIVB, SpoIVA, SpoVM, SpoVD, and SpoVE while the stability of SpoIIIL depends only on SpoIVB, SpoIVA, SpoVM, as well as SpoVID. How cells achieve the coordination between coat and cortex assembly across the intermembrane space still remains largely unclear. However, since the LysM domain of

SpoVID can bind to the substrate of MurAB, N-acetylglucosamine (GlcNAc) as well as Lipid II, and MurAB has been implicated in a very strong cortex assembly relationship with SpoIIIL, we strongly suggest that future work should probe this new found relationship trio between SpoIIIL, SpoVID and MurAB via more sophisticated protein-protein interaction studies like bacterial two-hybrid assays to reveal the nature of their possible interaction in relation to cortex assembly. Furthermore, we found that cortex assembly was obliterated in the absence of both *spoIIIL* and the peptidoglycan synthesis gene *murAB*, and that spores of the *ΔspoIIIL ΔmurAB* double mutant could not become phase bright. The *ΔspoIIIL ΔmurAB* double mutant spores did not survive the heat kill treatment or sporulation efficiency assay, ultimately yielding nil or dead spores compared to either the *ΔmurAB* single mutant which had ~44% sporulation efficiency or the *ΔspoIIIL* single mutant spores which had ~47% sporulation efficiency. Hence, the cortex assembly regulatory and signalling pathways as well as the genetic interactions involved has been illustrated in a new light.

Collectively, the accumulated evidence from this work has provided a significant leap in our understanding of spore development through the mid-stages to the later stages of sporulation in spore forming bacteria. This is a discovery worth targeting and deserving of further investigation. Because, if spore formation can be totally eliminated as is the case in this study, whilst allowing the attainment of all the benefits obtainable from diverse applications of industrially, medically, and environmentally beneficial spore forming bacteria, and the recurrence and transmission of infections by pathogenic spore forming bacteria completely prevented, then we have achieved a milestone in the study of cell differentiation in prokaryotes.

Keywords: *Bacillus subtilis*, Sporulation, SpoIIIL, Cortex Assembly Signalling

NOMENCLATURE

BS	*Bacillus subtilis*
α	alpha
A	alanine
amp	ampicillin
β	beta
cat	chloramphenicol resistance gene
CFP	cyan fluorescent protein
cfu	colony-forming unit
D	aspartic acid
DNA	deoxyribonucleic acid
DNaseI	deoxyribonuclease II
DSM	Difco Sporulation Medium
DTT	1,4-Dithiothreitol
FM4-64	N-(3-Triethylammoniumpropyl)-4-(6-(4-(Diethylamino) Phenyl) Hexatrienyl) Pyridinium Dibromide
EDTA	ethylenediaminetetraacetic acid
et al.	and others
erm	erythromycin resistance gene
F	phenylalanine
G	glycine
γ	gamma
g	gram (s)
GCW	germ cell wall
GFP	green fluorescent protein
HEPES	4-(2-hydroxyethyl)-1-piperazineethanesulfonic acid
His	histidine
hr	hour

IPTG	isopropyl-1-thio-β-D-galactopyranoside
K	lysine
kan	kanamycin resistance gene
L	litre (s)
LB	Luria-Bertani broth (Lennox)
m	milli (10^{-3})
M	moles per litre
min	minutes
MQW	milli-Q purified water
mYPET	monomeric yellow fluorescent protein for energy transfer
N	asparagine
n	nano (10^{-9})
neo	neomycin resistance gene
ODx	optical density at (x refers to wavelength in nm)
opt	optimized
P	proline
p	probability
$P_{hyperspank}$	IPTG-hyper-inducible promoter
PAGE	polyacrylamide gel electrophoresis
PBS	phosphate buffered saline
PBP	penicillin binding protein
PCR	polymerase chain reaction
pH	power of Hydrogen
phleo	phleomycin resistance gene
PMSF	phenylmethylsulfonyl fluoride
R	arginine
RBS	ribosome binding site
RNase	ribonuclease A

rpm	revolutions per minute
SD	standard deviation
SDS	sodium dodecyl sulfate
σ	sigma
spec	spectinomycin resistance gene
T	threonine
tet	tetracycline resistance gene
TMA-DPH	(1-(4-Trimethylammoniumphenyl)-6-Phenyl-1,3,5-Hexatriene p-Toluenesulfonate)
Tn-seq	transposon sequencing
Tris	tris(hydroxymethyl)methylamine
U	units (enzyme activity)
UV	ultraviolet
V	volt(s)
v/v	volume per volume
W	watt
w/v	weight per volume
X-Gal	5-Bromo-4-Chloro-3-Indolyl β-D-Galactopyranoside
Y	tyrosine
YFP	yellow fluorescent protein
µ	micro (10^{-6})

LIST OF TABLES

LIST OF FIGURES

Table of Contents

Introduction

1.1 Preface and the applications of sporulation studies

The list of large-scale DNA sequenced microorganisms which had previously not included a paradigm for industrially, medically, and environmentally beneficial Gram-positive bacteria now contains *Bacillus subtilis* because of how intensely its biochemistry, physiology, and genetics have been studied over several decades [1]. *Bacillus*, being one of the most frequently employed prokaryotes that is used as an industrial cell factory for the making of vitamins, inositol, acetoin, hyaluronan, insecticides, recombinant proteins, and other chemicals, is favoured because its cultivation in large-scale production settings at high cell densities is easy and usually cost effective; [2–4] and the species *B. subtilis* can also form complex biofilms that can be utilized as living biological materials for the manufacture of many functional biomaterials, like surface growth factors, antibiotics, lysozyme, and antimicrobial peptides for medical purposes[3,4].

Presently, ~60% of the commercially available enzymes are made by *Bacillus* species[2]. Recently, it was shown that pro-inflammatory cytokines like IL-1 β, 6, 8, 12, 18, and TNF-α which are known to be active against COVID-19, are secreted in large amounts when neutrophils and monocytes are provoked by biosurfactant producing bacteria like *B. subtilis*[5,6]. Thus making the possible use of *B. subtilis* or its biomolecules as antigens (either in the form of a vaccine or a therapeutic agent), to trigger neutrophils and monocytes to produce IL-1 β, 6, 8, 12, 18, and TNF-α, which can act against COVID-19, a promising pursuit. Additionally, besides being an well-known multifunctional probiotic, with huge potential for prohibiting the growth of pathogenic bacteria and amplifying nutrient uptake, *B. subtilis* has now been applied in astropharmacy, where its space-hardy spore-forming strains are engineered to make two pharmaceutical peptides that are vital for astronaut health namely: teriparatide (an anabolic agent for fighting osteoporosis) and filgrastim (an effective panacea for radiation-induced neutropenia)[4,7]. These and more are benefits accruable from diverse applications of spore forming bacteria like *B. subtilis*.

Nevertheless, bacterial spores are relevant and incessant food contaminants, and the spore forming bacteria are much commonly implicated in food and product safety, as well as in food and product quality considerations[8,9]. It is increasingly disturbing that the shelf life of pasteurized milk is chiefly determined by the ubiquity and growth of Gram-positive, rod shaped aerobic endospore formers, of which species of the *Bacillus cereus* group are the most far-reaching and the products contaminated include various formats of dairy products, milk,

cheese, yoghurt etc[10,11]. Another very important source of concern is that a recent emergence of strains of *B. cereus* that bring about anthrax-like diseases which result in identical symptoms and death toll as those brought about by *B. anthracis*, have now been reported in mammals and humans[12].

However, since new antibiotic resistant bacterial strains constantly emerge and evade counter measures via sporulation or otherwise, there is always the need to continuously innovate and develop not just nascent antibacterial materials[13], but also subtle anti-sporulation genetic modifications which would allow the attainment of all the benefits obtainable from diverse applications of spore forming bacteria, whilst preventing the formation of its resistant, disease-causing, food- or product-contaminating spores. Hence, this project is inclined towards the development of ways by which sporulation can be subtly and effectively prevented not only in the disease-causing spore-formers, but also in the industrially, medically, and environmentally beneficial spore forming bacteria.

The process of spore formation involves several morphological changes, as well as dedicated genetic programs that have been studied beyond 50 years and represent one of the most elaborately characterized developmental pathways in modern day molecular microbiology[14]. *B. subtilis* is a model organism for fundamental research as well as an industrial workhorse and studies with *B. subtilis* gain from the ease genetic manipulation, nevertheless, its profound process of sporulation encompasses many cellular events and involves hundreds of genes, many of which have poorly understood functions[15,16]. Cell differentiation however, is a basic biological process and spore formation by *B. subtilis* is a archaic system of cell differentiation that has now become an archetype for the investigation of cell differentiation in prokaryotes[17].

Bacillus subtilis is a soil-inhabiting, aerobic, Gram-positive rod, classified phylogenetically under the group Firmicutes (recently renamed as Bacillota)[18], which comprises also of genera notorious for entering a developmental pathway termed sporulation[1]. Sporulation is a process whereby actively growing vegetative bacterial cells differentiate into dormant and highly-resistant cells called endospores (also termed “forespores” or “spores”), in response to starvation stress[19,20,21]. In the event of starvation, *B. subtilis* ceases to grow and initiates certain first aid responses by amplifying metabolic activity just to circumvent its situation and these activities include commencement of motility and chemotaxis, making of hydrolases (including proteases and carbohydrases) as well as antibiotics in order to persist vegetatively

and re-establish normal growth but then continues into sporulation if this first aid attempt fails[22]. When *B. subtilis* finally goes into sporulation, the resultant spores can survive harsh environmental conditions, such as desiccation, elimination by cell-wall-degrading enzymes, increased temperatures, UV radiation, digestion by protozoans, detergents, acids, extremes of physical and chemical conditions and even antibiotics[17,23,24]. Spores can spread and remain dormant for many years in a variety of ecosystems ranging from deep into the earth's crust and the oceans, to the stratosphere, as plant or animal disease causal agents, symbionts or commensals, or even as part of the human gut microbiota where they could form healthy symbiotic and commensal associations upon exposure to nutrients, thus germinating and proliferating into vegetatively growing cells, and restoring bacterial populations in the environment[25–27].

B. *subtilis* 168 has a genome of over 4,214,810 base pairs comprising 4,100 protein-coding genes that have been completely sequenced[22]. Out of these, 148 genes have been implicated in sporulation and exhibit sporulation defects. Most recently, 24 additional genes which had previously not been associated with spore formation were discovered[14], including *spoIIIL* – the subject of this thesis.

SpoIIIL, a 59 amino acids protein, transcribed in the forespore under σ^F control [28], predicted by certain bioinformatics tool (e.g phobius) to contain a patch of hydrophobic residues at the C-terminus, was not only found to participate in intercellular signalling pathways during sporulation but was also discovered to take part in the activation of the late forespore specific sigma factor σ^G [28]. This discovery was made possible via transposon sequencing (Tn-seq), a powerful technique usually employed to discover and further characterize novel genes and pathways involved in sporulation[28]. SpoIIIL is thus believed to be an A-Q complex protein[28]. Although a lot is not currently documented in literature about the sporulation gene *spoIIIL*, it still does not fall short of being regarded highly in *Bacillus subtilis* sporulation studies.

1.2 Brief overview of the stages of sporulation in *Bacillus subtilis*

In laboratory conditions, the *B*. *subtilis* sporulation program is completed between 5 to 7 hours. The sporulation program is controlled by the sporulation regulator Spo0A and five known σ factors (σ^H, σ^F, σ^E, σ^K, and σ^G) that are activated in a stepwise manner[17,29–35]. The initiation of sporulation is directed by two transcriptional regulators, namely Spo0A and the stationary phase σ factor σ^H [24,28,35–37] resulting in the polar division of the starving cell into two

compartments; the smaller forespore, as well as the bigger mother cell which not only nurtures the developing forespore but also subsequently surrounds it with two bilayer membranes in a process called engulfment[38–42].

These regulators direct the production of proteins which initiate the very early steps of spore development: e.g. inhibition of new cycles of DNA replication, remodelling of the chromosomes and shifting of the cell division site to one pole of the cell[20,43–46](Fig. 1.1). Polar division is a hallmark of sporulation and divides the starving cell into two compartments: the bigger mother cell and the smaller forespore that develops into the spore within the mother cell (Fig. 1.1). The mother cell contributes to forespore maturation, but then lyses afterwards[24,28,47–49].

After polar division, the forespore-specific σ factor, σ^F, becomes activated and drives the expression of an array of forespore proteins, including two signalling proteins responsible for activation of σ^E in the mother cell[50–53]. σ^E directs the expression of many proteins, some of which orchestrate cell wall remodelling of the polar septum and mother cell membrane migration around the forespore in a phagocytic-like process called engulfment[54–56]. Upon engulfment completion, the forespore is suspended in the mother cell cytoplasm as a free protoplast (or endospore) fenced in by two membranes, an inner membrane gotten from the forespore and an outer membrane gotten from the mother cell[29,57,58].

During engulfment, a very interesting and highly-conserved transenvelope protein complex, called the A-Q complex, also described as a feeding tube apparatus, is believed to traverse the two bilayer membranes, assembling in the membranes surrounding the forespore,[14,59,60] creating a direct conduit between the mother cell and the forespore, and aiding the maturation of the forespore by functioning as a specialized secretion system which contributes to spore shape, as well as the transcriptional potential of the spore[56,61,62].

This complex is believed to maintain the physiology of the forespore and the activity of the late forespore σ factor, σ^G [14,47,63]. The activitation of σ^G leads to a signalling cascade which then activates the second mother cell transcription factor σ^K [41,59,60]. Furthermore, during engulfment, the primordial germ cell wall is synthesized from the forespore side while the thick spore cortex peptidoglycan layer is synthesized from the mother cell side[25,58,64].

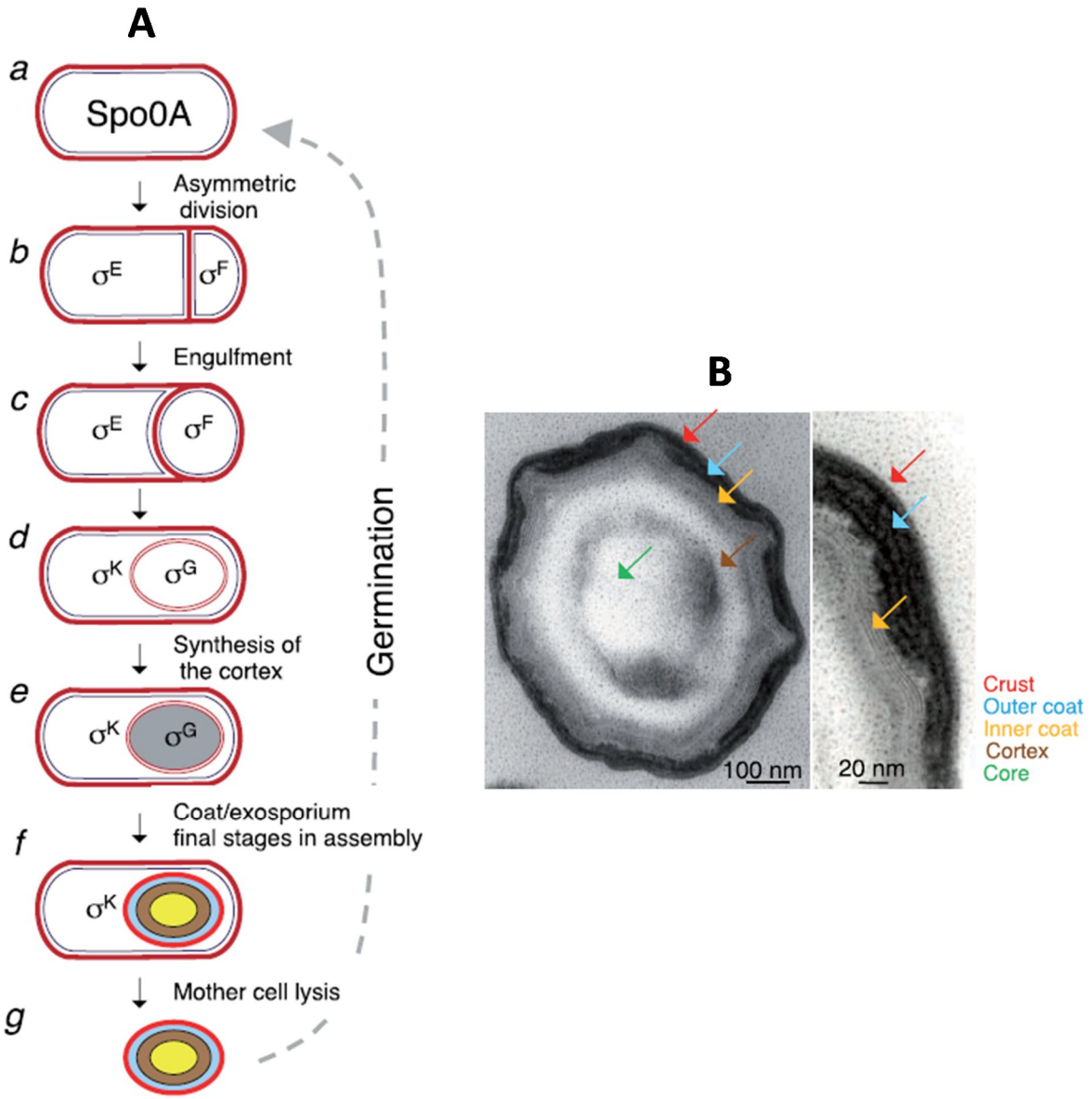

Fig 1.1. Sporulation in *Bacillus subtilis*: showing (A) *a-g:* The main stages of sporulation and the order of sporulation-specific transcription factor activation and (B) Transmission electron microscopy (TEM) image of a thin cross section of a *B. subtilis* spore showing the main structures of the spore and a magnified view of the spore surface layers on the right panel. Adapted from[25].

Proteins made in the mother cell under σ^E and σ^K control, are responsible for orchestrating the assembly and modification of the cortex, which is present between the mother cell and forespore membranes, as well as a multi-layered proteinaceous coat on top the forespore surface[21,25,65]. In the forespore, σ^G transcribes certain genes which encode several proteins that bind and compact DNA in order to protect the spore chromosome, as well as a membrane complex that imports dipicolinic acid which aids in spore dehydration[14,21,26]. Finally, under the

mother cell σ factor σ^K, a group of enzymes degrade the cell wall of the mother cell, leading to its death by cell lysis, and release of the fully mature endospore into the environment[25,46,50,66,67].

1.3 Sporulation in *B. subtilis* – a Review of the essentials

Sporulation in *B. subtilis* is likely the best-comprehended and most productive example of cellular differentiation and development for understanding both the expansive themes and the molecular fundaments in developmental biology[36,43,68]. The recognition of successive stages of sporulation by Roman numerals thus goes by the convention introduced by Ryter[17] which is now globally adopted. Generally, the nomenclature ascribed to sporulation genes are termed according to the morphological stages at which their inherent mutations stop spore development[68]. For instance, mutations in *spoII* genes arrest advancement at stage II and do not permit advancement to stage III whereas, genes whose products are vital for the beginning and proper formation of asymmetrically positioned septum are allocated the *spo0* initials[68].

1.3.1 Stage 0 - Decision to sporulate and cessation of exponential growth:

According to Errington, in this stage there is normal proliferation of the vegetative rod-shaped cells in a good growth medium like other rod-shaped bacteria cells wherein cells double in length and partition centrally to yield two identical daughter cells[37], and the main vegetative housekeeping σ factor during this phase is σ^A [17,69]. Although recently, pioneering electron-microscopic studies have revealed cells in a sporulation medium that have ceased growing exponentially and are yet to show overt changes in morphology[34,36]. Either way, expression of a factor known as Sda is induced to truncate sporulation if conditions are not favourable for the initiation of DNA replication or if the cell contains actively replicating chromosomes[34,36]. The characteristic morphological remodeling that takes place during sporulation are linked to universal changes in gene expression, that are facilitated and carried out by the turning on of the alternative RNA polymerase σ factors[42].

1.3.2 Stage I - Axial filament formation and ensuring correct chromosome copy number:

Phosphorylation of the transcription factor Spo0A oversees the decision to start sporulation and *spo0* mutants are impaired in the signal transduction structure initiating sporulation

[9,33,36,42,69]. Activation of σ^H (also acknowledged as the alternative σ factor or the transition-state regulator) and Spo0A (the response regulator, via Spo0F and Spo0B mediated phosphorylation- Spo0A-PO_4) in the predivisional cell results in the expression of factors important for axial filament formation, asymmetric partitioning, and compartmentalization of gene expression including the activation of genes that encode the initial compartmentalized σ factors, σ^F and σ^E, and their regulators[9,17,35,42,44,69]. For example, the *spoIIA* and *spoIIG* operons that encode the prespore- and mother cell-specific transcription factors σ^F and σ^E respectively, *spoIIE* encoding a bifunctional protein phosphatase vital for asymmetric partitioning and σ^F activation, as well as *racA* gene which encodes the effector of axial filament formation, are all under the control of Spo0A[50], although σ^F and σ^E become active only after asymmetric division is complete[52,62]. At the start of sporulation, the cell contains two chromosomes: one for the mother cell and one for the forespore[40]. The duplicated chromosomes form a condensed serpentine-like structure known as the axial filament which stretches from one pole of the cell to the other[40]. The RacA protein which is vital for anchoring both chromosomes to the cell poles in order to promote proper chromosome segregation, affixes to GC-rich inverted repeats close to the origin of replication and localizes to the cell poles via its connection with DivIVA, which reciprocally localizes to the two poles of the cell via the recognition of highly negatively curved membranes thereby ensuring that each daughter cell gets one origin of replication and consequently, one chromosome[40]. Hence, activation or repression of transcription is decided by the binding of Spo0A-PO4 to a 7-bp sequence, TGNCGAA, where N represents any nucleotide, in or close to promoters recognized by the vegetative σ factor σ^A as well as the alternative σ factor σ^H resulting in universal variances in gene expression, and changing the expression profile of more than 500 genes representing roughly one-eighth of all genes in *B. subtilis*[17,70]. However, the degree of Spo0A phosphorylation decides the response dynamics of the system as well as a battery of physiological outcomes, ranging from the making of biofilms and becoming cannibalistic (when Spo0A is phosphorylated at reduced levels), to sporulation (when Spo0A is phosphorylated at increased levels)[8,40,42,69] and KinA is the main histidine kinase culpable for initiation of sporulation[33,42,51,69] although there are several histidine kinases (KinA, KinB, KinC, KinD, and KinE) each of which respond to a different stimuli[35,40,71]. Overexpression of KinA (or KinB) during exponential growth or above certain threshold can also induce sporulation regardless of nutrient availability[36,42,69]. Summarily, in this stage, an axial filament of

chromatin is formed wherein two copies of chromosomes (or an incompletely replicated chromosome) condense and elongate forming a stretched continuum across the long axis of the cell[17].

1.3.3 Stage II - Asymmetric septation:

Asymmetric division which involves the changeover from a medial septum to an asymmetric septum, marks the start of this stage dividing the cell at a subpolar site into two unequally sized daughter cells; the larger mother cell and a smaller prespore[17,37,40,52,61,68,72]. This transition to a polar septum depends on increased FtsZ levels and the production of SpoIIE which somehow recruits FtsZ to polar sites[40]. Once asymmetric division is complete, SpoIIE dephosphorylates SpoIIAA, which binds and sequesters SpoIIAB (an anti-sigma factor holding σ^F inactive) thereby causing σ^F to assume activity in the prespore, rapidly followed by SpoIIR-mediated σ^E activation in the mother cell[40,42,50]. σ^E however, is usually produced as an inactive pro-σ^E precursor that needs *spoIIGA* for processing to its mature form[40]. Two unusual steps are involved during prespore chromosome segregation. Initially, a section of the chromosome that is centred approximately on the *oriC* region (where bidirectional chromosome replication is originated) reaches the cell pole whilst making of the sporulation septum traps ~30% of the chromosome within the smaller prespore compartment[43,50] (Fig 1.2). Afterwards, the rest of the chromosome ~70% which is situated farther away from the *oriC*, is then rapidly pumped via the septum by a DNA conveyer known as SpoIIIE which is also required for membrane fusion, yielding two cells with dissimilar volumes but similar genomes[43,50,72,73]. Thus, finalization of the specialized spore (polar) septum is the hallmark of this stage[17,53] as the edges of the septum starts advancing towards the proximal cell pole[36] (Fig 1.2). Both σ^F and σ^E mutants arrest at asymmetric division[62]. Additionally, recent studies opines that SpoIIIE, SpoIIIM, and PbpG work together to manage the synthesis of peptidoglycan around the septal pore during chromosome translocation, and as a result, compartmentalization in the event of septal peptidoglycan hydrolysis is ensured[73].

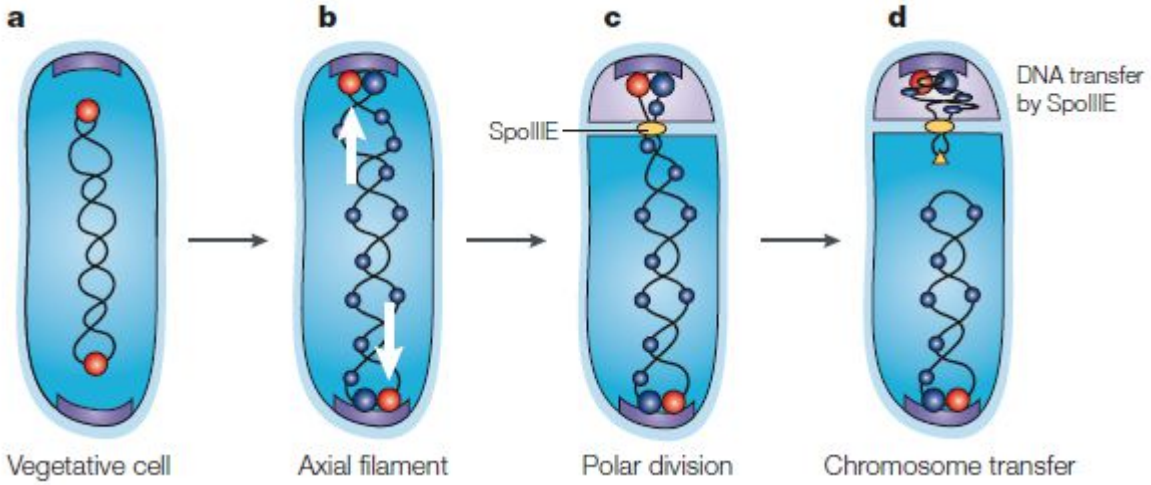

Fig 1.2 Prespore chromosome segregation showing: (A) affixing of Spo0J protein to areas around the *oriC* portions of the chromosome forming a condensed foci vital for optimal chromosome segregation in the vegetative cell. The *oriC*/Spo0J complexes (red) are affixed at about the one-quarter and three-quarter positions across the length of the cell. (B) advancement of the *oriC* regions towards the cell poles whilst being affixed to the poles via the combined action of a protein known as Soj (not represented) and RacA (blue), alongside the polar anchor protein, DivIVA (purple) at the initial stages of sporulation. (C) trapping of ~30% of the chromosome which is affixed to the *oriC* region in the prespore compartment as a consequence of asymmetric division. (D) recruitment of the SpoIIIE protein (yellow) to the leading edge of the septum where it makes a pore through which it conveys the left over parts of the chromosome, and thus finalizing prespore chromosome partitioning. Adapted from[43].

1.3.4 Stage III - Engulfment:

The prespore is thereafter engulfed by the mother cell in an operation widely known as engulfment and consists of several distinct intermediary steps which involves an initial SpoIIB mediated septal thinning of the polar septum whilst the prespore bulges into the mothercell and the septal membrane completes its migration around both sides of the prespore[17,43,61,66,70,74]. At the end of the membrane migration around the prespore, the membranes join at the cell pole, disjoining from the prespore, liberating and allowing it to float freely as a protoplast within the mother cell marking the end of stage III[17,55,61]. It is thought that FisB, a mother cell protein fortified at the regions of membrane fission during engulfment and vital for optimal membrane fission is responsible for membrane fission towards the end of engulfment[40]. Apparently, FisB associates preferentially alongside the phospholipid cardiolipin that is supposedly fortified across negatively curved leaflets of membranes and for membrane scission to occur, FisB would interact *in trans* with cardiolipin

fortified membranes at the leading edge of the engulfing membrane causing an instability of the two membranes[40]. As a consequence of engulfment completion, the free floating protoplast is now fenced in by two membranes: its own, termed the inner forespore membrane (IFM), as well as a second membrane acquired from the mother cell, termed the outer forespore membrane (OFM), and both membranes together sandwich and define the intermembrane space[74]. A third outermost mother cell cytoplasmic membrane however, envelops the first two membranes and the forespore[55]. Three mother cell hydrolase proteins namely SpoIID, SpoIIM and SpoIIP with PG degradation activity form a complex known as (DMP) and mediates PG synthesis at the leading end of the engulfing membrane as well as the incomplete dissolution of the septal PG to remove steric blocks that could hinder the advancement of the mother cell membrane around the prespore[36,40,66,75–78]. The DMP complex is recruited to the polar septum by SpoIIB and without SpoIIB, there is a partial mislocalisation of the DMP complex, resulting in a sloppy peptidoglycan hydrolysis and faulty engulfment[79]. SpoIID is a lytic transglycosylase that cuts glycan strands which do not have stem peptides, while SpoIIP is an amidase and endopeptidase that cuts out the stem peptides off the glycan strands, and SpoIIM is a polytopic membrane protein believed to act as a scaffold for the other two enzymes fastened to the membrane [79]. By thinning the peptidoglycan layer of the polar septum, the DMP hydrolase complex which is also necessary for septal thinning to proceed to the ends of the septum, allows the formation of a channel consisting of parts controlled by both forespore-specific σ^F and mother cell-specific σ^E [55,62,77,79]. This renowned 'feeding tube' channel or 'transenvelope complex', is composed of σ^F controlled SpoIIQ, as well as σ^E controlled SpoIIIAA-AH (A-Q complex), and not only connects the mothercell and forespore compartments, while serving as a means by which the mother cell nurtures the forespore, but also is a requirement for σ^G activation and maintenance in the forespore[38,60–62,77,80] (Fig 1.3). Technically, there appears to be a need to nurture the forespore in some way, because post engulfment, as the forespore is secluded from the mother cell, its metabolic capability is diminished[40].

The A-Q complex besides having a zipper-like inter-action between its component forespore protein SpoIIQ and its mother cell counterpart SpoIIIAH which is vital for the progression of engulfment if the DMP activity is reduced (Fig 1.3), or in the absence of SpoIIB, also possesses certain similarites to secretion systems and conveys non-defined mini molecules or

substances required for σ^G activation into the forespore[60–62,75,80]. Recently, two new proteins namely: YrvJ, a putative PG hydrolase, as well as MurAB, a PG precursor synthesis enzyme were reported to be required for efficient engulfment if the DMP complex is impaired, while MurAB is also required if the SpoIIIAH-SpoIIQ complex is absent[79]. MurAB is an alternative form of the vital *B. subtilis* protein MurAA, which acts as a UDP-N-acetylglucosamine 1-carboxyvinyltransferase, catalyzing the initial devoted action of peptidoglycan precursor synthesis; the conversion of UDP-N-acetylglucosamine to UDP-N-acetylglucosamine enolpyruvate which happens before the formation of UDP-N-acetylmuramic acid (Fig 1.5)[79,81].

Different lines of gene expression action the engulfment of the prespore by the mother cell resulting to the synthesis of the late compartment-unique σ factors[82]. However, at this stage, the membranes enveloping the prespore (now known as the forespore) portray a very shapeless outlook owing probably to the absence of the peptidoglycan layer which provides a definite form[37] even though it is now suggested that the forespore makes two functionally redundant class A penicillin-binding proteins (PBPs), namely PbpG and PbpF, that produce a slim layer of spore peptidoglycan known as the germ cell wall[73,83].

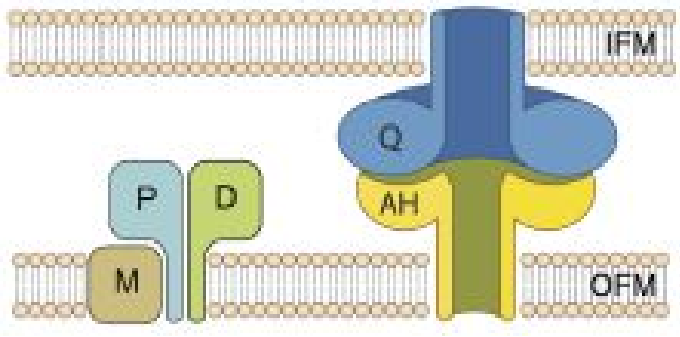

Fig 1.3 Schematic representation of the DMP complex and the SpoIIQ-SpoIIIAH complex in the intermembrane space during sporulation: showing **t**he DMP complex (SpoIID, D in green; SpoIIP, P in light blue; and SpoIIM, M, in brown) vital for peptidoglycan hydrolysis and remodelling during engulfment (II-IV). SpoIIQ (blue) traversing the inner forespore membrane (IFM) and SpoIIIAH (yellow) traversing the outer forespore membrane (OFM), together alongside extra *spoIIIA*-encoded proteins (unshown) constitute a multimeric ring suggested to fashion a channel that permits intercommunication between mother cell and the forespore. The A-Q and the DMP complexes participate in engulfment and are vital for sporulation (III-V). Adapted from[77]

1.3.5 Stage IV - Initiation of cortex and coat assembly:

At this stage, following engulfment, σ^G which drives a nascent transcriptional program encoding determinants vital for the activation of the late sporulation sigma factor σ^K becomes

active inside the forespore, while σ^K, the mother cell specific sigma factor produced as an inert pro-σ^K protein, becomes activated in the mother cell[61,62,74,82]. σ^K expression which needs both σ^E and SpoIIID, a σ^E-regulated transcription factor, also needs proteolytic processing by the intramembrane protease SpoIVFB that cuts out the inhibitory pro-peptide off of σ^K akin to σ^E [35,62]. SpoIVB can free the inhibition enforced by SpoIVFA and BofA by chopping SpoIVFA at multiple sites and by turning on the alternate protease CtpB, which could also cut SpoIVFA (Fig 1.4)[40,84]. Since the activity of SpoIVFB relies upon the σ^F-/σ^G-dependent protease SpoIVB, the activation of σ^K in the mother cell is hence tightly linked to the activity of σ^G in the forespore and active σ^K triggers the expression of genes whose products are vital for the synthesis of the cortex and coat[62]. The unique oval-like shape of the mature spore starts becoming obvious as two PG layers namely; the primordial germ cell wall as well as the modified form of cell wall layer known as the cortex peptidoglycan or simply cortex, are being synthesized in the intermembrane space between the forespore membranes[37,42,82,85,86]. Thus, cortex layer synthesis is the main event of this stage[36]. A σ^G mutant can complete engulfment but would fail to generate σ^K-dependent cortex or coat while the σ^K mutant would also phenocopy the σ^G mutant[62].

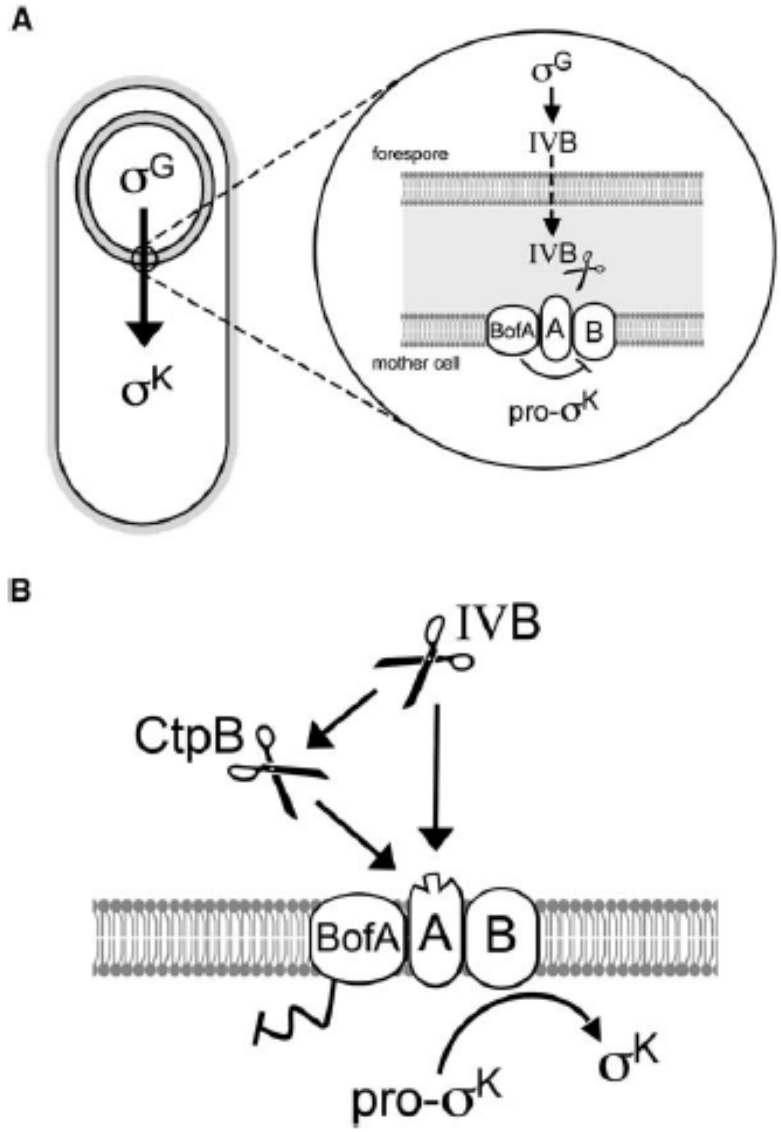

Fig 1.4 Schematic representation of σ^K activation by SpoIVB during sporulation: showing **(A)** Following finalization of engulfment, a σ^G controlled signal transduction pathway in the forespore turns σ^K on in the mother cell. σ^K is firstly produced as an inert precursor protein (pro-σ^K). Proteolytic processing of pro-σ^K within the mother cell needs the membrane-embedded metalloprotease SpoIVFB designated as B in the figurewhile SpoIVFB is being held inactive by two other membrane proteins, SpoIVFA designated as A in the figure as well as BofA. SpoIVB, the forespore signalling protein designated as IVB in the figure is produced under σ^G control and released into the area inbetween the mother-cell and forespore membranes (illustrated in gray). The scissors represents the serine protease SpoIVB, and protease activity is usually needed in order to free the inhibition enforced upon SpoIVFB by SpoIVFA as well as BofA. **(B)** Pro-σ^K processing is induced by two SpoIVB-dependent pathways. SpoIVB initiates pro-σ^K activation directly by cutting SpoIVFA at one of two sites as well as indirectly by bringing about the activation of the serine protease CtpB. Activated CtpB, reciprocally, ccuts the extra-cellular region of SpoIVFA. Adapted from[84]

1.3.6 Stage V - Synthesis of cortex PG, coat assembly, and precursor modification:

Around similar time-point as the cortex is being synthesized inbetween the forespore membranes, the deposition of a protective proteinaceous coat layer on the outside surface of the engulfed spore commences[37,66,82,85] resulting in the encasement of the mature spore into two different concentric shells: an outer shell known as the "coat" consisting of ~70 or ~80 proteins, and an inner shell known as the "cortex" composed of specialized peptidoglycan[40,87]. Together both shells function to shield the maturing spore away from environmental stress[40].

Peptidoglycan is a large polymer comprising of extended glycan strands made by repeating units of *N*-acetyl glucosamine-*N*-acetyl muramic acid, that are cross-linked via pentapeptide chains, supplies mechanical intergity to the cell encasement, and preserves cell shape[76]. This spore peptidoglycan resides between the inner forespore membrane and the outer forespore membrane and is made up of two layers namely: an inner germ cell wall and an outer cortex[40]. The outer cortex is made up of specialized peptidoglycan layer which protects the spore from heat and desiccation[40]. While the germ cell wall is a thin layer bordering the inner forespore membrane and is similar in structure as a vegetative cell wall, the cortex however is different in structure from the vegetative cell wall in that the repetitiveness of transpeptidation between glycan chains and the relative abundance of muramic lactam are both reduced[40]. These structural alterations in the cortex that differentiates it from the germ cell wall are brought about by low molecular weight penicillin binding proteins usually harbouring D,D-carboxypeptidase activity (the eradication of terminal D-alanine residues), as well as the hydrolases CwlD and PdaA that function in the manufacture of muramic lactam from muramic acid[40,88]. Germination is blocked in mutants whose cortex is deficient in Muramic lactam but this can be remedied by exogenous lysozyme treatment[40].

It is fascinating that the amount of crosslinking allover the cortex is non-uniform, but instead increases stepwisely towards the external cortex layers and that the disruption of this crosslinking gradient does not seem to confer serious effects on spore core dehydration indicating that a wide gradient of cortex crosslinking is supposedly sufficient to ensure the dehydration of the spore core[40].

Synthesis of both cortex peptidoglycan and vegetative cell wall transpire through similar mechanism. The production and modification of peptidoglycan precursors occur in the mother cell cytosol and is effected by the Mur proteins (designated *mur(AA)BCDEFG*) and *mraY* which

also modify peptidoglycan precursors during the synthesis of vegetative cell wall (see Fig 1.5). However, for sporulation, manufacture of Mur proteins is upregulated by σ^K [40,81,89]. MurAA (or MurAB) and MurB catalyses UDP-MurNAc synthesis using UDP-GlcNAc and phosphoenolpyruvate after which the pentapeptide moiety is then combined in a stepwise manner by MurC, MurD, MurE, and MurF which joins L-ala, D-glu, diaminopimelic acid (DAP), as well as the dipeptide, D-ala-D-ala respectively[81]. MraY then catalysis the translocation of MurNAc-pentapeptide-1-phosphate into the membrane compartment by creating a covalent bond with a membrane embedded undecaprenyl-phosphate molecule thereby forming Lipid I. Finally, UDP-GlcNAc derived GlcNAc is then added to the 4-hydroxyl of MurNAc by MurG to form Lipid II[81].

After proper modification, the PG precursors are tethered to the outer forespore membrane via the creation of lipid intermediary compounds Lipid I and Lipid II and subsequently flipped over the membrane into the intermembrane space between the outer and inner forespore membrane by a Lipid II flippase [40]. Lipid II, which is a disaccharide pentapeptide tethered to an isoprenoid, has to go through the membrane in order to be polymerized and as soon as the flipping or translocation is done via some undefined process, polymerization of the disaccharides commences resulting in the cross-linking of the peptides by the responsible penicillin binding proteins (PBPs)[90] (see Fig 1.5). The *E. coli* FtsW protein which is a member of the SEDS (shape, elongation, division, and sporulation) group exhibits *in vitro* flippase activity, and SpoVE which is also a SEDS protein is thought to be its sporulation-specific homolog. Also, the *E. coli* MviN/MurJ protein had been proposed to be a Lipid II flippase, and its sporulation specific homolog was identified to be SpoVB[40]. Both SpoVE and SpoVB are suspected to be sporulation-specific Lipid II flippases and mutations in either *spoVE* or *spoVB* or even *spoVD* truncates cortex assembly resulting in the buildup of surplus levels of PG precursors in the mother cell compartment[40,89,90]. Following translocation into the membrane space, high molecular weight penicillin-binding proteins (PBPs) SpoVE and SpoVD, produce a meshwork of PG that constitutes the cortex in the process whereby lipid-tethered precursors are compiled into glycan chains through a SpoVE-catalyzed tranglycosylation, while peptide crosslinks are formed between the glycan strands via a SpoVD-catalyzed transpeptidation (Fig 1.5)[40]. These peptides are then cross-linked in a process whereby a terminal D alanine is eliminated by a transpeptidase and a new peptide bond is created between the second D-

alanine residue from the peptide side chain as well as the diaminopimelic acid (Dpm) residue from a peptide side chain in a different glycan strand[88]. A non vital class B penicillin binding protein SpoVD, is reliant upon SpoVE, and SpoVD shields SpoVE away from in vivo proteolysis[90]. Experiments like co-immunoprecipitations or fluorescence resonance energy transfer opines that an interaction exists between SpoVE and SpoVD, while experiments like co-affinity purification conducted in *Escherichia coli* showed that the interaction between SpoVE and SpoVD is direct[90]. The cortex PG after synthesis by the synthases SpoVD and SpoVE, is now required to undergo certain modifications by the hydrolases CwlD and PdaA which are vital in the creation of muramic δ-lactam and the reduction in peptide tethered-linkagess[40,91].

The coat basically, is portrayed as having four distinct layers namely: the basement layer, the inner coat, the outer coat, as well as the crust, and proteins within the coat can be subdivided into six classes depending on their cellular localization dynamics[40] (see Fig 1.1B).

One of the initial coat proteins to be situated on the forespore externa is SpoVM[40,87]. SpoVM, a small 26-amino acid protein exclusively manufactured in the mother cell compartment, recognizes the forespore membrane's positive curvature (as opposed to the mother cell's negative membrane curvature) and tethers the next coat protein SpoIVA, a soluble morphogenetic and structural component of the coats basement layer, to the coat[40,87]. SpoIVA, a static cytoskeletal component, then hydrolyses ATP to catalyse its irreversible self-assembly on the forespore surface forming the coats basement layer which then serves as a scaffold upon which every other coat proteins are deposited[40,87] (see Fig 1.5B).

A knockout of either *spoVM* or *spoIVA* truncates the induction of coat assembly and eliminates cortex assembly whether or not the coat is spatially disassociated from the cortex by the outer forespore membrane, thus suggesting that both coat and cortex assembly are intimately linked[40,91]. Recently, CmpA, a 37-amino acid sprotein encoded by a mother cell peculiar sporulation gene was discovered functioning with SpoVM in the coordination of cortex assembly although cells undergoing sporulation are also capable of initiating a SpoVM and SpoIVA mediated cortex assembly without it[40]. Another important mother cell produced coat protein that describes a comprehensive group of firmicute proteins possessing a characteristic N-terminal domain as well as a C-terminal LysM harbouring PG-binding regions is SpoVID, and SpoVID drives coat "encasement" in a step wherein coat proteins completely encapsulate the developing forespore[40,87]. SpoVID is a well-characterized protein that is been said to tether

the outer layers of the coat to the basement platform generated by SpoIVA, and SpoVID acts as the fundamental checkpoint that connects the composing of the coat and cortex[87]. The very mechanism that ascertains the coordinated assembly of the coat and cortex has long been unknown but recently, it was discovered that SpoVID guides the degree of polymerization of the coat basement layer through a linkage to a functioning intra-cellular LysM region which effects the ceasation of sporulation whenever coat assembly is not properly commenced; and that the erroneous assembly of the coat uncovers and reveals the SpoVID LysM region, which when exposed, segregates and withdraws lipid II in order to arrest cortex assembly[87].

Furthermore, the proper coupling of the distinct layers of the coat usually depends upon one main morphogenetic protein that defines it except for the crust which is dependent on two[40]. For instance, knocking out *spoIVA* causes an improper coupling of the resultant basement layer and consequently, all other subsequent layers; while knocking out *safA*, *cotE*, or *cotZ* and *cotY* causes an impaired coupling of the inner coat, the outer coat, as well as the crust respectively[40]. However, it is not yet completely clear how the assembly of both shells are intimately coordinated[40,91].

Once the cortex and coat are being properly generated, huge quantities of dipicolinic acid gets synthesized within the mother cell compartment while the forespore absorbes the dipicolinic acid alongside divalent cations (mostly Ca^{2+}) in a process whereby the engulfed forespore becomes dehydrated and mineralized resulting in the phase-bright appearance of the forespore[82,92].

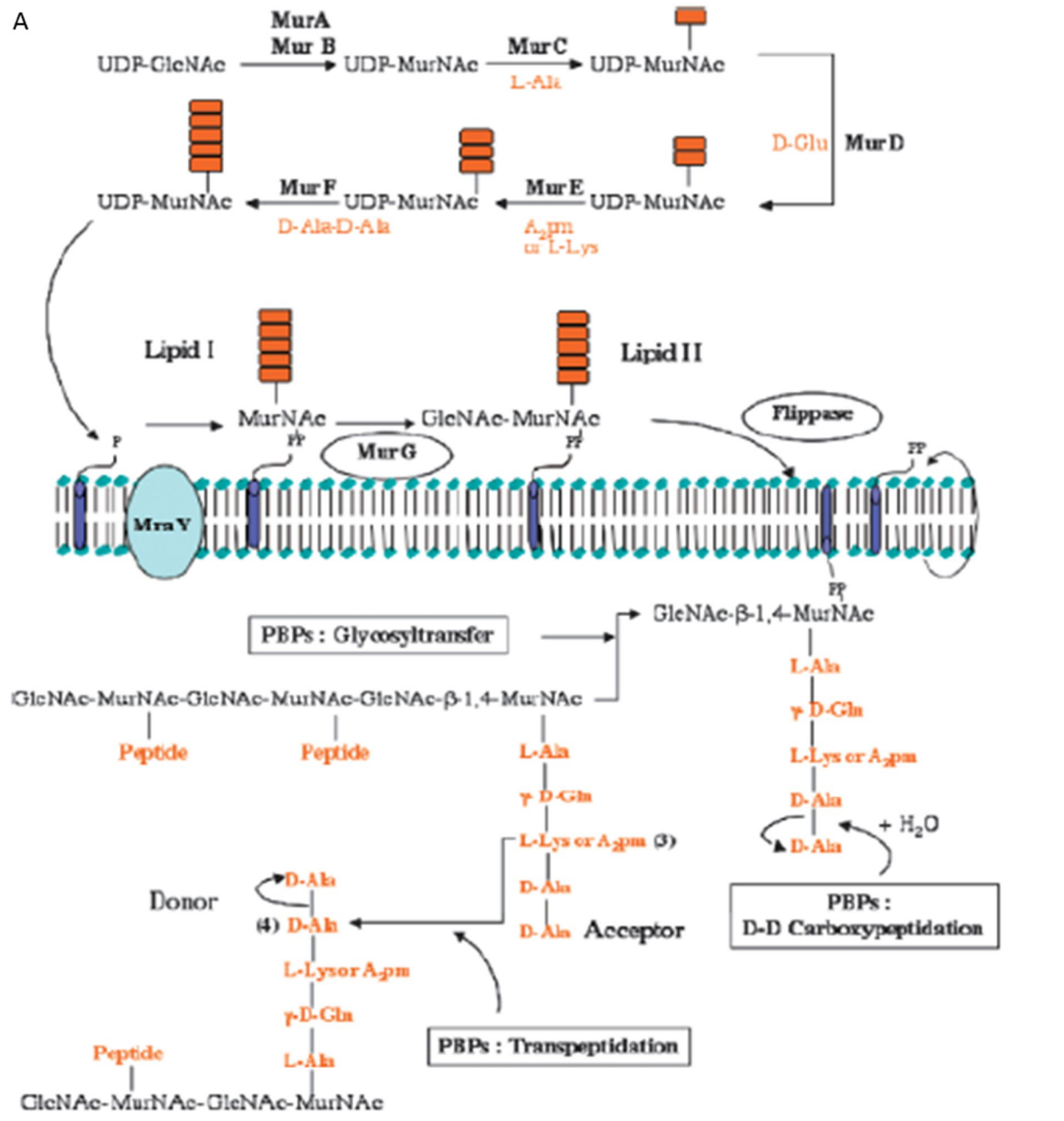
A
MurA
Mur B
UDP-GlcNAc
UDP-MurNAc
MurC
L-Ala
UDP-MurNAc
D-Glu
MurD
UDP-MurNAc
MurF
D-Ala-D-Ala
UDP-MurNAc
MurE
A2pm
or L-Lys
UDP-MurNAc
Lipid I
Lipid II
MurNAc
GlcNAc-MurNAc
MurG
Flippase
MraY
PBPs : Glycosyltransfer
GlcNAc-β-1,4-MurNAc
L-Ala
γ-D-Glu
L-Lys or A2pm
D-Ala
D-Ala
+ H2O
GlcNAc-MurNAc-GlcNAc-MurNAc-GlcNAc-β-1,4-MurNAc
Peptide
Peptide
L-Ala
γ-D-Glu
L-Lys or A2pm (3)
D-Ala
D-Ala
Acceptor
PBPs :
D-D Carboxypeptidation
Donor
D-Ala
(4) D-Ala
L-Lys or A2pm
γ-D-Glu
L-Ala
PBPs : Transpeptidation
Peptide
GlcNAc-MurNAc-GlcNAc-MurNAc
B
outer spore membrane
inner spore membrane
coat
cortex
germ cell wall
SpoVID
SafA
SpoIVA
SpoVM
muramic δ-lactam
peptide cross-link

Fig 1.5 Schematic representation of the cortex and coat synthesis during sporulation showing: (A) The synthesis and assembly of the building blocks of peptidoglycan occur in a stepwise manner in the cytoplasm; after which the linking of the PG building blocks to a membrane-associated undecaprenyl group (generating Lipid I) takes places, leading to further modifications with a GlcNAc group (to create Lipid II). Lipid II is then 'flipped' to opposite side of the membrane. This lipid II which is now situated on the external area of the bacterial membrane functions as the substrate that is then utilized for PBPs-catalyzed glycosyltransfer and transpeptidation reactions. Adapted from[93] (B) A model showing the germ cell wall and the cortex sandwiched in between the inner forespore membrane and the outer forespore membrane, as well as a few vital coat proteins. Adapted from[91].

1.3.7 Stage VI - Maturation:

This is also known as the maturation stage and final period of spore development during which the spore sequentially develops its characteristic features of resistance to UV and high temperatures, dormancy, and germinability with little or no obvious changes in forespore morphology[36,66,82,94].

1.3.8 Stage VII - Lysis:

Upon full maturation of the forespore, the mother cell compartment lysis resulting in the subsequent liberation of the fully mature spore unto the environment and marking this stage as well as the whole sporulation process as complete[61,66,82,94]. It is probably noteworthy to state that within the inter-compartment sigma factor regulatory arrangements embeds some battery of feedback and feedforward loops which permit the replacement of the functions of early sigma factors (σ^F and σ^E) by the later functioning sigma factors (σ^G and σ^K) in their respective compartments[62]. For example, gene products that are controlled by σ^E activate σ^K and also down-regulate gene expression controlled by σ^E in the process, while an anti-σ^F sigma factor controlled by σ^F in reciprocity enhances the activation of σ^G [62]. Finally, as the liberated spore finds itself situated in a nutrient-fortified environment following its eventual release, the cortex PG becomes specifically hydrolysed by the cortex-lytic enzymes SleB and CwlJ which are not only redundant in function but also exhibits its specificity by recognizing muramic lactam. This results in germination and outgrowth consequently allowing the cell to resume its normal vegetative growth cycle[8,40,82].

1.4 Specialized secretion systems and the A-Q complex

The A-Q complex has been described as a new type of specialized secretion system since its components share amino acid sequence and structural similarity to proteins present in well-

studied specialized secretion systems[26,42,60,95]. Specialized secretion systems can be described as molecular nanomachines which facilitate the ATP-driven transport and movement of molecules (proteins, DNA and metabolites) across the bacterial cell envelopes or membranes in Gram-positive and Gram-negative bacteria[14,21,59]. Bacterial secretion systems are classed into different types depending on the function, structure and mechanism of substrate translocation exhibited. Of particular interest are components of the Type II, Type III and Type IV secretion systems which share sequence and structural similarities to proteins of the A-Q complex (Fig 1.6).

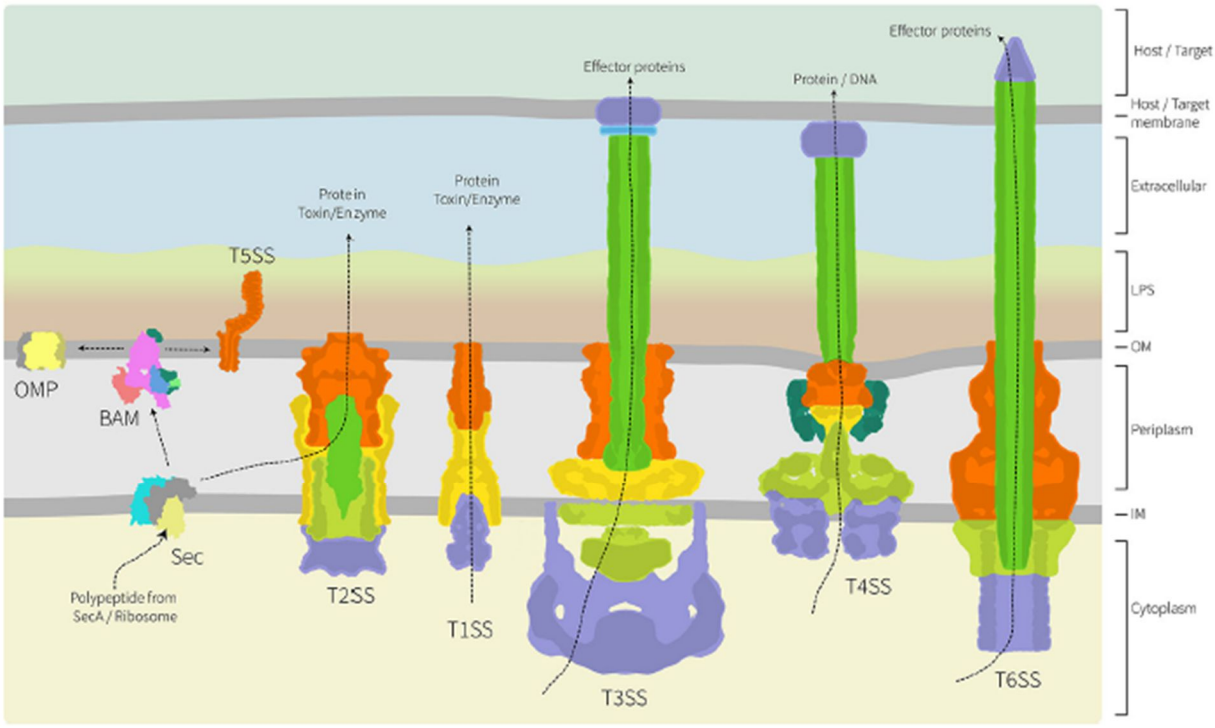

Fig 1.6 Structural description of the main protein secretion arrangements present in Gram-negative bacteria: showing the T1SS, T3SS, T4SS, and T6SS, which transport substrates directly through membranes from the cytoplasm and the T2SS, which conveys proteins from the periplasm[96].

1.4.1 Components of the A-Q complex

During engulfment, the highly-conserved A-Q complex is organized in the forespore membranes and appears to establish a channel between the mother cell and the nascent forespore[14,21,47,63] (Figures 1.3, 1.7 & 1.8).

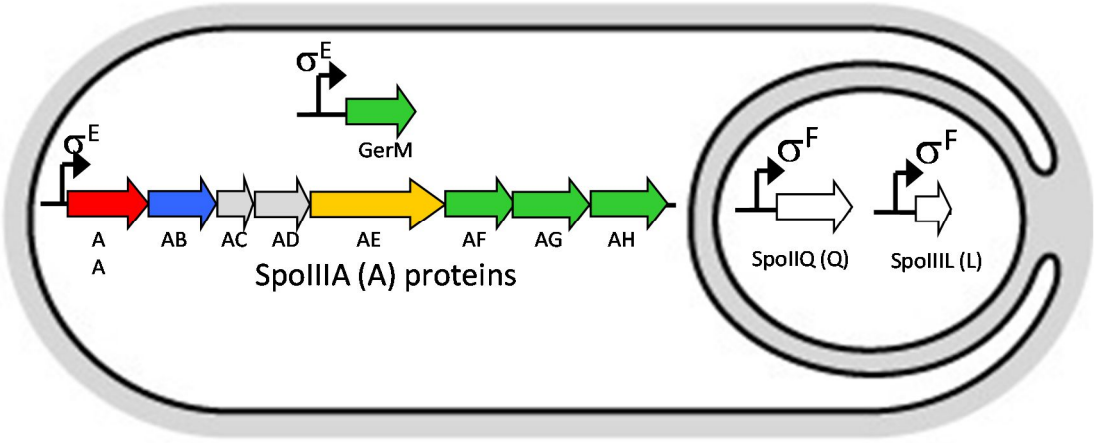

Fig 1.7 Proteins of the SpoIIIA-SpoIIQ (A-Q) complex. The A-Q complex constitutes not less than nine proteins including the forespore protein SpoIIQ (transcribed under the control of σ^F) and at least eight mother cell proteins (SpoIIIAA, SpoIIIAB, SpoIIIAC, SpoIIIAD, SpoIIIAE, SpoIIIAF, SpoIIIAG, and SpoIIIAH), all of which are encoded in the *spoIIIA* operon (transcribed under σ^E). In addition to these proteins, two other factors, namely GerM and SpoIIIL, have recently been implicated in the A-Q complex and are transcribed under σ^E and σ^F control, respectively[21]. All proteins, except SpoIIIAA, GerM and SpoIIIL are integral membrane proteins. SpoIIIAA is cytoplasmatic, GerM a lipoprotein and SpoIIIL of still undefined topology[21,38].

1.4.2 Similarity of A-Q complex proteins to specialized secretion systems

The A-Q complex proteins share homologies with certain proteins of other secretion systems as shown in the Table 1.1. The most common homologies are shared between the T2SS, T3SS, and T4SS, which are all present within Gram-negative bacteria.

	Size (residues)	Topology and homology regions[a]	Protein homologue (% of sequence identity)[b]	Function of the homologue
SpoIIIAA	307		VirB11 (18%) from T4P/GspE from T2SS (18%)	VirB11/GspE: ATPase involved in substrate export and pilus biogenesis
SpoIIIAB	171		GspF from T2SS (16%)	ATPase membrane anchor
SpoIIIAC	68	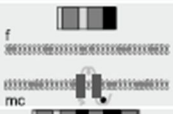	NI	NI
SpoIIIAD	133	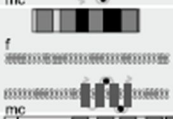	NI	NI
SpoIIIAE	399	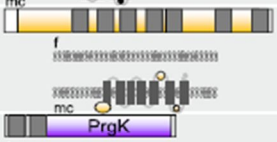	Permease domain of the multidrug transporter ABCG2 (11%)	Transport of various drugs through the cytoplasmic membrane
SpoIIIAF	206		RBM2 of PrgK from T3SS (12%)	Ring-building motif, part of the inner-membrane platform
SpoIIIAG	229		RBM2 of PrgK from T3SS (17%)/RBM3 of FliF from flagella (14%)	Ring-building motif, part of the inner-membrane platform
SpoIIIAH	218		RBM2 of PrgK from T3SS (17%)	Ring-building motif, part of the inner-membrane platform
SpoIIQ	283	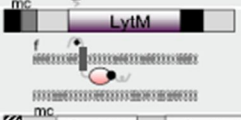	LytM from the *S. aureus* cell wall synthesis machinery (20%)	Hydrolysis of the Gly-Gly bond in the pentaglycine inter-peptide link found in the staphylococcal cell wall
GerM	366	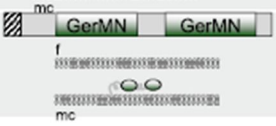	NI Belongs to the GerMN protein family (PF10646)	NI

Table 1.1 Homologies of the A-Q complex proteins to proteins of other secretion systems. Adapted from[21].

1.4.3 Localization of A-Q complex proteins

The A-Q complex is organized in the membranes encompassing around the spore, with the extracellular domain of SpoIIQ interacting with the extracellular domain of SpoIIIAH to form a transenvelope connection betwixt the larger mother cell and the smaller forespore[14,21,26,97–99]. Consistent with this interaction, the localization of SpoIIIAH in the forespore outer membranes depends on SpoIIQ[14,21,63,98]. As depicted in Figure 1.8, SpoIIQ localization to the forespore septal membrane relies upon both SpoIIIAH and GerM[21,46,60]. Reciprocally, GerM requires SpoIIQ for its localization in the forespore outer membrane[21,60]. Proper assembly of

this protein triad (SpoIIQ, GerM, SpoIIIAH) enables the accurate localization of SpoIIIAG on the septal membrane of the larger mother cell, because if any of these three proteins is knocked out, SpoIIIAG localization becomes compromised[21,60].

Although the localization of the other components of the A-Q complex is yet to be established, the current model is that they all depend on the SpoIIQ/ GerM / SpoIIIAH triad[21,60].

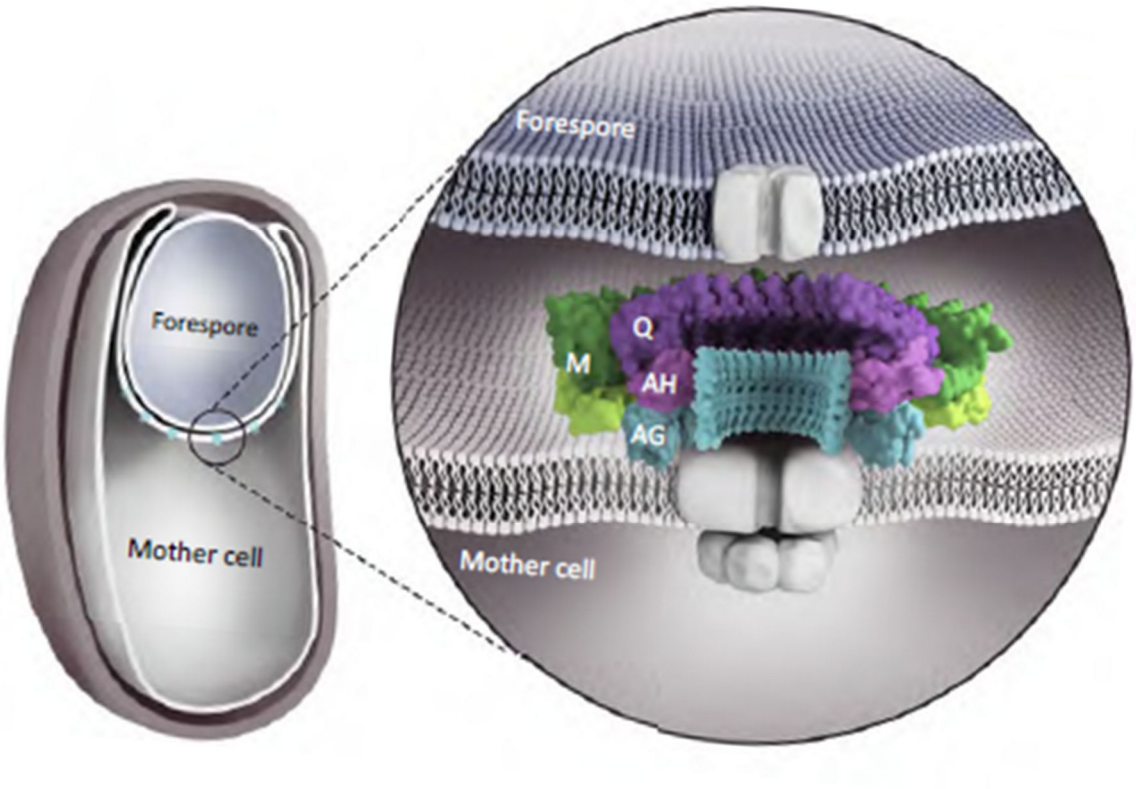

Fig 1.8 Illustration of the stacked ring formation of the A-Q complex in *Bacillus subtilis*: highlighting the integral mother cell proteins SpoIIIAG (teal), SpoIIIAH (pink), GerM (green), as well as the forespore protein SpoIIQ (purple). The remaining SpoIIIA-SpoIIQ complex proteins SpoIIIAB-SpoIIIAF, depicted as a single complex in gray, is also shown to possess a hypothetical membrane pore that is still unproven. The complex proteins are assumed to form a channel-like conduit which connects the mother and the forespore by stacking upon each other in the form of rings. SpoIIIAA is shown as a hexamer, as a consequence of its resemblance to ATPases of some other specialized secretion systems. As already described in literature, the presence of a pore in the forespore membrane is already established although the protein culprit remains yet to be identified. Adapted from[21]. It is important to state that the structural arrangements of the proteins in the cartoon above is however mostly hypothetical.

1.4.4 Phenotypes of the A-Q complex mutants

Mutants in any of the A-Q complex genes display two characteristic phenotypes: 1) smaller forespores with abnormally shaped membranes (Fig. 1.9B), and 2) limited forespore transcriptional potential, which results in decreased σ^G-dependent transcription (see Fig 1.9A)[47,54,99]. The data shown in Figure 1.9C suggests that some components of the A-Q complex are not absolutely required for sporulation. SpoIIIAA-G mutants have a very severe sporulation defect (0.001%, relative to wild type cells)[100] as well as SpoIIQ (0.01%)[47,75,99]. On the other hand, the sporulation efficiency of SpoIIIAH and GerM mutants, averaging 3.4%[100] and 4.6%[60] spores respectively, suggests that both proteins are less relevant for sporulation compared to SpoIIIAA-G. The SpoIIIL mutant produces ~50% spores (this work) and thus this protein is less important for sporulation compared to the other proteins in the table.

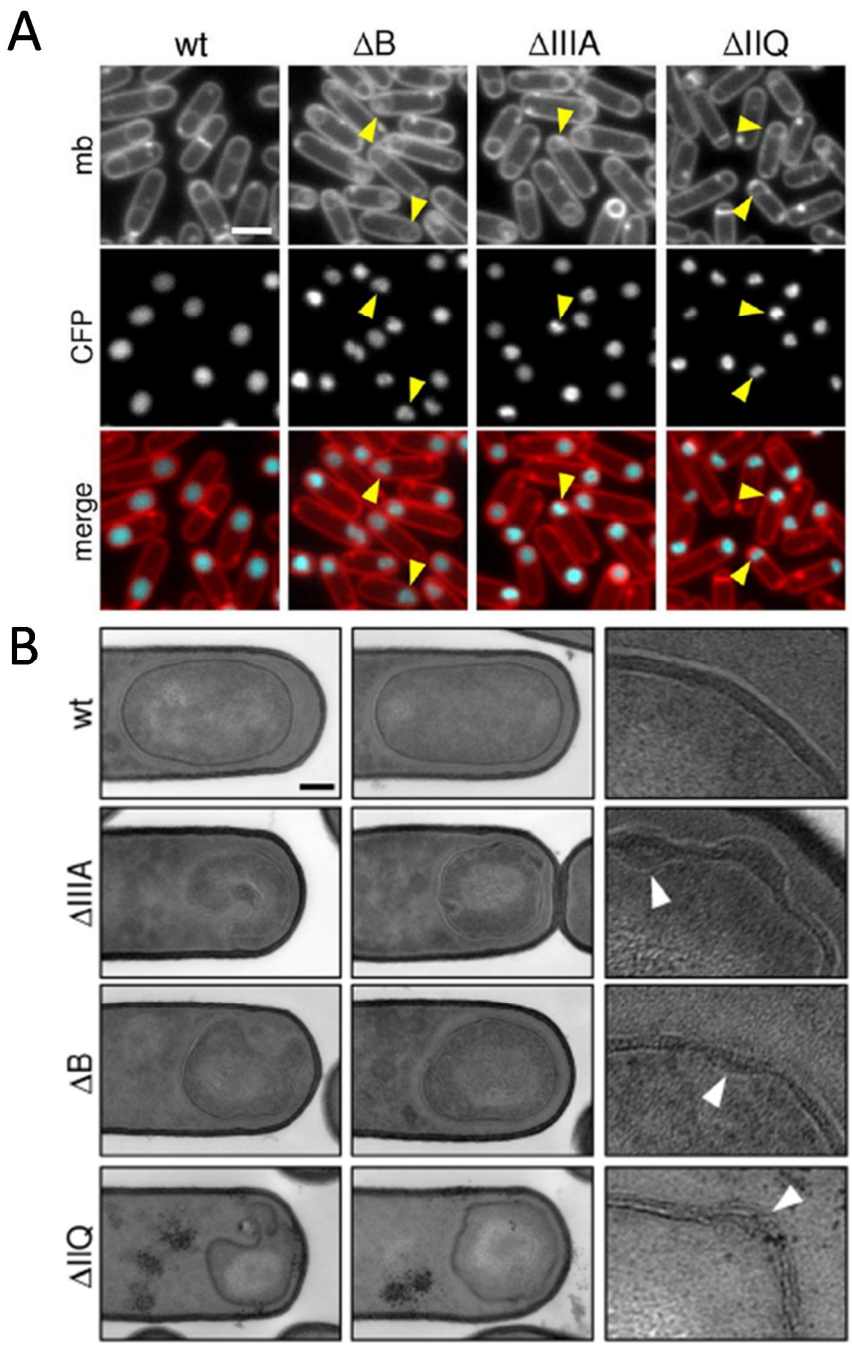

Null mutant	Spores %
AA AB AC AD AE AF AG	0.001
AH	3.4
GerM	4.6
SpoIIIL	50
Q	0.01

Fig 1.9 Phenotypes of the A-Q complex mutants: showing σG activity and morphological defects (A), forespore morphology and membrane defects (B) and sporulation efficiency data (C). (A) Represents fluorescence microscopy images of *B. subtilis* forespore at hour 3 after start of sporulation in otherwise wild-type (WT), Δ*spoIIIA* mutant, Δ*spoIIIAB* mutant, and Δ*spoIIQ* mutant, all strains have a forespore reporter (P*spoIIQ*-cfp; false-colored blue in the lower panel) for good visualization of the illustrated forespore cytoplasm, the membranes (mb) from the same field were visualized using the fluorescent dye TMA-DPH is false colored red in the lower panel). Carets illustrates instances of ''collapsed'' forespores. Scale bar, 1 µm (B) Electron microscopy images of *B. subtilis* forespore at hour 3 after start of sporulation in otherwise wild-type (WT), Δ*spoIIIA* mutant, Δ*spoIIIAB* mutant, and Δ*spoIIQ* mutant. Two examples are shown for each strain in the first two columns and the last

column is a 5x enlargement of the forespore membranes. The carets show the bulged or deformed membranes. Scale bar, 200 nm. (C) Sporulation efficiency data of 36 hr cultures determined as a total number of heat resistant colony forming units compared to wild type after 20 min heat treatment at 80°C[47,75,80].

1.4.5 Hypothetical functions for the A-Q complex

At least two main models have been used to describe the function of the A-Q complex and how it contributes to normal spore size and transcriptional potential in the forespore. In the first model referred to as the feeding tube model, the A-Q complex forms as a gap-like junction through which the forespore is fed mother-cell derived metabolites[21,54,99]. This model takes into consideration the fact that the forespore becomes separated from the external environment during engulfment as it is internalized inside the mother-cell, and would therefore depend on the mother cell for macromolecule biosynthesis and transcription[21,99]. Interestingly, current knowledge suggests that the complex is still required for forespore transcription, even when the forespore still enjoys access to the external environment (for example, in mutants impaired in engulfment where the forespore does not become internalized within the mother cell). Thus, the A-Q complex functions during spore development also whilst the forespore has access to the outside environment[21]. In the second model referred to as the secretion model, the A-Q complex acts to translocate certain yet-to-be-defined proteins into the forespore[21]. However, studies using compartment-specific fluorescent proteins have failed to observe cross-compartment leakiness of fluorescent proteins[21,98]. Thus, despite these two models, the exact function of the A-Q complex remains unclear.

1.4.6 SpoIIIL and its relationship to the A-Q complex

spoIIIL is transcribed within the forespore under σ^F control[14]. Interestingly, *spoIIIL* is also transcribed as a component of the *comG* operon, which encodes the competence machinery that resembles a Type IV pilus, and is involved in DNA uptake[101]. The significance of *spoIIIL* transcription within the *comG* operon is unclear, as is its role, if any, in the competence machinery.

SpoIIIL is partially required for σ^G activity and a Δ*spoIIIL* deletion mutant has a sporulation efficiency between 30 - 50%[14]. Furthermore, a subpopulation of cells in the Δ*spoIIIL* mutant produces smaller forespores, with reduced or no σ^G activity[14]. Importantly, combining the Δ*spoIIIL* deletion with another mutant of the A-Q complex which exhibits a mild defect (for

e.g, Δ*spoIIIAH*), resulted in severe reduction in sporulation efficiency (0.0004%)[14]. The Δ*spoIIIAH* deletion results in 1-10% heat-resistant spores, and not all forespores are defective in σ activity or spore size[14,47]. However, when combined with Δ*spoIIIL,* almost no σ^G activity was seen and all forespores had a notable size change relative to wild-type (see Fig. 1.10)[14]. Although these observations point to the possibility that SpoIIIL is likely an accessory component of the SpoIIIA-SpoIIQ complex, it remains unclear if this is really the case. Thus, this project is focused on understanding the function of SpoIIIL and determining its relationship with the A-Q complex or other processes occurring during spore development.

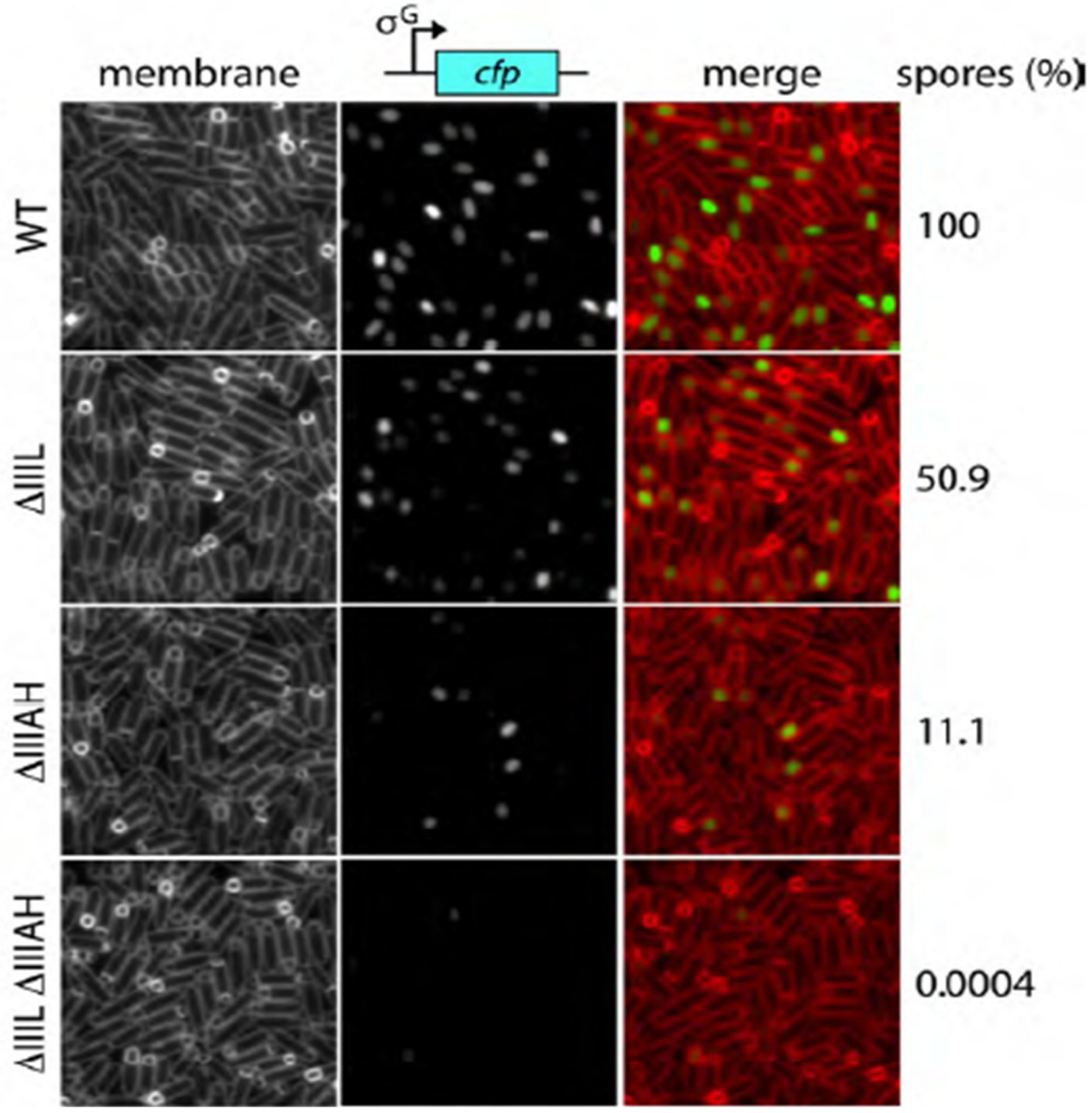

Fig 1.10 σ^G activity and sporulation efficiency of Δ*spoIIIL* mutants: WT, Δ*spoIIIL* (Δ*IIIL*), Δ*spoIIIAH* (Δ*IIIAH*), and Δ*spoIIIL* Δ*spoIIIAH* (Δ*IIIL* Δ*IIIAH*) double mutant strains were imaged via fluorescence microscopy at hour 3.5 from

the start of sporulation. σ^G activity was visualized using a transcriptional fusion of a σ^G responsive forespore promoter (P*sspB*) to cyan fluorescent protein (*cfp*), shown in green in the merge. Sporulation efficiencies relative to wild type at hour 30 after the onset of sporulation (T30) are stated on the right. Adapted from[14].

1.5 Thesis aims and approaches at the start of the project

1.5.1 Aim 1: Defining the extent to which SpoIIIL functions in the A-Q complex

Although existing σ^G activity and spore shape data suggest that SpoIIIL is required for the function of the A-Q complex[14], this data is qualitative and does not provide detailed information regarding the genetic penetrance of the *spoIIIL* mutant defect. Thus, it remains mostly unclear to what extent SpoIIIL actually participates in the complex's role in σ^G activity and spore shape.

To further define the extent to which SpoIIIL functions in the A-Q complex, I will validate existing data and additional mutants using a quantitative imaging approach. Here, I will construct a dual-reporter strain that will allow quantitative examination of σ^G activity and spore size in the same cell, using large population of cells (Fig 1.11). This dual reporter strain will contain a cyan fluorescent protein (CFP) fused to a σ^F-dependent promoter that will allow the quantification of spore size and a yellow fluorescent protein (YFP) fused to a σ^G-dependent promoter that will facilitate the quantification of σ^G activity. The images will then be analysed using ImageJ and the image analysis plugin MicrobeJ[102], which facilitates segmentation of the fluorescent signals and gathering of single cell data values that include: roundness, size and signal intensity. Using this dual reporter strain, it will therefore be possible to quantitatively measure and correlate σ^G activity and spore shape in individual cells within large populations, which has not previously been done before[14].

Previous work examined σ^G activity and spore shape qualitatively in the Δ*spoIIIL* mutant alone, or in combination with the Δ*spoIIIAH* mutant. For my project, I will repeat these analyses using the above approach and test additional mutants, such as the *gerM* deletion mutant. Like SpoIIIL, GerM is only partially involved in the A-Q complex. To further verify SpoIIIL's contribution to the A-Q complex, I will construct a Δ*gerM* Δ*spoIIIL* double mutant and examine its effect on σ^G activity and spore shape, to explore any potential synergy between SpoIIIL and GerM, which would indicate a functional role of SpoIIIL that is dependent on the A-Q complex. The Kolmogorov-Smirnov test (to compare differences in population distributions) as well the

chi-squared test (to compare frequencies of certain subpopulations) will be performed to infer statistical significance.

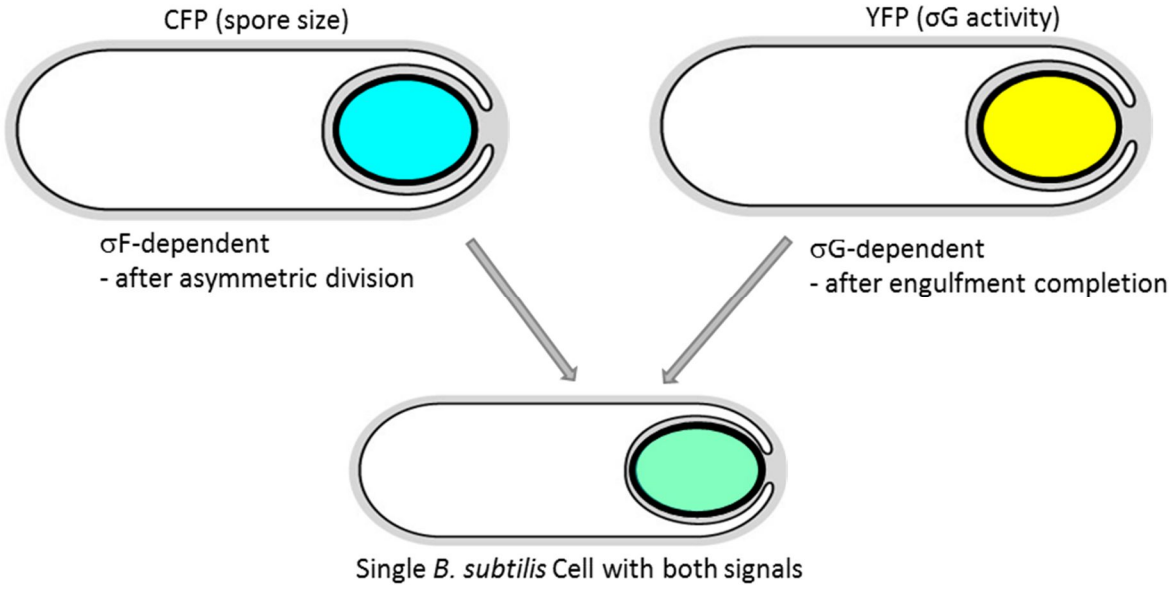

Fig 1.11 Illustration of the newly constructed dual reporter strains for the measurement of σ^G activity and spore size: The dual reporter strain will contain a cyan fluorescence protein (CFP) fused to a σ^F-dependent promoter and yellow fluorescence protein (YFP) fused to a σ^G-dependent promoter. The CFP reporter will allow for examination of spore size during development and and σ^G activity measurements at later stages of development. I will induce sporulation of the cells by resuspension method and collect imaging data at various time-points as the spores develop, in order to obtain spore size and σ^G activity data overtime, using fluorescence microscopy (available in the Microbial Imaging Facility, UTS): See Fig. 1.12A.

1.5.2 Aim 2: Identify, validate and characterize genes that may function with SpoIIIL in sporulation

Very little is known about the genetic network of *spoIIIL*. Because genes rarely function in isolation, the genetic network of *spoIIIL* was probed using a transposon-sequencing (Tn-seq) genetic screen of a Δ*spoIIIL* mutant (unpublished; conducted previously by Dr. Chris Rodrigues). Tn-seq is a powerful method that utilizes the ability of transposons, a type of mobile genetic element, to insert themselves throughout the genome[14]. Insertion of a transposon into a gene is probably more likely if its disruption does not severely impact survival[14]. Therefore, genes that resist transposon insertion are often biologically significant in the genetic background and conditions tested[14]. Tn-seq involves growing a mariner-based transposon library in wild-type cells and any chosen mutant in a sporulation medium, taking samples at the onset of starvation (T0), and after sporulation (24 h – 30 h, T24 or T30) and

then subjecting the samples to heat treatment at 80°C for 20 min (see Figs 1.12A and B)[14]. Transposon mutants that produces spores harbouring transposon insertions survive the heat-treatment, whereas transposon mutants that do not produce spores do not[14]. DNA sequencing and mapping of the transposon-insertions onto the genome unmasks genes, which do or do not habour transposon-insertions, revealing genes that are important for sporulation in different genetic backgrounds (see Fig 4.1 results section).

Using this approach on wild-type and Δ*spoIIIL* deletion strains, Tn-seq revealed genes that become more important for sporulation in the Δ*spoIIIL* mutant compared to otherwise wild-type cells. From the available Tn-seq data, I will firstly identify a list of top 20 genes (geneX^{top20}) using the Sanger Artemis Genome Browser and Annotation tool[14], which allows visualization of the transposon-sequencing data. Next, I will generate double mutants of Δ*spoIIIL* ΔgeneX^{top20} and perform sporulation efficiency (heat-kill) assays to test if these mutants produce fewer spores compared to the Δ*spoIIIL* single mutant, thus validating the Tn-seq data. The sporulation efficiency (heat-kill) assay calculates sporulation efficiency in 24-36 h cultures by determining the number of heat-resistant (80°C for 20 min) colony forming units (CFUs) of any strain compared to the number of wild-type heat-resistant CFUs. Finally, double knockouts with severe sporulation defects (i.e. > 5-fold reduction in sporulation relative to Δ*spoIIIL*), will be examined further for defects in σ^G activity and spore shape, using the same image analysis strategy applied in Aim 1. By assaying the sporulation efficiency, σ^G activity and spore shape of Δ*spoIIIL* Δ*gene*X^{top20} mutants, I will be able to define possible genetic relationships and interaction networks involving *spoIIIL* (see methods section 2.8).

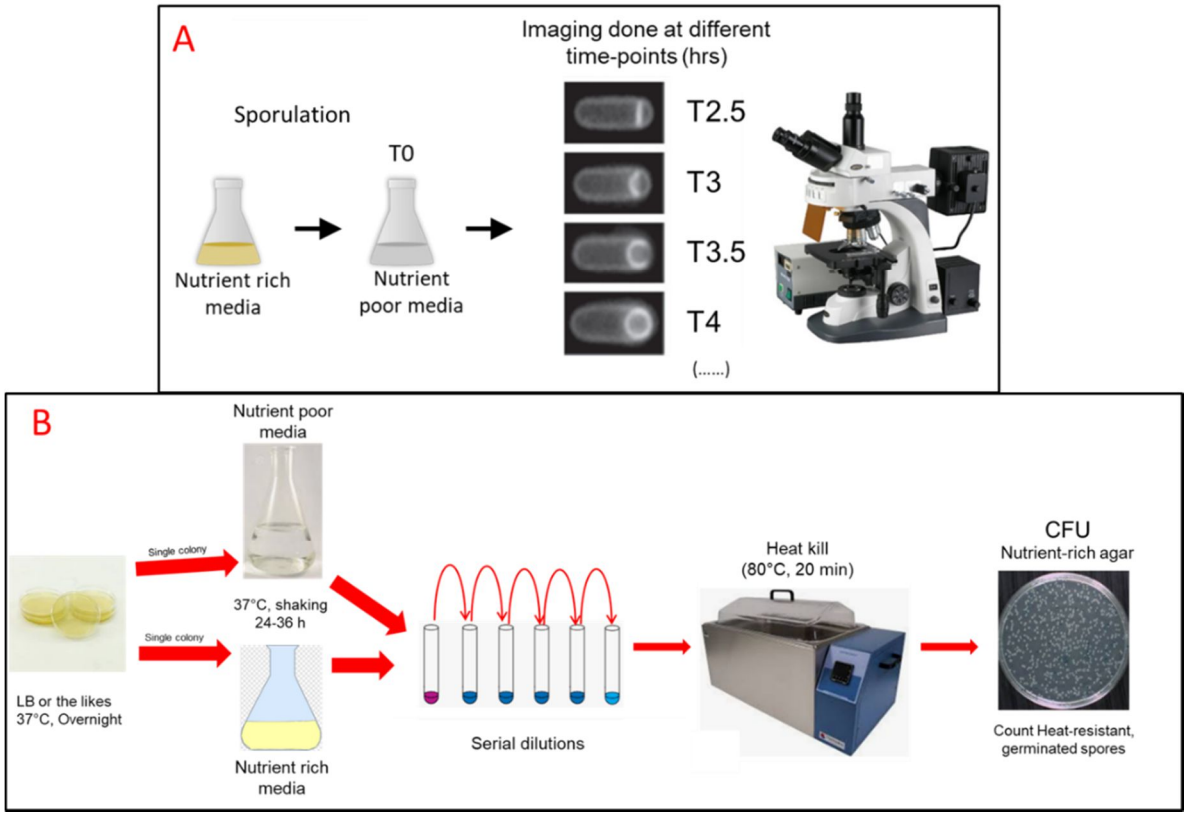

Fig 1.12 Illustration of *B. subtilis* fluorescence imaging **(A)** and sporulation efficiency (heat Kill) **(B)** protocols. For (A), Cells will be grown in nutrient rich medium at 37°C, and transferred into nutrient poor medium (this is T0) to trigger sporulation of the cells. Samples will be collected, concentrated by centrifugation, resuspended in the membrane dye TMA-DPH, fixed on 2 % agarose pads and imaged at certain time points after the onset of sporulation. For (B), Sporulation will be induced in the cells either by resuspension method[14,103] which involves transferring the cells to nutrient poor medium or by nutrient exhaustion method[14,104] which involves growing the cells in a nutrient rich medium until the nutrients in the medium is depleted. Cells will then be incubated at 37°C, for 24 – 36 h after which the cultures will be serially diluted, exposed to heat treatment 80°C, 20 min and plated on nutrient rich medium to obtain heat-resistant colony forming units (CFUs).

1.5.3 Aim 3: Define the localization, topology and important domains / conserved residues of SpoIIIL

The localization of a protein in the cell can provide insights into its function[105]. To determine the localization of SpoIIIL, I will construct two C-terminal fluorescent protein fusions to SpoIIIL, with green fluorescent protein (GFP) and mCherry, using standard molecular cloning techniques (Fig 1.13). The fluorescent proteins will be introduced into *B. subtilis* cells and then examined using fluorescence microscopy to visualize SpoIIIL's subcellular localization.

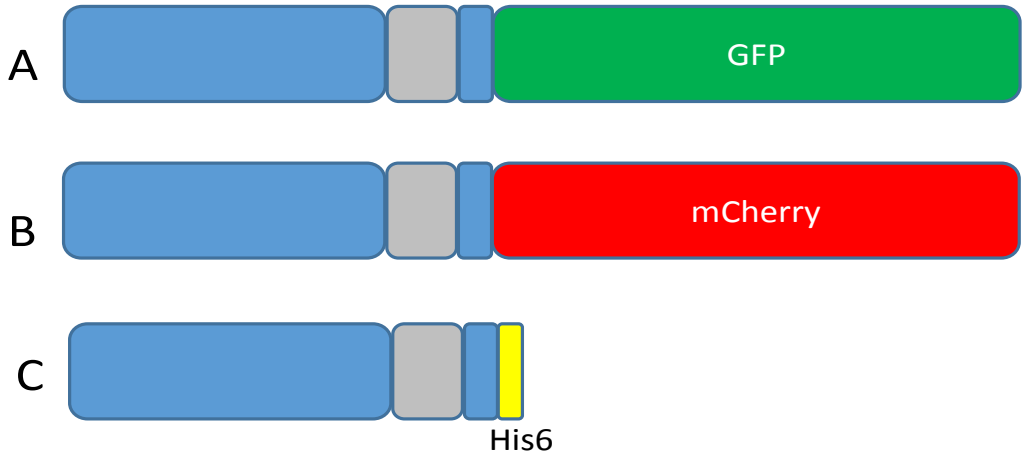

Fig 1.13 Depiction of C-terminal fluorescent fusions of *spoIIIL*: showing (A) *spoIIIL* fused to GFP (B) *spoIIIL* fused to mCherry (C) *spoIIIL* fused to Hexahistidine (His6).

SpoIIIL is predicted to contain a C-terminal hydrophobic patch, which may associate SpoIIIL with the spore membrane (unpublished observation, C. Rodrigues). If SpoIIIL is indeed membrane-associated, defining its topology may help to better understand its function. Topology describes the approximate orientation of membrane proteins through the membrane by identifying protein domains that are surface-exposed or cytoplasmic. To determine the topology of SpoIIIL, I will perform a protease accessibility assay on sporulating cells that have been protoplasted. The principle of this assay is that proteins which are surface exposed will be accessible to degradation by a proteolytic enzyme (e.g. trypsin), while proteins which are cytoplasmic will remain protected[60,74]. Since SpoIIIL is produced in the forespore, and since engulfed forespores would be inaccessible to trypsin digestion, the assay will be done using Δ*spoIIQ* mutants, which are defective in engulfment[19]. Since we do not have an antibody to SpoIIIL, a SpoIIIL-His6 or SpoIIIL-GFP construct will be used with planned detection with anti-His antibodies or anti-GFP antibodies respectively.

A protein might contain certain sequences or conserved residues/domains which could be found in related orthologs. These conserved residues and homologous sequences are sometimes responsible for certain vital functions of the protein. For SpoIIIL, it is not yet known whether such conserved residues or domains exist in its protein sequence. To identify the important domains and conserved residues in SpoIIIL, I will compare SpoIIIL's amino acid sequence with orthologs from other bacilli and other spore-forming Firmicutes or distant relatives using sequence alignment tools such as the META server, HHPred, PSI-PRED, MODELLER[106–110]. I will then perform site-directed mutagenesis to introduce point mutations

in the genetic sequence of SpoIIIL (in the context of SpoIIIL-His6), that will replace one or more highly-conserved amino acids with an alanine. Afterwards, I will then conduct sporulation efficiency assays, σ^G activity assays and spore size/shape assays on these mutants, as explained above in Aim 1, to investigate the importance of these mutations and whether the mutations affect the function of SpoIIIL.

1.5.4 Aim 4: Identify SpoIIIL protein-protein interaction partners

Proteins rarely function in isolation. To identify SpoIIIL's protein-protein interaction partners, I will perform protein pull-down assays by using SpoIIIL-GFP/His6 as the bait. For the pull-down assays, cell lysates obtained from sporulating cells will be incubated with GFP/His6 -antibody coupled resin, washed in buffers, and bound proteins will be eluted and visualized on SDS-PAGE gels. The eluted proteins will then be identified by mass spectrometry (at UTS, in collaboration with Matt Padula).

To determine the functional significance of SpoIIIL protein interactions identified by pull-down assays, double mutants of potential interacting partners with *spoIIIL* will be generated and characterized through sporulation efficiency assays, complementation assays, and fluorescence microscopy to quantify their effects on spore shape and σ^G activity.

1.6 Project Significance

By understanding the function of SpoIIIL in the A–Q complex during spore development, we will be able to understand more about the function of the poorly-characterized and mysterious A-Q complex, and potentially reveal connections between SpoIIIL and other processes occurring during sporulation. Thus, by understanding the molecular function of SpoIIIL, and how it participates in other biological processes, we can begin to reveal the complexity of how bacteria build spores. More broadly, this project may reveal new weaknesses in the sporulation program that may aid in developing ways to prevent sporulation in disease-causing spore-formers.

Materials and Methods

2.1 Chemicals, reagents and solutions

The chemicals and antibodies employed in this study are listed in Table 2.1. The buffers and solutions used throughout this work are listed in Table 2.2.

Table 2.1: Routine chemicals and reagents

Reagents	Source	Identifier
Antibodies		
THE^{TM} His Tag Antibody, mAb, Mouse	GenScript	Cat#A00186
anti-FtsZ	(Hajduk et al., 2019)	N/A
anti-SpoIIIAG	(Doan et al., 2009)	N/A
Chemicals		
FM4-64	Thermo Fisher Scientific	Cat#T13320
TMA-DPH	Thermo Fisher Scientific	Cat#T204
X-Gal	Invitrogen Life Technologies	Cat#15520-034

Table 2.2: Routine Buffer and solutions

Buffers / Solutions	Constituents*
PBS	137 mM NaCl, 2.7 mM KCl, 10.1 mM Na_2HPO4, 1.8 mM KH_2PO_4; pH 7
Lysis buffer (DNA extraction)	20 mM Tris pH 7.5, 50 mM EDTA, 100 mM NaCl
1X SMM	1 M sucrose, 40 mM maleic acid, 40 mM $MgCl_2.6H_2O$, pH 6.5
Lysis buffer (SDS-PAGE)	20 mM Tris pH 7.5, 10 mM EDTA, 1 mg/mL lysozyme, 1 mM PMSF, 10 µg/mL DNAse I, 100 µg/mL RNase A
Sample Buffer (2X)	4% SDS, 250 mM Tris pH 6.8, 20% glycerol, 10mM EDTA, BPB (40 µl of 1% stock)
SDS running buffer (10X)	0.2 M Tris base, 1.5 M Glycine, 35 mM SDS
Western transfer buffer	20 mM tris base, 0.15 M glycine, 3.5 mM SDS, 20% MeOH (v/v)
SDS-PAGE loading buffer	62.5 mM Tris-HCl pH 6.8, 10% (v/v) glycerol, 5% (v/v) 2-mercaptoethanol, 2% (w/v) SDS, 0.1% bromophenol blue; pH 8.5

Hypotonic buffer	20 mM Hepes 8 (Na+), 200 mM NaCl, 1 mM DTT, 1 mM $MgCl_2$, 1 mM $CaCl_2$, 1 mM PMSF, 0.5 µg/mL leupeptin, 0.7 µg/mL pepstatin A; pH 8
G2 buffer	20 % (w/v) glycerol, 20 mM HEPES, 200 mM NaCl, 1 mM DTT, 1 mM PMSF, 0.5 µg/mL leupeptin, 0.7 µg/mL pepstatin A; pH 8
Elution buffer	2 % (w/v) SDS, 125 mM Tris-HCl; pH 6.8
TBE	89 mM Tris-HCl, 89 mM boric acid, 2.5 mM EDTA, pH 8.3

*the solutions listed here used (1X), unless specified otherwise.

2.2 *Bacillus subtilis* strains

The *Bacillus subtilis* strains employed in this work were all obtained from strain 168 or PY79[15,111] as well as in the Rodrigues lab and are listed in Table 2.3 below.

Table 2.3: *Bacillus subtilis* strains

Strains	Genotype*	Source
bDR2413 (168)	wild-type	[15]
bPO001	*yqzE::erm*	bCR1236
bPO002	*yycR::PsspB-rbsopt-cfp (phleo), spoIIIL::erm*	This study
bPO003	*yycR::PsspB-rbsopt-cfp (phleo), spoIIIAH::spec, spoIIIL::erm*	This study
bPO004	*amyE::PspoIIQ-cfp(Bs) (cat), spoIIIL::erm*	This study
bPO005	*amyE::PspoIIQ-cfp(Bs) (cat), spoIIIL::erm, spoIIIAH (spec)*	This study
bPO006	*yhcN::kan*	This study
bPO007	*amyE::PspoIIQ-yfp (JF)(cat)*	This study
bPO008	*yycR::PsspB-rbsopt-cfp (phleo), amyE::PspoIIQ-yfp (JF)(cat)*	This study
bPO009	*yycR::PsspB-rbsopt-cfp (phleo), spoIIIAH (spec), amyE::PspoIIQ-yfp (JF)(cat)*	This study
bPO010	*yycR::PsspB-rbsopt-cfp (phleo), spoIIIL::erm, amyE::PspoIIQ-yfp (JF)(cat)*	This study
bPO011	*yycR::PsspB-rbsopt-cfp (phleo), spoIIIAH::spec, spoIIIL::erm, amyE::PspoIIQ-yfp (JF)(cat)*	This study
bPO012	*pbpf::kan, spoIIIL::erm*	This study
bPO013	*ywnB::kan, spoIIIL::erm*	This study
bPO014	*yydJ::kan, spoIIIL::erm*	This study
bPO015	*yydI::kan, spoIIIL:::erm*	This study
bPO016	*acuC::kan, spoIIIL::erm*	This study
bPO017	*apt::kan, spoIIIL::erm*	This study
bPO018	*rocR::kan, spoIIIL::erm*	This study
bPO019	*spsD::kan, spoIIIL::erm*	This study
bPO020	*ydhC::kan, spoIIIL::erm*	This study
bPO021	*tenI::kan, spoIIIL::erm*	This study

bPO022	*glpD::kan, spoIIIL::erm*	This study
bPO023	*adcC::kan, spoIIIL::erm*	This study
bPO024	*fbp::kan, spoIIIL::erm*	This study
bPO025	*mcsB::kan, spoIIIL::erm*	This study
bPO026	*engD::kan, spoIIIL::erm or yyaF::kan, spoIIIL::erm*	This study
bPO027	*ytvI::kan, spoIIIL::erm*	This study
bPO028	*thiD::kan, spoIIIL::erm, or yjbV::kan, spoIIIL::erm*	This study
bPO029	*yhcN::kan, spoIIIL::erm*	This study
bPO030	*yqzE::erm*	This study
bPO032	*spoIIIL::erm, ctpB::kan*	This study
bPO033	*spoIIIL::erm, safA::kan*	This study
bPO034	*spoIIIL::erm, ydcC::*markerless	This study
bPO035	*murAB::erm, spoIIIL::*markerless	This study
bPO036	*spoIIIL::*markerless	This study
bPO037	*spoIIIAH::kan, spoIIIL::erm*	This study
bPO038	*yhdG::Pspank-yqzE (phleo)*	This study
bPO039	*yhdG::PyqzE-yqzE (tet)*	This study
bPO040	*yhdG::Pspank-yqzE (phleo)*	This study
bPO041	*yhdG::PyqzE-yqzE (tet)*	This study
bPO042	*yhdG::Pspank-yqzE (phleo), spoIIIAH::kan, spoIIIL::erm*	This study
bPO043	*yhdG::PyqzE-yqzE (tet), spoIIIAH::kan, spoIIIL::erm*	This study
bPO044	*yhdG::Pspank-yqzE (phleo), spoIIIL::erm*	This study
bPO045	*yhdG::PyqzE-yqzE (tet), spoIIIL::erm*	This study
bPO046	*yhdG::PsspB-rbsopt-yfp (tet), amyE::PspoIIQ-cfp (BS)(cat)*	This study
bPO047	*yhdG::PsspB-rbsopt-yfp (tet), amyE::PspoIIQ-cfp (BS)(cat), spoIIIAH (spec)*	This study
bPO048	*spoIIIL::erm, yhdG::PsspB-rbsopt-yfp (tet), amyE::PspoIIQ-cfp (BS)(cat)*	This study
bPO049	*yhdG::PsspB-rbsopt-yfp (tet), amyE::PspoIIQ-cfp (BS)(cat), spoIIIAH::spec, spoIIIL::erm*	This study
bPO050	*yhdG::PsspB-optRBS-yfp(tet)*	This study
bPO051	*sigG::neo*	This study
bPO052	*sigG::neo, yhdG::PsspB-optRBS-yfp (tet)*	This study
bPO053	*SpoIIIL::erm, spoIIB::cat*	This study
bPO054	*SpoIIIL::*markerless*, gerM::erm*	This study
bPO055	*spoIIIAG::erm*	This study
bPO056	*yhdG::PspoIIIA(2)-spoIIIAG (K223E) (kan)*	This study
bPO057	*yhdG::PspoIIIA(2)-spoIIIAG (K223E) (kan)*	This study
bPO058	*spoIIIAG::erm, yhdG::PspoIIIA(2)-spoIIIAG (K223E) (kan)]168*	This study
bPO059	*yhdG::PspoIIIA(2)-spoIIIAG (K223E) (kan), spoIIIAG::*markerless	This study
bPO060	*spoIIIL::erm, yhdG::PspoIIIA(2)-spoIIIAG (K223E) (kan), spoIIIAG::*markerless	This study
bPO061	*gerM::erm*	This study
bPO062	*yhdG::spec, spoIIIL::erm*	This study
bPO063	*yhdG::PsspB-optRBS-yfp (tet), SpoIIIL::erm*	This study
bPO064	*yhdG::PsspB-optRBS-yfp (tet), SpoIIB::cat*	This study

bPO065	*yhdG::PsspB-optRBS-yfp (tet), SpoIIIL::erm, spoIIB::cat*	This study
bPO066	*yhdG::PsspB-optRBS-yfp (tet), SpoIIIL::*markerless*, gerM::erm*	This study
bPO067	*ycgO::PsspB-optRBS-yfp(spec), spoIIIAG::*markerless*, yhdG::PspoIIIA(2)-spoIIIAG (K223E) (kan)*	This study
bPO068	*ycgO::PsspB-optRBS-yfp(spec), spoIIIL::erm, spoIIIAG::*markerless*, yhdG::PspoIIIA(2)-spoIIIAG (K223E) (kan)*	This study
bPO069	*yhdG::PsspB-optRBS-yfp (tet), gerM::erm*	This study
bPO070	*amyE::PspoIIQ-cfp(Bs) (cat), yhdG::PsspB-optRBS-yfp (tet), SpoIIIL::erm*	This study
bPO071	*amyE::PspoIIQ-cfp(Bs) (cat), yhdG::PsspB-optRBS-yfp(tet), gerM(erm)*	This study
bPO072	*amyE::PspoIIQ-cfp(Bs) (cat), yhdG::PsspB-optRBS-yfp (tet), SpoIIIL::*markerless*, gerM::erm*	This study
bPO073	*amyE::PspoIIQ-optRBS-cfp (kan), yhdG::PsspB-optRBS-yfp(tet)*	This study
bPO074	*amyE::PspoIIQ-optRBS-cfp (kan), yhdG::PsspB-optRBS-yfp (tet), SpoIIIL::erm*	This study
bPO075	*amyE::PspoIIQ-optRBS-cfp (kan), yhdG::PsspB-optRBS-yfp (tet), SpoIIB::cat*	This study
bPO076	*amyE::PspoIIQ-optRBS-cfp (kan), yhdG::PsspB-optRBS-yfp (tet), SpoIIIL::erm, spoIIB::cat*	This study
bPO077	*ycgO::PsspB-optRBS-yfp(spec)*	This study
bPO078	*amyE::PspoIIQ-cfp(Bs) (cat), ycgO::PsspB-optRBS-yfp(spec)*	This study
bPO079	*SpoIIIL::erm, amyE::PspoIIQ-cfp(Bs) (cat), ycgO::PsspB-optRBS-yfp(spec)*	This study
bPO080	*amyE::PspoIIQ-cfp(Bs)(cat), ycgO::PsspB-optRBS-yfp(spec), spoIIIAG::*markerless*, yhdG::PspoIIIA(2)-spoIIIAG (K223E) (kan)*	This study
bPO081	*amyE::PspoIIQ-cfp(Bs) (cat), ycgO::PsspB-optRBS-yfp(spec), spoIIIL::erm, spoIIIAG::*markerless*, yhdG::PspoIIIA(2)-spoIIIAG (K223E) (kan)*	This study
bPO082	*yhdG::PspoIIIL-spoIIIL-His6(tet), spoIIIL::erm*	This study
bPO083	*yhdG::PspoIIIL-spoIIIL-sfGFP(cat), spoIIIL::erm*	This study
bPO084	*yhdG::PspoIIIL-spoIIIL-mCherry(cat), spoIIIL::erm*	This study
bPO085	*spoIIQ::tet, yhdG::PspoIIIL-spoIIIL-sfGFP(cat), spoIIIL::erm*	This study
bPO086	*pbpF::kan, yhdG::PsspB-optRBS-yfp(tet), amyE::PspoIIQ-cfp (BS)(cat)*	This study
bPO087	*pbpF::kan, spoIIIL::erm, yhdG::PsspB-optRBS-yfp(tet), amyE::PspoIIQ-cfp (BS)(cat)*	This study
bPO088	*spsD::kan. yhdG::PsspB-optRBS-yfp(tet), amyE::PspoIIQ-cfp (BS)(cat)*	This study
bPO089	*spsD::kan, spoIIIL::erm, yhdG::PsspB-optRBS-yfp(tet), amyE::PspoIIQ-cfp (BS)(cat)*	This study
bPO090	*mcsB::kan, yhdG::PsspB-optRBS-yfp(tet), amyE::PspoIIQ-cfp (BS)(cat)*	This study
bPO091	*mcsB::kan, spoIIIL::erm, yhdG::PsspB-optRBS-yfp(tet), amyE::PspoIIQ-cfp (BS)(cat)*	This study

bPO092	*thiD::kan, yhdG::PsspB-optRBS-yfp(tet), amyE::PspoIIQ-cfp(BS)(cat)*	This study
bPO093	*thiD::kan, spoIIIL::erm, yhdG::PsspB-optRBS-yfp(tet), amyE::PspoIIQ-cfp (BS)(cat)*	This study
bPO094	*ctpB::kan, yhdG::PsspB-optRBS-yfp(tet), amyE::PspoIIQ-cfp(BS)(cat)*	This study
bPO095	*ctpB::kan, spoIIIL::erm, yhdG::PsspB-optRBS-yfp(tet), amyE::PspoIIQ-cfp (BS)(cat)*	This study
bPO096	*ydcC::erm, yhdG::PsspB-optRBS-yfp(tet), amyE::PspoIIQ-cfp(BS)(cat)*	This study
bPO097	*yhdG::PsspB-opt-RBS-yfp(tet), spoIIIL::erm, ydcC::markerless*	This study
bPO098	*amyE::PspoIIQ-cfp(Bs) (cat), yhdG::PsspB-opt-RBS-yfp(tet), spoIIIL::erm, ydcC::*markerless	This study
bPO099	*murAB::erm, yhdG::PsspB-optRBS-yfp(tet), amyE::PspoIIQ-cfp(BS)(cat)*	This study
bPO100	*yhdG::PsspB-optRBS-yfp(tet), murAB::erm, spoIIIL::*markerless	This study
bPO101	*amyE::PspoIIQ-cfp(Bs)(cat), yhdG::PsspB-optRBS-yfp(tet), murAB::erm, spoIIIL::*markerless	This study
bPO102	*spoIIQ::tet*	This study
bPO103	*sacA::PspoIIQ-cfp-spoIIQ (spec), spoIIQ::tet*	This study
bPO104	*sacA::PspoIIQ-cfp-spoIIQ (spec)*	This study
bPO105	*spoIIIL::erm, sacA::PspoIIQ-cfp-spoIIQ (spec), spoIIQ::tet*	This study
bPO106	*yhdG::PspoIIIL-spoIIIL-mCherry(cat), spoIIIL::erm, sacA::PspoIIQ-cfp-spoIIQ (spec), spoIIQ::tet*	This study
bPO107	*spoIIQ::cat, yhdG::PspoIIIL-spoIIIL-His6(tet), spoIIIL::erm*	This study
bPO108	*amyE::PspoIIQ-cfp(Bs) (cat), sacA::PspoIIQ-optRBS-malF (TM1,2)-yfp (spec)*	This study
bPO109	*sacA::PspoIIQ-optRBS-malF (TM1,2)-yfp (spec), amyE::PspoIIQ-cfp(Bs)(cat), yunB::tet*	This study
bPO110	*sacA::PspoIIQ-optRBS-malF (TM1,2)-yfp (spec), amyE::PspoIIQ-cfp(Bs)(cat), spoIIIL::erm*	This study
bPO111	*spoIIIL(erm), sacA::PspoIIQ-optRBS-malF (TM1,2)-yfp (spec), amyE::PspoIIQ-cfp(Bs) (cat), yunB::tet*	This study
bPO112	*spoIIIL::erm, cotEΩcotE-gfp (spec)*	This study
bPO113	*spoIII::erm, spoVIDΩspoVID-gfp (spec)*	This study
bPO114	*spoIIIL::erm, ycgO::PsafA-safA-mYPET (spec)*	This study
bPO115	*spoIIIL::erm, spoVMΩspoVM-gfp (spec)*	This study
bPO116	*spoIIIL::erm, ycgO::PspoIVA-mYPET-spoIVA (cat)*	This study
bPO117	*pbpF::kan, spoIIIL::erm, cotEΩcotE-gfp(spec)*	This study
bPO118	*pbpF::kan, spoIII::erm, spoVIDΩspoVID-gfp (spec)*	This study
bPO119	*pbpF::kan, spoIIIL::erm, ycgO::PsafA-safA-mYPET (spec)*	This study
bPO120	*pbpF::kan, spoIIIL::erm, spoVMΩspoVM-gfp (spec)*	This study
bPO121	*pbpF::kan, spoIIIL::erm, ycgO::PspoIVA-mYPET-spoIVA (cat)*	This study
bPO122	*cotEΩcotE-gfp (spec), spoIIIL::erm, ydcC::*markerless	This study
bPO123	*spoVIDΩspoVID-gfp (spec), spoIIIL::erm, ydcC::*markerless	This study
bPO124	*ycgO::PsafA-safA-mYPET (spec), spoIIIL::erm, ydcC::*markerless	This study

bPO125	*ycgO::PspoIVA-mYPET-spoIVA (cat), spoIIIL::erm, ydcC::*markerless	This study
bPO126	*spoVMΩspoVM-gfp (spec), spoIIIL::erm, ydcC::*markerless	This study
bPO127	*cotEΩcotE-gfp (spec), spoIIIL::*markerless*, gerM::erm*	This study
bPO128	*spoVIDΩspoVID-gfp (spec), spoIIIL::*markerless*, gerM::erm*	This study
bPO129	*ycgO::PsafA-safA-mYPET (spec), SpoIIIL::*markerless*, gerM::erm*	This study
bPO130	*ycgO::PspoIVA-mYPET-spoIVA(cat), spoIIIL::*markerless*, gerM::erm*	This study
bPO131	*spoVMΩspoVM-gfp (spec), spoIIIL::*markerless*, gerM::erm*	This study
bPO132	*ycgO::PydcC-optRBS-sGFP(15aa)-ydcC (spec), spoIIIL::erm, ydcC::*markerless	This study
bPO133	*safA::kan, ycgO::PydcC-optRBS-sGFP(15aa)-ydcC (spec), spoIIIL::erm, ydcC::*markerless	This study
bPO134	*spoVID::kan, ycgO::PydcC-optRBS-sGFP(15aa)-ydcC (spec), spoIIIL::erm, ydcC::*markerless	This study
bPO135	*pbpG::kan, ycgO::PydcC-optRBS-sGFP(15aa)-ydcC (spec), spoIIIL::erm, ydcC::*markerless	This study
bPO136	*safA::kan, yhdG::PsspB-rbsopt-yfp (tet), amyE::PspoIIQ-cfp (BS)(cat)*	This study
bPO137	*safA::kan, spoIIIL::erm, yhdG::PsspB-rbsopt-yfp (tet), amyE::PspoIIQ-cfp (BS)(cat)*	This study
bPO138	*cotE::kan, yhdG::PsspB-rbsopt-yfp (tet), amyE::PspoIIQ-cfp (BS)(cat)*	This study
bPO139	*cotE::kan, spoIIIL::erm, yhdG::PsspB-rbsopt-yfp(tet), amyE::PspoIIQ-cfp(BS)(cat)*	This study
bPO140	*spoIVD::kan, yhdG::PsspB-rbsopt-yfp (tet), amyE::PspoIIQ-cfp (BS)(cat)*	This study
bPO141	*spoVID::kan, spoIIIL::erm, yhdG::PsspB-rbsopt-yfp (tet), amyE::PspoIIQ-cfp (BS)(cat)*	This study
bPO142	*pbpG::kan*	This study
bPO143	*yhdG::PspoIIIL-spoIIIL-sfGFP(cat), murAB::erm, spoIIIL::*markerless	This study
bPO144	*spoVD::spec, yhdG::PspoIIIL-spoIIIL-sfGFP(cat), spoIIIL::erm*	This study
bPO145	*spoVE::kan, yhdG::PspoIIIL-spoIIIL-sfGFP(cat), spoIIIL::erm*	This study
bPO146	*spoVD::spec, spoVE::kan, yhdG::PspoIIIL-spoIIIL-sfGFP(cat), spoIIIL::erm*	This study
bPO147	*spoIII::erm, spoVD::spec, ycgO::PspoVD-mYPET-spoVD (cat)*	This study
bPO148	*spoIIIL::erm, spoVE::kan, ycgO::spoVE-mYPET (cat)*	This study
bPO149	*spoIVA::spec, yhdG::PspoIIIL-spoIIIL-sfGFP(cat), spoIIIL::erm*	This study
bPO150	*spoVID::kan, yhdG::PspoIIIL-spoIIIL-sfGFP(cat), spoIIIL::erm*	This study
bPO151	*safA::kan, yhdG::PspoIIIL-spoIIIL-sfGFP(cat), spoIIIL::erm*	This study
bPO152	*cotE::kan, yhdG::PspoIIIL-spoIIIL-sfGFP(cat), spoIIIL::erm*	This study
bPO153	*yhdG::PspoIIIL-spoIIIL-sfGFP(cat), spoIIIL::*markerless	This study
bPO154	*spoVM::erm, yhdG::PspoIIIL-spoIIIL-sfGFP(cat), spoIIIL::*markerless	This study
bPO155	*cwlD::kan, yhdG::PspoIIIL-spoIIIL-sfGFP(cat), spoIIIL::*markerless	This study

bPO156	*pdaA::kan, yhdG::PspoIIIL-spoIIIL-sfGFP(cat), spoIIIL::*markerless	This study
bPO157	*ctpB::kan, yhdG::PspoIIIL-spoIIIL-sfGFP(cat), spoIIIL::*markerless	This study
bPO158	*spoIVB::spec, yhdG::PspoIIIL-spoIIIL-sfGFP(cat), spoIIIL::*markerless	This study
bPO159	*spoIVCB::kan, yhdG::PspoIIIL-spoIIIL-sfGFP(cat), spoIIIL::*markerless	This study
bPO160	*LonB::cat*	This study
bPO161	*LonB::kan, yhdG::PspoIIIL-spoIIIL-sfGFP(cat), spoIIIL::*markerless	This study
bPO162	*LonB::kan*	This study
bPO163	*spoVD::spec, yhdG::PsspB-rbsopt-yfp (tet), amyE::PspoIIQ-cfp (BS)(cat)*	This study
bPO164	*spoVE::kan, spoVD::spec, yhdG::PsspB-rbsopt-yfp (tet), amyE::PspoIIQ-cfp (BS)(cat)*	This study
bPO165	*cwlD::kan*	This study
bPO166	*cwlD::*markerless	This study
bPO167	*pdaA::kan, cwlD::*markerless	This study
bPO168	*spoIIIL::erm, pdaA::kan, cwlD::*markerless	This study
bPO169	*yhdG::PspoIIIL-spoIIIL-sfGFP(cat), spoIIIL::erm, pdaA::kan, cwlD::*markerless	This study
bPO170	*murAB::erm, cwlD::*markerless	This study
bPO171	*murAB::markerless, cwlD::*markerless	This study
bPO172	*spoIIIL::erm, murAB::markerless, cwlD::*markerless	This study
bPO173	*pdaA::kan, spoIIIL::erm, murAB::markerless, cwlD::*markerless	This study
bPO174	*yhdG::PspoIIIL-spoIIIL-sfGFP(cat), pdaA::kan, spoIIIL::erm, murAB::markerless, cwlD::*markerless	This study
bPO175	*sigG::neo, yhdG::PspoIIIL-spoIIIL-sfGFP(cat), spoIIIL::markerless*	This study
bPO176	*pbpG::kan, yhdG::PspoIIIL-spoIIIL-sfGFP(cat), spoIIIL::*markerless	This study
bPO177	*pbpF::kan, yhdG::PspoIIIL-spoIIIL-sfGFP(cat), spoIIIL::*markerless	This study
bPO178	*spoIIIL::erm, pbpG::kan, pbpF::*markerless	This study
bPO179	*yhdG::PspoIIIL-spoIIIL-sfGFP(cat), spoIIIL::erm, pbpG::kan, pbpF::*markerless	This study
bPO180	*yhdG::PspoIIIL-spoIIIL-sfGFP(cat), spoIIIL::erm, ydcC::*markerless	This study
bPO181	*spsD::kan, yhdG::PspoIIIL-spoIIIL-sfGFP(cat), spoIIIL::erm*	This study
bPO182	*mcsB::kan, yhdG::PspoIIIL-spoIIIL-sfGFP(cat), spoIIIL::erm*	This study
bPO183	*thiD:kan, yhdG::PspoIIIL-spoIIIL-sfGFP(cat), spoIIIL::erm*	This study
bPO184	*yhdG::PxylA-gfp (tet)*	This study
bPO185	*yhdG::spec*	This study
bPO186	*ycgO::cat*	This study
bPO187	*spoIIIL::erm, yhdG::PspoIIIL-spoIIIL-gfp (N4A) (cat)*	This study
bPO188	*spoIIIL::erm, yhdG::PspoIIIL-spoIIIL-gfp (D5A) (cat)*	This study
bPO189	*spoIIIL::erm, yhdG::PspoIIIL-spoIIIL-gfp (Y6A) (cat)*	This study
bPO190	*spoIIIL::erm, yhdG::PspoIIIL-spoIIIL-gfp (K8A) (cat)*	This study
bPO191	*spoIIIL::erm, yhdG::PspoIIIL-spoIIIL-gfp (T11A) (cat)*	This study
bPO192	*spoIIIL::erm, yhdG::PspoIIIL-spoIIIL-gfp (R25A) (cat)*	This study
bPO193	*spoIIIL::erm, yhdG::PspoIIIL-spoIIIL-gfp (P38A) (cat)*	This study
bPO194	*spoIIIL::erm, yhdG::PspoIIIL-spoIIIL-gfp (F44A) (cat)*	This study

bPO195	*spoIIIL::erm, yhdG::PspoIIIL-spoIIIL-gfp (G45A) (cat)*	This study
bPO196	*spoIIIL::erm, yhdG::PspoIIIL-spoIIIL-gfp (P48A) (cat)*	This study
bPO197	*slp::kan*	This study
bPO198	*wprA::kan*	This study
bPO199	*yybT::kan*	This study
bPO200	*lacA::spoIVB(S378A) (tet)*	This study
bPO201	*lacA::spoIVB(S378A) (tet), spoIVB::spec, yhdG::PspoIIIL-spoIIIL-sfGFP(cat), spoIIIL::*markerless	This study
bPO202	*yhdG::PspoIVB-spoIVB-sfgfp (cat)*	This study
bPO203	*yhdG::PspoIVB-spoIVB(S378A)-sfgfp (cat)*	This study
bPO204	*spoIVB::spec, yhdG::PspoIVB-spoIVB(S378A)-sfgfp (cat)*	This study
bPO205	*yhdG::PspoIVB-spoIVB-sfgfp (cat), spoIVB::spec, spoIIIL::erm*	This study
bPO206	*yhdG::PspoIVB-spoIVB(S378A)-sfgfp (cat), spoIVB::spec, spoIIIL::erm*	This study
bPO207	*slp::kan, spoIIIL::erm*	This study
bPO208	*wprA::kan, spoIIIL::erm*	This study
bPO209	*yybT::kan, spoIIIL::erm*	This study
bPO210	*slp::kan, yhdG::PspoIIIL-spoIIIL-sfGFP(cat), spoIIIL::erm*	This study
bPO211	*wprA::kan,yhdG::PspoIIIL-spoIIIL-sfGFP(cat), spoIIIL::erm*	This study
bPO212	*yybT::kan, yhdG::PspoIIIL-spoIIIL-sfGFP(cat), spoIIIL::erm*	This study
bPO215	*yhdG::PspoIIIL-sfGFP-spoIIIL(cat), spoIIIL::erm [isolate B]*	This study
bPO216	*yhdG::PspoIIIL-sfGFP-spoIIIL(cat) [isolate B]*	This study
bPO217	*spoIIQ::tet, yhdG::PspoIIIL-sfGFP-spoIIIL(cat), spoIIIL::erm*	This study

*Antibiotic resistance genes are labelled as the following: erm, Erythromycin; cat, Chloramphenicol; kan, Kanamycin; neo, neomycin; phleo, Phleomycin; spec, spectinomycin and tet, Tetracycline. The antibiotic cassettes in some strains were looped out using the Cre/lox system leaving the lox72 site [112].

2.3 *Bacillus subtilis* growth media

Vegetative cells (except wild-type) were grown on Luria-Bertani broth (LB) (Lennox) agar plates (1.5% w/v) with antibiotics to select for the growth of strains harbouring antibiotic resistance cassettes. The antibiotics were used for strain selection, as listed in Table 2.4. B. subtilis strains were stored as 1.8 mL glycerol stocks (14% v/v) at –80°C. Sporulation was performed using either exhaustion or resuspension method (see section 2.9).

In the exhaustion method wherein nutrients in the medium are gradually used up over time before the cells start sporulating, the cells were cultivated in Difco Sporulation Medium (DSM) that was prepared as detailed previously[104], whereas the resuspension method involved growing the cells in a nutrient deficient Resuspension Medium as described previously[113,114] thereby forcing the cells to immediately enter into sporulation upon inoculation.

Table 2.4: Antibiotics used for selecting *Bacillus subtilis*

Antibiotic	Working concentration (µg/mL)*
Ampicillin	100
Chloramphenicol	5
Erythromycin	1
Kanamycin	10
Neomycin	2.5
Phleomycin	2
Spectinomycin	100
Tetracycline	10

*Stock solutions were prepared by dissolving antibiotics either in ethanol or purified, deionised water (Milli-Q water, MQW) and sterilized by filtration (0.2 µm filter). All antibiotics were stored at –20°C.

2.4 Sporulation efficiency (Heat-kill) Assay

The sporulation efficiency (heat-kill) assay calculates sporulation efficiency in 24-36 h cultures by determining the number of heat-resistant (80°C for 20 min) colony forming units (CFUs) of any strain in comparison to the number of wild-type heat-resistant CFUs. Sporulation was induced by resuspension at 37°C based on the Sterlini-Mandelstam method or via the exhaustion of nutrients usually in the supplemented Difco Sporulation Medium (DSM)[104]. Usually, a single colony was inoculated into a glass tube containing 2 mL of DSM media and incubated at 37^{O}C on a roller drum for 24‑30 hours (hrs). After 24 h (T24) or 30 h (T30), the cultures were serially diluted in 1X TBase Medium, and exposed to heat treatment at 80°C for 20 minutes in a water bath in order to kill off any residual non-sporulating cells and allow for the selection of only the surviving heat-resistant spores which will subsequently be plated on nutrient rich media (like LB Lennox agar plates) and incubated overnight at 37°C. The number of heat-resistant spores obtained were then quantified by counting the number of colony-forming units per ml of culture (cfu/ml) for each strain assayed. Sporulation efficiency of any mutant strain was determined as the percentage of spores produced relative to the wild-type.

2.5 Transformation and storage of B. subtilis strains

In this study, *B. subtilis* strains were usually generated by transformation to integrate specific genetic material, genomic DNA or plasmid vectors harbouring an antibiotic resistance gene,

into the genome via homologous recombination[115]. The desired genetic material was selected on Lennox LB agar plates which always contained the antibiotic of interest. The process of transformation involves the following multiple steps:

A) A single colony from the recipient strain was resuspended in 1 mL solution of 1X MC medium [900 µL ddH_2O, 100 µL 10X MC medium[116], 10 µL tryptophan (2 mg/mL), 3 µL 1 M $MgSO_4$] for 4 hrs on a roller drum at 37°C until the early stationary phase in order to induce competence[117].

B) 2 µL of genomic DNA (gDNA) from the donor strain or plasmid DNA were innoculated into 200 µL of the above competent cell culture and then incubated for 2 hrs on a roller drum at 37 °C.

C) The 200 µL culture from the step above was plated onto LB (Lennox) agar plates containing the antibiotic used to select the gene of interest and incubated overnight at 37°C.

D) On the following day, the antibiotic-resistant colonies were re-streaked on LB (Lennox) agar plates containing the initial antibiotic marker to confirm the successful uptake of the donor genetic material and screened for pre-existing antibiotic marker(s) of the recipient strain, if any, by streaking on plates containing antibiotics and incubated overnight at 37°C.

E) Finally, a single colony that acquired the resistance to all expected antibiotic markers (donor and recipient) was cultured in 2 mL LB (Lennox) for 2.5 hrs on a roller drum at 37°C and stored as 1.8 mL glycerol stocks (14% v/v) at -80 °C for further use. The deletion mutant strains were either derived from the *Bacillus* knock-out collection (Addgene)[118], or from pre-existing *B. subtilis* strains found in the Rodrigues laboratory collections, using the above transformation approach.

2.6 Genomic DNA extraction

To obtain genomic DNA, a standard phenol/chloroform extraction protocol was used. Usually, a fresh single colony of the strain of interest was cultured in 2 mL LB broth (Lennox) for 3 hrs on a roller drum or rotating incubator at 37°C, until mid-exponential phase. Next, ~1.5 – 4.5 mL of the culture was pelleted by centrifugation on a bench-top centrifuge (11,000 rpm for 1 min), after which the cell pellet was resuspended in 500 µL of lysis buffer (Table 2.2), 50 µL of lysozyme (20 mg/mL) added to the mix, and incubated at 37°C for 15 mins. After incubation,

60 µL of 10% (w/v) sarkosyl detergent was added to complete cell lysis and membrane solubilization. Then, 600 µL of phenol was added, the mixture vigorously vortexed for 10 seconds and then centrifuged for 5 mins at 11,000 rpm in order to separate the aqueous and organic phases of the mixture. The top aqueous phase was pipetted out of the mixture into a fresh tube and 600 µL of 1:1 phenolchloroform mixture was added, and vortexed. The mixture was centrifuged as described above and then the top aqueous layer was moved into a fresh tube (usually 1.5 ml Eppendorf cup), to which 60 µL of 3 M NaOAc was added to facilitate DNA precipitation. In order to precipitate the gDNA into a pellet, 1 mL of 100% ethanol was added to the mix and the tube was gentle inverted several times, followed by centrifugation (11,000 rpm for 1 min). Following precipitation of the gDNA, the supernatant was discarded, and the gDNA pellet was re-solubilized in 500 µL of ddH_2O and stored at -20°C for subsequent use in the lab.

2.7 General molecular biology methods

In this study, the DNA fragments were cloned into ectopic-integration, double cross-over plasmid vectors using standard molecular biology approaches as described below.

2.7.1 Polymerase chain reaction

Polymerase Chain Reaction (PCR) was employed to amplify DNA fragments (inserts), utilized for cloning into plasmid vectors, confirmation of *B. subtilis* mutants and isothermal assembly. The final volume of the PCR reaction was set to 25 µL and was comprised of 10.5 µL of ddH2O, 1 µL of template DNA (either plasmid or *B. subtilis* genomic DNA), 0.5 µL of each primer (10 µM) (listed in Table 2.5) and 12.5 µL of 2X PCR mix (from pre-existing stock in the Rodrigues lab). The 2X PCR mix contained 2 mM nucleotides (dNTPs), Phusion DNA polymerase (2000 units/mL, New England Biolabs), and Phusion polymerase buffer (2X concentration, New England Biolabs). Usually, the PCR reaction was incubated in an Eppendorf Mastercycler Nexus Thermal Cycler and set to 30 cycles with an annealing temperature of 55°C and amplification temperature of 72°C. Based on the size of the amplified DNA fragment, the extension time was adjusted. The PCR products used in cloning or isothermal assembly were purified using the Isolate II PCR and Gel Kit manufactured by Bioline following the manufacturer's protocol. In this study, the primers employed for PCR reactions are listed in Table 2.5

Table 2.5: Primers employed for PCR

Primer	Sequence*
oPO1	TATCACATTGAAGGGGCAGGC
oPO2	CTGTTCTTATCCTTTACGGCTC
oPO3	CTATTGCTGGTAACGCTTTCAAG
oPO4	GATGAGTACCATGCTCCATTTG
oPO5	TGTCAGAGGATTCGTTTGAAGC
oPO6	AGCGCTTCAAGCACAGGTGAA
oPO7	ACGAAGTGAATATCCCGCCAT
oPO8	AGTGACGCAAACCTCGACAGT
oPO9	GCTTCGTATAGCGGTCATTAC
oPO10	GTAAAGCCTGGAATGGACGGCT
oPO11	GTGCGTGTTGTACACGTCTAC
oPO12	TCGCCTCAGTCATCTCTGAATC
oPO13	GCTGATCAGCCTGAGAAAGCA
oPO14	GATGTCAGAAAGTGTTGCGAC
oPO15	TGAAGTCATCGGATGCAGCCG
oPO16	CCACGGTTCTTTCGAAACTTTG
oPO17	CACATGGAGCTGACAGATACT
oPO18	AGACCGACTTCAACGATCGCT
oPO19	GATGTTCTGAAACAATGATACAATG
oPO20	TTTTTATTTAGTATGGTTGGGTTAACTGG
oPO21	ACATAAGGAGGAACTACTATGAGT
oPO22	CACACAGCAGACTGCTATTTCC
oPO23	cgcGAATTCatgaaaatggaatctagcaggcatgg
oPO24	gcgGGATCCttaatggtgatggtgatgatgTTTTTTCCGTTTCAGCCAAAGTCGGAAGCC
oPO25	cgcCTCGAGttttttccgtttcagccaaagtcggaagcc
oPO26	cgcGAATTCatcaacttaagagtgtcaacgg (oCR467)
oPO27	GCTCACAGAGAACAGATTGGTGGTATGGTGAAAACGAATGATTATGTTAAATATATG
oPO28	ACGGAGCTCTGCTCTTCTACCTTATTTTTTCCGTTTCAGCC

oPO29	GAGGTGATCACGTGAAAACGGCTGATTATGTTAAATATATGA
oPO30	TCATATATTTAACATAATCAGCCGTTTTCACGTGATCACCTC
oPO31	TGATCACGTGAAAACGAATGCTTATGTTAAATATATGACGC
oPO32	GCGTCATATATTTAACATAAGCATTCGTTTTCACGTGATCA
oPO33	ATCACGTGAAAACGAATGATGCTGTTAAATATATGACGCAGC
oPO34	GCTGCGTCATATATTTAACAGCATCATTCGTTTTCACGTGAT
oPO35	TGAAAACGAATGATTATGTTGCATATATGACGCAGCAATTTG
oPO36	CAAATTGCTGCGTCATATATGCAACATAATCATTCGTTTTCA
oPO37	ATGATTATGTTAAATATATGGCGCAGCAATTTGTCAAATAT
oPO38	ATATTTGACAAATTGCTGCGCCATATATTTAACATAATCAT
oPO39	TAGATACTCCGAGAGATGAGGCAAAAGAACGAAAAGAGGTGC
oPO40	GCACCTCTTTTCGTTCTTTTGCCTCATCTCTCGGAGTATCTA
oPO41	TGCGGAAAGAAACAAAAACGGCTGTTTCCCAGCAGTGGTTCG
oPO42	CGAACCACTGCTGGGAAACAGCCGTTTTTGTTTCTTTCCGCA
oPO43	CGCCTGTTTCCCAGCAGTGGGCCGGTATTTTACCCTATGGCT
oPO44	AGCCATAGGGTAAAATACCGGCCCACTGCTGGGAAACAGGCG
oPO45	TGTTTCCCAGCAGTGGTTCGCTATTTTACCCTATGGCTTCC
oPO46	GGAAGCCATAGGGTAAAATAGCGAACCACTGCTGGGAAACA
oPO47	AGCAGTGGTTCGGTATTTTAGCCTATGGCTTCCGACTTTGG
oPO48	CCAAAGTCGGAAGCCATAGGCTAAAATACCGAACCACTGCT
oPO49	TAG ATA CTC CGA GAG ATG AGG AAA AAG AAC GAA AAG AGG TGC
oPO50	GCA CCT CTT TTC GTT CTT TTT CCT CAT CTC TCG GAG TAT CTA
oPO51	GAG ATG AGC GAA AAG AAC GAG ATG AGG TGC GGA AAG AAA CAA
oPO52	TTG TTT CTT TCC GCA CCT CAT CTC GTT CTT TTC GCT CAT CTC
oPO54	ATAATCATTCGTTTTCACGTGATC
oPO55	CGTGAAAACGAATGATTATTCTAAAGGTGAAGAACTGTTC
oPO56	cgcCTCGAGgccgcttgagcctccagatgatccTTTGTAGAGCTCATCCATGCCGTGCG
oPO57	cgcCTCGAGGTGAAAACGAATGATTATG
oPO58	cgcGGATCCttaTTTTTTCCGTTTCAGCCAAAGTCGGAAGCC
oPO59	GCAATACATACTCGTTCGTTTC
oPO60	TCGCTCATTCGTTTGATGTGCC

oPO61	CTGTTTGAACTTGAGACGATTCCGGG
oPO62	GCATATGCCCAACGCTCAATG

*capital letters indicate restriction sites

2.7.2 DNA agarose gel electrophoresis

To confirm the size of a PCR product after PCR, DNA agarose gel electrophoresis was usually performed. Agarose gels (Bioline) 1% (w/v) were prepared with 0.5X TBE buffer (Table 2.2) and contained the GelRed DNA stain (1:10,000, Biotium) to enable the visualization of DNA bands. Usually, 2 µL volume of the PCR product was added to 8 µL of ddH_2O and 2 µL of 6X loading dye (New England Biolabs) for loading onto each of the agarose gel wells. The 2-Log DNA ladder (New England Biolabs) was applied to estimate the size of DNA bands. Electrophoresis of the DNA agarose gel occurred inside a Mini-Sub Cell GT chamber (Bio-Rad) at 120 V for 1 hr (Bio-Rad PowerPac Basic). Finally, the resolved gel was analyzed using the Syngene InGenius3 software.

2.7.3 Restriction digest

To digest DNA (plasmid or PCR product), the final volume of a restriction digest reaction was set to 30 µL comprising of 4 µL of DNA, 3 µL CutSmart buffer (10X concentration, New England Biolabs), 1 µL of each restriction enzyme (100,000 units/mL, New England Biolabs), and 21 µL of MQH_2O. After preparing the mixtures, the digestion reactions were incubated at 37°C for 2 hrs to allow for enzyme activity after which the digested products were run on an agarose gel as described above. Subsequently, the DNA bands were excised from the gel using a scalpel on a UV light panel and the DNA from the gel excision fragments was purified using the Isolate II PCR and Gel Kit (Bioline) based on the manufacturer's protocol.

2.7.4 Molecular cloning of plasmid vectors into *Escherichia coli*

The ligation reaction containing the insert and vector was adjusted to a final volume of 10 µL with 3 µL of insert DNA, 1 µL of vector DNA, 1 µL of T4 DNA ligase (400,000 units/mL, New England Biolabs), 1 µL of 10X T4 DNA ligase buffer (New England Biolabs), and 4 µL of ddH_2O. Also, two control reactions were prepared: a vector only control that contained ddH2O instead of the insert to check for vector self-ligation, and a vector only without ligase control where the insert and T4 DNA ligase were replaced with ddH_2O to check for undigested vector. The three ligation reactions were incubated at room temperature (RT) for 30 mins and then

incubated with 100 µL of chemically-competent E. coli cells (rubidium chloride, RbCl) (unpublished Rodrigues laboratory protocol) for 15 mins on ice. Next, the cells were heatshocked at exactly 42°C for 90 seconds to allow for uptake of ligated plasmids after which the tubes containing the heat-shocked cells were kept on ice for 5 mins. Then, 900 µL of LB broth (Lennox) was added to each tube, followed by incubation at 37°C for 20 mins. The cells were then centrifuged (11,000 rpm for 1 min) and 900 µL of the supernatant was removed. The pellet was resuspended in the remaining 100 µL of the supernatant. Alternatively, after adding 900 µl LB to each tube, incubation could be done with shaking at 37°C, 200rpm for Ihr to allow enough time for the cells to recover, and the spinning down of cells step skipped. Usually, if this alternative step is followed, then the whole cell suspension ~1000 µl could be plated on LB agar which contained ampicillin (100 µg/mL), and incubated overnight at 37°C (two plates each for the controls and the test reaction).

Finally, the resuspended cells were plated on LB agar (Lennox) plates containing ampicillin (100 µg/mL), and incubated overnight at 37°C. On the following day, 4 colonies from the plate containing the vector and insert reaction were patched on LB agar (Lennox) plates containing ampicillin (100 µg/mL) and separately inoculated into LB broth (Lennox) with ampicillin (100 µg/mL) for overnight growth on a roller drum at 37°C. The following day, plasmid extraction from the 4 cultures was performed using the Bioline Isolate II Plasmid Mini Kit according to the manufacturer's protocol and the purified plasmids digested as described above to confirm the presence of inserts. Sequencing of plasmid inserts was performed through AGRF (Australian Genome Research Facility Ltd) to ensure that the desired inserts devoid of mutations were present. E. coli isolates containing the correct insert were stored as 1.8 mL glycerol stocks (14% v/v). The plasmids generated in this study are listed in Table 2.6.

Table 2.6: Plasmids list of the generated constructs.

Plasmid	Description	Source
pPO01	yhdG::PsspB-optRBS-yfp(phleo)	This study
pPOO2	yhdG::PsspB-optRBS-yfp(tet)	This study
pPO03	yhdG::PspoIIIL-spoIIIL-His6(tet)	This study
pPO04	yhdG::PspoIIIL-spoIIIL-sfGFP(cat)	This study
pPO05	yhdG::PspoIIIL-spoIIIL-mCherry(cat)	This study

pPO06	ycgO::PsspB-optRBS-yfp(spec)	This study
pHC055	His6-SUMO-spoIIIL (amp)	This study
pPO07	yhdG::PspoIIIL-spoIIIL-mEos4b (cat)	This study
pPO08	yhdG::PspoIIIL-sfGFP-spoIIIL(cat), spoIIIL::erm	This study

2.7.5 Plasmid construction

pPO001 [*yhdG::PsspB-optRBS-yfp (phleo)*] was generated in a three-way ligation with *Eco*RI-*Xho*I PCR product containing the *PsspB* sequence/region (oligonucleotide primers oPO19 & oPO20 and 168 genomic DNA as template), *Xho*I-*Bam*HI PCR product containing *optRBS-yfp (phleo)* (oligo nucleotide primers oPO21 & oAT093 and the plasmid pJL009 as template), as well as qAT079 digested with *Eco*RI and *Bam*HI. qAT079 (*yhdG::phleo*) is an ectopic integration vector for double cross over integration at the non-essential *yhdG* locus (C. Rodrigues – laboratory stock).

pPO002 [*yhdG::PsspB-optRBS-yfp(tet)*] was generated in a two-way ligation with *Eco*RI- *Bam*HI PCR product containing the *PsspB-optRBS-yfp* gene sequence using pPO01 as template and pBB281 digested with *Eco*RI and *Bam*HI. pBB281 (*yhdG::tet*) is an ectopic integration vector for double cross over integration at the non-essential *yhdG* locus (C. Rodrigues – laboratory stock).

pPO003 [*yhdG::PspoIIIL-spoIIIL-His6(tet)*] was generated in a two-way ligation with *Eco*RI-*Bam*HI PCR product containing *yhdG::PspoIIIL-spoIIIL-His6* sequence (oligonucleotide primers oPO24 & oPO26 and the plasmid pCR218 as template) and pCR218 digested with *Eco*RI-*Bam*HI. pCR218 [*yhdG-PyqzE-yqzE(tet)*] is an ectopic integration vector for double cross over integration at the non-essential *yhdG* locus (C. Rodrigues – laboratory stock).

pPO004 [*yhdG::PspoIIIL-spoIIIL-sfGFP(cat)*] was generated in a two-way ligation with *Eco*RI-*Xho*I PCR product containing *PspoIIIL-spoIIIL* gene sequence (oligonucleotide primers oPO25 & oPO26 and the plasmid pCR218 as template) and pCR227 digested with *Eco*RI-*Xho*I. pCR227 [*yhdG-PgerM-gerM-sfGFP(cat)*] is an ectopic integration vector for double cross over integration at the non-essential *yhdG* locus (C. Rodrigues – laboratory stock).

pPO005 [*yhdG::PspoIIIL-spoIIIL-mCherry(cat)*] was generated in a two-way ligation with *Eco*RI-*Xho*I PCR product containing *PspoIIIL-spoIIIL* gene sequence (oligonucleotide primers oPO25

& oPO26 and the plasmid pCR218 as template) and pCR228 digested with *Eco*RI-*Xho*I. pCR228 [*yhdG-PgerM-gerM-mCherry(cat)*] is an ectopic integration vector for double cross over integration at the non-essential *yhdG* locus (C. Rodrigues – laboratory stock).

pPO006 [*ycgO::PsspB-optRBS-yfp(spec)*] *)*] was generated in a two-way ligation with *Eco*RI-*Bam*HI PCR product containing *PsspB-optRBS-yfp* genetic sequence (oligonucleotide primers oPO19 & oAT93 and the plasmid pPO01 as template) and qAT001(pKM083) digested with *Eco*RI-*Bam*HI. pKM083 (*ycgO::spec*) is an ectopic integration vector for double cross over integration at the non-essential *yhdG* locus (C. Rodrigues – laboratory stock).

pPO007 [*yhdG::PspoIIIL-spoIIIL-mEos4b (cat)*] was generated in a three-way ligation with *Eco*RI-*Bam*HI *PspoIIIL-spoIIIL* PCR product containing the *PspoIIIL-spoIIIL* genetic sequence (oligonucleotide primers oPO25 & oPO26 and 168 genomic DNA as template), *mEos4b* PCR product containing the *mEos4b* gene sequence (oligonucleotide primers oHC158 and oHC159 and *mEos4b* gBlock as template), and pCR228 digested with *Eco*RI-*Bam*HI.

pPO008 [*yhdG::PspoIIIL-sfGFP-spoIIIL(cat)*] was generated in a three-way ligation with *EcoRI-XhoI PCR product containing PspoIIIL-sfGFP* gene sequence (oligonucleotide primers oPO26 & oPO56 and 168 gDNA, as well as pPO04 as templates), *XhoI-Bam*HI PCR product containing *spoIIIL* gene sequence (oligonucleotide primers oPO57 & oPO58 and 168 gDNA as template), and pCR227 digested with *Eco*RI-*Bam*HI. The *EcoRI-XhoI PCR product containing PspoIIIL-sfGFP* was initially a Gibson assembly product comprising of two pieces: (a) *EcoRI-PspoIIIL-* PCR product (oligonucleotide primers oPO26 & oPO54 and 168 gDNA as template), and (b) *sfGFP-Xho*I PCR product (oligonucleotide primers oPO55 & oPO56 and pPO04 as template).

2.7.6 Enzymatic isothermal assembly

In this work, enzymatic isothermal assembly was used to join two or more DNA sequences[119]. The DNA fragments were designed to have terminal sequence overlap of ~20-25 base pairs (bp) in order to allow for covalent joining of fragments. The final volume of the isothermal assembly reaction was adjusted to 20 µL and comprised of 6 µL of ddH_2O, 2 µL of each DNA piece (plasmid or gDNA), and 10 µL of 2X Isothermal mix (unpublished, Rodrigues Laboratory protocol). The reaction was usually performed on an Eppendorf Mastercycler Nexus Thermal Cycler at 50°C for 30 mins[119] after which, DNA agarose gel electrophoresis was employed to ascertain the size of the covalently combined DNA fragments.

2.8 Transposon insertion sequencing

The *magellan6x* transposon libraries were constructed as described earlier for WT (bDR2413), and Δ*spoIIIL* formerly known as *yqzE* libraries[28,120,121]. About 750,000 transformant colonies from each library were harvested, aliquoted, and frozen. The aliquots were thawed on ice, resuspended and washed in DSM, and diluted into 50 mL DSM at an OD600 of 0.05. Samples were collected at the onset of starvation (T0) & 24 hrs later (T24), when most cells had developed into spores. The sporulating cultures (T24) samples were heat-killed at 80°C for 20 mins to eradicate any existing vegetative cells, non-mature spores and mutants that failed to develop into heat resistant spores. After the heat-kill treatment, the spores were plated on LB agar to allow for germination. About 750,000 colonies from germinated spores from each assayed time point were harvested and resuspended in LB broth (Lennox). A 30 µL aliquot of this cell suspension was used for genomic DNA extraction. Subsequently, the genomic DNA was digested with MmeI enzyme to cut the MmeI restriction site inserted at the inverted repeat sequences of the *magellan6x* transposon. Barcode adapters were ligated onto the MmeI digested DNA and the transposon-chromosome junctions were amplified in 16 cycles of PCR. Agarose gel electrophoresis was employed to separate the amplification products while the band of interest was purified and posted for sequencing on the Illumina HiSeq platform using TruSeq reagents (Tufts University, TUCF Genomics facility). The transposon insertions or reads were mapped to the chromosome of *B. subtilis* 168 (NCBI NC_000964.3) to identify sites that accepted >1 read at each TA site. Genes whose reads were statistically underrepresented were ascertained using the Mann Whitney *U* test, while genes whose reads were statistically overrepresented were identified via a sliding window Mann Whitney *U* test using a 13 TA site window size across every TA sites that registered ≥ 1 read in the control experiments. Furthermore, transposon insertion profiles were visually inspected using the Sanger Artemis Genome Browser and Annotation tool.

2.9 Microscopy techniques (Fluorescence microscopy)

For the live-cell fluorescence imaging employed in this work, , cells were usually grown in nutrient rich medium at 37°C, and transferred into nutrient poor (resuspension) medium at 37˚C (this is time-point 0; T0) to trigger sporulation of the cells according to the method of Sterlini-Mandelstam[113] described above. 200 µL of the sporulating cells were collected at certain time points after the onset of sporulation (T0), and concentrated by centrifugation

(11,000 rpm for 30 seconds) and resuspended in 10 µL of the semi-permeable membrane dye TMA-DPH (1-(4-trimethyammoniumphenyl)-6-Phenyl-1,3,5-Hexatriene *p*-toluenesulfonate) (0.05 mM) spread and fixed on 2% (w/v) agarose gel pads which were prepared with resuspension medium, and subsequently set using a (Bio-Rad) Gene Frame. Next, a coverslip (0.13-0.16 mm thickness) was used to seal the Gene Frame. Images of the fixed cells were acquired via classic epifluorescence microscopy employing a Zeiss Axioplan 2 Microscope already equipped with a 100x objective (N/A 1.4). The DAPI filter was employed to excite the TMA-DPH membrane dye usually with an exposure time of around 400 milliseconds. CFP, GFP, and YFP filters were employed with exposure times of 600, 800, and 1000 milliseconds, respectively.

2.10 Immunoblot analysis

Whole-cell lysates from sporulating cells (by resuspension) were fashioned in the Rodrigues lab as previously described[73,85,91,97]. At defined time-points, the sporulating cells were collected and pelleted by centrifugation (4000 rpm for 5 mins), after which the pellets were lysed using SDS-Lysis buffer (Table 2.2) and incubated at 37°C for 10 min after which 50 µL SDS-Sample buffer containing 10% (v/v) 2-mercaptoethanol was added. Thereafter, the samples were heated usually for 15 mins at 50°C before sample loading. Equivalent loading was based on OD_{600} at the time of harvest. Samples were separated on a 17.5% polyacrylamide gel and transferred to a Polyvinylidene fluoride (PVDF) membrane (BioRad). Membranes were usually blocked with 5% non-fat milk (Coles) with 0.5% Tween-20 for 1 hr. Blocked membranes were probed with anti-GFP (1:5000) (BioRad), anti-His (1:4000) (Genscript), anti-SpoIIIAG (1:10000)[85] or anti-FtsZ [1:30000][122] primary antibodies diluted in 1X PBS with 5% (w/v) non-fat milk and 0.05% (v/v) Tween-20 at 4°C overnight with gentle rocking. The primary antibodies were detected using horseradish-peroxidase conjugated anti-mouse or anti-rabbit antibodies (BioRad) and detected using Western Lightning ECL reagent (ChemiDoc XRS+ imaging system) (BioRad) based on the manufacturers instructions.

2.11 Protease accessibility assay

For this work, protease accessibility assays were done on sporulating cells (by resuspension) lacking the SpoIIQ (Q) protein to make sure that the membrane proteins present in the inner and outer forespore membranes would not be artificially inaccessible due to protoplast

engulfment[75,123]. 25 mL of sporulating cell culture was harvested by centrifugation (4000 rpm, for 5 mins) at 2.5 hrs after the onset of sporulation, washed, and resuspended in 2 mL 1X SMM buffer (Table 2.2) after which the cells were then protoplasted using lysozyme (5 mg/mL final concentration) for 10 mins with gentle agitation. Harvesting of the protoplasts was done by centrifugation and later resuspension in 1 mL of 1X SMM. Next, 100 µL of protoplasts were incubated with either trypsin (30 µg/mL final concentration) (Worthington), trypsin and Triton X-100 (Sigma-Aldrich, 2% final concentration), or 1X SMM for 30 mins or 60 min at 30°C. The reactions were ended by the incorporation of 100 µL 2X SDS sample buffer and incubation for 5 mins at 95 °C. ~ 5 - 10 µl from each reaction were assayed by immunoblot.

2.12 Quantification and statistical analysis

2.12.1 Sporulation Efficiency Analysis

All the obtained sporulation efficiency data are the average (± SD) of 3 biological replicates.

All obtained microscopic images were processed by adjusting the image brightness and contrast using the Fiji software[102,124]. All the quantifications were done using the manual counting tool within the Fiji software, and the raw data were then exported into Excel for the purpose of data collation and generation of graphs. The criteria described below, as well as in the results and legends, were employed to quantify each phenotype.

(a) Quantification of SpoIIIL-GFP uniform vs patchy phenotypes (Figures 3.1, 3.2, 3.3, 5.2, 5.4):

based on TMA-DPH membrane staining, any engulfed forespores showing normal uniform & regular SpoIIIL-GFP localization pattern around the forespore membrane (fluorescence signals false-coloured green) was classified as uniform localization, while any abnormal looking forespores with non-uniform, irregular, or mislocalized patterns often presenting as green fluorescent patches or zig-zag stripes in the forespore cytoplasm, are considered patchy phenotypes. The percentages of each phenotype (average frequency ± SD of 3 biological replicates) were calculated based on the total number of engulfed forespores assayed at T3.5 & T5.5. n>300 per replicate, per time-point, per strain.

(b) Quantification of phase bright vs phase dark phenotypes (Figures 4.3 & 5.7)

based on TMA-DPH membrane staining and brightfield microscopy, any forespores whose cytoplasm have become either completely or partially light gray or somewhat whitish in colour was classified as phase bright, while any forespores devoid of these light gray or

whitish cytoplasmic patterns often presenting as a completely dark cytoplasm, are considered non-phase bright or phase dark phenotypes. The percentages of each phenotype (average frequency ± SD of 2 biological replicates) were calculated based on the total number of forespores assayed at T4, T7, T9, & T30. n>400 per replicate, per time-point, per strain.

(c) Analysis of σ^F dependent P*spoIIQ*-CFP and σ^G dependent P*sspB*-YFP signal intensity for spore size & σ^G measurements respectively (Figures 3.1 & 3.2):

The MicrobeJ plugin fashioned for the Fiji software was used to detect the signal intensities of the σ^F dependent P*spoIIQ*-CFP and the σ^G dependent P*sspB*-YFP fluorescence which translated as the spore size & σ^G measurements respectively. The actual steps involved were as follows:

- Open Image J, from Plugins tab open Microbe J
- Open your CFP and YFP pictures, hovering around the Image with the Mouse, on a blank part of the Image, get the value of the background e.g 5.0
- Go to process, Subtract background, type 5.0. or use CTRL P
    - Click Preview and Sliding background for windows
- In ImageJ, goto plugins, open microbeJ. From Images tab, in MicrobeJ, goto Channels, choose yfp channel 1 and cfp channel 2 (or the other way round). Merge both pictures (using the rectangular folder-like tab on the right). Then close previous yfp and cfp images leaving only the merged image open.
- To change unit to microns after merging: In ImageJ, Goto Image, properties, in unit length delete inch, write microns. In pixel width and pixel height, type 0.064935. in voxel depth delete everything. Tick global and click okay.
- In MicrobeJ, click Images Tab, click the arrow at Im, select the image youre working on.
- In MicrobeJ, goto Bacteria, load Presets by clicking the folder at the bottom left hand side of the dialog box. Load presets.
- Once loaded, tick intensity on the right (if not ticked). Optional: Modify your preset settings to include or exclude certain cells, spores, or weird shapes.
- In MicrobeJ, In Bacteria, choose smoothed or medial.

- Click the yellow pencil at the bottom right to see the appearance of the image. The spore should look encircled in green, with a few having red circles. You can zoom in and out the image holding down CTRL, and scrolling the mouse.
- For manual editing (e.g selecting each spore, deleting, or splitting joint spores into separate spores), use the edit panel on the right of the ImageJ software.
- After manual editing, get results by clicking the coloured square at the bottom right(far end) of the MicrobeJ dialogue box. Note: Optional: To analyse only a portion of the image, from ImageJ, click the square tab. And draw out the region of interest on the merged image.
- A new dialogue box opens up, "ResultsJ 5.131(20) beta. In this new dialogue box, click bacteria. A spreadsheet opens up. In shape column, right click the + sign and click roundness (optional: or aspect ratio or area, or length).
- For results: click the save tab on the top right to save, results as .res files. Then, right click on the spreadsheet to save the table as .csv files. These .csv files are the raw data that gets displayed on the MicrobeJ results table, and are then exported into Excel for data collation, further analysis and the generation of graphs. Optional: to save presets as .xml files, in MicrobeJ, click the save button in the middle, down below on the MicrobeJ interface.

The percentages of each phenotype (average frequency ± SD of 3 biological replicates) were calculated based on the total number of forespores assayed at T2.5, T3, T3.5, T4, T4.5, & T5. n>800 per replicate, per time-point, per strain.

SpoIIIL is required for σ^G regulation, forespore morphology, and undergoes proteolysis within the forespore

3.1 Disclaimer

This is to acknowledge that Dr. Chris Rodrigues and Dr. Helena Chan oversaw the stage 1 and stage 2 assessment documents from which this Chapter derives. But Helena and Chris were not involved in compiling, editing, or reading this chapter as it is, in this thesis. Dr. Chris Rodrigues, Odika Chimezie Progress, and Ms Salwa Souka planned the experiments to make the ten different single mutations (N4A, D5A, Y6A, K8A, T11A, R25A, P38A, F44A, G45A, and P48A) in SpoIIIL ORF found in section 3.3.6. Ms Salwa Souka constructed the ten different single mutations (N4A, D5A, Y6A, K8A, T11A, R25A, P38A, F44A, G45A, and P48A) in SpoIIIL ORF, and Salwa did the first biological replicate of the heat-kills and first biological replicate of the imaging data found in section 3.3.6. Although the imaging data done by Salwa is not in this thesis. Dr. Helena Chan has contributed to the work presented in this chapter, by doing the fluorescence microscopy imaging of MalF-GFP and SpoIIIL-GFP presented in Figure 3.3.5.

3.2 Introduction to Results

As previously stated, SpoIIIL is believed to be an A-Q complex protein[28]. Here however, we present data which suggests otherwise. Furthermore, we provide certain striking findings which in addition to the findings previously published[28], also strongly suggest that SpoIIIL does actually take part in σ^G activation as previously reported[14], albeit in a manner which ensures the timely activation of σ^G. However, during this spoIIIL-mediated σ^G activation, SpoIIIL localizes uniformly on the forespore periphery and inner membrane but later undergoes some proteolytic processing resulting in a change in its localization pattern from the initial uniform peripherial localization to a subsequent patchy-like cytoplasmic localization. It is suspected that this second localization pattern of SpoIIIL which appears as patches in the forespore cytoplasm is the conformation required to interact with σ^G conferring an inhibitory effect upon σ^G (Fig 3.1 D) thereby actively ensuring the down regulation of σ^G activity. This is because we observed that the time point (T3-T4; Fig 3.3 A & D) during which the localization pattern of SpoIIIL begins to change coincides with the time point during which σ^G activity begins to decline (Fig 3.1 D) in the wild type.

3.3 Results

3.3.1 SpoIIIL is required for spore shape and the timing of σ^G activity

It has been previously reported that in the absence of SpoIIIL, the forespores appear rounder and with reduced σ^G activity, resulting in approximately 50% heat-resistant spores (relative to WT)[28]. In order to confirm and reproduce these previously reported findings quantitatively, and to re-validate these phenotypes, we utilized a dual-reporter strain containing two fluorescent reporters: P_{spoIIQ}-*cfp*, and P_{sspB}-*yfp*, under the control of forespore promoters recognized by the early and late forespore sigma factors σ^F and σ^G, respectively (Fig 3.1 A). σ^F is active in the forespore before σ^G, so σ^F-dependent CFP fluorescence serves as a proxy for identifying the forespore using image segmentation (see Materials and Methods) and measuring forespore shape (more precisely, "roundness"). The σ^G-dependent YFP fluorescence allows for quantification of σ^G activity. To compare forespore shape and σ^G activity in WT cells and the Δ*spoIIIL* mutant, we examined P_{spoIIQ}-*cfp*, and P_{sspB}-*yfp* signal during a sporulation time course. Roundness in MicrobeJ goes by the heading "**round**", and can be defined by the following equation thus: 4A/(pi*Major Axis^2), where A = area and Major Axis = the major axis of best fit ellipse which is the longest distance or length between two points on

the circumference of the object being measured (in this case, "spore") that also cuts exactly across the centre of the object[125,126]. A value of 1.0 designates perfect roundness. Therefore, forespores with values closer to 1.0 are rounder and less oblong than forespores with values closer to 0. Additionally, roundness is also the inverse of Aspect Ratio (**AR**).

In terms of forespore shape, in WT cells, consistent with previous reports[28,38,123] the developing forespore became less round (i.e. more oblong) over time and most forespores developed an oblong appearance (less roundness) at later stages of development: at T5, the average forespore roundness in WT forespores was 0.74 $\pm$ 0.076 (Fig 3.1 E). In comparison, in the Δ*spoIIIL* mutant, a majority of the developing forespores became rounder than WT overtime. At T5, the average forespore roundness in the Δ*spoIIIL* mutant was 0.82 $\pm$ 0.084 (Fig 3.1 E). Statistical analysis indicated that the forespore shape differences between WT and Δ*spoIIIL* mutant at T5 were statistically significant (P<0.05, Kolmogorov-Smirnov test). While 46.9% of WT forespore had a roundness between 0.7-0.8, only 19.6% of Δ*spoIIIL* mutant spores fell within this same range of roundness (Fig 3.1 F). Conversely, 54.4% of Δ*spoIIIL* mutant forespores had roundness values between 0.8 – 0.9 as opposed to just 16 % of WT forespores in this same range of roundness. These results confirm that SpoIIIL is indeed required for the correct formation of forespore shape.

σ^G-dependent YFP fluorescence in the Δ*spoIIIL* mutant forespores was 18.7 $\pm$ 22.2 a.u and at T5 it was 40 $\pm$ 25 a.u (Fig 3.1 D). These results suggest that while *spoIIIL* is required for the proper timing of σ^G activity it is not required for maintaining σ^G activity late into development.

To gain more insight into the relationship between σ^G activity and forespore shape, we examined σ^G activity and forespore shape at an individual cell level, utilizing scatter plots populating σ^G-dependent fluorescence against forespore roundness at T.3.5 and T4.5 (Fig 3.1 B). In WT, comparing T3.5 and T4.5, there is a shift towards forespores becoming oblong (less round) and harbouring low σ^G activity later in development. To facilitate comparisons, and given the trend of the WT population shown in Fig. 3.1B, we determined the fraction of forespores at T.4.5 that harbour σ^G fluorescence below average as well as roundness below mean average (denoted by the grey shaded area on Fig. 3.1B - roundness >= 0.75 and σ^G-dependent fluorescence <= 28.7). Mean average is similar in different strains. We considered these forespores to be over-representative of the WT phenotype in that they are more oblong

than average and harbour less σ^G activity than average: 44.9% of the WT forespores had these characteristics.

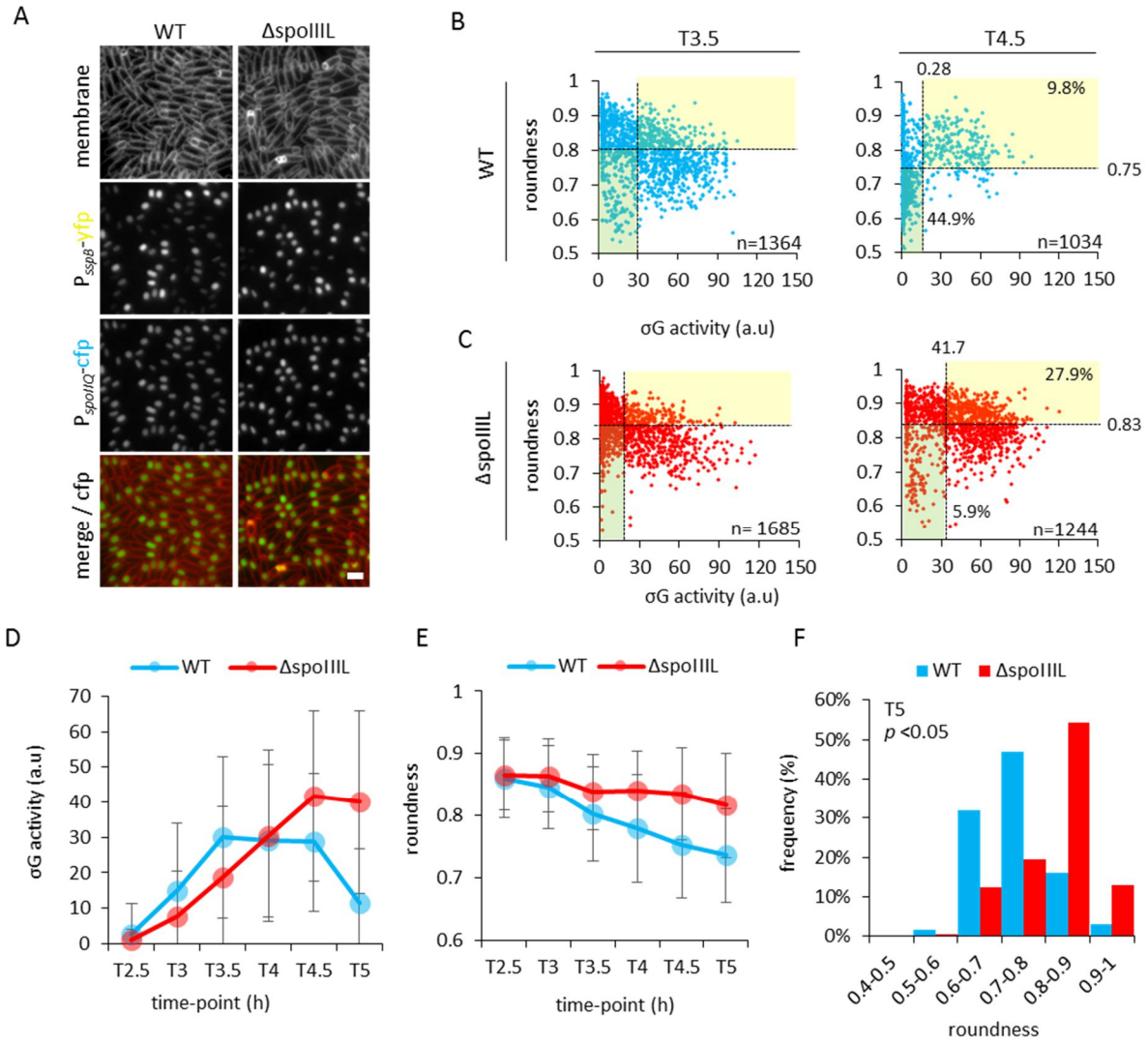

Fig 3.1 Defects of *the ΔspoIIIL* single mutant in forespore shape (roundness), and σG activity. (A) Representative fluorescence microscopy images describing two fluorescent reporters: (P*spoIIQ-cfp*, false-coloured green in merged images and P*sspB-yfp*, also false-coloured green in merged images, under the control of forespore promoters recognized by the early and late forespore sigma factors σF and σ^G respectively). Cell membranes were visualised using TMA-DPH fluorescent membrane dye and are false-coloured red in merged images. **(B)** Scatter plots populating σ^G-dependent YFP fluorescence against forespore roundness at T.3.5 and T4.5 for wild type (WT), or **(C)** for *ΔspoIIIL* strains. **(D)** σ^G activity overtime for WT and *ΔspoIIIL* strains, **(E)** forespore roundness over time for WT and *ΔspoIIIL* strains, **(F)** Frequency distribution histogram of forespore roundness for WT (blue) and *ΔspoIIIL* single mutant (red) strains at T5, n>800. Error bars for D) and E) represent standard deviation of the population.

In terms of σ^G activity, in WT cells σ^G-dependent YFP fluorescence increased overtime, peaked at T3.5 and then declined between T4 and T5 (Fig 3.1 D). At T3.5, the average σ^G-dependent fluorescence in WT forespores was 30.2 $\pm$ 25 a.u and at T5, it was 11.5 $\pm$ 15 a.u (Fig 3.1 D). Interestingly, contrary to the idea that SpoIIIL plays a role in σ^G activity, in the Δ*spoIIIL* mutant forespores σ^G-dependent YFP fluorescence increased slightly later compared to WT, and on average remained at higher levels for a longer period of time (Fig 3.1 D).

For comparison, only 5.9% of the Δ*spoIIIL* forespores were within these same WT parameters (Fig. 3.1C). Interestingly, in the Δ*spoIIIL* mutant alone, comparing T3.5 and T4.5, a number of forespores maintain their roundness and high-levels of σ^G-dependent YFP fluorescence as they develop (27.9%, green shaded area on Fig. 3.1C - corresponding to forespores with roundness >= 0.83 and σ^G-dependent fluorescence >= 41.7). For comparison, only 9.8% of the WT forespores were within these same Δ*spoIIIL* parameters (Fig. 3.1C). That the Δ*spoIIIL* mutant harbours rounder forespores with high levels of σ^G activity runs against the idea that SpoIIIL is in the A-Q complex genetic pathway, because A-Q complex mutants are characterized by low σ^G activity and rounder forespores.

Collectively, the time course and single cell data suggest that SpoIIIL may not function in the A-Q complex genetic pathway, as it retains σ^G dependent fluorescence well into development, and some of its forespores are rounder with high σ^G activity.

3.3.2 SpoIIIL does not synergize with the A-Q complex mutants in a similar manner

The above data in section 3.2.1 suggest that SpoIIIL may not function in the A-Q complex genetic pathway. To explore this possibility further, we performed synergy studies with *spoIIIL* and other A-Q complex genes because synergistic phenotypes are expected for the double mutant of *spoIIIL* and any of the A-Q complex proteins if the role of *spoIIIL* in maintaining forespore morphology as well as σ^G activity is related to the same role of the A–Q complex[123]. As discussed in the Introduction (Section 1), deletion of A-Q complex genes is known to result in decreased σ^G activity, rounder forespores and reduced sporulation efficiency. If SpoIIIL participates in the A-Q complex pathway for σ^G activity and forespore shape, as hypothesized in the literature[28], then one might expect double mutants of Δ*spoIIIL* with A-Q complex mutants to exhibit synergistic defects both in terms of σ^G activity and forespore shape. So, to test this idea, we took advantage of three A-Q complex mutants, Δ*spoIIIAH*, Δ*gerM* and

Δ*spoIIIAG** (SpoIIIAG^{K223E}, a mutant of SpoIIIAG that is defective in oligomeric ring formation and exhibits reduced sporulation efficiency, impaired σ^G activity, as well as smaller forespores)[38,41,56,80,123]. Unlike deletion of other A-Q complex genes, these mutants are partially defective in σ^G activity and forespore shape, and result in relatively mild defects in sporulation efficiency. The reported sporulation efficiency of Δ*spoIIIAH* is 5% or 3.4% [38,123] and 4.6% for Δ*gerM* [127] while Δ*spoIIIAG** produces 22.3% spores[123]. We combined these A-Q complex mutants with the Δ*spoIIIL* mutant to generate Δ*spoIIIL* Δ*spoIIIAH*, Δ*spoIIIL* Δ*gerM* and Δ*spoIIIL* Δ*spoIIIAG** in the context of the dual-reporter strain described above in section 3.2.1. With these strains we then examined sporulation efficiency at T30, as well as σ^G activity and forespore shape at T4.5, at a single cell level. As controls, we examined sporulation efficiency, σ^G activity and forespore shape in the Δ*spoIIIAH*, Δ*gerM* and SpoIIIAG* single mutants alone (otherwise WT for *spoIIIL*).

In the Δ*spoIIIAH* single mutant, consistent with previous data[28,38,67] and when compared to WT, a large proportion of the forespores (88%) were rounder and had less σ^G activity (green shaded area on Fig. 3.2 B – corresponding to forespores with σ^G-dependent YFP fluorescence <= 12.5 and roundness >= 0.74) while only about 2.8% of the forespores had the roundness and σ^G activity similar to WT (gray shaded area on Fig. 3.2 B – corresponding to forespores with σ^G-dependent YFP fluorescence <=12.5 and roundness <= 0.74). Furthermore, consistent with previous data, the Δ*spoIIIAH* single mutant had low sporulation efficiency (1.3%, Fig. 3.2 E). In the Δ*spoIIIL* Δ*spoIIIAH* double mutant, when compared to the Δ*spoIIIAH* single mutant, there was an obvious shift towards forespores becoming rounder (closer to perfect roundness 1) and harbouring low levels of σ^G-dependent YFP fluorescence: 61.7% of the forespores (green shaded area on Fig. 3.2B – corresponding to forespores with σ^G-dependent YFP fluorescence <=5.8 and roundness >= 0.88), whereas only 6.7% were rounder while also retaining the most σ^G activity (orange shaded area on Fig. 3.2 B – corresponding to forespores with σ^G-dependent YFP fluorescence >=5.8 and roundness >= 0.88). The green shaded area highlights the category of double mutant forespores that become more extreme in terms of A-Q complex mutant phenotypes (i.e. much rounder spores with least σ^G-dependent YFP fluorescence) while the orange shaded area highlights the category of double mutant forespores that are much rounder but retain σ^G activity. The forespores of this double mutant also had a much lower and drastically reduced sporulation efficiency of 0% (Fig. 3.2 E).

In the *spoIIIAG** single mutant, consistent with previous data[123] and when compared to WT, a large proportion of the spores (82%) were rounder and had less σ^G activity (green shaded area on Fig. 3.2 C – corresponding to forespores with σ^G-dependent YFP fluorescence <= 13.4 and roundness >= 0.75) while only about 2.4% of the forespores had the roundness and σ^G activity similar to WT (gray shaded area on Fig. 3.2 C – corresponding to forespores with σ^G-dependent YFP fluorescence <=13.4 and roundness <= 0.75). Inconsistent with published data[123], the forespores of this mutant had a low sporulation efficiency of 2.15% (Fig. 3.2 E) similar to that of the Δ*spoIIIAH* single mutant. In the Δ*spoIIIL* Δ*spoIIIAG** double mutant, when compared to the s*poIIIAG** single mutant, there was also an obvious shift towards forespores becoming rounder (closer to perfect roundness 1) and harbouring low levels of σ^G-dependent YFP fluorescence as seen in 64.4% of the forespores (green shaded area on Fig. 3.2 C – corresponding to forespores with σ^G-dependent YFP fluorescence <=6.9 and roundness >= 0.88), while only 9.3% were rounder and also had the most σ^G activity (orange shaded area on Fig. 3.2 C – corresponding to forespores with σ^G-dependent YFP fluorescence >=6.9 and roundness >= 0.88). The green shaded area highlights the category of double mutant forespores that become more extreme in terms of A-Q complex mutant phenotypes (i.e. much rounder spores with least σ^G-dependent YFP fluorescence) while the orange shaded area highlights the category of double mutant forespores that are much rounder but retain σ^G activity. The forespores of this double mutant also had a much lower sporulation efficiency of 0.0003% (Fig. 3.2 E).

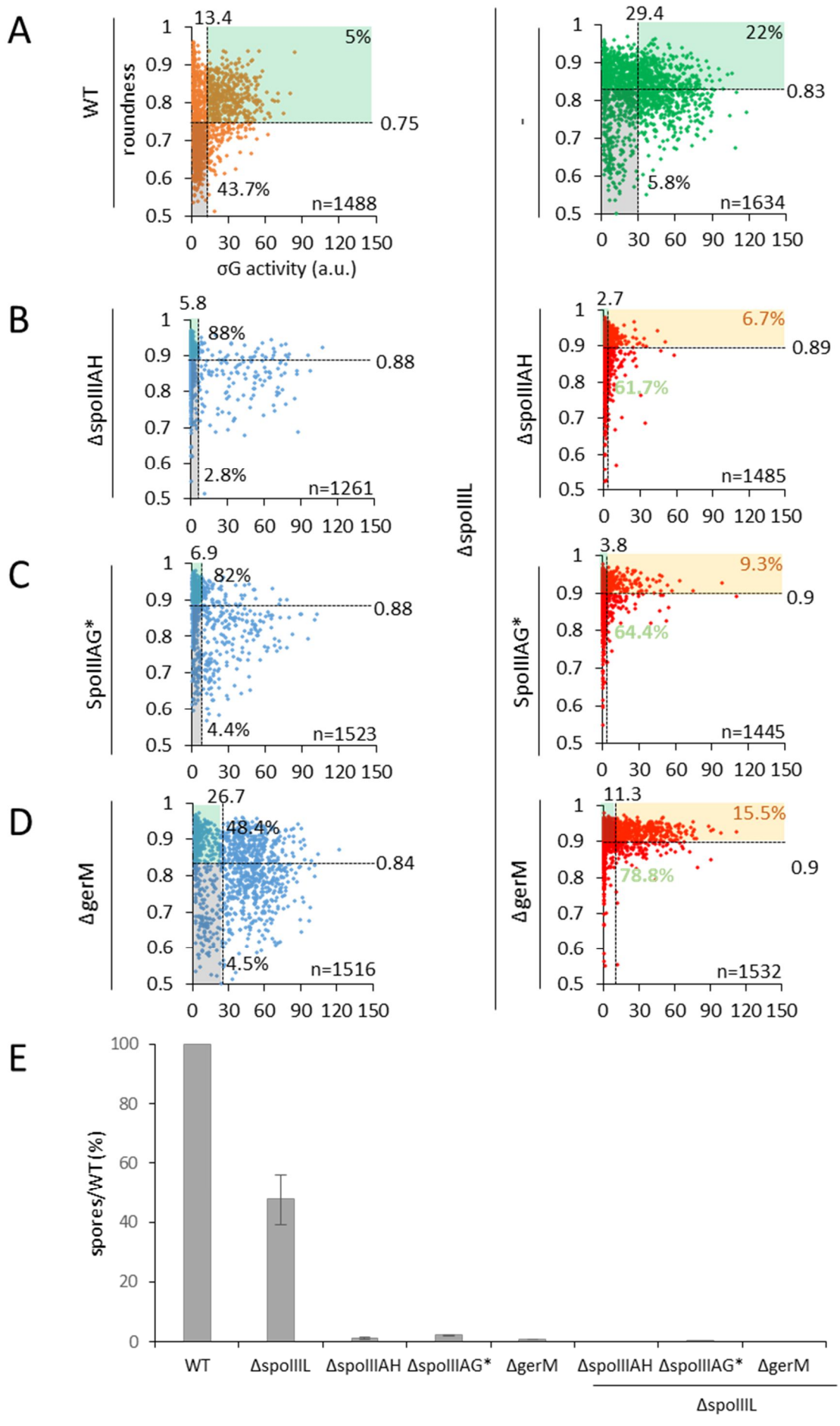
A
WT
roundness
13.4
5%
0.75
43.7%
n=1488
σG activity (a.u.)
-
29.4
22%
0.83
5.8%
n=1634
B
ΔspoIIIAH
5.8
88%
0.88
2.8%
n=1261
ΔspoIIIL
2.7
6.7%
0.89
61.7%
n=1485
C
SpoIIIAG*
6.9
82%
0.88
4.4%
n=1523
3.8
9.3%
0.9
64.4%
n=1445
D
ΔgerM
26.7
48.4%
0.84
4.5%
n=1516
11.3
15.5%
0.9
78.8%
n=1532
E
spores/WT (%)
WT
ΔspoIIIL
ΔspoIIIAH
ΔspoIIIAG*
ΔgerM
ΔspoIIIAH ΔspoIIIL
ΔspoIIIAG* ΔspoIIIL
ΔgerM ΔspoIIIL

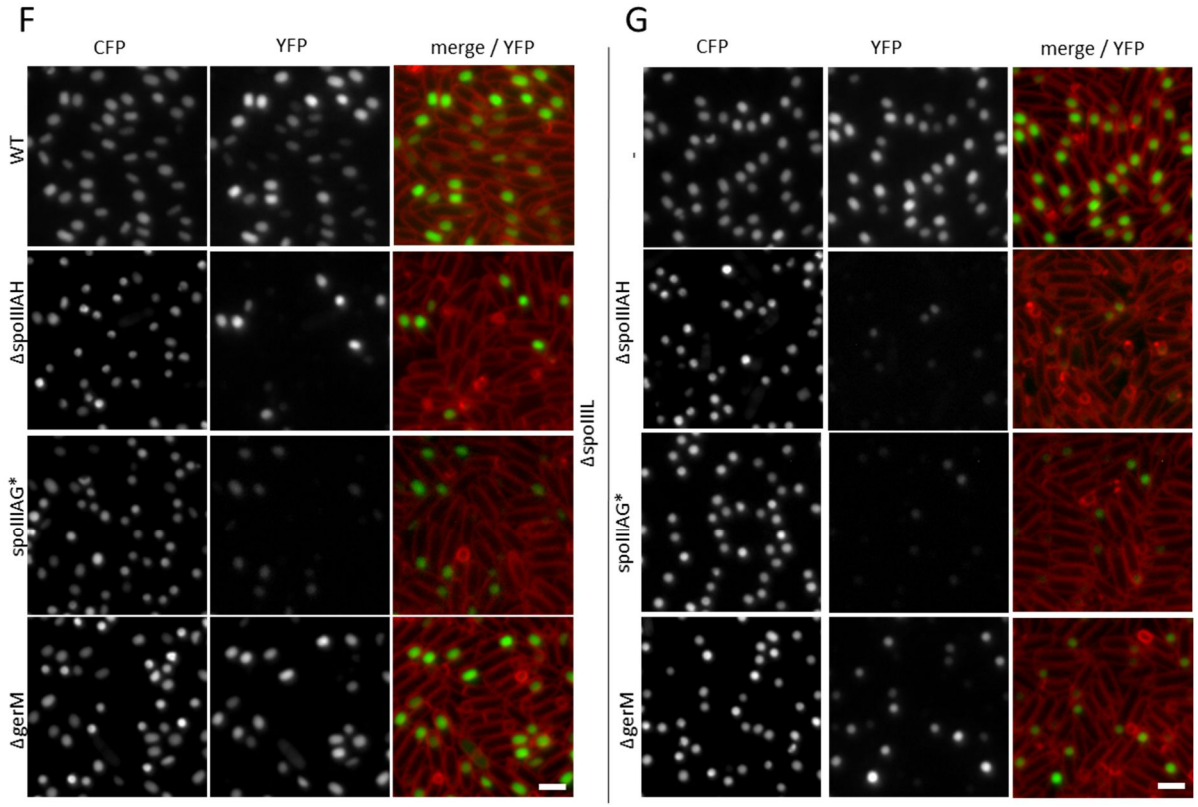

Fig 3.2 Synergistic defects of *the ΔspoIIIAH, ΔspoIIIAG*, ΔgerM* single mutants and their double mutants with *ΔspoIIIL* in forespore shape (roundness), σG activity and sporulation efficiency. (A) Scatter plots populating σG-dependent YFP fluorescence against forespore roundness at T4.5 for wild type (WT), or **(B)** for *ΔspoIIIAH* single mutant and *ΔspoIIIAH ΔspoIIIL* double mutant strains or **(C)** for *ΔspoIIIAG** single mutant and *ΔspoIIIAG* ΔspoIIIL double mutant* strains or **(D)** for *ΔgerM* single mutant and *ΔgerM ΔspoIIIL* double mutant strains. **(E)** Average sporulation efficiency data for WT, *ΔspoIIIL*, *ΔspoIIIAH, ΔspoIIIAG**, *ΔgerM* single mutants and the *ΔspoIIIAH ΔspoIIIL*, *ΔspoIIIAG* ΔspoIIIL*, *ΔgerM ΔspoIIIL* double mutants. Sporulation efficiency assays and microscopic image analyses were done as stated in the materials and methods section of this work. Error bars represent standard deviation of three biological replicates. **(F)** Representative fluorescence microscopy images at hour 4.5 (T4.5) after the onset of sporulation showing the intensity of σG-dependent YFP fluorescence for WT, *ΔspoIIIL*, *ΔspoIIIAH, ΔspoIIIAG**, *ΔgerM* single mutants and **(G)** for *ΔspoIIIAH ΔspoIIIL*, *ΔspoIIIAG* ΔspoIIIL*, *ΔgerM ΔspoIIIL* double mutants. σG-dependent YFP fluorescence was visualised using a YFP-fused σ^G-responsive forespore promoter (P*sspB-yfp*, false-coloured green in merged images). Cell membranes were visualised using TMA-DPH fluorescent membrane dye and are false-coloured red in merged images. Scale bar = 2 μm.

In the Δ*gerM* single mutant, consistent with previous data[127], and when compared to WT, almost 50% of the spores (48.4%) were rounder and had less σ^G activity (green shaded area on Fig. 3.2 D – corresponding to forespores with σ^G-dependent YFP fluorescence <= 13.4 and roundness >= 0.75) while only about 4.5% of the forespores had the roundness and σ^G activity similar to WT (gray shaded area on Fig. 3.2 D – corresponding to forespores with σ^G-dependent

YFP fluorescence <=13.4 and roundness <= 0.75). Similar to published data[127], the forespores of this single mutant also had low sporulation efficiency 0.79% (Fig. 3.2 E). In the Δ*spoIIIL* Δ*gerM* double mutant, when compared to the Δ*gerM* single mutant, there was also an obvious shift towards forespores becoming rounder (closer to perfect roundness 1) and harbouring low levels of σ^G-dependent YFP fluorescence as seen in 78.8% of the forespores (green shaded area on Fig. 3.2 D – corresponding to forespores with σ^G-dependent YFP fluorescence <=26.7 and roundness >= 0.84), while only 15.5% were rounder and also had the most σ^G activity (orange shaded area on Fig. 3.2 D – corresponding to forespores with σ^G -dependent YFP fluorescence >=26.7 and roundness >= 0.84). The green shaded area highlights the category of double mutant forespores that become more extreme in terms of A-Q complex mutant phenotypes (i.e. much rounder spores with least σ^G-dependent YFP fluorescence) while the orange shaded area highlights the category of double mutant forespores that are much rounder but retain σ^G activity. The forespores of this double mutant also had a much lower and drastically reduced sporulation efficiency of 0% (Fig. 3.2 E).

Summarily, neither the percentages of the forespores (61.7%, 64.4%, 78.8%) in the green shaded area for the A-Q complex double mutants assayed (Δ*spoIIIL* Δ*spoIIIAH*, Δ*spoIIIL* s*poIIIAG**, Δ*spoIIIL* Δ*gerM*) respectively are all similar nor the percentages of the forespores (6.7%, 9.3%, 15.5%) in the orange shaded area for the A-Q complex double mutants assayed (Δ*spoIIIL* Δ*spoIIIAH*, Δ*spoIIIL* s*poIIIAG**, Δ*spoIIIL* Δ*gerM*) respectively are all similar (Fig 3.2 B, C & D). This phenomenon of inconsistent synergy is also seen in the sporulation efficiency data (0%, 0.0003%, 0%) respectively of the A-Q complex double mutants assayed (Δ*spoIIIL* Δ*spoIIIAH*, Δ*spoIIIL* s*poIIIAG**, Δ*spoIIIL* Δ*gerM*) (see also Appendix I, Figure S3.2, S3.3, & S3.4). Collectively, these results therefore support the idea that SpoIIIL is unlikely to function in the A-Q complex pathway. However, another case scenario could be the possibility that SpoIIIL functions in the pathway of some but not all the A-Q complex mutants resulting thus in the so called inconsistent synergy.

3.3.3 SpoIIIL localizes uniformly in the spore membrane and changes overtime

To further determine if SpoIIIL is a component of the A-Q complex, we examined its localization pattern in the forespore. A-Q complex proteins have been shown to localize to the engulfing membranes of the developing forespore[91]. If SpoIIIL is part of the A-Q complex, then

we might expect it to also localize to the engulfing membranes of the forespore, from the forespore side. To do this, we first constructed and validated a C-terminal GFP fluorescent fusion to SpoIIIL: SpoIIIL-GFP (see Materials and Methods). To test if SpoIIIL-GFP is functional, SpoIIIL-GFP was inserted at an ectopic locus (*yhdG*) in a strain harbouring a deletion of *spoIIIL*, and the sporulation efficiency of the resulting strain was examined using the heat-kill assay. SpoIIIL-GFP was fully functional as the sole source of SpoIIIL, as it complemented the *spoIIIL* mutant and produced 93% heat-resistant spores (relative to WT, Fig. 3.3 E). Having validated SpoIIIL-GFP, we then examined its localization during a sporulation time course.

As shown in Fig. 3.3 A, we did not observe SpoIIIL-GFP localization at the engulfing membrane at early time points (between T2 and T3), as the GFP signal was not seen forming a curved pattern that follows the engulfing membrane. Instead SpoIIIL-GFP appeared to localize uniformly throughout the forespore membranes, with some cytoplasmic signal. Thus, the localization of SpoIIIL-GFP is different from what has been reported for the A-Q complex proteins[38,80,127–129].

Interestingly, at T3.5 we noticed a change in SpoIIIL-GFP localization: although most forespores harboured uniform SpoIIIL-GFP localization at the membrane, a subset of them appeared to display SpoIIIL-GFP as “patches” in the membrane or in the cytoplasm (Fig. 3.3 B). Strikingly, at a later time point (T5.5), most forespores harboured the patchy SpoIIIL-GFP localization. These results suggest that SpoIIIL-GFP undergoes a change in localization at later stages of development. Consistent with this idea, quantification of the uniform and patchy localization of the SpoIIIL-GFP at T3.5 and T5.5 suggests a dramatic change in localization: at T3.5 90% of forespores had uniform localisation of SpoIIIL-GFP and 10% had patchy localization, whereas at T5.5 17% spores had uniform and 83% spores had patchy localization (Fig. 3.3 C). Thus, SpoIIIL initially localizes uniformly in the forespore membrane and then undergoes a change in localization as the forespore matures.

The above localization data suggest that SpoIIIL does not become enriched in the engulfing membrane, and therefore is unlikely to be a component of the A-Q complex.

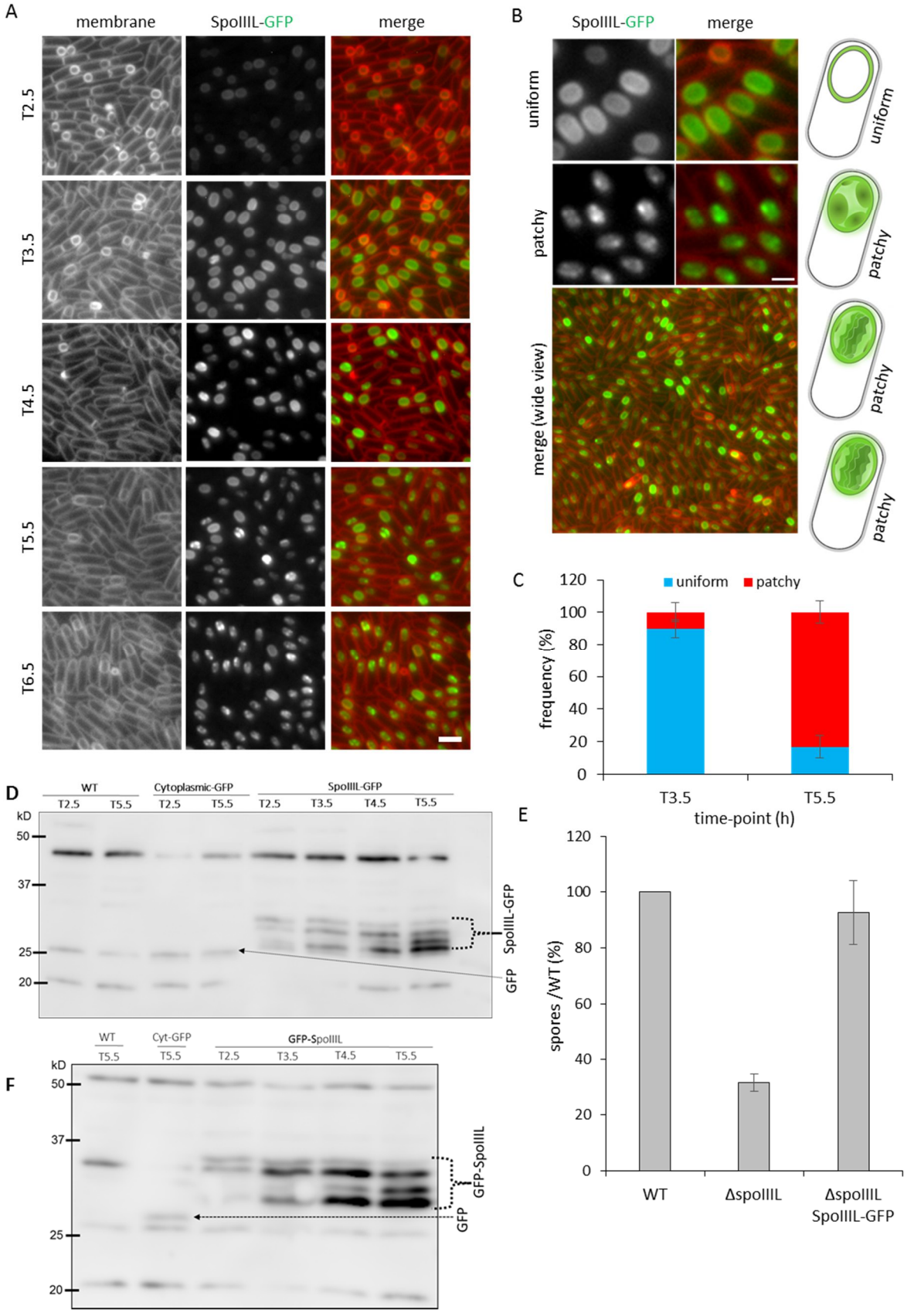

Fig 3.3 SpoIIIL-GFP localization in sporulating cells. (A) Fluorescence localization of SpoIIIL-GFP during a sporulation time-course. GFP signal is false-coloured green in the merged images. Cell membranes were visualised using TMA-DPH fluorescent membrane dye and are false-coloured red in merged images. Scale bar =

2 µm. **(B)** Close-up of SpoIIIL-GFP localization at time-points T3.5 and T5.5, and wider view of a T5.5 merge, after the onset of sporulation. Fluorescence signals are false-coloured as in (A). Scale bar = 1 µm. **(C)** Quantification histogram showing proportion of cells (% ± STDEV, 3 biological replicates) with uniform (blue) and patchy (red) SpoIIIL-GFP localization in wild-type cells at T3.5 and T5.5 after the onset of sporulation. n > 300 per replicate, per time-point, per strain. **(D)** Immunoblot analysis of SpoIIIL-GFP in cell lysates of sporulating WT cells collected every hour between T2.5 and T5.5. As controls, a cell lysate from sporulating cells collected at T2.5 & T5.5 from a WT strain that does not contain GFP, and a cell lysate collected at T2.5 & T5.5 from a strain expressing cytoplasmic GFP were included. SpoIIIL-GFP was immunodetected using anti-GFP antibodies. The position of SpoIIIL-GFP (~36.9 kDa) and GFP (~27.3 kDa) are indicated. **(E)** Average sporulation efficiency data for WT, Δ*spoIIIL* single mutant, and a Δ*spoIIIL* single mutant containing SpoIIIL-GFP at an ectopic locus. Sporulation efficiency assays were done as described in the materials and methods section of this work. Error bars represent standard deviation of three biological replicates. **(F)** Immunoblot analysis of GFP-SpoIIIL in cell lysates of sporulating WT cells collected every hour between T2.5 and T5.5. As controls, a cell lysate from sporulating cells collected at T5.5 from a WT strain that does not contain GFP, and a cell lysate collected at T5.5 from a strain expressing cytoplasmic GFP were included. SpoIIIL-GFP was immunodetected using anti-GFP antibodies. The position of GFP-SpoIIIL and GFP (~27.3 kDa) are indicated.

3.3.4 The C- and N- terminal GFP fusions of SpoIIIL localizes in the same manner and are both not membrane exposed

The above data suggests that SpoIIIL initially localizes uniformly in the forespore membrane before undergoing a change in its localization. However, it was not clear whether this change was a consequence of the fusion of GFP to the C-terminal end of the SpoIIIL ORF since the microscopic imaging data obtained so far has been with the C-terminal fusion of GFP to SpoIIIL. We therefore hypothesized that perhaps, a fusion of GFP to the N-terminal of end of the SpoIIIL ORF could yield a different result. In order to determine whether the change in SpoIIIL localization from uniform to patchy localization was not just the consequence of the fusion of GFP to the C-terminal end of the SpoIIIL ORF, we constructed an N-terminal fusion of GFP to the SpoIIIL ORF and imaged this strain under a fluorescence microscope hourly between timepoints T2.5 and T6.5. To test if GFP-SpoIIIL is functional, GFP-SpoIIIL was inserted at an ectopic locus (*yhdG*) in a strain harbouring a deletion of *spoIIIL*, and the sporulation efficiency of the resulting strain was examined using the heat-kill assay. GFP-SpoIIIL was fully functional as the sole source of SpoIIIL, as it complemented the *spoIIIL* mutant and produced 83% heat-resistant spores relative to WT (Appendix I, Figure S3.1).

Interestingly, the microscopic data obtained from this experiment suggested that both the C-terminal and N-terminal fusion of GFP to the SpoIIIL ORF behaved similarly under the fluorescence microscope. Thus, the change in SpoIIIL localization from the initial uniform localization pattern observed around T3.5 to the patchy localization pattern observed at later timepoints around T5.5 after the onset of sporulation, was consistent both in the C-terminal fusion, and in the N-terminal fusion of GFP to the SpoIIIL ORF (Fig 3.4 A & B).

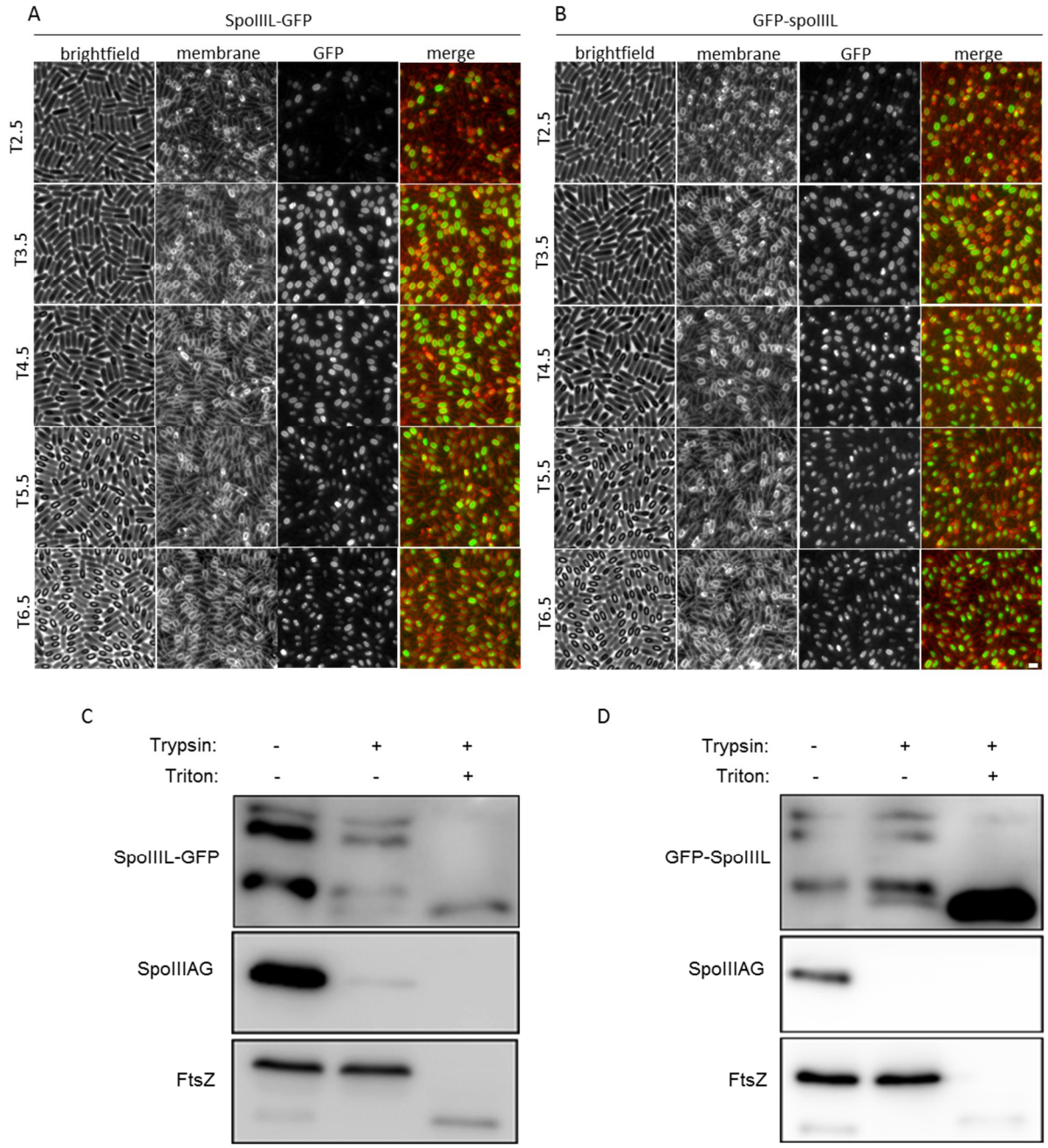

Fig 3.4 The C- and N- terminal GFP fusions of SpoIIIL localizes in the same manner. Fluorescence localization of SpoIIIL-GFP (A) and GFP-SpoIIIL (B) during a sporulation time-course, T2.5, T3.5, T4.5, T5.5, & T6.5. GFP signal is false-coloured green in the merged images. Cell membranes were visualised using TMA-DPH fluorescent

membrane dye and are false-coloured red in merged images. Scale bar = 2 µm. SpoIIIL-GFP & GFP-SpoIIIL are both not surface-exposed and thus are not accessible to digestion by trypsin. Immunoblot analysis of protoplasted sporulating cells using anti-GFP antibodies. Cells expressed SpoIIIL-GFP (C), or GFP-SpoIIIL (D) as the sole source of SpoIIIL in strain *ΔspoIIQ ΔspoIIIL* (bPO85) or (bPO217) respectively. Cells were treated with trypsin in the presence and absence of the detergent Triton X-100. Consistent with the prediction that SpoIIIL is not likely membrane-anchored but might contain some transmembrane segments, it was not susceptible to trypsin digestion in the absence of Triton X-100. As controls, the immunoblot was performed for a membrane protein with an extracellular domain (SpoIIIAG) and for a cytoplasmic protein (FtsZ).

Furthermore, our bioinformatics analysis of SpoIIIL suggested that it contains a patch of hydrophobic residues at the C-terminus as shown by the bioinformatics tool phobius employed for the prediction of transmembrane topology from the amino acid sequence of a protein[130] (see Figure S6.2). But It was not certain whether this segment is definitely transmembrane or cytoplasmic or some sort of amphipathic helices. It might be noteworthy to state that amphipathic helices have separate hydrophobic and polar residues between two interphases of the helix which allows the helices to adsorb at polar and non-polar interfaces such as the lipid surfaces of cellular organelles. Since the topology of SpoIIIL was not yet reported anywhere in literature, and considering the initial fluorescence microscopy imaging data of SpoIIIL (Fig 3.3), we therefore predicted that SpoIIIL could be anchored in the forespore membrane via its hydrophobic segment, while its mostly non-cytoplasmic N-terminal region would be suspended within the forespore cytoplasm. To test these bioinformatic predictions, we investigated the topology of SpoIIIL using a protease accessibility assay[131].

Usually in the protease accessibility assay, cells are protoplasted so that proteins displayed at the cell surface would be directly accessible to the protease Trypsin, and then digested. But, if the protein in question resides in the cytoplasm, it would be inaccessible to protease digestion unless the membrane is solubilized by a detergent that solubilizes the membranes but does not interfere with trypsin proteolysis; in our case Triton X-100. To perform this assay, we expressed either SpoIIIL-GFP or GFP-SpoIIIL as the sole source of SpoIIIL in *ΔspoIIQ ΔspoIIIL* sporulating cells to ensure that the membrane proteins present in the inner and outer forespore membranes, probably including SpoIIIL, would not be artificially inaccessible as a result of protoplast engulfment[75]. Three reactions were included in the assay. The first reaction did not include the addition of any reagents to the protoplasted cells, while the second control reaction included the addition of trypsin to the protoplasted cells in order to

digest any surface-exposed proteins. Finally, in the third reaction, protoplasts were incubated in the presence of trypsin and Triton X-100.

In this experiment, we employed two control reactions using a cytoplasmic protein FtsZ as well as SpoIIIAG, a protein previously shown to have a surface-exposed domain[123]. By immunoblotting with anti-FtsZ antibodies, we showed that FtsZ could only be digested by trypsin when Triton X-100 was added to the reaction (Figure 3.4.C & D; Appendix I, Figure S3.5). Since SpoIIIAG is a membrane protein with an extracellular domain, immunoblot analysis using anti- AG antibodies to the SpoIIIAG extracellular domain showed that it was accessible to the protease trypsin and was digested in the reaction devoid of Triton X-100 (Figure 3.4 C & D). For either SpoIIIL-GFP or GFP-SpoIIIL immunoblotting, we used anti-GFP antibodies.

Consistent with the bioinformatics predictions that SpoIIIL is not likely membrane-anchored but might contain some hydrophobic segments, and unlike the control SpoIIIAG, both SpoIIIL-GFP and GFP-SpoIIIL were not susceptible to trypsin digestion in the absence of Triton X-100. This result indicates that SpoIIIL is not a membrane-embedded protein regardless of whether it contains a patch of hydrophobic residues anywhere in its ORF or not. Thus, this conclusion does not rule out the fact that SpoIIIL may contain hydrophobic residues which are amphipathic in nature, and could explain why SpoIIIL localizes close to the forespore membrane like a peripheral membrane protein.

3.3.5 The C- terminal GFP fusion of SpoIIIL localizes differently from the C- terminal GFP fusion of a classical membrane protein, MalF

Since we are certain that SpoIIIL localizes uniformly around the forespore membrane at early timepoints after the onset of sporulation and changes to a patchy-like phenotype at later timepoints after the onset of sporulation, we hypothesized that may be this phenomenon was not unique to SpoIIIL alone afterall. We reasoned that may be, other classical membrane associated proteins could exhibit this similar phenomenon as SpoIIIL.

In order to ascertain that the characteristic localization phenotype of SpoIIIL wherein it localizes uniformly around the forespore membrane at early timepoints and subsequently as cytoplasmic patches in the forespore at later timepoints after the onset of sporulation was unique to SpoIIIL alone, we took advantage of a strain in the Rodrigues lab wherein GFP was

already expressed at the C-terminus of a classical membrane protein MalF, and imaged it hourly between T3 & T7, alongside SpoIIIL-GFP under a fluorescence microscope, after the onset of Sporulation.

While MalF-GFP localized uniformly around the membrane surrounding the forespore across all timepoints assayed, SpoIIIL-GFP on the other hand retained its characteristics uniform localization at early timepoints after the onset of sporulation around T3 and changed to a patchy phenotype later around T5 after the onset of sporulation (Fig 3.5).

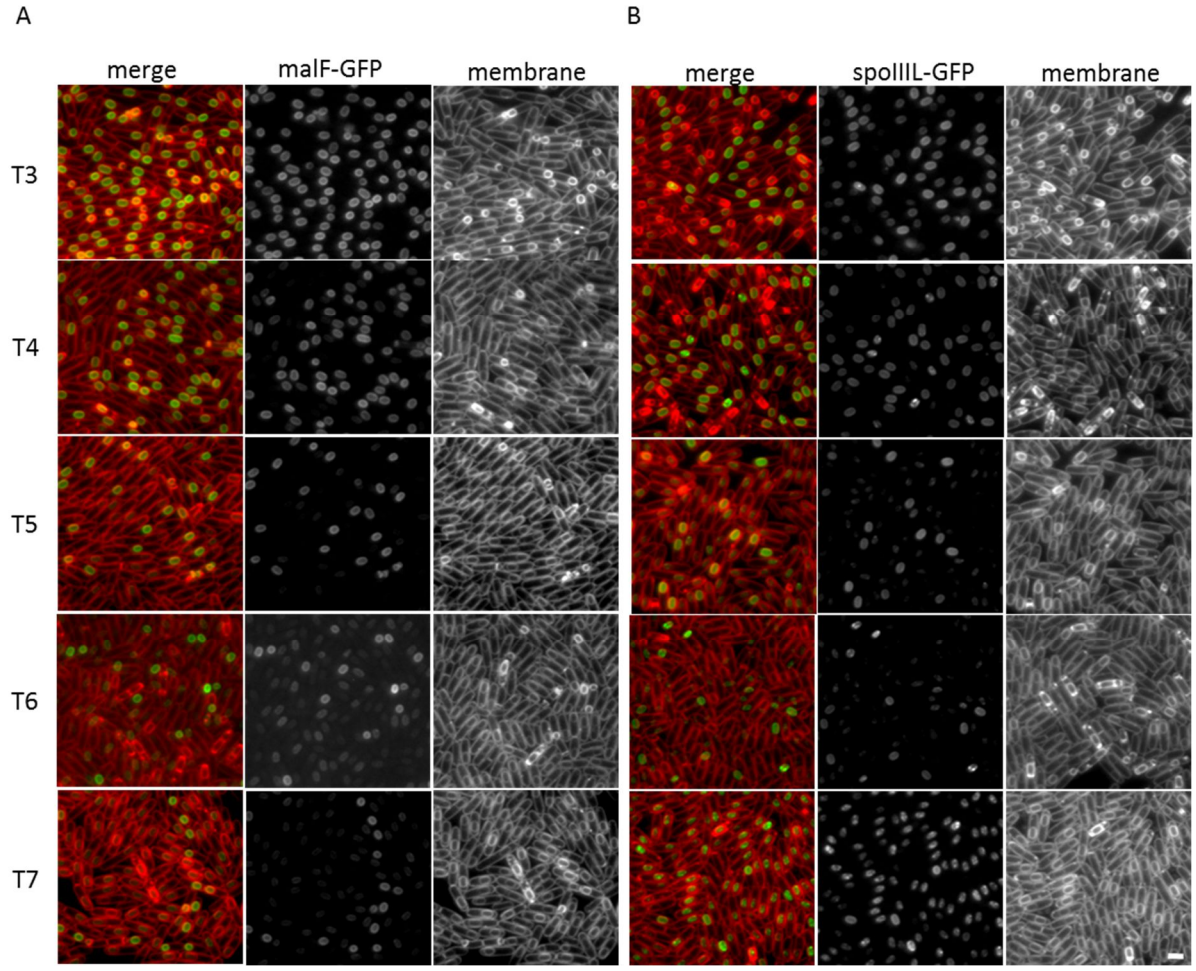

Fig 3.5 The C- terminal GFP fusion of SpoIIIL localizes differently from the C- terminal GFP fusion of a classical membrane protein, MalF. Fluorescence localization of MalF-GFP (A) and SpoIIIL-GFP (B) during a sporulation time-course, T3, T4, T5, T6, & T7. GFP signal is false-coloured green in the merged images. Cell membranes were visualised using TMA-DPH fluorescent membrane dye and are then false-coloured red in merged images. Scale bar = 2 μm.

Therefore, this data confirms that the change in SpoIIIL's localization pattern from uniform around the forespore membrane at early timepoints after the onset of sporulation, to patchy-

like patterns within the forespore cytoplasm at later timepoints after the onset of sporulation, is a special feature of SpoIIIL.

3.3.6 Ten different single mutations (N4A, D5A, Y6A, K8A, T11A, R25A, P38A, F44A, G45A, and P48A) in the SpoIIIL ORF do not disrupt normal SpoIIIL localization pattern

Site-directed mutagenesis is a molecular genetics approach that assists in deciphering protein structure-function relationships and fathoming protein-protein interactions, and involves the substitution of single non-alanine residues with alanine to generate mutant libraries for functional testing. This tool facilitates the discovery of residues in a protein ORF that are not only essential to a proteins' function and structure but also critical in the proteins interactions and behaviours within its native milieu[132].

The data above (section 3.3.4) indicates that SpoIIIL is not a membrane-embedded protein although it was predicted to also contain a patch of hydrophobic residues at the C-terminus of its ORF among other residues. Recall, It was not certain whether this hydrophobic residues containing segment constitutes amphipathic helices in the SpoIIIL ORF. Since amphipathic helices have separate hydrophobic and polar residues between two interphases of the helix which allows them to adsorb at polar and non-polar interfaces such as the lipid surfaces of cellular organelles, one might suspect that the predicted amphipathic nature of the SpoIIIL ORF may contribute to the ability of SpoIIIL to localize around the forespore membrane.

We therefore hypothesized that particular residues in the SpoIIIL ORF may be responsible for certain characteristic functions or features of SpoIIIL such as its localization around the forespore membrane (as seen in section 3.3.5), and that altering or disrupting the native structure or conformation of SpoIIIL by replacing one or more conserved residues of the SpoIIIL ORF with a physicochemically innocuous residue like alanine, could result in a significant change in SpoIIIL's phenotype and function.

In order to ascertain whether any single amino acid residue in the SpoIIIL ORF is responsible for the observed SpoIIIL phenotype, we constructed and localized 10 different single mutations of the SpoIIIL ORF by replacing 10 different conserved amino acid residues[133] in the SpoIIIL ORF with alanine (see Figure S6.3) and imaged the 10 different strains under a fluorescence microscope at T3.5 when most forespores harbour uniform SpoIIIL-GFP localization and at T5.5 when most forespores harbour patchy SpoIIIL-GFP localization, after

the onset of sporulation (Fig 3.6 A & B). Before the imaging, we tested whether the 10 different single mutation harbouring strains of SpoIIIL-GFP were functional, by inserting each SpoIIIL-GFP ORF harbouring a single amino acid residue substitution with alanine, at an ectopic locus (yhdG) in a strain harbouring a deletion of spoIIIL, and examining the sporulation efficiency of the resulting strains via heat-kill assay (see methods section). In all ten single mutation strains assayed, SpoIIIL-GFP appeared fully functional as the sole source of SpoIIIL, as it complemented the spoIIIL mutant and produced mostly ~ 100% heat-resistant spores (relative to WT, Fig. 3.6 C) except for the G45A mutation where glycine was replaced with alanine at the 45th amino acid position of the SpoIIIL ORF, which yielded ~ 70% heat-resistant spores. Glycine to Alanine switching has been predicted to bring about moderate and localised structural alterations, alongside a heightened dynamic in the backbone and modifications to the hydrogen bonding style of the protein[134]. This may suggest that a certain measure of flexibility or rigidity in the structure of SpoIIIL is required for its optimal function and localization around the forespore inner membrane.

However, the data obtained revealed no significant alteration or change in the localization pattern of SpoIIIL across all the 10 single mutations assayed when compared to wild type (Fig. 3.6 A & B). It is not clear whether the effect of the substitution of a single amino acid residue in the SpoIIIL ORF with alanine was too negligible to elicit a significant structure-function defect in SpoIIIL or whether the cell successfully compensated for alterations resulting from the site-directed mutagenesis of SpoIIIL.

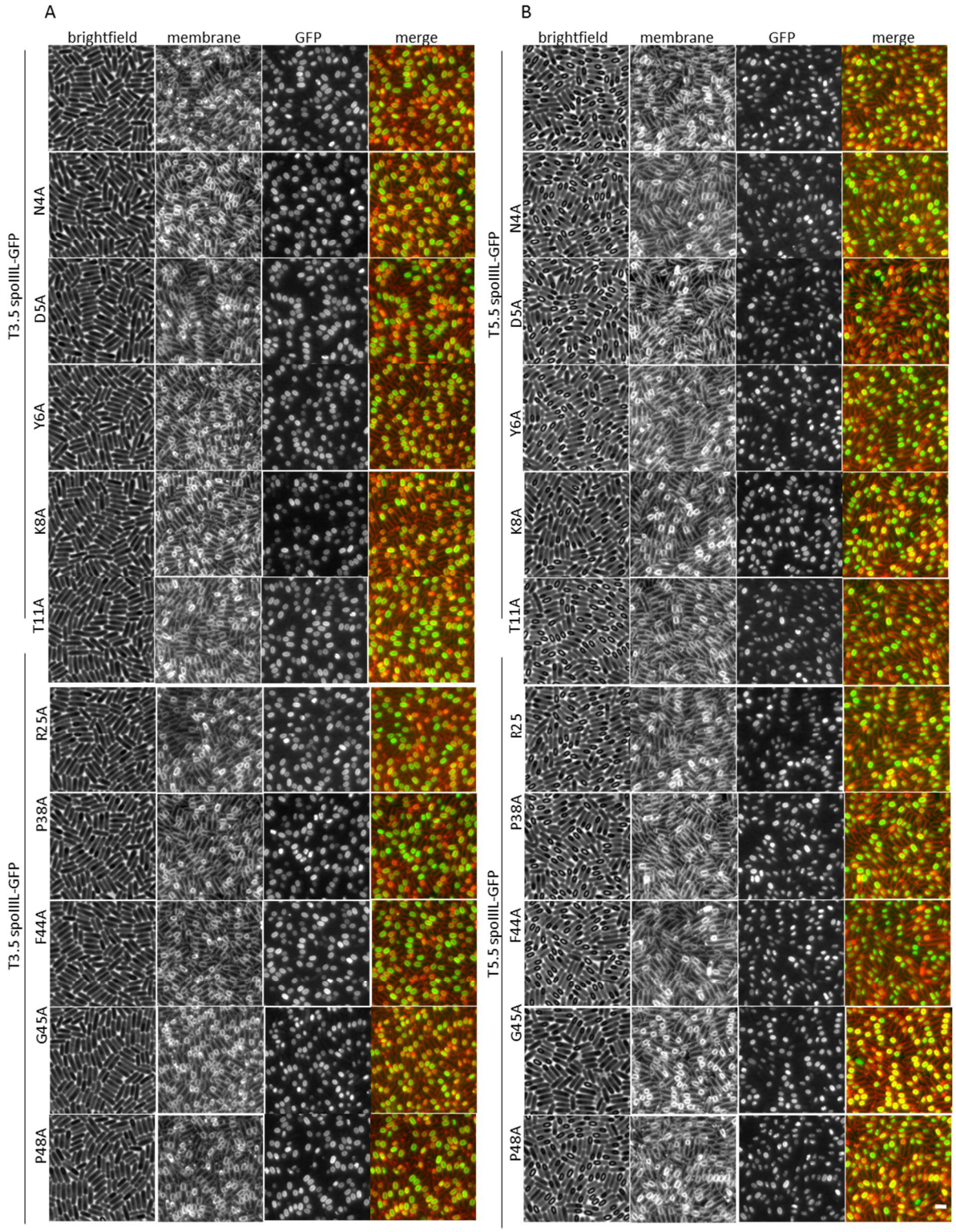
A
brightfield
membrane
GFP
merge
T3.5 spoIIIL-GFP
N4A
D5A
Y6A
K8A
T11A
R25A
P38A
F44A
G45A
P48A
B
T5.5 spoIIIL-GFP
R25

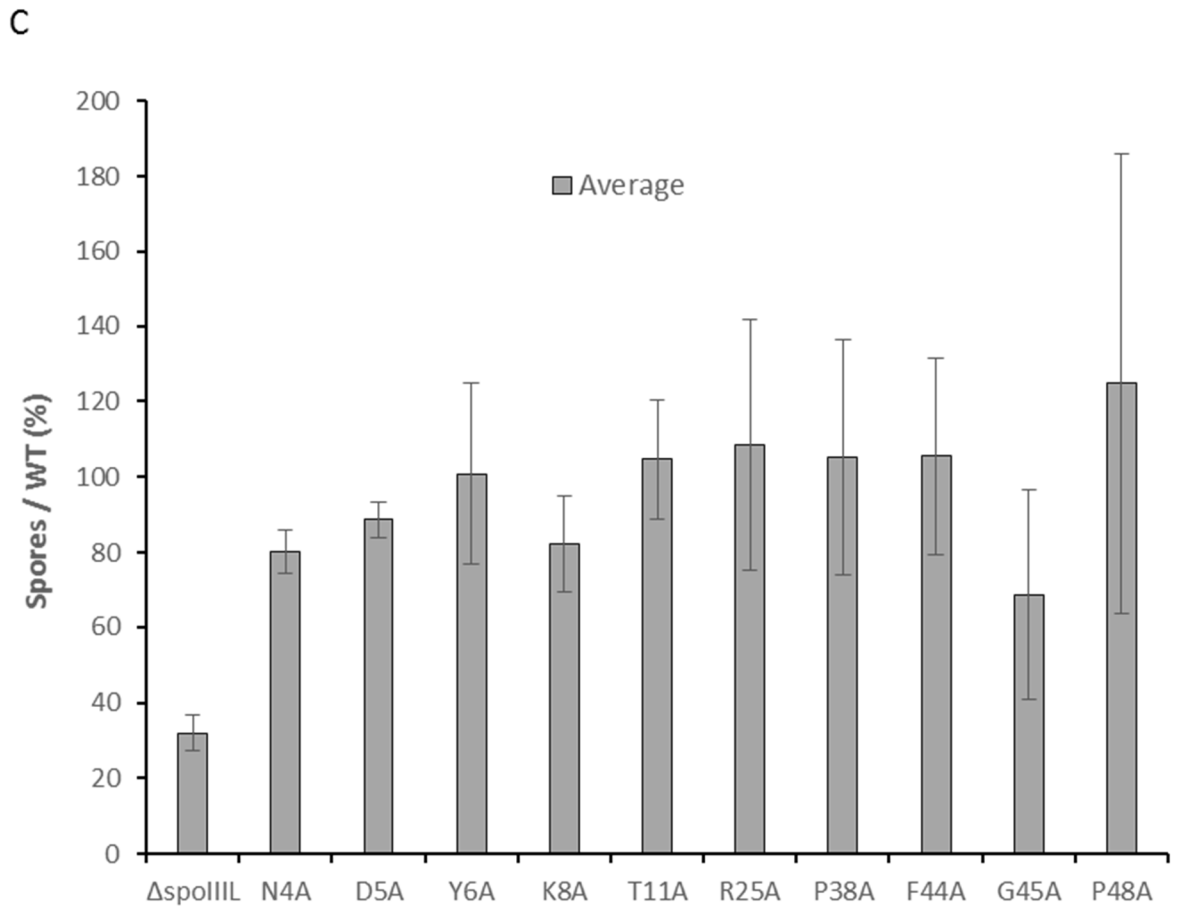

Fig 3.6 Ten different single mutations (N4A, D5A, Y6A, K8A, T11A, R25A, P38A, F44A, G45A, and P48A) in the SpoIIIL ORF do not disrupt normal SpoIIIL localization pattern. Fluorescence localization of SpoIIIL-GFP in 10 different single mutations in SpoIIIL ORF at T3.5 (A) and at T5.5 (B) after the onset of sporulation. GFP signal is false-coloured green in the merged images. Cell membranes were visualised using TMA-DPH fluorescent membrane dye and are then false-coloured red in merged images. Scale bar = 2 µm. (C) Average sporulation efficiency data for WT, Δ*spoIIIL* single mutant, and 10 different single mutation strains of the SpoIIIL ORF. Sporulation efficiency assays were done as described in the materials and methods section of this work. Error bars represent standard deviation of 2 biological replicates.

3.3.7 The change in SpoIIIL-GFP localization is due to proteolysis

The above data suggests SpoIIIL undergoes a change in localization. We hypothesized that this change in localization could be the result of proteolytic processing or cleavage of the GFP portion of SpoIIIL-GFP (these hypotheses are not mutually exclusive). To further investigate the change of SpoIIIL-GFP localization from uniform to patchy during spore development, we conducted immunoblot analysis of SpoIIIL-GFP in cell lysates of sporulating cells collected every hour between T2.5 and T5.5. As controls, we included a cell lysate from sporulating cells

collected at T5.5 from a WT strain that does not contain GFP. Anti-GFP antibodies were used to detect SpoIIIL-GFP in the immunoblot.

As shown in the immunoblot data in Fig. 3.3 D & F, a band corresponding to green fluorescent protein (GFP, ~27.3 kDa) was observed in the control lysates containing cytoplasmic GFP at T2.5 & T5.5 in the N-terminal fusion and C-terminal fusion of GFP to SpoIIIL.

For the wild-type lysates containing SpoIIIL fused to GFP, at T2.5 – T5.5, when counting downwards from higher molecular weight to lower molecular weight, four bands corresponding to the size of SpoIIIL-sfGFP (~36.9 kDa) were detected (see Fig 3.3 D&F). These four bands were not detected in the control lysates. At T2.5 and T3.5, all the visible bands (usually the first and topmost band, the second band, and the bottom or fourth band) appeared fainter compared to bands seen at later time points. At T4.5 and T5.5, all the visible bands were bolder except the top most or first band corresponding to full-length SpoIIIL-GFP which was usually observed to become fainter. Also, the third band was always observed to increase its intensity with time. Generally, the intensity of the full-length SpoIIIL-GFP band decreased over time, while the intensity of SpoIIIL-GFP cleavage products increased with time. This pattern is suggestive of the accumulation of SpoIIIL-GFP's products of proteolytic processing at later stages of spore maturation. This was consistent with the hypothesis that the patchy phenotype of SpoIIIL-GFP observed at later time points in spore development (Fig. 3.3 B) might be the direct result of some form of proteolytic processing or degradation.

The data presented so far suggests that the change in SpoIIIL-GFP localization from uniform to patchy during development is the result of proteolysis. To begin to understand the mechanism of SpoIIIL proteolysis, we hypothesized that SpoIIIL-GFP proteolysis may require a specific protease in the forespore. The forespore harbours three known proteases, SpoIVB, LonB, CtpB under σ^F control. SpoIVB is a serine protease that participates in pro-σ^K processing in the mother cell and in CtpB cleavage[84]. Although this protease is transcribed in very low amounts under σ^F control, a large portion of its transcription in the forespore is σ^G-dependent[84,114,135]. CtpB shares certain similarities with SpoIVB in that it is also a serine protease which takes part in pro-σ^K processing and functions in the intracellular space between the mother cell and the forespore[24,84,136]. CtpB is transcribed under the control of both σ^E and σ^G [84].

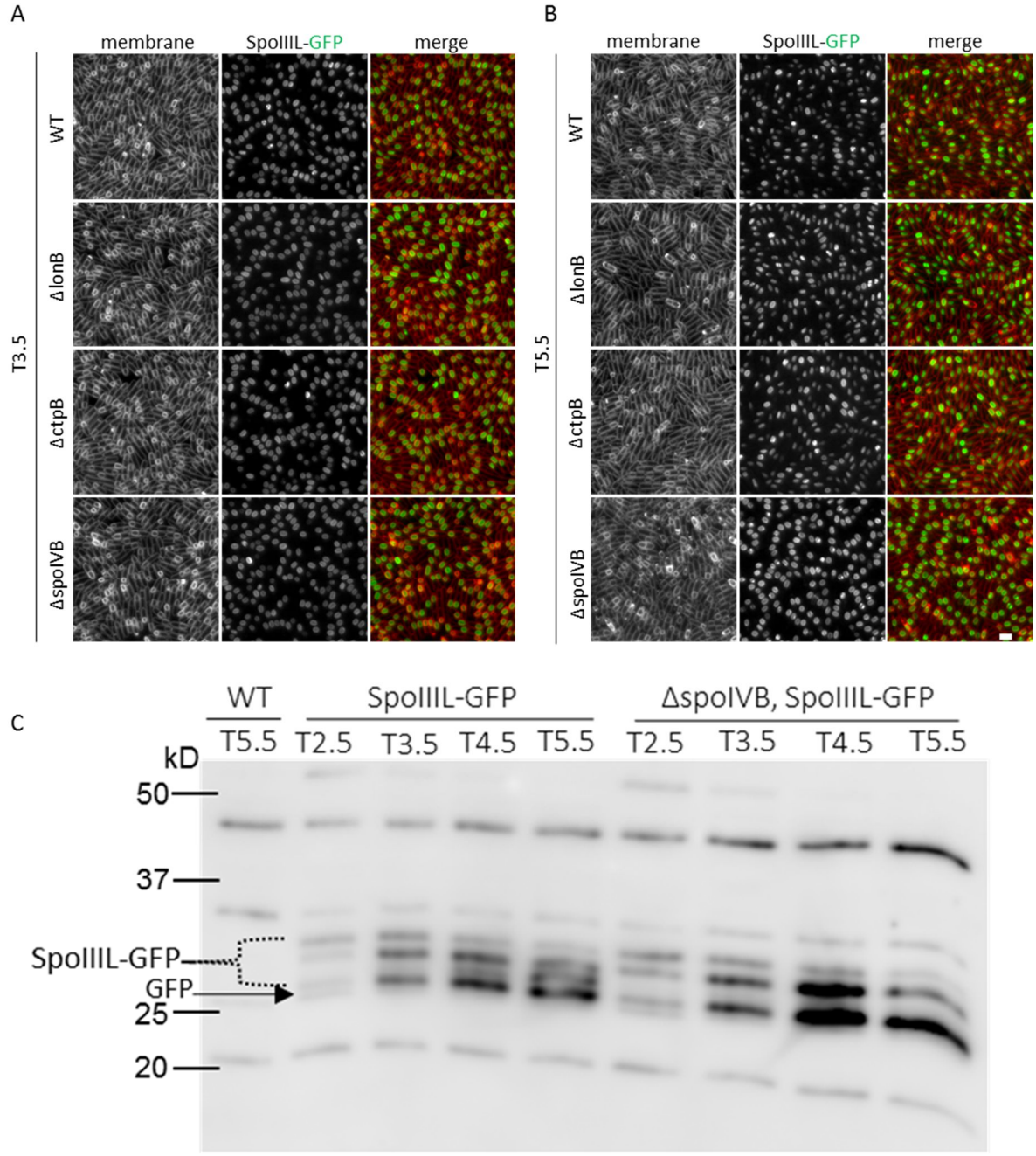

Fig 3.7 SpoIIIL-GFP proteolysis depends on SpoIVB. Fluorescence localization of SpoIIIL-GFP in WT cells as well as in the absence of three forespore proteases LonB, CtpB and SpoIVB at T3.5 when most forespores harbour uniform SpoIIIL-GFP localization **(A)** and at T5.5 when most forespores harbour patchy SpoIIIL-GFP localization **(B).** GFP signal is false-coloured green in the merged images. Cell membranes were visualised using TMA-DPH fluorescent membrane dye and are false-coloured red in merged images. Scale bar = 2 µm. **(C)** Immunoblot analysis of SpoIIIL-GFP in cell lysates of sporulating WT and *ΔspoIVB* single mutant strains collected every hour between T2.5 and T5.5. As controls, a cell lysate from sporulating cells collected at T5.5 from a WT strain that does not contain GFP was included. SpoIIIL-GFP was immunodetected using anti-GFP antibodies. The position of SpoIIIL-GFP and GFP are indicated.

LonB on the other hand is a Lon-like ATP-dependent protease that functions in protein quality control, and has been shown to localize in the forespore membranes early during spore development and in the entire forespore at later stages of spore development[137,138]. We reasoned that one or more of these forespore proteases may be involved in SpoIIIL proteolysis and the change in localization pattern from uniform to patchy.

To test this we localized SpoIIIL-GFP in the absence of these proteases at T3.5 when most forespores harbour uniform SpoIIIL-GFP localization and at T5.5 when most forespores harbour patchy SpoIIIL-GFP localization. If our hypothesis is correct, then we would expect to observe less forespores with patchy SpoIIIL-GFP localization at T5.5, compared to WT, in one or more of the protease mutant backgrounds.

In the Δ*lonB* mutant or Δ*ctpB* mutant background, there was no obvious difference in the localization pattern of SpoIIIL compared to WT. Like WT, in these two mutants, most forespores harboured patchy SpoIIIL-GFP localization at T5.5. Strikingly, in the Δ*spoIVB* mutant, most forespores retained the uniform SpoIIIL-GFP localization observed at T3.5, at T5.5 (Fig 3.2.7 A & B). In contrast to WT forespores, quantification of the number of forespores with uniform and patchy SpoIIIL-GFP localization in the Δ*spoIVB* mutant revealed that 36% were patchy and 64% were uniform at T5.5 (Fig 3.8). Therefore, the change in SpoIIIL-GFP localization from uniform to patchy is connected to the forespore protease SpoIVB (Fig 3.7 A & B) but not to LonB or CtpB.

Interestingly, when the Immunoblot analysis of SpoIIIL-GFP in cell lysates of sporulating WT strains as described earlier in this same section was repeated for the *ΔspoIVB* single mutant strain, when counting downwards from higher molecular weight to lower molecular weight, it was observed that the third band was absent at all time points. This was however in contrast to what was observed for the wild type immunoblot results where all four bands were always present (Fig 3.7 C). In summary, these results suggest that the protease SpoIVB is particularly required for the proteolysis of SpoIIIL.

3.3.8 The forespore protease SpoIVB, and its catalytic site (SpoIVB*) are required for SpoIIIL localization & stability

The above data (section 3.3.7) suggests that SpoIVB is required for the proteolysis and change in localization of SpoIIIL. Now that we know that the forespore protease SpoIVB is largely

responsible for the proteolysis of SpoIIIL, we wondered whether the catalytic site of SpoIVB is actually responsible for the observed change in the localization pattern of SpoIIIL from uniform localization at early time points T2.5 and T3.5 after the onset of sporulation, to the patchy phenotype observed at later time points T4.5, T5.5, and T6.5 after the onset of sporulation. Hence, we took advantage of a Δ*spoIVB** strain that is defective only in the catalytic site of SpoIVB, and imaged it under a fluorescence microscope at T3.5 and T5.5 after the onset of sporulation. Thus, in the Δ*spoIVB** mutant, the SpoIVB protein is present but cannot carry out its protease activity[139] and consequently may not be able to elicit the proteolysis of SpoIIIL-GFP which had resulted in the SpoIIIL's patchy phenotype observed at T5.5 (Fig 3.7 B)

If our hypothesis is correct, then we would also expect to observe much less or no forespores with patchy SpoIIIL-GFP localization at T5.5 as was observed in the Δ*spoIVB* mutant, compared to WT. As hypothesized, spores of the Δ*spoIVB** mutant behaved like those of the Δ*spoIVB* mutant, showing much less or no cytoplasmic patches at T5.5 compared to WT (Fig 3.8 A - F). In contrast to WT forespores where 83% were patchy and 17% were uniform at T5.5, quantification of the number of forespores with uniform and patchy SpoIIIL-GFP localization in the Δ*spoIVB** mutant revealed that 30% were patchy and 70% were uniform at T5.5 (Fig 3.8 D-F). And this Δ*spoIVB** mutant quantification data was consistent with the Δ*spoIVB* single mutant data where 24% spores were patchy and 75% spore were uniform at T5.5 h after the onset of sporulation.

To further investigate whether the catalytic site of the SpoIVB* mutant particularly mediates the resultant patchy-cytoplasmic phenotype observed in WT as well as the hypothesized accumulation of SpoIIIL-GFP's products of proteolytic processing at later stages of spore maturation (Fig 3.3), we conducted an immunoblot assay of SpoIIIL-GFP in cell lysates of sporulating ΔspoIVB single mutant, and Δ*spoIVB** catalytic mutants strains at T3.5 when most forespores harbour uniform SpoIIIL-GFP localization and at T5.5 when most forespores harbour patchy SpoIIIL-GFP localization (Fig 3.8 G). As controls, a cell lysate from sporulating cells collected at T5.5 from a WT strain that does not contain GFP was included. SpoIIIL-GFP was immunodetected using anti-GFP antibodies, and its position on the blot is indicated accordingly.

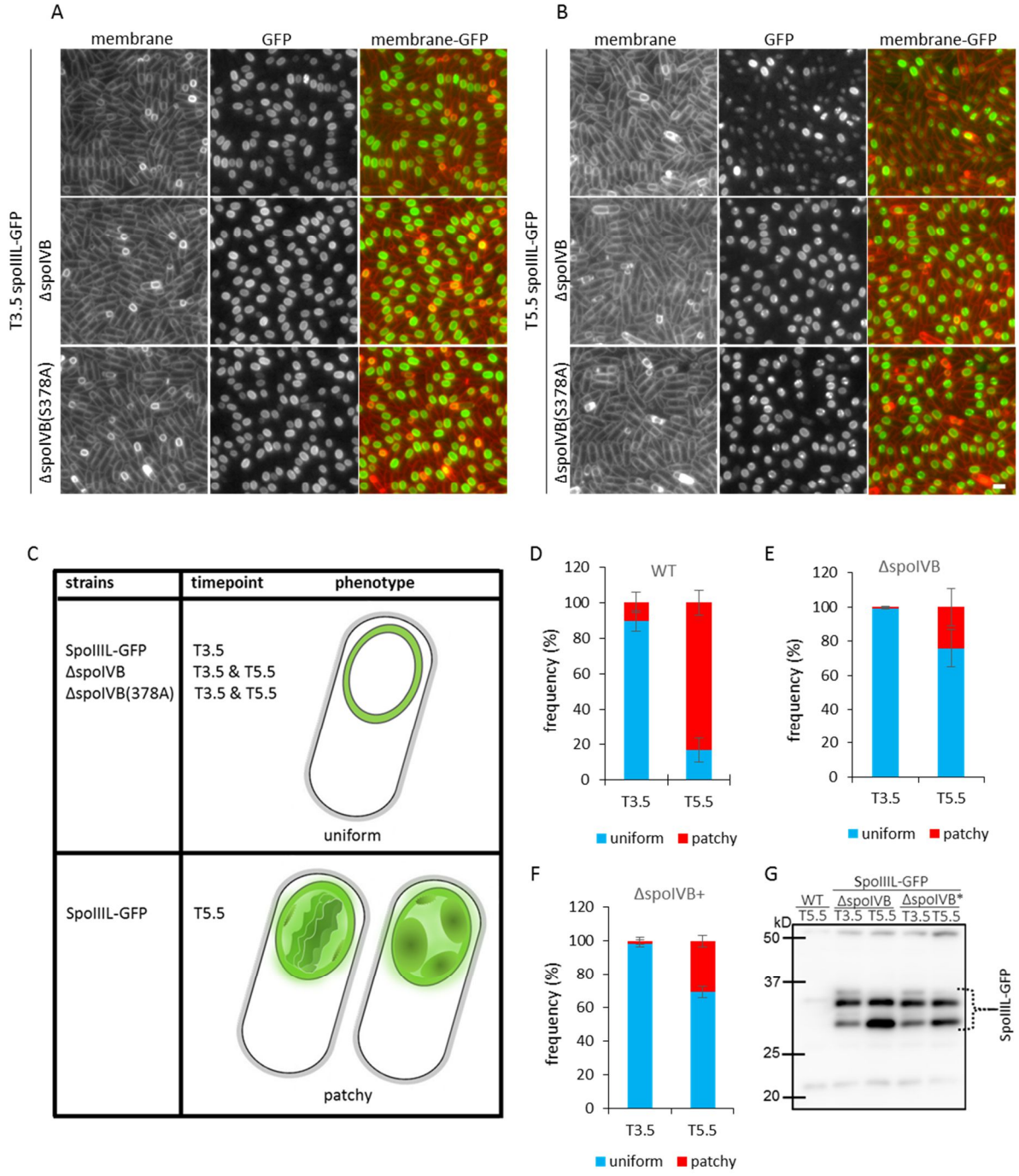

Fig 3.8 SpoIVB, and the SpoIVB*catalytic mutant influences SpoIIIL localization. Fluorescence localization of SpoIIIL-GFP in WT cells, *ΔspoIVB* single mutant, and Δ*spoIVB** catalytic mutants strains at T3.5 when most forespores harbour uniform SpoIIIL-GFP localization (A) and at T5.5 when most forespores harbour patchy SpoIIIL-GFP localization (B). GFP signal is false-coloured green in the merged images. Cell membranes were visualised using TMA-DPH fluorescent membrane dye and are false-coloured red in merged images. Scale bar = 2 µm. (C) Schematic description of the predominant SpoIIIL-GFP uniform and patchy (non-uniform) localization patterns in WT cells, *ΔspoIVB* single mutant, and Δ*spoIVB** catalytic mutant strains at time-points T3.5 and T5.5 after the onset of sporulation. (D) Quantification histogram showing proportion of cells (% ± STDEV, 3 biological

replicates) with uniform (blue) and patchy (red) SpoIIIL-GFP localization in WT cells at T3.5 and T5.5 after the onset of sporulation. n > 300 per replicate, per time-point, per strain. (E) Quantification histogram showing proportion of cells (% ± STDEV, 3 biological replicates) with uniform (blue) and patchy (red) SpoIIIL-GFP localization in ΔspoIVB single mutant strains at T3.5 and T5.5 after the onset of sporulation. n > 300 per replicate, per time-point, per strain. (F) Quantification histogram showing proportion of cells (% ± STDEV, 3 biological replicates) with uniform (blue) and patchy (red) SpoIIIL-GFP localization in *ΔspoIVB** catalytic mutant strains at T3.5 and T5.5 after the onset of sporulation. n > 300 per replicate, per time-point, per strain. (G) Immunoblot analysis of SpoIIIL-GFP in cell lysates of sporulating Δ*spoIVB* single mutant, and *ΔspoIVB** catalytic mutants strains at T3.5 when most forespores harbour uniform SpoIIIL-GFP localization (A) and at T5.5 when most forespores harbour patchy SpoIIIL-GFP localization. As controls, a cell lysate from sporulating cells collected at T5.5 from a WT strain that does not contain GFP was included. SpoIIIL-GFP was immunodetected using anti-GFP antibodies. The positions of SpoIIIL-GFP bands are indicated.

Consistent with our hypothesis, Immunoblot analysis of the Δ*spoIVB** catalytic mutant (Fig. 3.8 G) was similar to the immunoblot data obtained for the Δ*spoIVB* single mutant (Fig. 3.7 C, & Fig 3.8 G). The immunoblot data which would always show four bands in WT scenario at T5.5, only showed three bands for both the Δ*spoIVB* single mutant and the Δ*spoIVB** catalytic mutant. In both the Δ*spoIVB* single mutant and the Δ*spoIVB** catalytic mutant, when counting downwards from higher molecular weight to lower molecular weight, the top most SpoIIIL-GFP band was most faint at T5.5, while the intensity of the second and fourth bands increased at T5.5.

Generally, in the WT, when counting downwards from higher molecular weight to lower molecular weight, there appears to always be an increase in the intensity of the second, the third, and the fourth SpoIIIL-GFP protein bands, while the intensity of the first SpoIIIL-GFP band decreases over time as seen in the previous western blot images (like in Fig. 3.2). But in the Δ*spoIVB* single mutant and the Δ*spoIVB** catalytic mutant, the third band is absent at all time points assayed, while there is an observed increase in the intensity of the second and fourth protein bands at T5.5.

In summary, these results suggest that the catalytic site of SpoIVB as well as the protease SpoIVB itself, are both particularly required for the characteristic localization pattern and stability of SpoIIIL.

3.3.9 SpoIIQ, and consequently the engulfing membrane is required to maintain the stability and proper localization pattern of SpoIIIL

It is a well known fact that during engulfment, a transenvelope complex, called the A-Q complex, assembles in the membranes surrounding the forespore[14,59,127] (see introduction). Upon engulfment completion, the forespore becomes suspended in the mother cell cytoplasm as a free protoplast (or endospore) surrounded by two membranes, an inner membrane deriving from the forespore as well as an outer membrane deriving from the mother cell[29,57,58]. The A-Q complex assembles in these membranes enveloping the spore, with the extracellular domain of SpoIIQ interacting with the extracellular domain of SpoIIIAH to establish a transenvelope connection between the mother cell and the forespore[14,21,26,97–99]. Consistent with this interaction, SpoIIIAH localization within the forespore outer membranes depends on SpoIIQ[14,21,63,98]. It is believed that the A-Q complex proteins localize to the engulfing membranes and are required to maintain or mediate the physiology and transcription potential of the forespore, as well as the activity of the late forespore σ factor, σ^{G}[14,47,63]. Hence, the A-Q complex which is primarily stabilized by the SpoIIQ-AH interaction, is also required for the stability of the membranes encompassing around the forespore.

To determine if SpoIIQ and the membranes surrounding the forespore are required for the proper localization of SpoIIIL, we imaged SpoIIIL-GFP hourly on a time course under a fluorescence microscope from T1.5 to T6.5 after the onset of sporulation, both in WT condition and in the absence of SpoIIQ.

As hypothesized, the proper localization of SpoIIIL was significantly disrupted in the absence of SpoIIQ (Fig 3.9). The normal WT localization phenotype with SpoIIIL localizing uniformly around the forespore beginning at early timepoints T2.5 and also localizing within the forespore as patches at later timepoints beyond T3.5 was evident, but this was not the case in the SpoIIQ mutant. In the SpoIIQ single mutant however, SpoIIIL-GFP was seen as single or multiple green fluorescent foci or dots within the forespore cytoplasm. This data however prompted us to consider the possibility that SpoIIQ and consequently the membranes surrounding the forespore may also be influencing the stability of SpoIIIL.

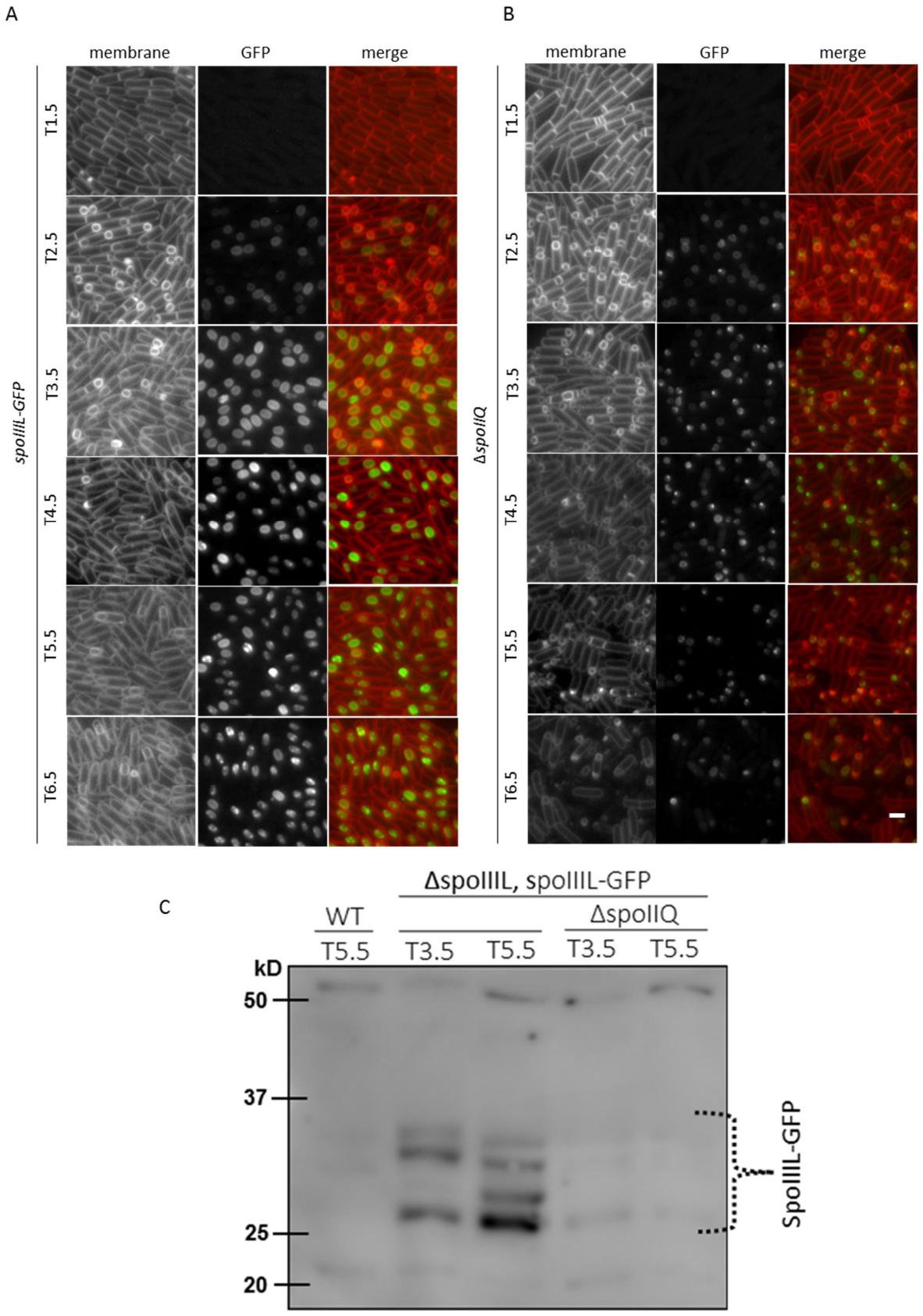

Fig 3.9 SpoIIQ is required for the stability and proper localization of SpoIIIL. Fluorescence localization of SpoIIIL-GFP in WT cells (A), and Δ*spoIIQ* single mutants (B), during a sporulation time-course. GFP signal is false-coloured green in the merged images. Cell membranes were visualised using TMA-DPH fluorescent membrane

dye and are false-coloured red in the merged images. Scale bar = 2 µm. (C) The A-Q Complex integral protein SpoIIQ and consequently, the engulfing membrane, influences SpoIIIL stability. Immunoblot analysis of SpoIIIL-GFP in cell lysates of sporulating WT cells as well as Δ*spoIIQ* single mutant strains at T3.5 and at T5.5. As controls, a cell lysate from sporulating cells collected at T5.5 from a WT strain that does not contain GFP was included. SpoIIIL-GFP was immunodetected using anti-GFP antibodies. The position of SpoIIIL-GFP four bands is indicated.

To further determine whether SpoIIQ and consequently the membranes surrounding the forespore are required for the stability of SpoIIIL, we performed Immunoblot analysis of SpoIIIL-GFP in cell lysates of sporulating WT cells as well as in cell lysates of Δ*spoIIQ* single mutant strains at T3.5 and at T5.5. As controls, a cell lysate from sporulating cells collected at T5.5 from a WT strain that does not contain GFP was included. SpoIIIL-GFP was immuno-detected using anti-GFP antibodies.

Generally, in the WT immunoblot at T5.5, when counting downwards from higher molecular weight to lower molecular weight, four SpoIIIL-GFP bands are always present. In the Δ*spoIIQ* single mutant however, all four bands usually observed in WT condition were either absent or too negligible to be noticed, at all time points assayed.

In summary, these results suggest that SpoIIQ and consequently the membranes surrounding the forespore are required for the proper localization pattern as well as the stability of SpoIIIL. This summary does not exclude the fact that the absence of SpoIIQ might be eliciting a much wider spectrum of cellular effects upon the forespore and that SpoIIIL may just be one of the recipients of this much wider spectrum of cellular effect.

3.4 Discussion

In this chapter, building upon our hypothesis that SpoIIIL is required for σ^G regulation, forespore morphology, and undergoes proteolysis within the forespore, we found that SpoIIIL contributes to the timely regulation of σ^G and that the σ^G dependent forespore resident protease SpoIVB and its catalytic site are required for the change in localization as well as the stability of SpoIIIL. We also found that the manner of localization of SpoIIIL is inconsistent with the characteristic localization pattern of the A-Q complex proteins thereby supporting our hypothesis that SpoIIIL is unlikely to be a component of the A-Q complex.

Furthermore, microscopic analysis revealed that the localization pattern of SpoIIIL remained consistent when either the C-terminal or N-terminal fusion of GFP to SpoIIIL ORF was analysed.

Also, site directed mutagenesis of the SpoIIIL ORF at 10 different sites also did not affect the localization phenotype of SpoIIIL. In summary, protease accessibility assay of both the C-terminal and N-terminal GFP fusions of SpoIIIL revealed that SpoIIIL is not surface exposed suggesting that SpoIIIL is inaccessible from the intermembrane space.

3.4.1 What is the role of SpoIIIL

Our data so far suggests that the role of SpoIIIL revolves mainly around spore shape and σ^G regulation (Fig 3.1 D & E). How SpoIIIL contributes to shape is not yet clear but may likely depend on its interaction with certain spore coat and cortex proteins since spore envelope composition and dynamics is strongly linked to shape[91]. Therefore, future work will investigate the relationship between SpoIIIL and key envelope proteins as well as proteins involved in envelope synthesis in order to reveal the exact mechanism by which SpoIIIL influences spore shape. Additionally, since *spoIIIL* is required for the proper timing of σ^G activity, but not for maintaining σ^G activity late into spore development (Fig 3.1 D), a possible role for SpoIIIL could be that it is involved in the regulation of σ^G activity. How SpoIIIL manages to contribute to the regulation of σ^G activity is also not completely clear. However, a possible explanation could be that a certain amount of indirect interaction of SpoIIIL with the forespore DNA, is important in order to ensure timely σ^G activation as well as timely σ^G downregulation. Interestingly, this inference is deduced from the observation that at T3.5 when SpoIIIL localized uniformly around the forespore membranes (Fig 3.3 A) and probably furthest away from the forespore DNA, σ^G activity was highest in the WT (Fig 3.1 D) and at time points around or after T5 when SpoIIIL started localizing as patches in the forespore cytoplasm, probably closer in proximity to the forespore DNA, that σ^G activity was also decreasing further. Future work encompassing SpoIIIL-DNA interactions as well as protein-DNA co-localization studies could reveal the possible underlying mechanisms of interaction and effects of proximity of SpoIIIL with the DNA during spore development.

3.4.2 What is the significance of SpoIIIL'S localization and SpoIVB mediated proteolysis

The localization pattern of SpoIIIL differs from the localization pattern of the A-Q complex proteins as already previously mentioned above because SpoIIIL is not enriched at the engulfing membrane. Certain *Bacillus subtilis* proteins which affect spore shape like SsdC localizes as a ring-like structure in the peripherial mothercell membrane towards the mother

cell proximal pole of the forespore[91]. Since SpoIIIL affects shape and shape is strongly linked to the spore envelope, some integral envelope proteins like SpoIVA, SpoVM and SpoVID have therefore been compared to SpoIIIL. These envelope proteins appear to closely follow the mother cell membrane as it engulfs the forespore and sometimes form an almost complete ring of fluorescence as seen with SpoIIIL[140]. Our data however does not suggest that SpoIIIL is an envelope protein considering the fact that it localizes in the cytoplasm at later stages of spore development and has not been implicated in successive scaffold formation like the envelope proteins.

An interesting question that remains unanswered is why the significant change in SpoIIIL localization from uniform localization around the membrane surrounding the forespore to patchy-like localization in the forespore cytoplasm. It is common knowledge that certain post-translational modifications of a protein often result in new or modified biological activities[141]. Although our data suggest that the forespore resident protease SpoIVB and its catalytic site are required for this change in localization as well as the stability of SpoIIIL (Fig 3.3 & Fig 3.7 A & B, & Fig 3.8), it is yet to be clearly established whether the change is directly related to SpoIIIL's function. Therefore, future work will seek to establish the link between the posttranslational modification of SpoIIIL and its consequent biological activity. Furthermore, highly sophisticated microscopic tools will be employed to reveal possible similarities between the localization pattern of SpoIIIL, the shape-influencing envelope proteins, as well as any sporulation protein that may localize in similar manner as SpoIIIL.

3.4.3 SpoIIIL is unlikely to be a component of the A-Q complex

In this study we have been able to show that the 59 amino acid, 9.6kDa forespore resident protein called SpoIIIL, that is transcribed under σ^{F} [28] and has a ~50% sporulation efficiency (Fig 3.2.E & 3.3E) is unlikely to be a component of the A-Q complex. Similar to what was obtained in this study (Fig 3.2 E), the reported sporulation efficiency for the A-Q complex single mutants is around 0.001 – 0.003% except Δ*spoIIIAH* and Δ*gerM* with ~5% [38,127], or Δ*spoIIQ* with 0.01% [127]. That the Δ*spoIIIL* single mutant shows a sporulation efficiency of ~50% clearly indicates that it really does not impact the cell as much as the other A-Q complex proteins do and therefore cannot be said to be as vital for sporulation as the other A-Q complex proteins.

Furthermore, the unquantified phenotypes of the A-Q complex proteins as previously reported also includes rounder & irregular forespores, as well as reduced σ^G activity [28,38,62,67,80,123,127,129]. In this work however, the roundness phenotype of the forespore as well as the σ^G activity has been quantified for SpoIIIL and for three select A-Q complex proteins namely SpoIIILAH, SpoIIIAG* and GerM (see section 3.3.2 and 3.3.3). Generally, spores of the Δ*spoIIIL* single mutant became rounder than WT overtime (Fig 3.1 E&F) but not rounder than the spores of the A-Q complex single mutants (Fig 3.2 A-D). Also, the defect in σ^G activity observed for the A-Q complex is generally more severe than that observed for SpoIIIL (Fig 3.2 A-D). It is common knowledge that the A-Q complex maintains the transcription potential as well as σ^G activity of the spore[80]. Our results suggest that while *spoIIIL* is required for the proper timing of σ^G activity, it is not required for maintaining σ^G activity late into development (Fig 3.1 D).

Summarily, the reported localization pattern of the A-Q complex proteins [38,80,127–129] is not consistent with the observed localization pattern of SpoIIIL (Fig 3.3 A & B). While the A-Q complex proteins are enriched in, and follow the engulfing membrane, SpoIIIL was not observed to behave in a similar manner. Instead, SpoIIIL was observed to localize uniformly around the forespore membrane at a time point that coincides with the completion of engulfment and changed its localization later in development to look like intriguing patchy-like structures in the forespore cytoplasm (Fig 3.3 A & B). The reason for the change in localization for SpoIIIL from uniform-membrane localization to patchy-cytoplasmic localization is not yet entirely clear. However, this manner of localization which is inconsistent with the characteristic localization pattern of the A-Q complex proteins only seem to further support our hypothesis that SpoIIIL is unlikely to be a component of the A-Q complex. This result chapter successfully leads us to the next result chapter where we see more of the connection between spore shape, cortex assembly and peptidoglycan precursor biosynthesis as well as the involvement of a strong genetic partner alongside SpoIIIL in the spore shape determination pathway.

SpoIIIL and MurAB are strongly required for cortex synthesis and sporogenesis

4.1 Disclaimer

This is to acknowledge that Chris Rodrigues, has contributed to the work presented in this chapter, by developing the Tn-seq screen on the SpoIIIL mutant and for providing all the Tn-seq data that was then used to identify potential hits in the *spoIIIL* mutant background.

4.2 Introduction to results

According to the data presented so far (in results section 3 above and in Meeske et al,[28]), SpoIIIL seems to be significantly involved in the spore shape determination pathway as well as in σ^G regulation pathway, although it was not clear whether SpoIIIL was more involved in either pathway than the other. In cells lacking SpoIIIL, the forespore becomes smaller and rounder, and σ^G activity is improperly regulated (Fig 3.1).

It is well documented that the development of the spore is intimately tied to the morphogenesis of its multi-layered envelope and the maintenance of bacterial shape is linked to the organization, assembly and remodelling of the cell envelope and sacculus[91,142–145].

In this chapter, following the transposon-sequencing data obtained by C. Rodrigues, and via microscopic and immunoblot analysis, we investigated the possible genetic pathways and essential genetic partners of the poorly-characterized gene renamed as *spoIIIL* (previously known as *yqzE*) during sporulation. Hence, we discovered that *murAB* is required for sporulation in cells lacking *spoIIIL* although MurAB is not required for the stability and localization of SpoIIIL. Finally, our data illustrated the strong synergy that exist between SpoIIIL and MurAB in the cortex assembly genetic pathway during sporulation in *B. subtilis*.

4.3 Results

4.3.1 Tn-seq rationale and the identification of MurAB

To get a clearer understanding of which pathway to better categorize SpoIIIL, a transposon sequencing (Tn-seq) experiment was performed[28,97]. Tn-seq is an analysis that is done to discover potential genes that become essential in a mutant background. This is indicated by the amount of transposable elements or transposons inserted by a transposase enzyme into the genetic sequence of the discovered genes. Thus, the discovered genes could reveal vital genetic interaction partners of SpoIIIL and the cellular pathways they are required in (see materials and methods section 2.8)[28,146–148].

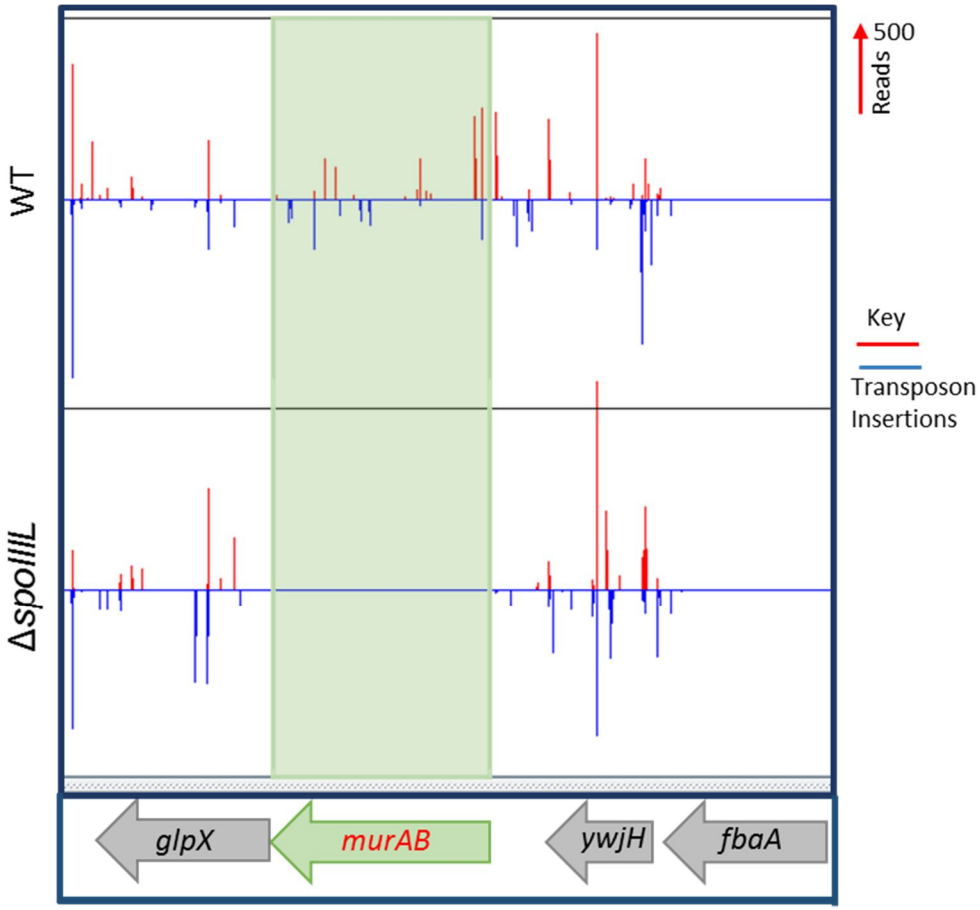

Fig 4.1: Transposon sequencing reveals genes that are important for sporulation in the absence of *spoIIIL*. (A) Tn-seq profile at the *murAB* genomic loci (shaded region) showing many transposon insertions in WT (bDR2413) and none in the *spoIIIL* mutant (bCR1236). Tn-seq profiles were prepared using the genome browser and annotation tool (Artemis) for all libraries after 24 hrs growth and sporulation in exhaustion medium. Height of vertical red or blue lines represent the number of transposon-sequencing reads at each position. Shaded regions illustrate the significant reduction in sequencing reads at the *murAB* loci.

For example, when a WT strain and a mutant strain like Δ*spoIIIL* are exposed to the same transposons or the same transposase enzyme which incorporates transposons into susceptible genes, the transposons are then incorporated into certain genes in both the WT strain and the Δ*spoIIIL* strain. If transposons are incorporated into a hypothetical "*gene A*" in the WT strain, but not incorporated into the same "*gene A*" in the Δ*spoIIIL* mutant, then "*gene A*", also refered to as a Tn-seq hit, is therefore considered to be essential for sporulation only in the Δ*spoIIIL* strain (see materials and methods section 2.8).

The analysis of the Tn-seq data identified a set of potential genes that appear to be required for sporulation specifically in the absence of *spoIIIL*. For instance, (in Fig 4.1 above), *murAB* accepts transposon insertions in the WT background.

Interestingly, validation of the Tn-seq screen revealed that *murAB* neither tolerated nor accepted transposon insertions in the Δ*spoIIIL* mutant strain when compared to the wild-type strain. Since transposon insertions were largely underrepresented in the *ΔspoIIIL* mutant especially at the *murAB* foci, *murAB* was therefore considered vital for sporulation in the *ΔspoIIIL* mutant background but not in the wild-type background.

4.3.2 The other Tn-seq hits SpsD, McsB, SsdC, PbpF, discovered alongside MurAB, neither synergizes strongly with SpoIIIL nor influences SpoIIIL localization

The Tn-seq data obtained so far (section 4.3.1) suggests that MurAB is required for sporulation in the absence of SpoIIIL. Considering the fact that the peptidoglycan precursor biosynthesis (UDP-N-acetylglucosamine 1-carboxyvinyltransferase) gene *murAB* which is also required for efficient spore engulfment[79,149,150] synergizes strongly with SpoIIIL, we wondered whether the other Tn-seq hits discovered alongside *murAB* also synergizes strongly with SpoIIIL in sporulation. This is usually the validation step required to determine how essential these genes are during sporulation when combined with *spoIIIL*. The discovered Tn-seq hits to be assayed were *spsD*, which takes part in spore coat polysaccharide synthesis, and is required for spore crust assembly and legionaminic acid synthesis[151]; *ctpB*, a carboxy-terminal processing serine protease that cuts *spoIVFA*, resulting in processing of pro-SigK as well as the control of sigK[25,84,135,136]; *mcsB*, a protein arginine kinase that tags proteins for degradation by ClpC-ClpP and is involved in the control of CtsR-dependent repression[152–154]; *thiD* a gene involved in thiamine pyrophosphate biosynthesis[155–157]; *pbpF*, a class A penicillin-binding

protein and bifunctional glycosyltransferase/transpeptidase that participates in synthesis of spore peptidoglycan[83,158,159]; and *ssdC* (formerly *ydcC*), a MucB/RseB-like protein that binds lipopolysaccharide in diderm bacteria, influences spore shape and the assembly of the spore cortex in monoderm *Bacillus subtilis* [28,91].

Hence, we made double mutants of *spoIIIL* with each of the discovered Tn-seq hits, and determined the average sporulation efficiency data for WT, and the following: *ΔspoIIIL ΔspsD*, *ΔspoIIIL ΔmcsB, ΔspoIIIL ΔssdC, ΔspoIIIL ΔpbpF* double mutant spores at T30 after the onset of sporulation. Sporulation efficiency assays were done as described in the materials and methods section of this work.

According to our hypothesis, we expect each pair of the Tn-seq hits double mutants with *spoIIIL* to exhibit a cumulative synergistic effect on the spore that would not be observed in the Tn-seq hits single mutants alone. However, if the double mutants with *spoIIIL* do not show significant synergy, it will be confirmed that the genes aren't really essential in sporulation under the *spoIIIL* single mutant background.

Interestingly, the average sporulation efficiency data of *ΔspoIIIL ΔpbpF* (~4%)*, ΔspoIIIL ΔspsD* (~5%)*, ΔspoIIIL ΔmcsB* (~5%)*, ΔspoIIIL ΔctpB* (~6%) were negligible compared to the average sporulation efficiency data of their corresponding single mutants *ΔpbpF* (~69%), *ΔspsD* (~30%), *ΔmcsB* (~76%), *ΔctpB* (~80%) respectively. While the average sporulation efficiency data for *ΔspoIIIL ΔssdC* was (~0.00004%) compared to its corresponding single mutant *ΔssdC* (~19%). Strikingly, the *ΔspoIIIL ΔmurAB* double mutant spores did not survive the heat kill or sporulation efficiency assay, ultimately yielding nil or dead spores compared to the *ΔmurAB* single mutant which had ~44% spores. Thus, all the double mutants assayed revealed no strong synergy except in the *ΔspoIIIL ΔssdC* and *ΔspoIIIL ΔmurAB* double mutants where sporulation was significantly impaired compared to what was observed separately for the *spoIIIL* or *ydcC* or *murAB* single mutants (Fig 4.2 C & Fig 4.4 B).

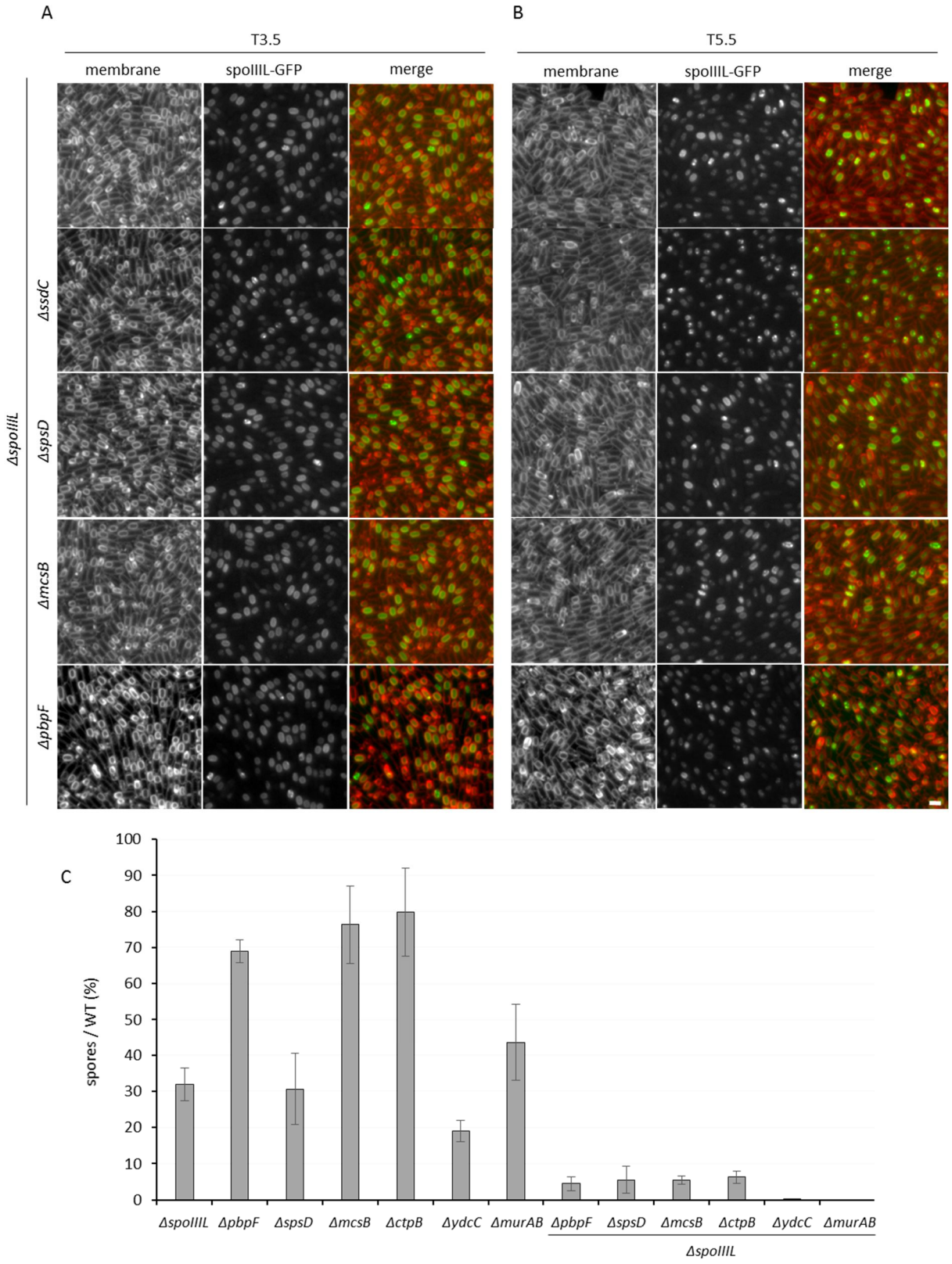

Fig 4.2 The other Tn-seq hits SpsD, McsB, SsdC, PbpF, discovered alongside MurAB, neither influences SpoIIIL localization nor synergizes strongly with SpoIIIL. Fluorescence localization of SpoIIIL-GFP in WT spores as well as in *ΔspoIIIL ΔspsD, ΔspoIIIL ΔmcsB, ΔspoIIIL ΔssdC, ΔspoIIIL ΔpbpF* double mutant spores at T3.5 when most

forespores harbour uniform SpoIIIL-GFP localization (A) and at T5.5 when most forespores harbour patchy SpoIIIL-GFP localization (B). GFP signal is false-coloured green in the merged images. Cell membranes were visualised using TMA-DPH fluorescent membrane dye and are false-coloured red in merged images. Scale bar = 2 µm. (C) Average sporulation efficiency data for WT, *ΔspoIIIL, ΔspsD, ΔmcsB, ΔssdC, ΔpbpF* single mutant spores. Sporulation efficiency assays were done as written in the materials and methods section of this work. Error bars represent standard deviation of three biological replicates.

Furthermore, we reasoned that although only *ssdC* and *murAB* showed strong synergy with *spoIIIL* in sporulation efficiency, it is also possible that via another genetic pathway, the discovered Tn-seq hits might be required for the localization of SpoIIIL. Recall, that it has already been reported that SsdC is most likely not a part of the developing forespore and is not enriched in the engulfing mother cell membrane even though it somehow affects spore shape[91].

To determine whether the Tn-seq hits are required for the characteristics localization phenotype of SpoIIIL, we expressed SpoIIIL-GFP as the sole source of SpoIIIL in the Δ*spsD*, Δ*mcsB*, Δ*ssdC*, Δ*pbpF*, Δ*ctpB* single mutant spores and imaged them at T3.5 when most forespores harbour uniform SpoIIIL-GFP localization and at T5.5 when most forespores harbour patchy SpoIIIL-GFP localization after the onset of sporulation.

Surprisingly, the Tn-seq hits were not required for SpoIIIL localization since there was no change in the usual localization pattern of SpoIIIL in the Tn-seq mutants assayed. Therefore, the Tn-seq hits SpsD, McsB, PbpF, and CtpB discovered alongside MurAB, neither influences SpoIIIL localization nor synergizes strongly with SpoIIIL in sporulation efficiency (Fig 4.2 & Fig 3.7).

4.3.3 MurAB does not influence SpoIIIL localization and stability

The data above (in section 4.3.2) indicated that the other Tn-seq genes discovered alongside *murAB* in the *spoIIIL* screen did not influence spoIIIL localization. Since *murAB* on the hand appears to synergize strongly with *spoIIIL* in sporulation, we expected that MurAB would also strongly influence SpoIIIL localization and stability.

To determine whether MurAB is particularly required for the characteristics localization phenotype of SpoIIIL, we expressed SpoIIIL-GFP as the sole source of SpoIIIL in the Δ*murAB* single mutant and imaged the spores at T3.5 when most forespores harbour uniform SpoIIIL-

GFP localization and at T5.5 when most forespores harbour patchy SpoIIIL-GFP localization after the onset of sporulation.

Surprisingly, *murAB* was not required for SpoIIIL localization. Upon closer observation, there was no observable change in the usual localization pattern of SpoIIIL-GFP in the Δ*murAB* single mutant when compared to WT. Therefore, MurAB does not influence SpoIIIL localization (Fig 4.3).

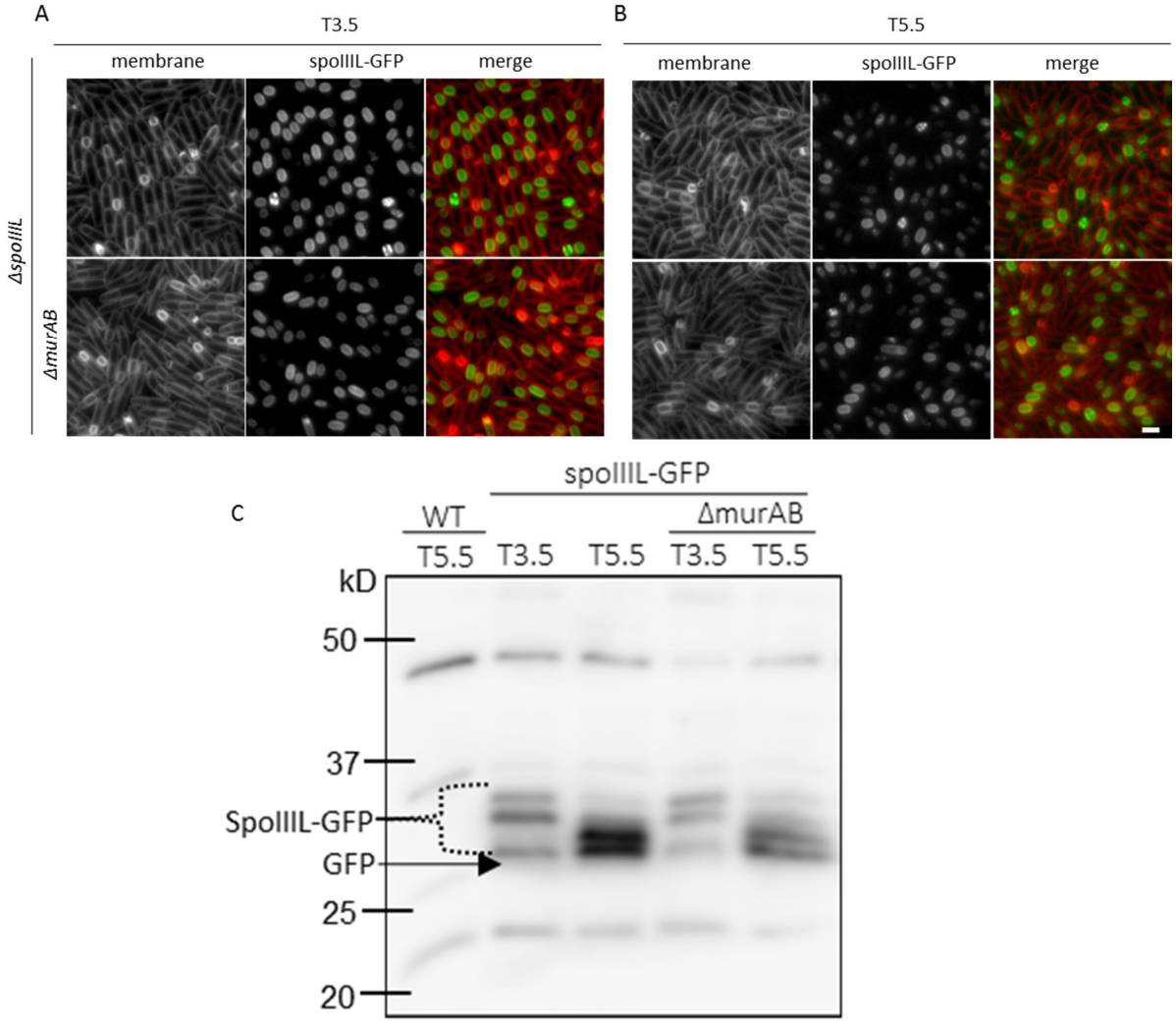

Fig 4.3 MurAB does not influence SpoIIIL localization and stability. Fluorescence localization of SpoIIIL-GFP in WT spores as well as in *ΔmurAB* single mutant spores at T3.5 when most forespores harbour uniform SpoIIIL-GFP localization (A) and at T5.5 when most forespores harbour patchy SpoIIIL-GFP localization (B). GFP signal is false-coloured green in the merged images. Cell membranes were visualised using TMA-DPH fluorescent membrane dye and are false-coloured red in the merged images. Scale bar = 2 µm. (C) Immunoblot analysis of SpoIIIL-GFP in cell lysates of sporulating WT and *ΔmurAB* single mutant strains collected at T3.5 and T5.5. As controls, a cell lysate from sporulating cells collected at T5.5 from a WT strain that does not contain GFP was included. SpoIIIL-GFP was immunodetected using anti-GFP antibodies. The position of SpoIIIL-GFP and GFP are indicated.

Furthermore, we reasoned that *murAB* may impact the stability of *spoIIIL*, considering the strong synergy in sporulation efficiency observed in the *ΔspoIIIL ΔmurAB* double mutant (Fig 4.4B) and the essentiality of the *murAB* gene observed in the *spoIIIL* Tn-seq screen (Fig 4.1).

To further determine whether *murAB* is required for the stability of *spoIIIL*, we performed Immunoblot analysis of SpoIIIL-GFP in cell lysates of sporulating WT cells as well as in cell lysates of the Δ*murAB* single mutant strains at T3.5 and at T5.5. As controls, a cell lysate from sporulating cells collected at T5.5 from a WT strain that does not contain GFP was included. SpoIIIL-GFP was immunodetected using anti-GFP antibodies. The position of SpoIIIL-GFP and GFP are indicated.

Generally, in the WT immunoblot at T5.5 when counting downwards from higher molecular weight to lower molecular weight, four SpoIIIL-GFP bands are always present. Unexpectedly, in the Δ*murAB* single mutant however, all four bands usually observed in WT condition were present in the Δ*murAB* single mutant, and the intensity of the bands were similar to what was obtained for the WT, at all time points assayed.

Summarily, these results indicates that MurAB is required neither for the proper localization nor the stability of SpoIIIL. The later suggesting that a direct protein-protein interaction between these two proteins is most unlikely.

4.3.4 *ΔspoIIIL ΔmurAB* forespores are severely impaired in cortex synthesis and sporogenesis

Spore development is intimately coupled to the morphogenesis of the spore envelope and the spore envelope is mainly composed of the outermost crust, the outer coat, the inner cortex layer, and the innermost germ cell layer[91]. Previous data in (section 4.3.2, Fig 4.2 C, & Fig 4.4 B) has shown that *ΔspoIIIL ΔmurAB* double mutant spores are severely deficient in sporulation. Since spore shape determination is also dependent on a properly assembled cortex and its peptidoglycan composition, and the spore cortex is largely responsible for the heat resistance and sporulation efficiency of spores, we reasoned that the severe deficiency in sporulation observed in the *ΔspoIIIL ΔmurAB* double mutant spores may be linked to an under-developed or immature cortex.

Proper cortex assembly results in a change in forespore refractivity, causing forespores to become phase bright as they mature[91]. An indirect technique involving the imaging of the

phase brightness of spores can be used to measure and analyse the level of development, maturity, and assembly of the spore cortex.

To determine whether *murAB* is required for proper cortex assembly, we performed phase bright imaging of the WT, Δ*spoIIIL*, Δ*murAB*, and Δ*spoIIIL* Δ*murAB* double mutant spores at T4, T7, T9, and T30 after the onset of sporulation and quantified the spores showing the proportion of cells (% ± STDEV, 2 biological replicates) with phase bright (blue) and phase dark (red) phenotype, per time-point, per strain (Fig 4.4 A & C).

At T4, the results show that about ~25% of the WT spores have become either completely or partially phase bright while only less than ~1% of the *ΔspoIIIL* mutant spores are either completely or partially phase bright.

At T7, about ~90% of WT spores have become either completely or partially phase bright, while around ~65% of the *ΔspoIIIL* mutant spores are either completely or partially phase bright.

At T9 however, the percentage of WT spores that have become either completely or partially phase bright remained at ~90% while the percentage of *ΔspoIIIL* mutant spores that have become either completely or partially phase bright rose to ~80%.

Furthermore, at T30, while the percentage of WT spores that have become either completely or partially phase bright remained at around ~92%, the percentage of *ΔspoIIIL* mutant spores that have become either completely or partially phase bright rose to ~92% suggesting that spores of the *ΔspoIIIL* single mutant undergoes a gradual and slower but eventual process of becoming phase bright compared to the WT. On the other hand, spores of the *ΔmurAB* single mutant appeared to mature slightly earlier than spores of the *ΔspoIIIL* single mutant but at a slower pace compared to the WT.

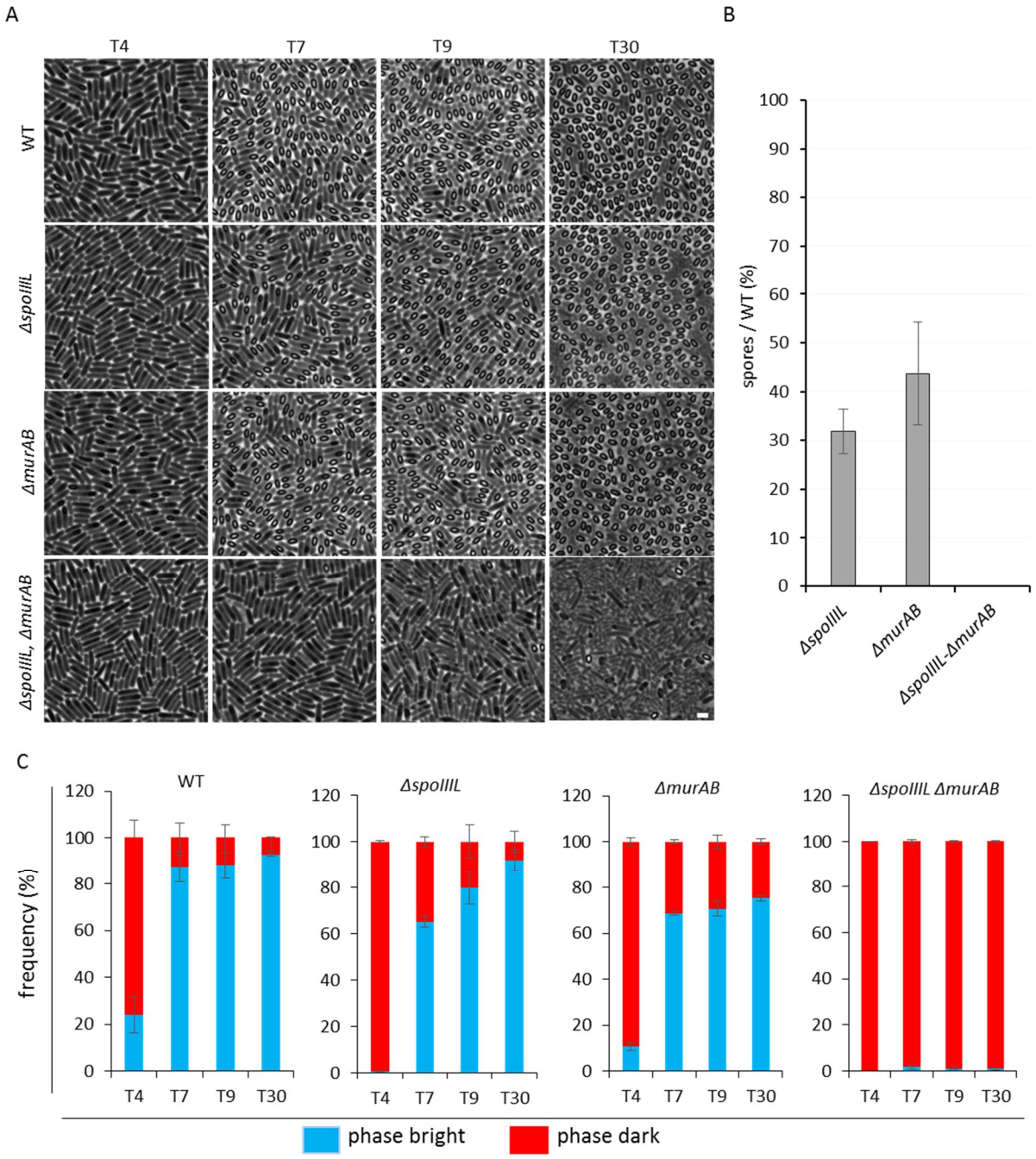

Fig 4.4 ***ΔspoIIIL ΔmurAB* impairs cortex synthesis.** (A) Microscopic imaging of the phase bright phenotype of WT, *ΔspoIIIL*, *ΔmurAB*, and *ΔspoIIIL ΔmurAB* double mutant spores at T4, T7, T9, and T30 after the start of sporulation. Cell membranes were visualised with TMA-DPH fluorescent membrane dye. Scale bar = 2 µm. (B) Average sporulation efficiency data for WT, *ΔspoIIIL*, *ΔmurAB*, and *ΔspoIIIL ΔmurAB* double mutant spores. Sporulation efficiency assays were done as inscribed in the materials and methods section of this work. Error bars represent standard deviation of three biological replicates. (C) Quantification histogram showing proportion of cells (% ± STDEV, 2 biological replicates) with phase bright (blue) and phase dark (red) phenotype in WT, *ΔspoIIIL*, *ΔmurAB*, and *ΔspoIIIL ΔmurAB* double mutant spores imaged at T4, T7, T9, and T30 after the onset of sporulation. n > 400 per replicate, per time-point, per strain.

Interestingly, cortex assembly (phase brightness) for the *ΔspoIIIL ΔmurAB* double mutant was slowest compared to WT or either of the *ΔspoIIIL* or *ΔmurAB* single mutants suggesting that a strong synergy exists between both single mutations in question. This is because the percentages of phase bright spores for the *ΔspoIIIL ΔmurAB* double mutant were ~0%, ~1.7%, ~1%, and ~0.8% at T4, T7, T9, and T30 for the double mutant respectively. Whereas, in comparison, the percentages of phase bright spores for the *ΔspoIIIL* single mutant were,~0.6%,~65%,~80%, and ~92% at T4, T7, T9, and T30 respectively and the percentages of phase bright spores for the *ΔmurAB* single mutant were, ~11%, ~68%, ~71%, and ~75% at T4, T7, T9, and T30 respectively (Fig 4.4 C).

Strikingly, at T9, the spores of the *ΔspoIIIL ΔmurAB* double mutant in general, exhibited great signs of senescence which became very evident at T30 where literally almost every spore seen under the microscopic was no longer viable (ie. dead and or lysed). But, this was never the case for any of the other three strains assayed (Fig 4.4 A). Thus, consistent with the phase bright microscopy experiments described earlier, these data indicate that *ΔspoIIIL ΔmurAB* double mutant is strongly impaired in cortex synthesis and assembly.

4.4 Discussion

In this chapter, building upon our hypothesis that SpoIIIL and MurAB are strongly required for cortex synthesis and sporogenesis, we found that the *murAB* which did not accept transposon insertions in the *ΔspoIIIL* mutant background as opposed to wild-type, also does not influence SpoIIIL localization and stability.

Furthermore, heat kill assays showed that the *ΔspoIIIL ΔmurAB* forespores are severely impaired in spore generation suggesting that a combination of both mutation brings sporulation completely to its knees. Surprisingly, employing protein-protein interaction assays, we found that MurAB does not affect the stability of SpoIIIL, suggesting that a direct protein-protein interaction between these two proteins is most unlikely even though these two proteins generate a very strong synergy together.

4.4.1 How does MurAB genetically Influence SpoIIIL?

The previous chapter led to our hypothesis that SpoIIIL and MurAB contributes to cortex assembly, and sporogenesis. In this chapter, we tested this hypothesis by examining the sporulation efficiency and cortex deficiency in *ΔspoIIIL ΔmurAB* forespores.

MurAB is a peptidoglycan precursor biosynthesis (UDP-N-acetylglucosamine 1-carboxyvinyltransferase) gene that is also required for efficient spore engulfment[79,149,150] and has been shown in this work to synergize strongly with SpoIIIL in Sporulation and in spore cortex assembly (Fig 4.4). Also, MurAB was found to be important only in situations where either the widely conserved and well-characterized DMP complex, consisting of SpoIID, SpoIIM, and SpoIIP which is required for forespore engulfment is compromised, or the widely conserved SpoIIIAH-SpoIIQ rachet-like mechanism which is required for engulfment efficiency is abolished[79]. In both scenario, forespore engulfment is the key process linking MurAB to the DMP and the A-Q complex. However, no similar connection has been reported to exist between SpoIIIL and either the DMP complex or the A-Q complex. Although it was previously thought that SpoIIIL is a component of the A-Q complex[28], it has now been shown in this work that SpoIIIL is not a component of the A-Q complex since it neither localizes like the A-Q complex genes by following the engulfing membrane, nor synergizes with the A-Q complex genes in a similar manner (sections 3.3.2 & 3.3.3). It would have been logical to think that MurAB and SpoIIIL could interact indirectly via the A-Q complex's participation in engulfment, had SpoIIIL been confirmed to be a component of the A-Q complex. Unfortunately, this is not the case.

Peptidoglycan precursor synthesis is an important step towards successful engulfment and cortex assembly. MurAB catalyzes the synthesis of UDP-MurNAc (Uridine-diphosphate N-acetylmuramic acid) from UDPGlcNAc (Uridine-diphosphate N-acetylglucosamine) and phosphoenolpyruvate which is the first devoted step during the biosynthesis of PG, an integral and essential component of the bacterial cell wall[81,150]. SpoIIIL on the other hand, has been shown in this work to be required for spore shape, cortex assembly, and the timing of σ^G activity (section 3.3.1). But, going by the fact that SpoIIIL is mainly enriched around the forespore membrane beginning at time-points T2.5 and reaching its peak enrichment at around T3.5 – T4.5, which overlaps with the time-point around engulfment completion (Fig 3.3), one might be tempted to suspect that SpoIIIL may not be unconnected with engulfment after all.

Furthermore, the DMP complex is required for engulfment while the SpoIIIAH-SpoIIQ interaction is believed to function like a zipper which stabilizes the engulfing membranes and helps the advancement of engulfment around the spore. Since MurAB becomes important in

the absence of either the DMP or the A-Q complex, and cortex assembly comes after engulfment[79], it would be logical to suppose an indirect interaction between MurAB and SpoIIIL at the stage immediately after engulfment during cortex synthesis and assembly. This hypothesis could be backed up by the fact that the *ΔspoIIIL ΔmurAB* double mutant forespores are severely impaired in cortex synthesis and consequently sporogenesis (section 4.3.4) even though the molecular processes underlying such interaction remains elusive.

Additionally, since recent studies have suggested that a combination of the *ΔmurAB* single mutant and mutants involved in engulfment enables the PG precursor synthesis role of MurAB which contributes to efficient engulfment, to become more prominent[79], one could begin to see SpoIIIL in another light; possibly as a tentative factor in engulfment.

Summarily, the exact direct or indirect mechanism by which *spoIIIL* interacts with *murAB* is yet to be elucidated but muropeptide analysis and more advanced protein-protein interaction analysis could assist future studies that seek to deconstruct the SpoIIIL-MurAB genetic interaction conundrum.

4.4.2 Why does MurAB not influence SpoIIIL localization and stability?

SpoIIIL is transcribed under the control of the initial forespore transcription factor σ^{F} [28] and has been shown to localize around the forespore membrane within the forespore cytoplasm, and SpoIIIL is also not surface exposed (results sections 3.3.3 & 3.3.4). MurAB on the other hand relies on the σ^{K} mediated upregulation for increased precursor synthesis in the mother cell compartment[89].

In light of this, one could easily arrive at the conclusion that SpoIIIL and MurAB are neither in the same cellular compartment nor in close vicinity within the cell to warrant or enable close genetic interactions or intracellular contact. Firstly, if both proteins in question are not in the same cellular compartment, it becomes tempting to rationalise that both proteins do not directly interact. Secondly, going by the cellular functions of MurAB being an enzyme with a known substrate (listed in section 4.4.1), SpoIIIL can also not be considered to be a substrate for MurAB and vice versa. Therefore, the supposed lack of direct interaction between MurAB and SpoIIIL, as well as the demarcation of both proteins by two membranes and an intermembrane space may contribute to the many possible reasons why MurAB does not influence the intracellular localization and stability of SpoIIIL.

Furthermore, several factors contribute to the stability of a protein invivo and in the case of SpoIIIL, these factors may not be limited to the influence of a single protein such as MurAB alone. Protein stability describes the potential of a particular pattern or patterns of a protein to survive over time and certain processes like protein unfolding, denaturation, degradation, conformational changes, enzymatic modifications and proteolytic cleavages may transform this 'pattern'[160]. Also, post-translational modifications (PTMs) can happen on certain specific amino acid residues situated within regulatory domains of specific proteins which are responsible for the control of a protein's stability[161]. Our fluorescence microscopy and immunoblot data in the previous chapter (section 3.3.8) rather showed a direct interaction between SpoIIIL and the forespore protease SpoIVB. Such interaction could leave SpoIIIL with some post-translational modification which contributes to the sequestration of SpoIIIL further deep into the forespore cytoplasm at later time-points (T5.5) during sporulation driving it physically further away from the forespore membrane and from the reach of MurAB which is on the opposite side of the membrane in the mother cell compartment.

In future works, several methods including but not limited to NMR, Raman microscopy, and more advanced fluorescence microscopy can be employed to investigate and follow protein structure, stability, synthesis and/or folding in cells including techniques, such as FReI (fast relaxation imaging) which allows for real-time assaying of a protein's thermal stability and folding kinetics within living cells with enhanced spatial resolution[162].

4.4.3 Why does SpoIIIL and MurAB double mutation significantly impact the cortex?

Based on the strong synergy observed in the *ΔspoIIIL ΔmurAB* double mutant forespores as regards cortex assembly and sporogenesis (Fig 4.4), we speculated that it is possible that a product of MurAB's enzymatic cascade or a vital process that MurAB is involved in during peptidoglycan precursor synthesis, could be strongly linked to SpoIIIL and SpoIIIL's intracellular activities including during σ^G regulation at the least upon the start of cortex synthesis and assembly. We therefore propose that future work should investigate SpoIIIL's σ^G regulation peak time-point which is between T3.5 and T4.5 after the onset of sporulation as well as any peptidoglycan precursor synthesis activity that occurs closest to the forespore membrane within the intermembrane space during this time-point.

Furthermore, MurAB is a alternative form of the essential *B. subtilis* protein MurAA, which acts as a UDP-N-acetylglucosamine 1-carboxyvinyltransferase, catalyzing the initial devoted

step of peptidoglycan precursor synthesis; which consists of the conversion of UDP-N-acetylglucosamine to UDP-N acetylglucosamine enolpyruvate that comes before the production of UDP-N-acetylmuramic acid[79]. It is possible that a different reaction pathway or product could be adopted or generated when either MurAA or MurAB (but not both) becomes the sole active paralog in the cell. We hypothesize that the data obtained for the *ΔspoIIIL ΔmurAB* double mutant forespores could be different when *ΔspoIIIL ΔmurAA* double mutant forespores are assayed instead. Either way, we are interested in discovering the exact convergence point for the activities of MurAB and SpoIIIL.

To investigate the exact convergence point of the activities of MurAB and SpoIIIL, what cellular pathways are mostly affected, and find out what products of peptidoglycan precursor biosynthesis that become more or less abundant in the cell when either MurAA or MurAB is the sole available paralog in the cell, an alternative analysis could be conducting muropeptide analysis in a *ΔspoIIIL ΔmurAA* double mutant where MurAB is the sole available paralog, as well as in a *ΔspoIIIL ΔmurAB* double mutant where MurAA is the sole available paralog in the cell. This experiment could reveal different possible pathways that the cell might adopt when MurAA or MurAB is the sole available paralog in the absence of SpoIIIL thereby providing indepth insight as to Why SpoIIIL and MurAB double mutation significantly impact the cortex. This leads us to the next result chapter where we see more of the cortex and coat proteins influencing SpoIIIL localization and stability.

The cortex and coat proteins are required for SpoIIIL localization and or stability

5.1 Disclaimer

This is to acknowledge that the work and experiments contained in this chapter was solely conducted by Odika Chimezie Progress

5.2 Introduction to Results

According to the data presented so far (in chapters 3 and 4 above), we have seen that the σ^F controlled forespore based protein SpoIIIL is either required for, or involved in σ^G regulation, forespore morphology, and undergoes proteolysis within the forespore. The data also elucidated the extent of cortex assembly and sporogenesis impairment incurred in cells of the *ΔspoIIIL ΔmurAB* double mutant.

In this chapter, knowing that the preservation of bacterial shape is linked to the organization, assembly and remodelling of the cell envelope[91], we therefore bring into consideration the many vital proteins involved in spore shape determination via spore cortex or coat synthesis as well as their relationship with SpoIIIL.

Hence, by employing several analytical and protein-protein interaction tools such as fluorescence microscopy, phase bright microscopy, heat kill assays, and western blots, we were able to deduce that the cortex and coat are required for the localization and or the stability of SpoIIIL.

Furthermore, our data illustrated the significance of σ^K as the "middle man" in the relationship between the forespore protease SpoIVB, and the cortex synthases SpoVD and spoVE and how this dynamic impacts SpoIIIL. Finally the intercellular or inter-compartmental effects of the coat proteins SpoIVA, SpoVM, and SpoVID upon SpoIIIL regarding its stability and localization, in the pathway towards cortex and coat assembly during sporulation in *B. subtilis* was also expatiated.

5.3 Results

5.3.1 SpoVD and SpoVE are required for SpoIIIL localization but not SpoIIIL stability

We previously reported (in section 3.3.3) that SpoIIIL localizes uniformly around the spore membrane at early time-points around T3.5 and changes overtime to a non-uniform patchy phenotype at later time-points around T5.5. The relationship between SpoIIIL and the cortex synthases responsible for PG synthesis is still not clear and we were interested in knowing whether the cortex synthases contribute to the observed change in SpoIIIL localization from uniform localization to patchy localization. Two vital enzymes that are important in cortex peptidoglycan synthesis in *B. subtilis* are the transpeptidase (SpoVD) and the transglycosylase (SpoVE). SpoVD is a class B penicillin binding protein that is thought to be directly responsible for cross-linking the peptidoglycan strands of the cortex while the product of spoVE is part of the SEDS group of proteins that usually participate in cell shape determination[89–91,163].

To get a better understanding of the relationship between SpoIIIL and cortex assembly, we expressed SpoIIIL-GFP in the absence of SpoVD or SpoVE or both and imaged the resultant spores under a fluorescence microscope at T3.5 when most forespores harbour uniform SpoIIIL-GFP localization and at T5.5 when most forespores harbour patchy SpoIIIL-GFP localization. We observed that the *ΔspoVD*, and *ΔspoVE* single mutants, as well as the *ΔspoVD ΔspoVE* double mutant seemed to have much less typical patches/clumps compared to the otherwise wild-type indicating that cortex assembly is required for the localization of SpoIIIL (Fig 5.1 A & B). Reciprocally, we also investigated whether SpoIIIL contributed to the localization of the cortex synthases by fusing either SpoVD or SpoVE to a fluorescent protein and imaging the cells under a fluorescent microscope at T3.5 and T5.5. The results obtained revealed that SpoIIIL is neither required for, nor involved in the localization of the cortex synthases (Appendix II, Figure S5.1).

During cortex assembly, the activities of SpoVD and SpoVE are interdependent meaning that either proteins cannot carry out their function in the absence of the other. Whereas the localization of SpoVD depends on SpoVE, SpoVD in turn protects SpoVE from *in vivo* proteolysis[89–91]. Therefore any phenotype observed in the absence of only one of the synthases is the same as the phenotype observed either in the absence of the other synthase or in the absence of both synthases. Hence, to more thoroughly characterize the impact of the cortex on the localization of SpoIIIL, we quantified the proportion of cells with uniform (blue)

and patchy (red) SpoIIIL-GFP localization in wild-type or *ΔspoVE* cells at T3.5 when most forespores harbour uniform SpoIIIL-GFP localization and at T5.5 when most forespores harbour patchy SpoIIIL-GFP localization after the onset of sporulation (Fig 5.1 C).

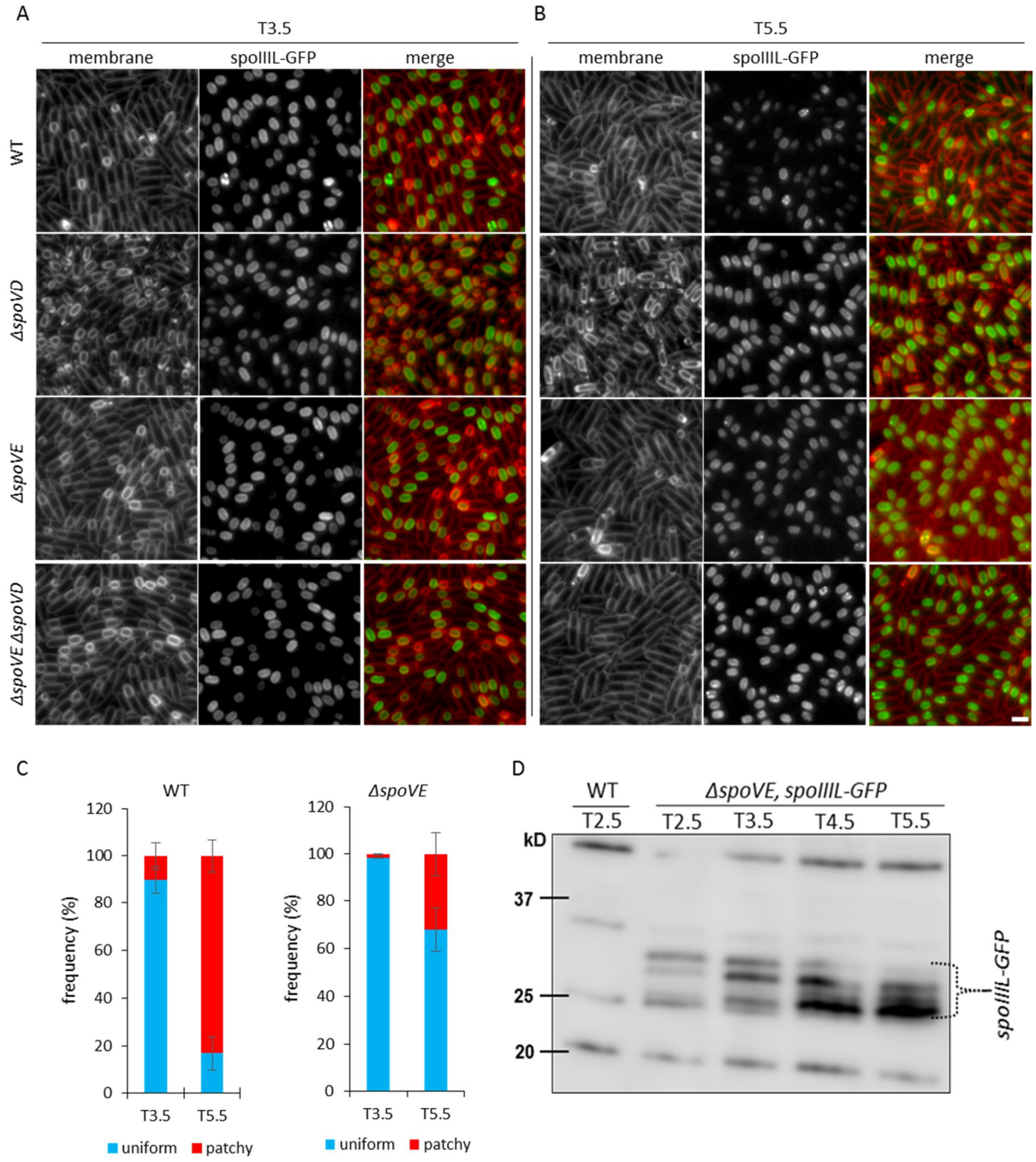

Fig 5.1 SpoVD and SpoVE influences SpoIIIL localization but not its stability. Fluorescence localization of SpoIIIL-GFP in WT cells as well as in the *ΔspoVD, ΔspoVE* single mutants, and the *ΔspoVD ΔspoVE* double mutant at T3.5 when most forespores harbour uniform SpoIIIL-GFP localization (A) and at T5.5 when most forespores harbour patchy SpoIIIL-GFP localization (B). GFP signal is false-coloured green in the merged images. Cell membranes were visualised using TMA-DPH fluorescent membrane dye and are false-coloured red in merged

images. Scale bar = 2 µm. C) Quantification histogram showing proportion of cells (% ± STDEV, 3 biological replicates) with uniform (blue) and patchy (red) SpoIIIL-GFP localization in WT or *ΔspoVE* cells at T3.5 and T5.5 after the onset of sporulation. n > 300 per replicate, per time-point, per strain. (D) SpoVD and SpoVE do not influence SpoIIIL stability. Immunoblot analysis of SpoIIIL-GFP in cell lysates of sporulating *ΔspoVE* single mutant strains collected every hour between T2.5 and T5.5. As control, a cell lysate from sporulating cells collected at T2.5 from a WT strain that does not contain GFP was included. SpoIIIL-GFP was immunodetected using anti-GFP antibodies. The position of SpoIIIL-GFP four bands is indicated.

In contrast to wild-type forespores where ~83% were patchy and ~17% were uniform at T5.5, quantification of the number of forespores with uniform and patchy SpoIIIL-GFP localization in the *ΔspoVE* single mutant revealed that ~32% were patchy and ~68% were uniform at T5.5 (Fig 5.1 C).

To further investigate whether the cortex or the cortex synthases contributes to the stability of SpoIIIL, we conducted an immunoblot assay of SpoIIIL-GFP in cell lysates of sporulating *ΔspoVE* single mutant, at T3.5 when most forespores harbour uniform SpoIIIL-GFP localization and at T5.5 when most forespores harbour patchy SpoIIIL-GFP localization (Fig 5.1 D). As control, a cell lysate from sporulating cells collected at T5.5 from a WT strain that does not contain GFP was included.

Interestingly, consistent with the result previously obtained for the wild-type condition where SpoIIIL-GFP was the only source of GFP in the cell (Fig. 3.3 D & F), Immunoblot data obtained for the *ΔspoVE* single mutant (Fig 5.1 D) was similar to the immunoblot data obtained for the wild-type (Fig. 3.3 D & F). The immunoblot data which would always show four bands in WT scenario at T5.5, also showed four bands for the Δ*spoVE* single mutant at T5.5.

Generally, in the WT condition where SpoIIIL-GFP was the only source of GFP in the cell, when counting downwards from higher molecular weight to lower molecular weight, four bands corresponding to the size of SpoIIIL-sfGFP (~36.9 kDa) were usually detected, and there appears to always be an increase in the intensity of the second, the third, and the fourth SpoIIIL-GFP protein bands over time, while the intensity of the first or top most SpoIIIL-GFP band decreases over time. This similar pattern was also observed in the Δ*spoVE* single mutant.

All together, these results suggest that the cortex synthases are required for the characteristic localization pattern but not the stability of SpoIIIL.

5.3.2 SpoIVA and SpoVM are required for SpoIIIL localization and stability

We have shown that SpoIIIL is required for spore shape (section 3.3.1) and cortex assembly (section 4.3.4). Since spore shape as well as proper cortex assembly also depends on the basement layer proteins SpoIVA and SpoVM, the encasement protein SpoIVD, as well as the inner coat protein SafA[91], we investigated the relationship between these proteins and SpoIIIL. Firstly, we wondered whether SpoIVA, SpoVM, SpoIVD, SafA and CotE (an outer coat protein) are required for the localization of SpoIIIL.

To test whether SpoIVA, SpoVM, SpoIVD, SafA, and CotE are required for SpoIIIL localization, we expressed SpoIIIL-GFP in the absence of these coat proteins and imaged the resultant spores under a fluorescence microscope at T3.5 when most forespores harbour uniform SpoIIIL-GFP localization and at T5.5 when most forespores harbour patchy SpoIIIL-GFP localization.

We noticed that the non-uniform patchy localization phenotype usually observed in the otherwise wild-type cells at T5.5 after the onset of sporulation (Fig 3.3) was absent in the *ΔspoIVA*, and *ΔspoVM* single mutants indicating that the basement layer proteins SpoIVA and SpoVM are required for the localization of SpoIIIL (Fig 5.2 A & B). Reciprocally, we also investigated whether SpoIIIL contributed to the localization of these coat proteins in question by fusing each of the coat proteins to a fluorescent protein and imaging the cells under a fluorescent microscope at T4, T5 and T6. The results obtained revealed that SpoIIIL is not required for the localization of the coat proteins SpoIVA, SpoVM, SpoIVD, SafA, and CotE (Appendix II, Figure S5.2 A, B, & C).

Since SpoIVA and SpoVM are both basement layer proteins and cells lacking either SpoIVA or SpoVM do not assemble the cortex[91], we decided to thoroughly characterize the impact of the *ΔspoIVA* single mutation on the localization of SpoIIIL by quantifying the proportion of cells with uniform (blue) and patchy (red) SpoIIIL-GFP localization in wild-type or *ΔspoIVA* single mutant cells at T3.5 when most forespores harbour uniform SpoIIIL-GFP localization and at T5.5 when most forespores harbour patchy SpoIIIL-GFP localization after the onset of sporulation.

In contrast to wild-type forespores where ~83% had patchy SpoIIIL-GFP phenotype and ~17% had uniform SpoIIIL-GFP phenotype at T5.5, quantification of the number of forespores with

uniform and patchy SpoIIIL-GFP localization in the *ΔspoIVA* single mutant revealed that ~6% had patchy SpoIIIL-GFP phenotype whereas ~94% had uniform SpoIIIL-GFP phenotype at T5.5 (Fig 5.2 C).

To further investigate whether the basement layer proteins SpoIVA or SpoVM, as well as the encasement protein SpoIVD contribute to the stability of SpoIIIL, we conducted an immunoblot assay of SpoIIIL-GFP in cell lysates of sporulating *ΔspoIVA, ΔspoVM, ΔspoVID* single mutants, at T3.5 when most forespores harbour uniform SpoIIIL-GFP localization and at T5.5 when most forespores harbour patchy SpoIIIL-GFP localization (Fig 5.2 D). As controls, a cell lysate from sporulating cells collected at T5.5 from a WT strain that does not contain GFP was included, as well as a cell lysate from sporulating cells collected at T3.5 and T5.5 from a WT strain expressing SpoIIIL-GFP from an ectopic locus as its only source of GFP.

Interestingly, inconsistent with the result previously obtained for the wild-type strain where SpoIIIL-GFP was the only source of GFP in the cell (Fig. 3.3 D & F), Immunoblot data obtained for the *ΔspoIVA, ΔspoVM,* and *ΔspoVID* single mutants was dissimilar to the immunoblot data obtained for the wild-type (Fig 5.2 D). The immunoblot data which would always show four SpoIIIL-GFP bands in wild-type scenario at T5.5, only showed three SpoIIIL-GFP bands for the *ΔspoIVA, ΔspoVM,* and *ΔspoVID* single mutants at T5.5 wherein the 3rd SpoIIIL-GFP band was absent.

Generally, in the WT condition where SpoIIIL-GFP was the only source of GFP in the cell, when counting downwards from higher molecular weight to lower molecular weight, four bands corresponding to the size of SpoIIIL-sfGFP (~36.9 kDa) were usually detected, and there appears to always be an increase in the intensity of the second, the third, and the fourth SpoIIIL-GFP protein bands over time, while the intensity of the first or top most SpoIIIL-GFP band decreases over time. This similar pattern was also observed in the Δ*spoVE* single mutant. In the *ΔspoIVA, ΔspoVM,* and *ΔspoVID* single mutants at T5.5, the 3rd SpoIIIL-GFP band was however absent.

All together, these results suggest that the basement layer proteins SpoIVA and SpoVM only are required for the characteristic localization pattern of SpoIIIL, while the basement layer proteins SpoIVA and SpoVM, as well as the encasement protein SpoVID are required for the stability of SpoIIIL.

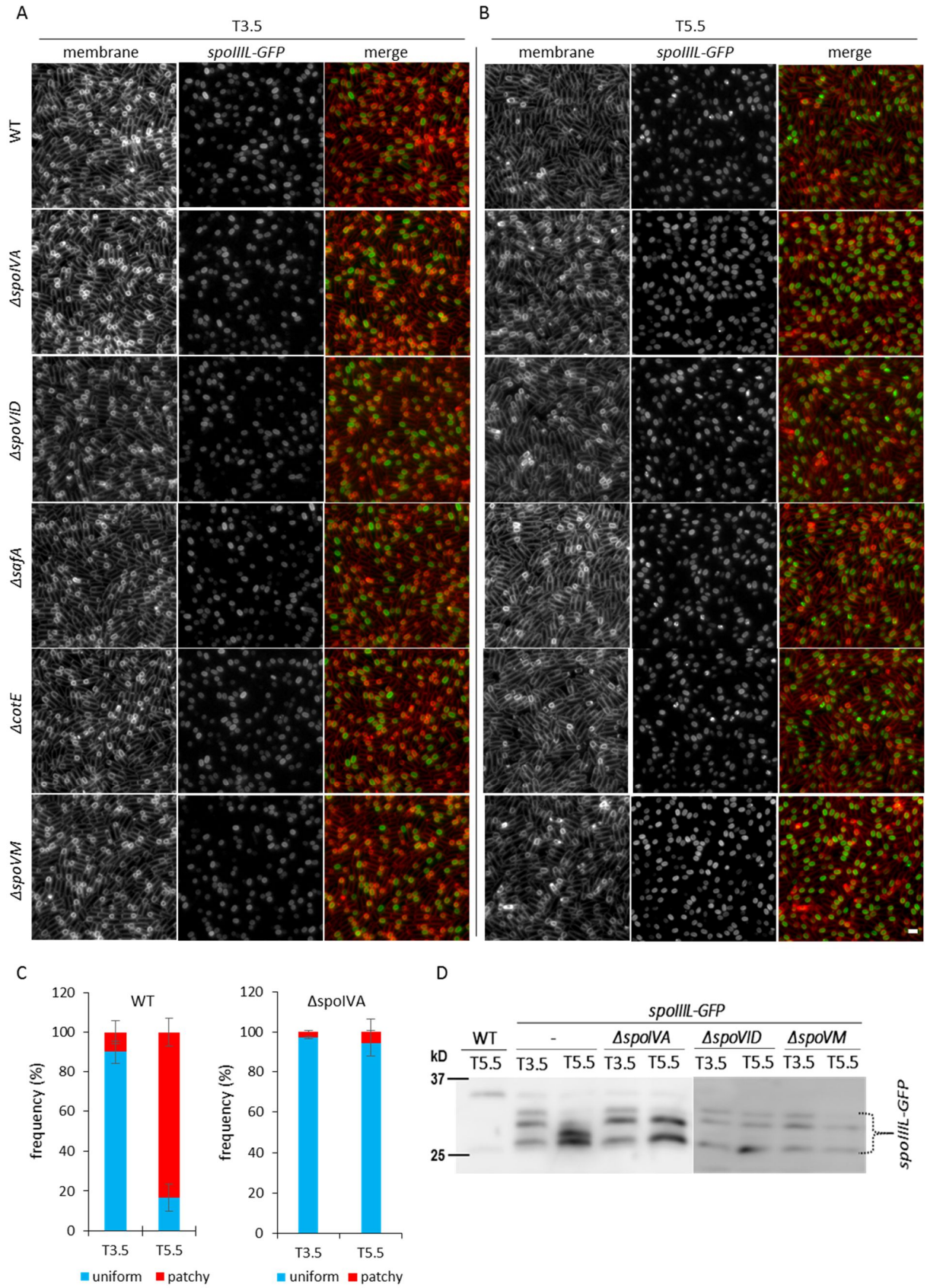

Fig 5.2 SpoIVA and SpoVM influences SpoIIIL localization and stability. Fluorescence localization of SpoIIIL-GFP in WT cells as well as in the *ΔspoIVA, ΔspoVID, ΔsafA, ΔcotE*, and *ΔspoVM* single mutants at T3.5 when most

forespores harbour uniform SpoIIIL-GFP localization (A) and at T5.5 when most forespores harbour patchy SpoIIIL-GFP localization (B). GFP signal is false-coloured green in the merged images. Cell membranes were visualised using TMA-DPH fluorescent membrane dye and are false-coloured red in merged images. Scale bar = 2 µm. (C) Quantification histogram presenting the proportion of cells (% ± STDEV, 3 biological replicates) with uniform (blue) and patchy (red) SpoIIIL-GFP localization in WT or *ΔspoIVA* cells at T3.5 and T5.5 after the onset of sporulation. n > 300 per replicate, per time-point, per strain. (D) SpoIVA, SpoVID, and SpoVM are required for SpoIIIL stability. Immunoblot analysis of SpoIIIL-GFP in cell lysates of sporulating *ΔspoIVA, ΔspoVID,* and *ΔspoVM* single mutant strains collected at T3.5 and T5.5. As control, a cell lysate from sporulating cells collected at T5.5 from a WT strain that does not contain GFP was included. SpoIIIL-GFP was immunodetected using anti-GFP antibodies.

5.3.3 CwlD and PdaA are not required for SpoIIIL localization

Since SpoIIIL localization depends on the peptidoglycan synthases SpoVD and SpoVE, we hypothesized that it is also possible for the localization of SpoIIIL to be dependent on the spore peptidoglycan modifying hydrolase enzymes CwlD and PdaA. CwlD (N-acetylmuramoyl-L-alanine amidase) as well as PdaA (N-acetylmuramic acid deacetylase gene) are required for the modification of the spore peptidoglycan after it is synthesized by the PG synthases enzymes SpoVD and SpoVE. CwlD and PdaA function in the production of muramic δ-lactam as well as the reduction in PG peptide cross links although the Loss of PdaA or CwlD has no effect on spore heat resistance but culminates in reduced germination efficiency[88,91,164–166]. Thus, if our hypothesis is correct, then we might see a change in the localization of SpoIIIL in the *ΔcwlD* or *ΔpdaA* single mutant.

To test whether the *ΔcwlD* or *ΔpdaA* single mutant is required for SpoIIIL localization, we expressed SpoIIIL-GFP in the absence of *cwlD* or *pdaA* and imaged the resultant spores under a fluorescence microscope at T3.5 when most forespores harbour uniform SpoIIIL-GFP localization and at T5.5 when most forespores harbour patchy SpoIIIL-GFP localization (Fig 5.3).

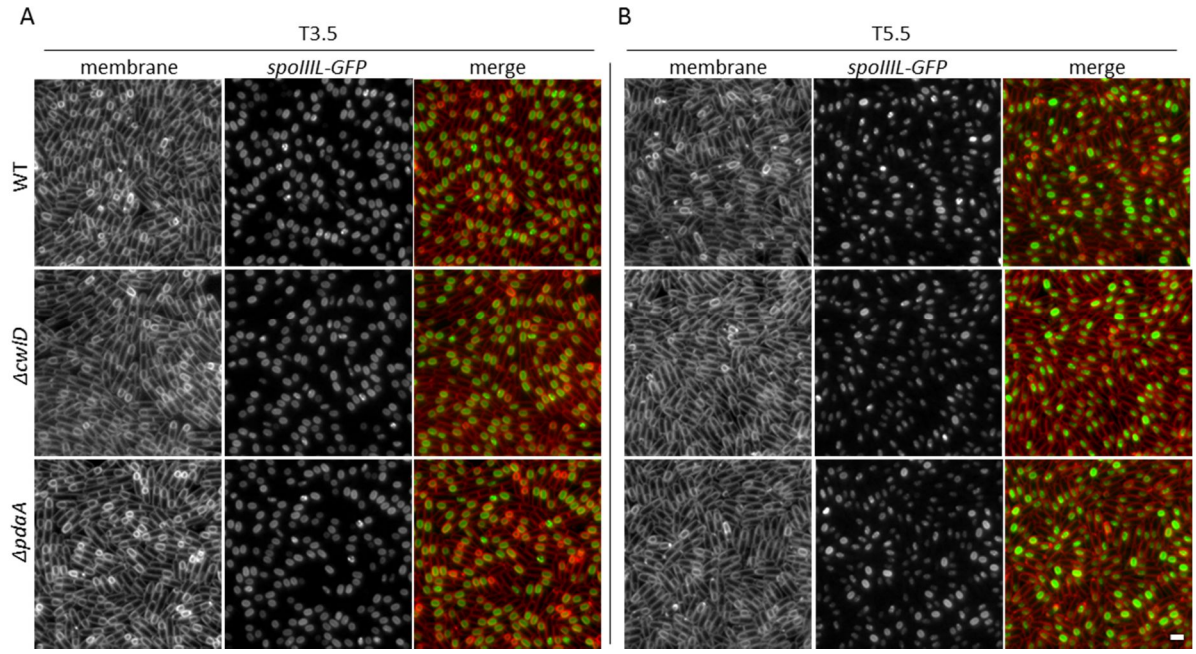

Fig 5.3 CwlD and PdaA do not influence SpoIIIL localization. Fluorescence localization of SpoIIIL-GFP in WT cells as well as in the *ΔcwlD*, and *ΔpdaA* single mutants at T3.5 when most forespores harbour uniform SpoIIIL-GFP localization (A) and at T5.5 when most forespores harbour patchy SpoIIIL-GFP localization (B). GFP signal is false-coloured green in the merged images. Cell membranes were visualised using TMA-DPH fluorescent membrane dye and are false-coloured red in the merged images. Scale bar = 2 µm.

Surprisingly, cells of the *ΔcwlD* or *ΔpdaA* single mutant, had similar uniform SpoIIIL-GFP localization phenotype as is usually observed in the otherwise wild-type cells at T3.5 after the onset of sporulation as well as similar patchy SpoIIIL-GFP localization phenotype as is usually observed in the otherwise wild-type cells at T5.5 after the onset of sporulation. Thus indicating that the PG modifying enzymes CwlD and PdaA are not required for the localization of SpoIIIL (Fig 5.3 A & B).

5.3.4 *ΔcwlD ΔpdaA* double mutation does not contribute to spore phase brightness in the *ΔspoIIIL* mutant

We have shown that in the absence of SpoIIIL there is delayed and reduced σ^G activity (Fig 3.1 D). Also, in the otherwise wild-type strain, the σ^G activity usually peaks at around T3.5, stays relatively at the same level before falling at around T4.5. Whereas, in the *ΔspoIIIL* single mutant, σ^G activity stays on for longer and rather peaks approximately one hour later at T4.5 before hesitantly commencing its fall (Fig 3.1 D). We have also seen that cortex assembly in the *ΔspoIIIL* single mutant is delayed compared to wild-type (Fig 4.4 C). It is reported that the spore peptidoglycan modifying enzymes CwlD and PdaA are both σ^G controlled and that the

cwlD mutant produces bright spores while the *pdaA*-deficient spores were bright by phase-contrast microscopy[89,166,167].

Since the hydrolases CwlD and PdaA which form muramic δ-lactam & reduce PG peptide cross links are σ^G controlled, and σ^G activity stays on for longer in the *ΔspoIIIL* single mutant, we hypothesized that this extended σ^G activity in the *ΔspoIIIL* single mutant, could cause an increased and extended activity window for CwlD & PdaA resulting in an excessive production of muramic δ-lactam as well as an excessive reduction or degradation of PG peptide cross links. A resultant effect which could be detrimental to the cortex, thereby completely disrupting or delaying cortex assembly in general. Recall that proper cortex assembly results in a change in forespore refractivity, causing forespores to become phase bright as they mature[91]. If our hypothesis is true, then cortex assembly which is envisaged as a measure of the phase brightness of spores would be adversely affected.

To determine whether the hypothesized excessive production of muramic δ-lactam and excessive degradation of PG peptide cross links supposedly elicited by *cwlD* and *pdaA* in the *ΔspoIIIL* single mutant is detrimental to proper cortex assembly, we performed phase bright imaging of the WT, *ΔspoIIIL*, *ΔcwlD ΔpdaA* double mutant, and *ΔspoIIIL ΔcwlD ΔpdaA* tripple mutant spores at T4, T7, T9, and T30 after the onset of sporulation and quantified the spores showing the proportion of cells (% ± STDEV, 2 biological replicates) with phase bright (blue) and phase dark (red) phenotype, per time-point, per strain (Fig 5.4 A & B).

The results suggest that at T4, ~25% of the WT spores have become either completely or partially phase bright while only less than 1% of the *ΔspoIIIL* mutant spores are either completely or partially phase bright. At T7 ~90% of WT spores have become either completely or partially phase bright while ~65% of the *ΔspoIIIL* mutant spores are either completely or partially phase bright. At T9 however, the percentage of WT spores that have become either completely or partially phase bright remained at ~90% while the percentage of *ΔspoIIIL* mutant spores that have become either completely or partially phase bright rose to ~80%.

Furthermore, at T30, while the percentage of WT spores that have become either completely or partially phase bright remained at around ~90%, the percentage of *ΔspoIIIL* mutant spores that have become either completely or partially phase bright rose to ~90%. Altogether, the

results suggests that spores of the *ΔspoIIIL* mutant undergo a gradual and slower but eventual process of becoming phase bright compared to the WT.

Summarily, the percentages of phase bright spores for the otherwise wild-type cells were, ~25%, ~87%, ~88%, and ~93% at T4, T7, T9, and T30 respectively while the percentages of phase bright spores for the *ΔspoIIIL* single mutant cells were, ~1%, ~65%, ~80%, and ~92% at T4, T7, T9, and T30 respectively. Also, the percentages of phase bright spores for the *ΔcwlD ΔpdaA* double mutant cells were ~18%, ~88%, ~90%, and ~90% at T4, T7, T9, and T30 respectively, whereas, in comparison, the percentages of phase bright spores for the *ΔspoIIIL ΔcwlD ΔpdaA* tripple mutant were,~1%,~67%,~86%, and ~88% at T4, T7, T9, and T30 respectively.

Interestingly, the results obtained for the *ΔcwlD ΔpdaA* double mutant was equivalent to what was obtained for the otherwise wild-type cells while the results obtained for the *ΔspoIIIL ΔcwlD ΔpdaA* tripple mutant was equivalent to what was obtained for the *ΔspoIIIL* single mutant alone suggesting that the *ΔcwlD ΔpdaA* double mutation does not contribute to the observed phase bright phenotype. Therefore, both the phase bright imaging data and the corresponding quantification data suggests that the hypothesized excessive production of muramic δ-lactam and the hypothesized excessive degradation of PG peptide cross links supposedly elicited by *cwlD* and *pdaA* in the *ΔspoIIIL* single mutant does not contribute to the observed phase bright phenotype.

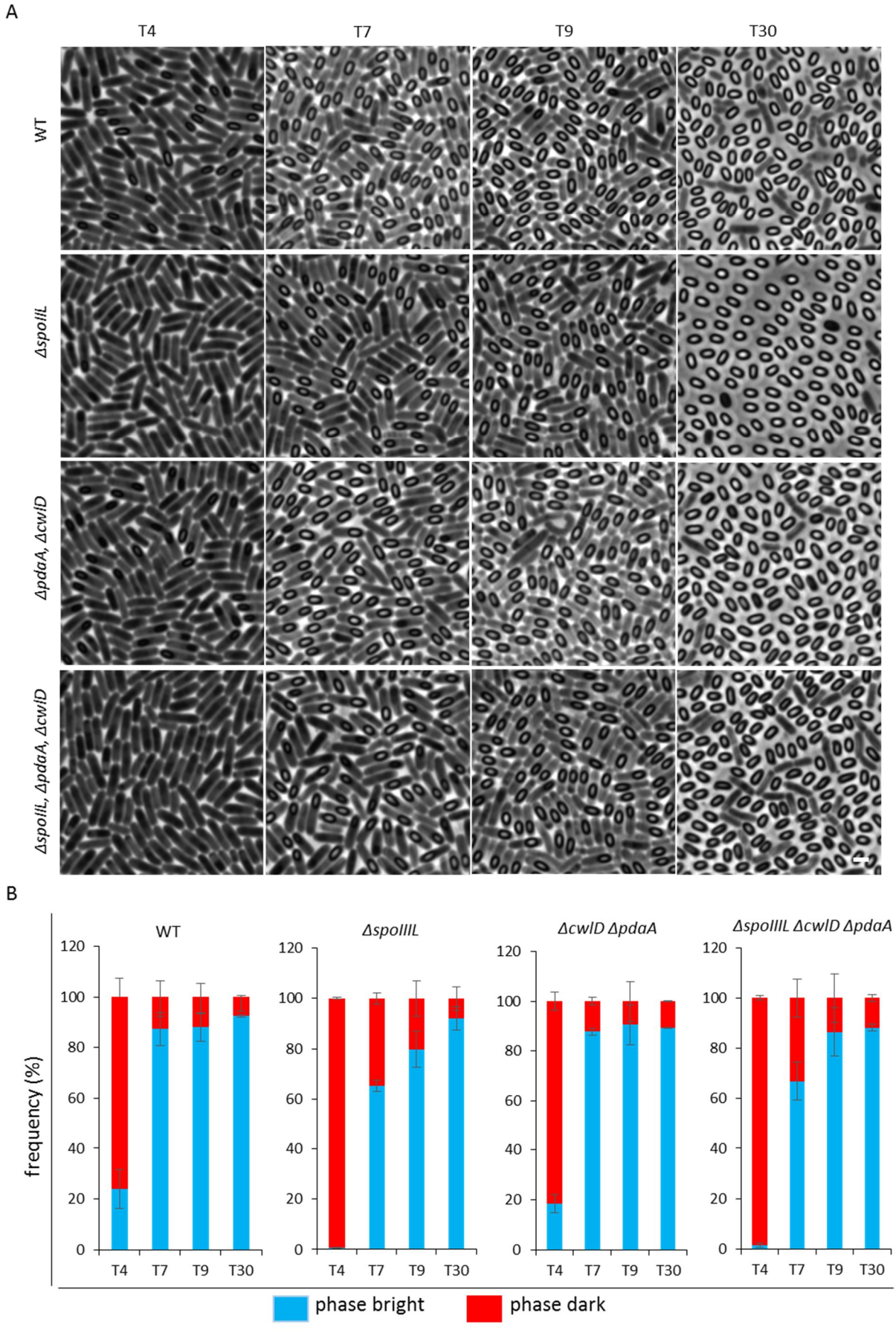
A
T4
T7
T9
T30
WT
ΔspoIIL
ΔpdaA, ΔcwlD
ΔspoIIL, ΔpdaA, ΔcwlD
B
WT
ΔspoIIIL
ΔcwlD ΔpdaA
ΔspoIIIL ΔcwlD ΔpdaA
frequency (%)
0
20
40
60
80
100
120
T4
T7
T9
T30
phase bright
phase dark

Fig 5.4 CwlD and PdaA do not influence cortex maturation. (A) Microscopic imaging of the phase bright phenotype of WT, *ΔspoIIIL, ΔcwlD ΔpdaA* double mutant, and *ΔspoIIIL ΔcwlD ΔpdaA* triple mutant spores at T4, T7, T9, and T30 after the start of sporulation. Cell membranes were visualised using TMA-DPH fluorescent membrane dye. Scale bar = 2 µm. (B) Quantification histogram presenting the proportion of cells (% ± STDEV, 2 biological replicates) with phase bright (blue) and phase dark (red) phenotype in wild-type (WT), *ΔspoIIIL* single mutant, *ΔcwlD ΔpdaA* double mutant, and *ΔspoIIIL ΔcwlD ΔpdaA* triple mutant spores imaged at T4, T7, T9, and T30 after the onset of sporulation. n > 400 per replicate, per time-point, per strain

5.3.5 PbpF & PbpG are both required for SpoIIIL localization

PbpF and PbpG are two forespore produced functionally redundant class A penicillin- binding proteins (PBPs), which produce a thin layer of spore PG known as the germ cell layer[73,83] and the germ cell layer is produced during engulfment[79,89]. Sporulating cells lacking either *pbpF* or *pbpG* produce nearly similar levels of spores as wild-type, but cells devoid of both genes are severely impaired in sporulation[73,83]. SpoIIIL localizes around the forespore membrane and the germ cell layer overlays the forespore membrane surface from the intermembrane space.

Since SpoIIIL localization also depends on the cortex peptidoglycan synthases SpoVD and SpoVE (section 5.3.1), we hypothesized that it is also possible for the localization of SpoIIIL to be dependent on the functionally redundant germ cell layer generating enzymes PbpF and PbpG. Thus, if our hypothesis is correct, then we might see a change in SpoIIIL localization in the *ΔpbpF ΔpbpG* double mutant.

To test whether the *ΔpbpF ΔpbpG* double mutation will result in a change in SpoIIIL localization, we expressed SpoIIIL-GFP in the absence of *pbpF* or *pbpG or both* and imaged the resultant spores under a fluorescence microscope at T3.5 when most forespores harbour uniform SpoIIIL-GFP localization and at T5.5 when most forespores harbour patchy SpoIIIL-GFP localization (Fig 5.5).

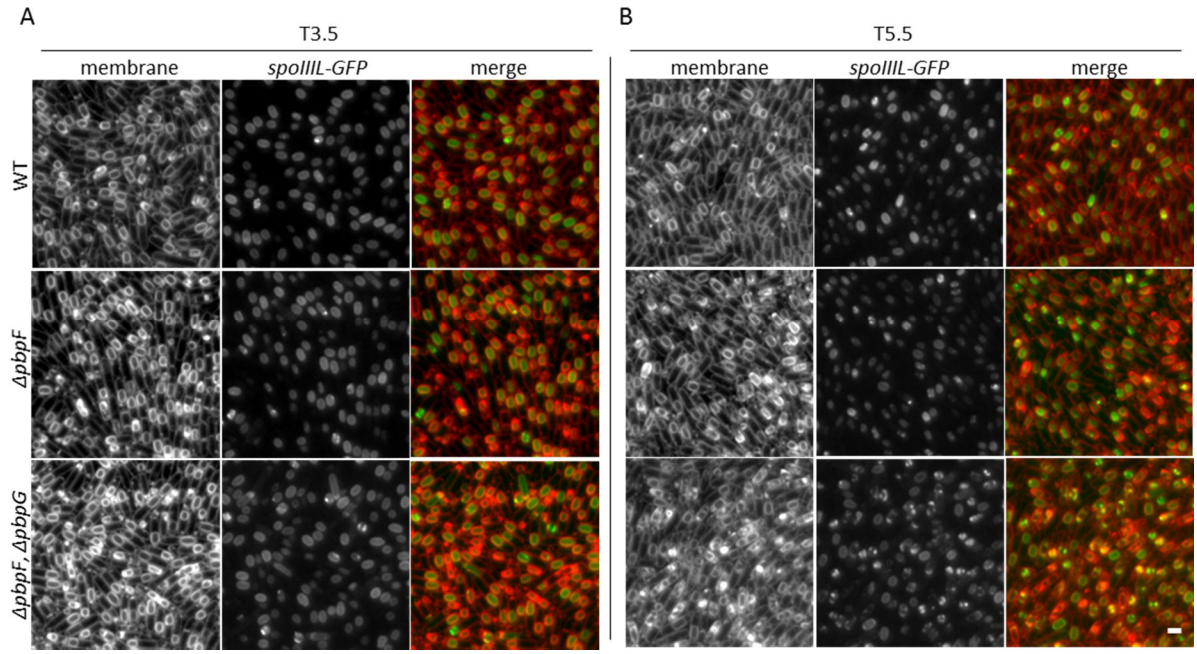

Fig 5.5 The germ cell layer PbpF & PbpG are both required for SpoIIIL localization. Fluorescence localization of SpoIIIL-GFP in WT spores as well as in *ΔpbpF*, and *ΔpbpG* single mutant spores at T3.5 when most forespores harbour uniform SpoIIIL-GFP localization (A) and at T5.5 when most forespores harbour patchy SpoIIIL-GFP localization (B). GFP signal is false-coloured green in the merged images. Cell membranes were visualised using TMA-DPH fluorescent membrane dye and are false-coloured red in the merged images. Scale bar = 2 µm.

Interestingly, and consistent with literature, we observed that the uniform SpoIIIL-GFP localization phenotype as is usually observed in the otherwise wild-type cells at T3.5 after the onset of sporulation as well as the patchy SpoIIIL-GFP localization phenotype that is usually observed in the otherwise wild-type cells at T5.5 after the onset of sporulation were present both in the wild-type and in the *ΔpbpF* single mutant.

However, as hypothesized, the *ΔpbpF ΔpbpG* double mutant had the uniform SpoIIIL-GFP localization phenotype which is usually observed in otherwise wild-type cells at T3.5 after the onset of sporulation but did not exactly have the patchy SpoIIIL-GFP localization phenotype that is usually observed in the otherwise wild-type cells at T5.5 after the onset of sporulation

Thus indicating that the germ cell layer or the germ cell layer generating duo PbpF and PbpG, are required for the localization of SpoIIIL (Fig 5.5 A & B).

5.3.6 SigK (SpoIVCB) is required for SpoIIIL localization and stability

We have shown that the forespore protease SpoIVB which sits upstream of σ^K activation cascade is required for the localization and stability of SpoIIIL (section 3.3.8). We have also

shown that the cortex peptidoglycan synthases SpoVD and SpoVE whose activities sit downstream of σ^K activation are also required for SpoIIIL localization but not SpoIIIL stability (section 5.3.1). Our data also elucidates how the peptidoglycan precursor synthesis gene *murAB* synergizes strongly with *spoIIIL* both in cortex assembly and in sporogenesis (section 4-3.4). Recall that SpoIIIL also ensures the timely downregulation of σ^G at around T4.5 which is also around the time-point for active cortex PG synthesis (Section 3.3.1).

Since σ^K activation is required for the synthesis of peptidoglycan precursors during the latter stages of sporulation and the timing of spore PG synthesis coincides with the timing of precursor synthesis[89], we wondered whether taking σ^K out of this dynamic relationship between SpoIIIL, the forespore protease SpoIVB, the cortex synthases SpoVD & SpoVE, as well as the peptidoglycan precursor biosynthesis, would influence the localization and stability of SpoIIIL.

To test whether SigK is required for SpoIIIL localization, we expressed SpoIIIL-GFP in a *ΔsigK* mutant and imaged the resultant spores under a fluorescence microscope at T3.5 when most forespores harbour uniform SpoIIIL-GFP localization and at T5.5 when most forespores harbour patchy SpoIIIL-GFP localization (Fig 5.6).

Interestingly, the localization of SpoIIIL in cells of the *ΔsigK* mutant appeared similar to that observed in otherwise wild-type cells at T3.5. That is, at T3.5, the uniform SpoIIIL-GFP localization phenotype usually observed in the otherwise wild-type cells after the onset of sporulation was also observed in cells of the *ΔsigK* mutant. However, at T5.5, both the localization of SpoIIIL in the *ΔsigK* mutant, as well as the cells of the *ΔsigK* mutant in general, did not appear exactly the same as they are in the otherwise wild-type cells. Firstly, cells of the *ΔsigK* single mutant generally appeared more slender & elongated than cells of the wild-type. Secondly, there was a difference in the appearance of the patchy SpoIIIL-GFP localization phenotype usually observed in the otherwise wild-type cells at T5.5, in the *ΔsigK* mutant.

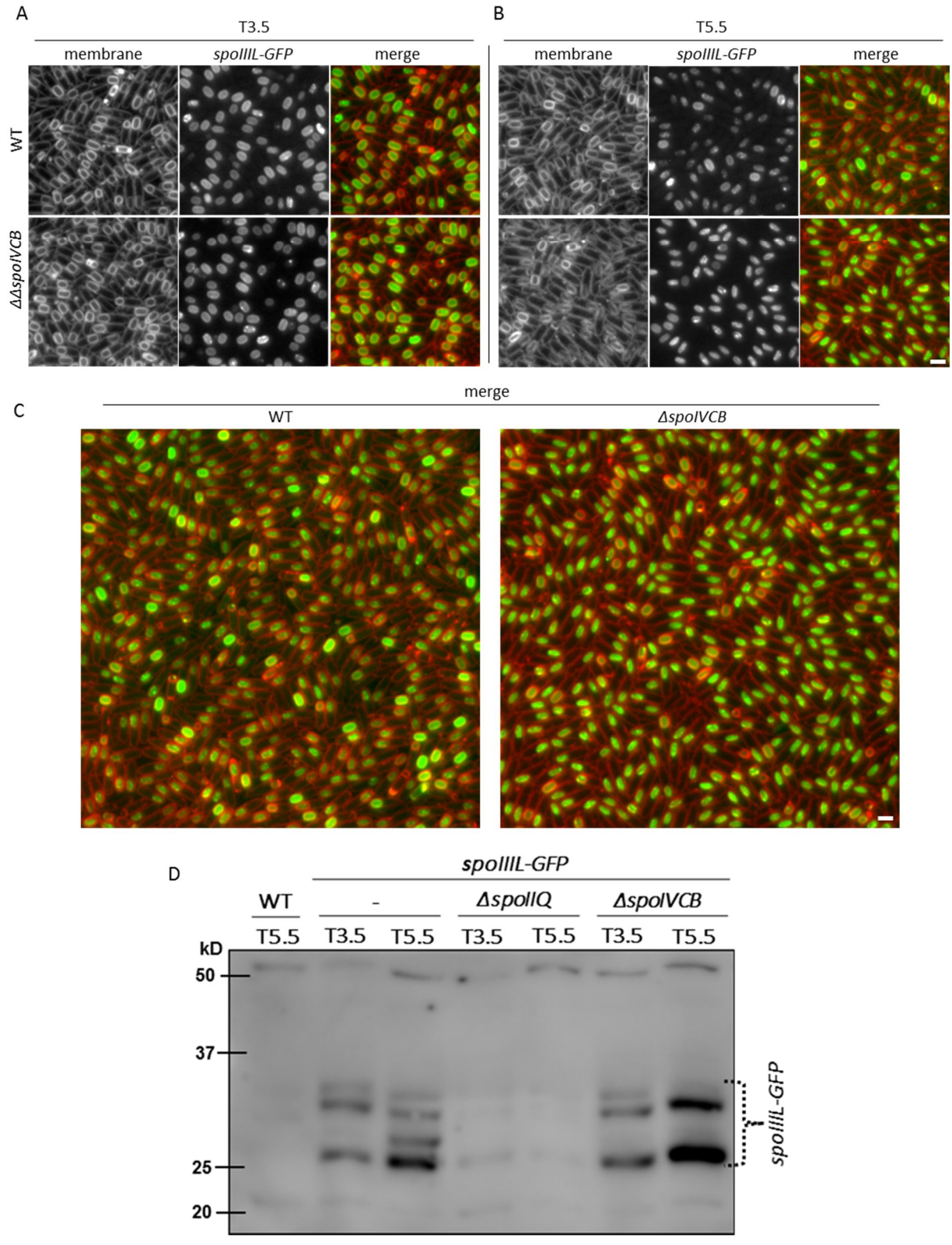

Fig 5.6 SigK (SpoIVCB) is required for SpoIIIL localization and stability. Fluorescence localization of SpoIIIL-GFP in WT spores as well as in *ΔsigK* single mutant spores at T3.5 when most forespores harbour uniform SpoIIIL-GFP localization (A) and at T5.5 when most forespores harbour patchy SpoIIIL-GFP localization (B). GFP signal is false-coloured green in the merged images. Cell membranes were visualised using TMA-DPH fluorescent membrane dye and are false-coloured red in the merged images. Scale bar = 2 µm. (C) Large area view of SpoIIIL-GFP

localization in WT spores, as well as in *ΔsigK* single mutant spores at T5.5 after the onset of sporulation. Fluorescence signals are false-coloured as in (A) & (B). Scale bar = 2 µm. (D) Immunoblot analysis of SpoIIIL-GFP in cell lysates of *ΔsigK* (Δ*spoICVB*) & *ΔspoIIQ* single mutant strains collected at T3.5 and T5.5. As controls, cell lysates of sporulating cells collected at T5.5 from a WT strain that does not contain GFP, as well as from a WT strain wherein SpoIIIL-GFP is integrated at an ectopic locus as the sole source of SpoIIL, was included. SpoIIIL-GFP was immunodetected using anti-GFP antibodies. The position of SpoIIIL-GFP four bands is indicated.

We do not know whether the slender elongated phenotype of the *ΔsigK* single mutant could be influencing the spatial configuration of the contents of the forespore including its proteins and consequently SpoIIIL. But what we do know is that, the above data suggests that σ^K is required for the proper localization of SpoIIIL (Fig 5.6 A, B, & C).

To further investigate whether σ^K is required for the stability of SpoIIIL, we conducted an immunoblot assay of SpoIIIL-GFP in cell lysates of sporulating *ΔsigK* (*ΔspoIVCB*) single mutant, at T3.5 when most forespores harbour uniform SpoIIIL-GFP localization and at T5.5 when most forespores harbour patchy SpoIIIL-GFP localization (Fig 5.6 D). As controls, a cell lysate from sporulating cells collected at T5.5 from a WT strain that does not contain GFP was included, as well cell lysates from sporulating cells collected at T3.5 and T5.5 from a WT strain expressing SpoIIIL-GFP from an ectopic locus as its only source of GFP.

Interestingly, inconsistent with the result obtained for the wild-type cells where SpoIIIL-GFP was the only source of GFP in the cell, Immunoblot data obtained for the *ΔsigK* (*ΔspoIVCB*) single mutant was dissimilar to the immunoblot data obtained for the wild-type (Fig 5.6 D). The immunoblot data which would always show four SpoIIIL-GFP bands in wild-type scenario at T5.5 when counting downwards from higher molecular weight to lower molecular weight, only showed three SpoIIIL-GFP bands for the *ΔsigK* (*ΔspoIVCB*) single mutant at T5.5 as the 3rd SpoIIIL-GFP band was absent.

All together, these results suggest that σ^K (SigK or SpoIVCB) is required both for the characteristic localization pattern of SpoIIIL, as well as for the stability of SpoIIIL.

5.4 Discussion

5.4.1 Why does the cortex and coat influence SpoIIIL localization and stability?

In the previous chapter, we saw how the *ΔspoIIIL ΔmurAB* double mutant forespores became severely deficient in sporogenesis and cortex assembly. In the chapter before that we also saw that SpoIIIL was required for σ^G regulation, forespore morphology, and undergoes a SpoIVB

mediated proteolysis within the forespore. Both chapters led us to probe more in-depth the involvement of SpoIIIL in spore shape determination by investigating SpoIIIL's relationship between the various factors involved in shape determination.

There are certain coat proteins that form the bedrock for the interaction between the coat and the cortex. SpoIVA, SpoVM, and SpoVID are some of the most important proteins in such interactions. While the enzymes responsible for synthesizing the cortex SpoVD and SpoVE contributed to the localization of SpoIIIL, it was surprising to discover that the stability of SpoIIIL was not dependent on the cortex synthesizing enzymes (Fig 5.1). Why the cortex synthases did not influence SpoIIIL stability but contributed immensely to its proper localization was not clear. However, we suspected that SpoIIIL could be interacting with the cortex via multiple possible pathways.

Furthermore, it is reported that the basement layer of the coat is required for the localization of all coat proteins and that cells lacking the coat basement layer proteins SpoIVA and SpoVM do not assemble the cortex[91]. While SpoVM is required for proper localization of SpoIVA to the outer membrane of the maturing forespore, mutations in spoIVA caused defects in cortex synthesis[89,168]. Thus, the attachment of the coat to the surface of the spore as well as the synthesis of the cortex both relies on the spore protein SpoIVA[168].

In our data, we saw that SpoIVA and SpoVM contributed both to the localization as well as the stability of SpoIIIL (Fig 5.2). This was a unique finding for us because it clearly meant that SpoIIIL which rather localized around the forespore membrane within the forespore cytoplasm and was not membrane exposed, was largely dependent on the coat for its proper localization and stability. How and why this was the case remains to be discovered.

Additionally, the encasement protein SpoIVD which is required by some coat proteins like SafA for their localization[91] also contributed to the stability of SpoIIIL but not its localization (Fig 5.2). This was an interesting result for us because SpoIVD which is an important coat protein could only but contribute to the stability of SpoIIIL and not its localization. Altogether, our data seems to notify us of the possibility that SpoIIIL interacts with the cortex and the coat via multiple pathways. It is possible that one of this pathway influences both the localization and stability of SpoIIIL, while the second pathway could be influencing either just the localization of SpoIIIL alone or the stability of SpoIIIL alone. But, the third pathway may not be influencing

either the localization of SpoIIIL or its stability but could be synergizing strongly with SpoIIIL in cortex assembly as in the case of the peptidoglycan precursor synthesis enzyme MurAB (section 4.3.3 & 4.3.4). However, consistent with literature where the loss of the PG modifying hydrolase enzymes CwlD and PdaA do not affect heat resistance[91], we observed also that CwlD and PdaA do not contribute to SpoIIIL's cortex assembly defect (Fig 5.4).

Bacterial shape and overall morphology is ultimately determined by the netlike PG sacculus. Whereas some morphological determinants can behave like a cytoskeleton to direct biosynthetic complexes spatiotemporally, various other major determinants of bacterial cell shape includes the spatiotemporal regulation of enzymes which modify the sacculus or PG after biosynthesis[169,170]. We are not certain whether to place SpoIIIL in the PG sacculus modifying category or in the cytoskeleton category but certain that our data has hinted that SpoIIIL is likely involved in more than one genetic pathway that culminates in spore envelope assembly.

5.4.2 How does SigK influence SpoIIIL stability and localization?

The forespore protease SpoIVB brings about the activation of σ^K [84]and contributes to the proper localization and stability of SpoIIIL (section 3.3.8) as well. The time point around which spore PG synthesis occurs coincides with the timepoint around which engulfment is completed by the mother cell membranes and the regulation of genes around this particular stage of sporulation is reliant upon σ^G activation in the forespore as well as the subsequent induction of σ^K activity in the larger mother cell compartment[89,171]. Thus, significant cortex synthesis begins only after engulfment is completed, bringing about the activation of σ^G in the forespore, and later the activation of σ^K in the larger mother cell[89,171]. Interestingly, this might explain the link between SpoIIIL, σ^G and σ^K seeing that SpoIIIL was already shown to ensure timely activation and down regulation of σ^G (Fig 3.1) around similar time-points T3.5 - T4.5 even though SpoIIIL has not been shown to be directly involved in σ^K regulation.

Importantly, a reduction in PG precursor biosynthesis around early sporulation stages, accompanied by a renewed precursor biosynthesis upon the activation of σ^K, functions as an instrument to regulate the timing of the synthesis of the spore cortex[89]. Recall that cortex synthases SpoVD and SpoVE influences SpoIIIL localization (Fig 5.1), while in the absence of both *spoIIIL* and the PG precursor biosynthesis enzyme *murAB*, cortex synthesis and spore

generation is greatly impaired or completely blocked (Fig 4.4). This indicates that SpoIIIL is actively involved around this same time-point in this stage of sporulation. Since σ^K activation at this stage of sporulation is required in order to activate the cortex synthesis enzymes SpoVD and SpoVE and to upregulate the precursor synthesis enzymes, we can therefore deduce that σ^K influences SpoIIIL stability and localization indirectly via its regulation of PG synthesis and PG synthesis enzymes although the exact molecular mechanism by which σ^K influences SpoIIIL is not completely clear. The significant proof of this remains that cells lacking both SpoIIIL and MurAB are blocked in σ^K mediated cortex assembly and consequently sporogenesis (Fig 4.4). This leads us to the next chapter where we attempt to illustrate the molecular mechanism and pathways that connect SpoIIIL, SpoIVB, SigG, SigK, SpoVD & SpoVE, MurAB, and cortex synthesis.

General Discussion

6.1 Overview

The process of spore formation involves several morphological changes, as well as dedicated genetic programs that have been investigated for more than 50 years and represent one of the most elaborately characterized developmental pathways in modern day molecular microbiology[14]. Cell differentiation however, is an elementary biological process and spore formation by *B. subtilis* is a very old system of cell differentiation that has now become an archetype for the investigation of cell differentiation in prokaryotes[82]. Most recently, 24 additional genes which had previously not been associated with spore formation were discovered[14], including SpoIIIL, a 59 amino acids protein, transcribed in the forespore under σ^F control, reported to take part in the activation of the late forespore specific sigma factor σ^G, and is believed to be an A-Q complex protein[28]. Reading further, one would see how we have been able to uncover a specialized role for SpoIIIL during Spore development and how SpoIIIL is involved in cortex assembly regulation and signalling.

At the beginning of this project, not much was known about SpoIIIL, so our aims included defining the extent to which SpoIIIL functions in the A-Q complex; Identifying, validating and characterizing genes that may function with SpoIIIL in sporulation; defining the localization, topology and important domains / conserved residues of SpoIIIL; as well as Identifying SpoIIIL protein-protein interaction partners. This would eventually enable us to reveal connections between SpoIIIL and other processes occurring during sporulation, and consequently, nascent weaknesses in the sporulation program that may aid in developing ways to prevent sporulation in disease-causing spore-formers would be discovered.

Whether SpoIIIL was really an A-Q complex protein was elusive at the start of this project. However, during the course of this thesis, it was discovered that SpoIIIL is not an A-Q complex protein. While the A-Q complex proteins are enriched in, and follow the engulfing membrane, SpoIIIL was not observed to behave in a similar manner. Instead, SpoIIIL was observed to localize uniformly around the forespore membrane at a time point that coincides with the completion of engulfment and changes its localization later during spore development to look like intriguing patchy-like structures in the forespore cytoplasm (Fig 3.3 A & B). Our results also suggested that whilst *spoIIIL* is required for the proper timing of σ^G activity, it is not required for maintaining σ^G activity late into development (Fig 3.1 D). Additionally, the roundness defect, sporulation in-efficiency, and the σ^G activity defects were all much more

severe in the well-known A-Q complex proteins assayed compared to SpoIIIL (Fig 3.1 & Fig 3.2).

This work combines a multitude of evidence generated via several analytical approaches to confirm that SpoIIIL which localizes uniformly around the forespore inner membrane and changes over time to look like intriguing patchy-like structures in the forespore cytoplasm (Fig 3.3), is not surface exposed (Fig 3.4), and that a forespore resident protease known as SpoIVB as well as the SpoIVB catalytic site are both required for the observed change in localization and stability of SpoIIIL (Fig 3.8). Furthermore, we saw that the absence of both SpoIIIL and MurAB, a protein wherein during Tn-seq experiments (section 4.3.1), transposon insertions were largely underrepresented in the *ΔspoIIIL* single mutant especially at the *murAB* foci compared to WT, severely impairs cortex synthesis and assembly (Fig 4.4). However, MurAB is required neither for the proper localization nor the stability of SpoIIIL (Fig 4.3).

Cortex assembly is required for the localization of SpoIIIL because the localization pattern of SpoIIIL is altered in the absence of the cortex synthases SpoVD and SpoVE. There is also no reported direct interaction between SpoIIIL and either proteins, and neither SpoVD nor SpoVE is required for the stability of SpoIIIL (Fig 5.1). Also, our data revealed that the basement layer proteins SpoIVA and SpoVM without which cells do not assemble the cortex, are required for both the localization and the stability of SpoIIIL (Fig 5.2), while the encasement protein SpoVID is required for the stability of SpoIIIL but not the localization of SpoIIIL (Fig 5.2). Finally, our data illustrated that σ^K (SigK or SpoIVCB) which is activated by the forespore protease SpoIVB is required both for the characteristic localization pattern of SpoIIIL, as well as for the stability of SpoIIIL. Accumulatively, the data generated in this thesis have brought a broader understanding of the mid-stages of spore development which can be summarized in a simple schematics called the “SpoIIIL-Cortex Assembly Signaling” (Figure 6.1).

6.2 The SpoIIIL-spore encasement relationship

Spore encasement transpires within two concentric shells namely: an outer proteinaceous ‘‘coat’’ and an inner peptidoglycan ‘‘cortex,’’ demarcated by a membrane. The proper assembly of the cortex is initiated only after the commencement of coat assembly, and an impaired induction of coat assembly prevents the assembly of the cortex. Successful binding and formation of the coat’s basement layer is also required to warrant cortex assembly[87,164].

As revealed in this thesis, we have seen that the proper localization of SpoIIIL depends on SpoIVB, SpoIVA, SpoVM, SpoVD, and SpoVE while the stability of SpoIIIL depends only on SpoIVB, SpoIVA, SpoVM, as well as SpoVID (see Table 6.1). The common cellular event that occurs in the absence of SpoIVB, SpoIVA, SpoVM, SpoVD, and SpoVE is that the cortex is not assembled (see Fig 6.1). We believe that the change in localization of SpoIIIL from uniform localization at early time-points after the onset of sporulation to intriguing patchy-like localization at later time-points after the onset of sporulation indicates the assembly of the cortex.

Table 6.1 SpoIIIL localization and stability determinants: showing the conditions wherein the localization and stability of SpoIIIL changes in relation to wild-type, as well as the cellular events that occur in such conditions.

Mutants (condition)	σ^K activation	Precursor synthesis	Cortex Assembly	Basement layer (coat assembly)	SpoVID-LysM-GlcNAc sequestration in mother cell	SpoVD/E activation
SpoIIIL localization determinants (localization different from wild-type)						
wild-type	yes	yes	yes	yes	no	yes
ΔspoIVB	no	no	no	yes	no	no
ΔspoIVA	yes	yes	no	no	yes	yes
ΔspoVM	yes	yes	no	no	yes	yes
ΔspoVD/E	yes	yes	no	yes	no	no
SpoIIIL stability determinants/ direct interaction partners (no 3rd band)						
wild-type	yes	yes	yes	yes	no	yes
ΔspoIVB	no	no	no	yes	no	no
ΔspoIVA	yes	yes	no	no	yes	yes
ΔspoVM	yes	yes	no	no	yes	yes
ΔspoVID	yes	yes	**Yes**	**Yes (defective)**	no	yes

However, since cortex assembly is reliant upon the successful initiation of the assembly of the coat, and a direct genetic interaction between SpoIIIL and the cortex synthases SpoVD and SpoVE is yet to be established, we propose that SpoIIIL interacts with the coat (or a component of the coat) in the coordination of cortex assembly and or in functioning as an indicator of spore encasement. Although, future work should test the possibility of a direct interaction between SpoIIIL and the spore cortex synthases SpoVD and SpoVE via approaches like the bacterial two-hybrid (see Future work section 6.3).

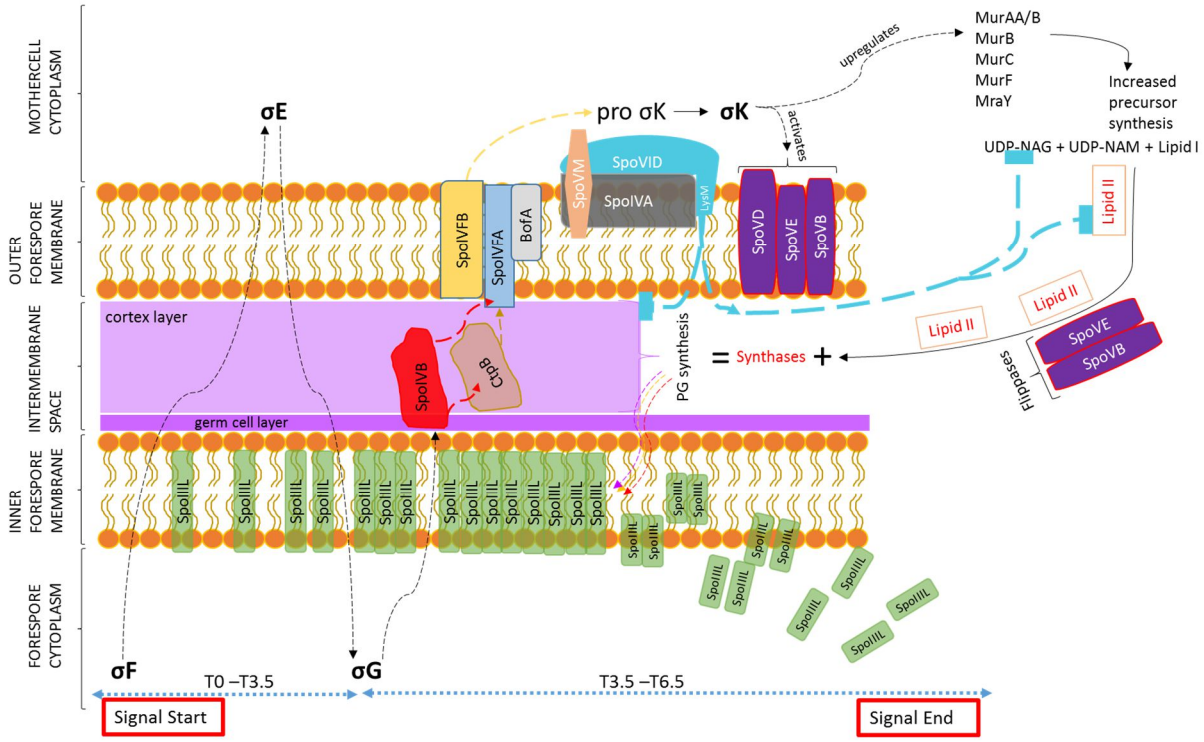

Fig 6.1 SpoIIIL- Cortex Assembly Signalling: showing the signal route from σ^F at early time-points after the onset of sporulation through σ^K at later time-points after the onset of sporulation and finally to cortex synthesis resulting in the proteolysis and precipitation of SpoIIIL into the forespore cytoplasm. SpoVID-LysM domain can prevent cortex synthesis if coat assembly is not properly initiated and it does this by binding to and sequestering N-acetylglucosamine (GlcNAc) present in lipid II and peptidoglycan preventing Lipid II flipping into the intermembrane space. Both SpoVE and SpoVB proteins are suspected flippases. The presence of Lipid II and the action of cortex synthases SpoVE and SpoVD in the intermembrane space ensures the commencement of cortex assembly. SpoIIIL precipitation into the forespore cytoplasm at later time-points supposedly after proteolysis by SpoIVB, indicates cortex assembly. SpoIVB-mediated pro-σ^K processing and σ^K activation resulting in the upregulation of the Mur genes (including MurAB and MraY) responsible for increased precursor biosynthesis and activation of the cortex synthases enzymes is also shown.

We make this proposal because of a very interesting discovery of this work which is that, in the absence of SpoIVB, SpoIVA, SpoVM, and SpoVID, a particular SpoIIIL protein band (third band counting from the top in SpoIIIL immunoblot assay) always disappear or goes missing. In otherwise wild-type scenario, SpoIIIL usually shows 4 bands in the immunoblot assay. However, the disappearance of the third band reduces the number of bands observable in the SpoIIIL immunoblot assay to three. It is not completely clear why this particular band disappears in the *ΔspoIVB*, *ΔspoIVA*, *ΔspoVM*, and *ΔspoVID* single mutants as opposed to the wild-type, whereas the same third protein band is always present in the *ΔspoVD* or *ΔspoVE* single mutant, or even in the *ΔspoVD ΔspoVE* double mutant (see Appendix III, Figure S6.1)

just as in wild-type. So, we suspect that this third SpoIIIL protein band is intimately involved in a direct or indirect SpoVID-mediated SpoIIIL-encasement-signaling. Recall that the proper localization of SpoIIIL depends on SpoIVB, SpoIVA, SpoVM, SpoVD, and SpoVE but not on SpoVID.

To buttress this point further, recently, SpoVID was shown to contain a functional intracellular LysM domain that could sequester lipid II and prevent cortex assembly when coat assembly is improperly initiated, and strikingly, cortex assembly is still possible in the absence of SpoVID[87]. We therefore hypothesized that the encasement protein SpoVID may be functioning more specifically with SpoIIIL. To support this hypothesis, we gathered that whereas the LysM domain inherent in the C-terminal of SpoVID is well known for binding N-acetylglucosamine (GlcNAc) abundant in the cell walls of plants, fungi, and bacteria (chitin or peptidoglycan for instance)[87], the precursor biosynthesis enzyme MurAB on the other hand utilizes UDP-GlcNAc and phosphoenolpyruvate to synthesize UDP-MurNAc during spore peptidoglycan synthesis which is a vital process in cortex assembly and consequently, spore formation.

Additionally, our Tn-seq data showed that MurAB is very important for spore formation in the absence of SpoIIIL, and cortex assembly is severely impaired if not completely blocked in the double mutant of *ΔspoIIIL ΔmurAB*. We therefore propose that SpoIIIL on the forespore side functions whether directly or indirectly with MurAB and SpoVID on the mother cell side to monitor and or regulate proper cortex assembly and encasement. We also suggest that the strong sporulation and cortex assembly synergy observed between SpoIIIL and MurAB is probably via SpoVID since SpoVID can bind to either UDP-GlcNAc (the substrate of MurAB) or Lipid II which is present in peptidoglycan, or cortex peptidoglycan directly via its LysM domain.

Interestingly, to sum it all up, SpoIIIL is transcribed under the transcription factor σ^F, and according to our results, ensures the timely activation of σ^G. We think that SpoIIIL ensures this timely activation of σ^G probably because SpoIIIL itself is also involved in cortex assembly and therefore is intimately linked in ensuring that σ^G is activated in time so that all the necessary σ^G-dependent resources required for the normal process of cortex assembly such as SpoIVB activation, pro-σ^K processing, activation of the cortex PG synthases SpoVD/E, upregulation of the Mur genes as well as increased precursor synthesis will occur or be supplied right on time, to avoid any cortex assembly anomaly. Strikingly, the precipitation of SpoIIIL from the forespore inner membrane where it is uniformly localized prior to the commencement of

cortex assembly, into the forespore cytoplasm presenting as intriguing patchy-like structures as a result of proteolysis by SpoIVB, apparently becomes the prime indicator and signal of cortex assembly. We therefore propose using Fig 6.1 and Table 6.1 that this is supposedly how the 59 amino acid, 9.6kDa protein SpoIIIL, is involved in cortex assembly regulation and signalling.

6.3 Future Work

This thesis has demonstrated that a small protein such as SpoIIIL could actually be so intricately involved in complex processes like cortex assembly and even play vital roles such as ensuring that important factors responsible for various stages of such a process are properly regulated. Collectively, the accumulated evidence from this work has provided a significant leap in our understanding of spore development through the mid-stages to the later stages of sporulation in spore forming bacteria.

One important aspect of this work that remains unresolved is whether or not SpoIIIL maintains a direct genetic interaction with the cortex synthases, as well as the peptidoglycan precursor biosynthesis enzyme, MurAB. However future work can probe this new found relationship trio between SpoIIIL, SpoVID and MurAB via more sophisticated protein-protein interaction studies like bacterial two-hybrid assays. Since the role of SpoVID in linking the coordination between coat and cortex assembly during encasement was only recently discovered, and SpoVID directly binds to the substrate utilized by MurAB for precursor synthesis, it would be fascinating to unravel the nature of this relationship between MurAB and SpoVID, as well.

Also, the SpoIIIL immunoblot assay, reveals four similar sized protein bands that are usually observed in otherwise wild-type scenario. A particular SpoIIIL protein band (third band counting from the top in SpoIIIL immunoblot assay) which always disappear in the absence of SpoIVB, SpoIVA, SpoVM, and SpoVID could be analysed using state of the art chromatographic and NMR spectroscopy techniques to ascertain its amino acid composition and sequence in relation to the other three bands on the immunoblot. It would actually be interesting to ascertain the exact nature of each protein band observed in SpoIIIL immunoblot because it is not common to come across a small 9.6kDa protein like SpoIIIL which displays four different bands on an immunoblot. So may be the chromatographic analysis of the four SpoIIIL bands could reveal cleavage information surrounding the proteolysis of SpoIIIL since we already

know that the forespore protease SpoIVB as well as the SpoIVB catalytic site are both required for the proteolytic event that results in the precipitation of SpoIIIL into the forespore cytoplasm at later time-points after the onset of sporulation. With this in mind, one could easily be tempted to speculate that the four SpoIIIL bands are likely different active forms or versions of SpoIIIL.

Finally, a high point of this study which is of striking medical significance is the data in chapter 4 of this thesis which demonstrates that in the absence of both SpoIIIL and MurAB, cortex assembly is abolished and spore formation in *Bacillus subtilis* is rendered next to impossible. This is a discovery worth targeting and deserving of further investigation. Because, if spore formation can be totally eliminated as is the case in this study, and the recurrence and transmission of infections by pathogenic spore forming bacteria completely prevented, then we have achieved a milestone in the study of cell differentiation in prokaryotes.

6.4 Concluding Remarks

Summarily, this thesis has moved a step further in advancing the knowledge of how bacteria differentiate into spores. The cortex assembly regulatory and signalling pathways as well as the genetic interactions involved has been illustrated in a new light. Coordination of coat and cortex synthesis has long been an incompletely defined vital process during sporulation. Now SpoIIIL could probably be used as a signal for cortex assembly when further studies are being undertaken regarding the coat and cortex synthesis.

Appendices

Appendix I

Supplementary figures

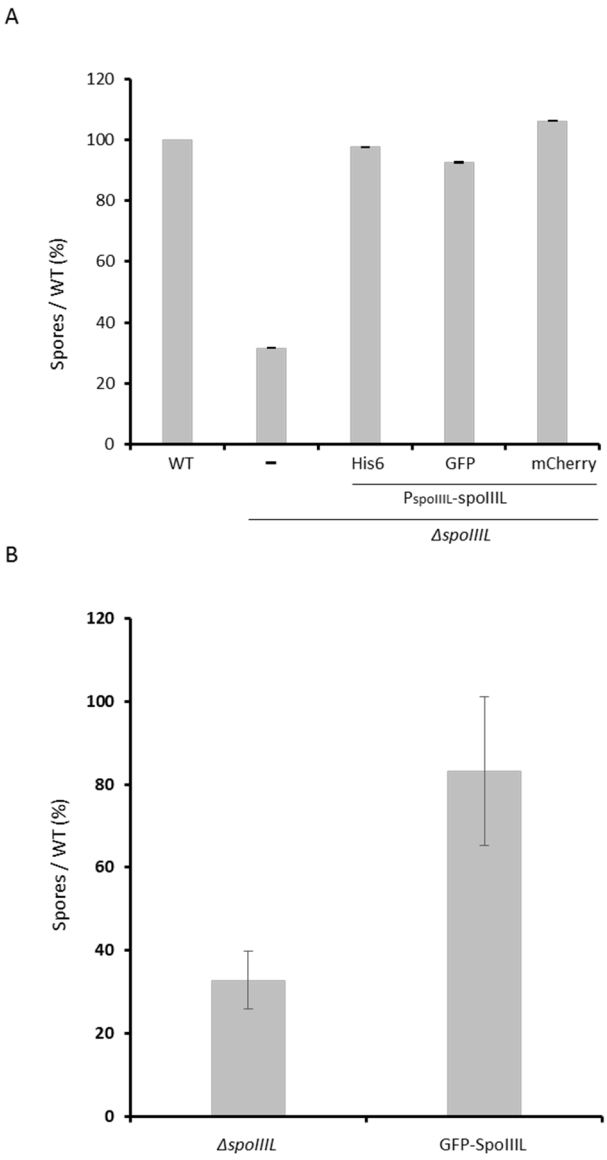

Figure S3.1: **Complementation graph of SpoIIIL(IIIL)**. showing **A)** WT, Δ*spoIIIL, and* complementation strains of three C-terminus tagged Δ*spoIIIL mutants* expressing SpoIIIL from an ectopic locus under its native promoter. Sporulation efficiency assays and the microscopic image analysis were done as described in the materials and methods section of this work. Error bars represent standard error of the mean from at least two biological replicates. **B)** Δ*spoIIIL, and* complementation strain of an N-terminus tagged Δ*spoIIIL mutant* expressing SpoIIIL from an ectopic locus under its native promoter. WT value is automatically set at 100%. Sporulation efficiency assays and the microscopic image analysis were done as stated in the materials and methods section of this work. Error bars represent standard error of the mean from at least two biological replicates.

Appendix I (Supplementary figures)

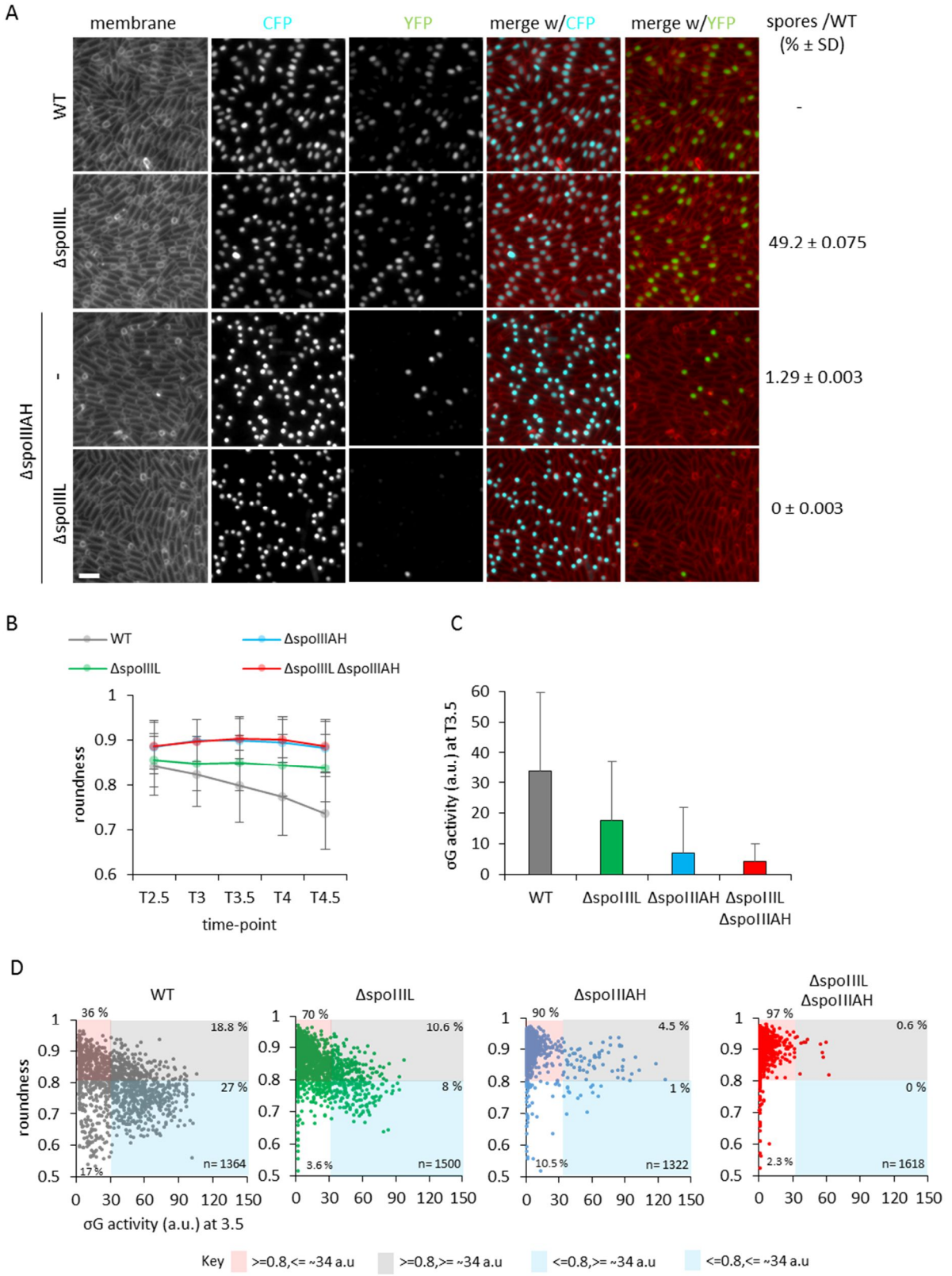

Figure S3.2: Synergistic defects of *the ΔspoIIIL ΔspoIIIAH* double mutant in σ^G activity, forespore shape (roundness), and sporulation efficiency. Representative images are wild type, *ΔspoIIIL, ΔspoIIIAH* and *ΔspoIIIL ΔspoIIIAH* at hour 4 **(A)** showing the roundness defects **(B)**, σ^G activity at hour 3.5 **(c)**, and the population data at hour 3.5 for roundness plotted against σ^G activity **(D)**. Sporulation efficiency assays and the microscopic image analysis were done as described in the materials and methods section of this work. Scale bars are 3 µm.

Appendix I (Supplementary figures)

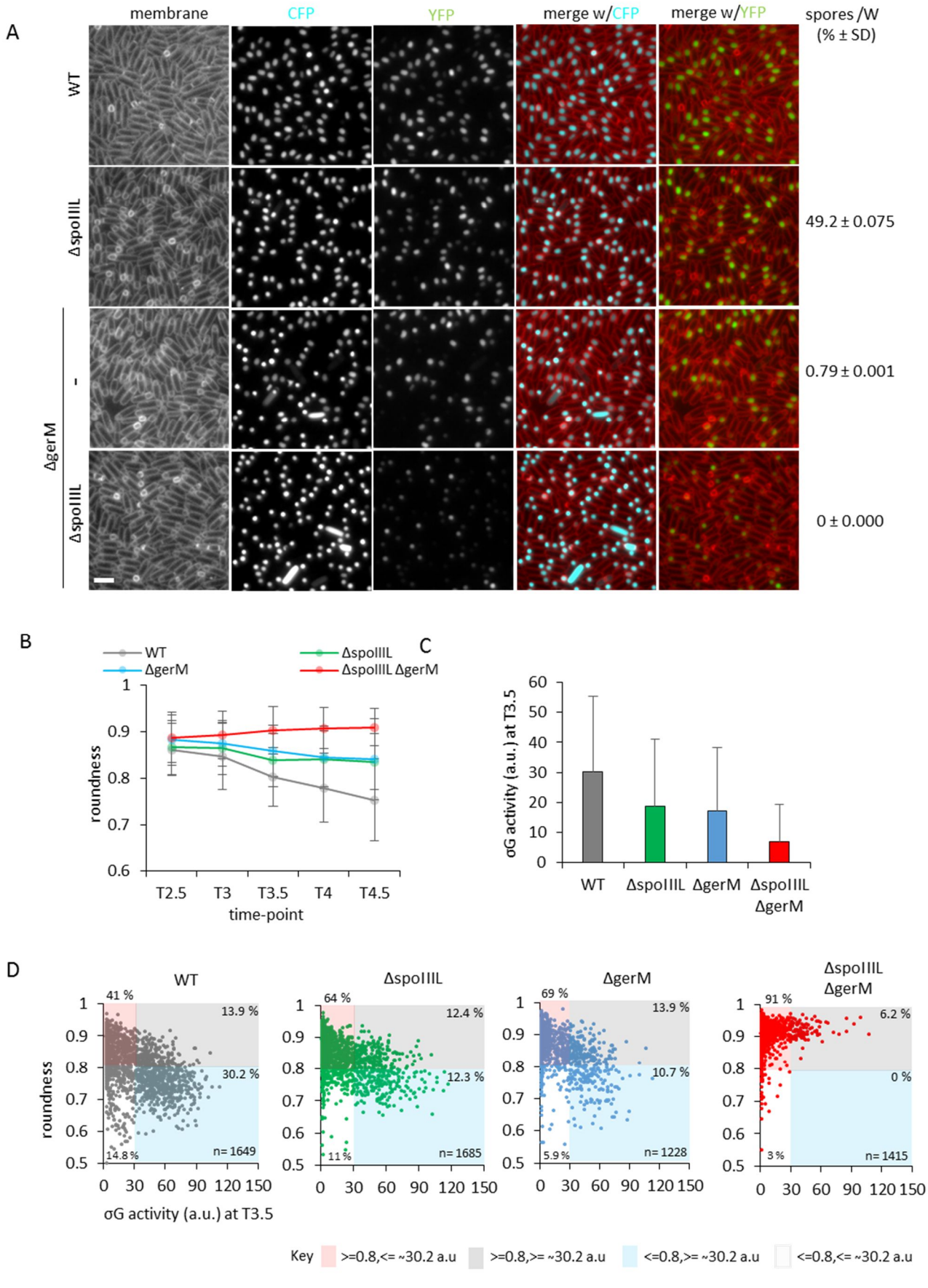

Figure S3.3: Synergistic defects of *the ΔspoIIIL ΔgerM* double mutant in σ^G activity, forespore shape (roundness), and sporulation efficiency. Representative images are wild type, *ΔspoIIIL, ΔgerM* and *ΔspoIIIL ΔgerM* at hour 4 **(A)** showing the roundness defects **(B)**, σ^G activity at hour 3.5 **(c)**, and the population data at hour 3.5 for roundness plotted against σ^G activity **(D)**. Sporulation efficiency assays and the microscopic image analysis were done as described in the materials and methods section of this work. Scale bars are 3 μm.

Appendix I (Supplementary figures)

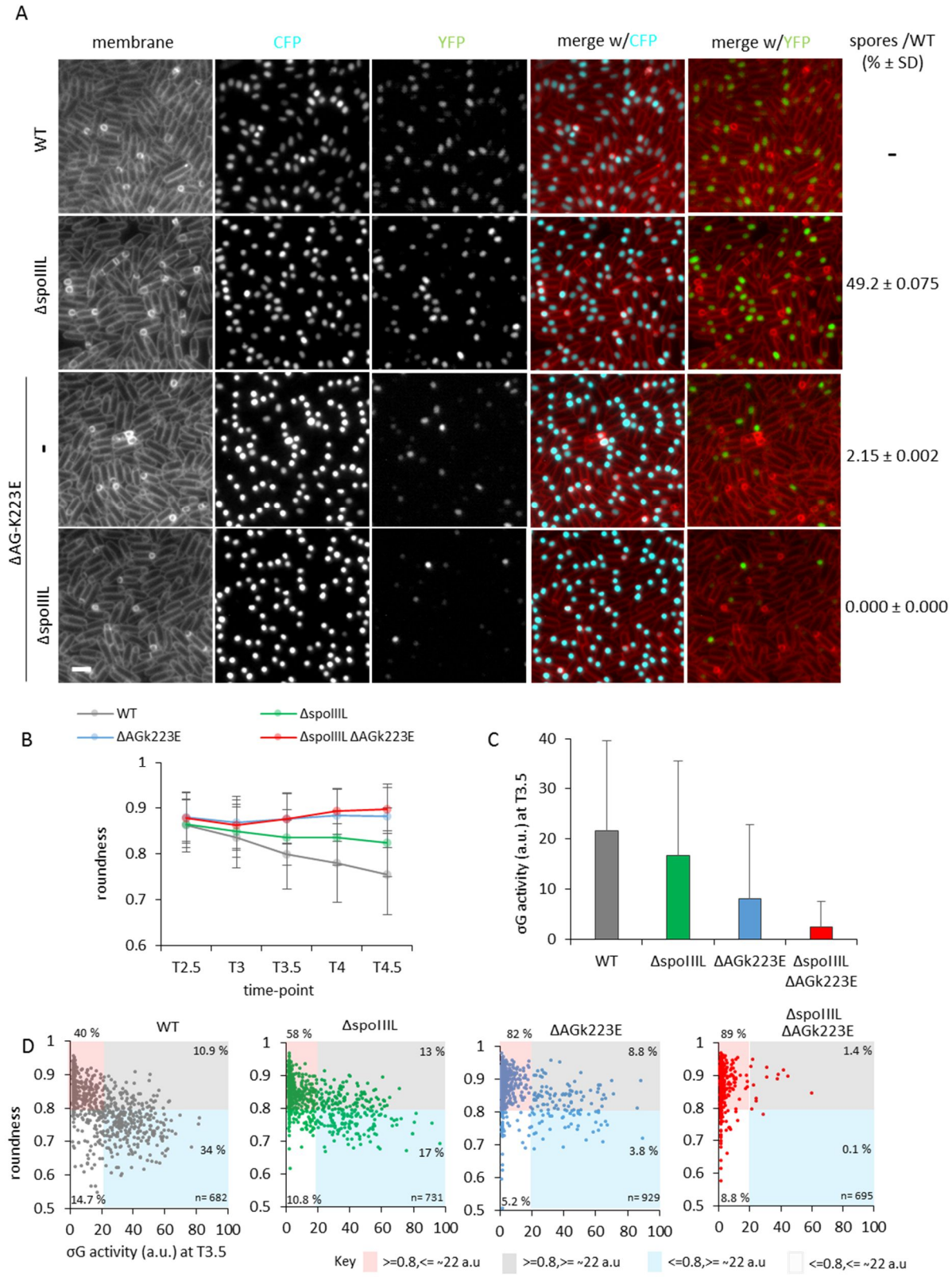

Figure S3.4: Synergistic defects of *the ΔspoIIIL ΔspoIIIAG-K223E* double mutant in $^{\sigma}$G activity, forespore shape (roundness), and sporulation efficiency. Representative images are wild-type, *ΔspoIIIL, ΔspoIIIAG-K223E,* and *ΔspoIIIL ΔspoIIIAG-K223E* double mutant at hour 4 **(A)** showing the roundness defects **(B)**, $^{\sigma}$G activity at hour 3.5 **(c)**, and the population data at hour 3.5 for roundness plotted against $^{\sigma}$G activity **(D)**. Sporulation efficiency assays and the microscopic image analysis were done as described in the materials and methods section of this work. Scale bars are 3 µm.

Appendix I

Supplementary figures

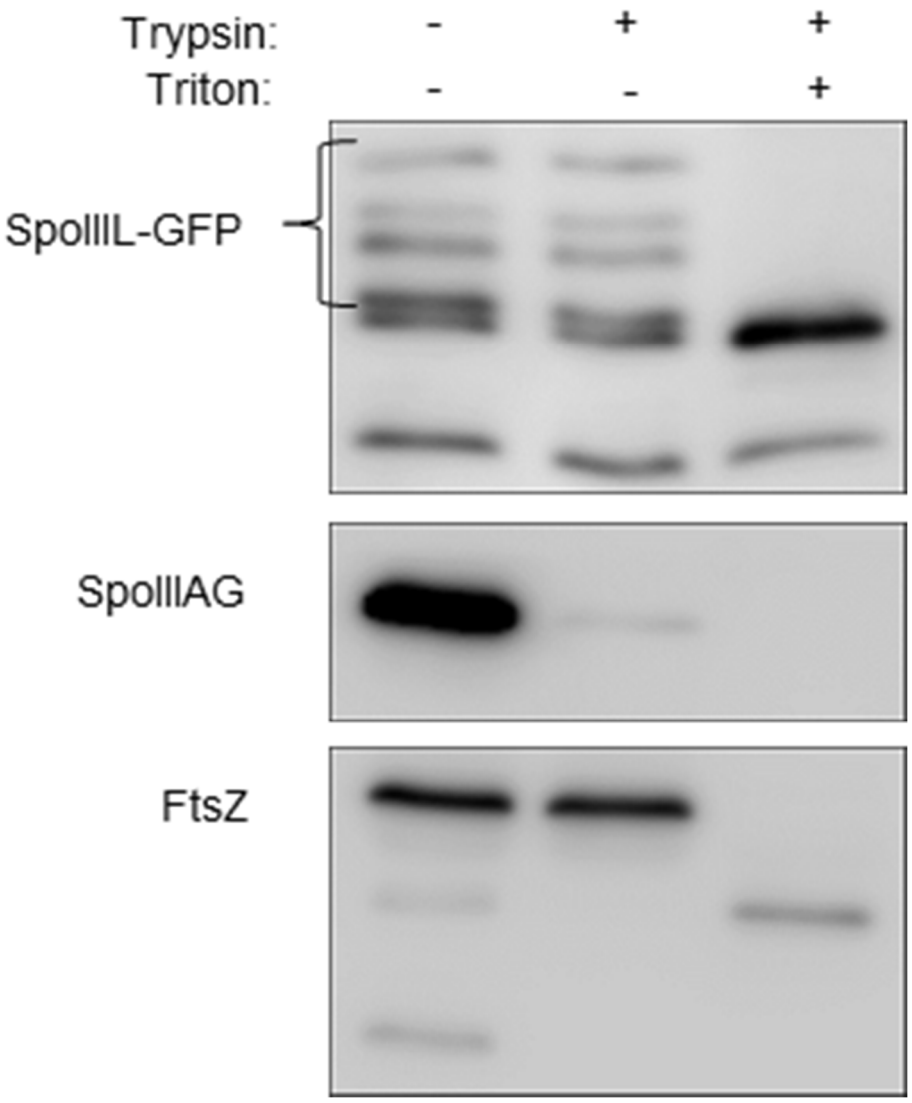

Figure S3.5: SpoIIIL-GFP is not surface-exposed and thus is not accessible to digestion by trypsin. Immunoblot analysis of protoplasted sporulating cells using anti-GFP antibodies. Cells expressed SpoIIIL-GFP as the sole source of SpoIIIL in strain *ΔspoIIQ ΔspoIIIL* (bPO85) respectively. Cells were treated with trypsin in the presence and absence of the detergent Triton X-100. Consistent with the prediction that SpoIIIL is not likely membrane-anchored but might contain some transmembrane segments, it was not susceptible to trypsin digestion in the absence of Triton X-100. As controls, the immunoblot was performed for a membrane protein housing an extracellular domain (SpoIIIAG) as well as for the cytoplasmic protein (FtsZ).

Appendix II

Supplementary figures

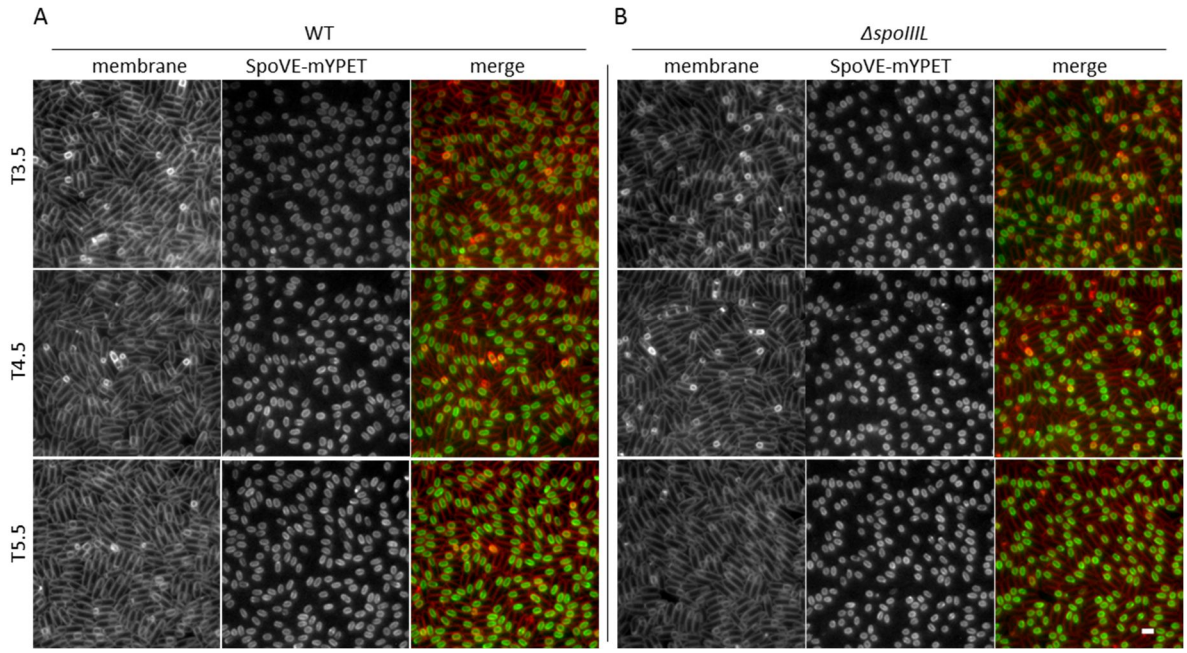

Figure S5.1: **SpoIIIL does not influences the localization of SpoVE**: Fluorescence localization of SpoVE-mYPET in otherwise WT cells (A), as well as in the *ΔspoIIIL* single mutant (B) at T3.5, T4.5, and at T5.5. Fluorescence signal is false-coloured green in the merged images. Cell membranes were visualised using TMA-DPH fluorescent membrane dye and are false-coloured red in the merged images. Scale bar = 2 µm.

Appendix II

Supplementary figures

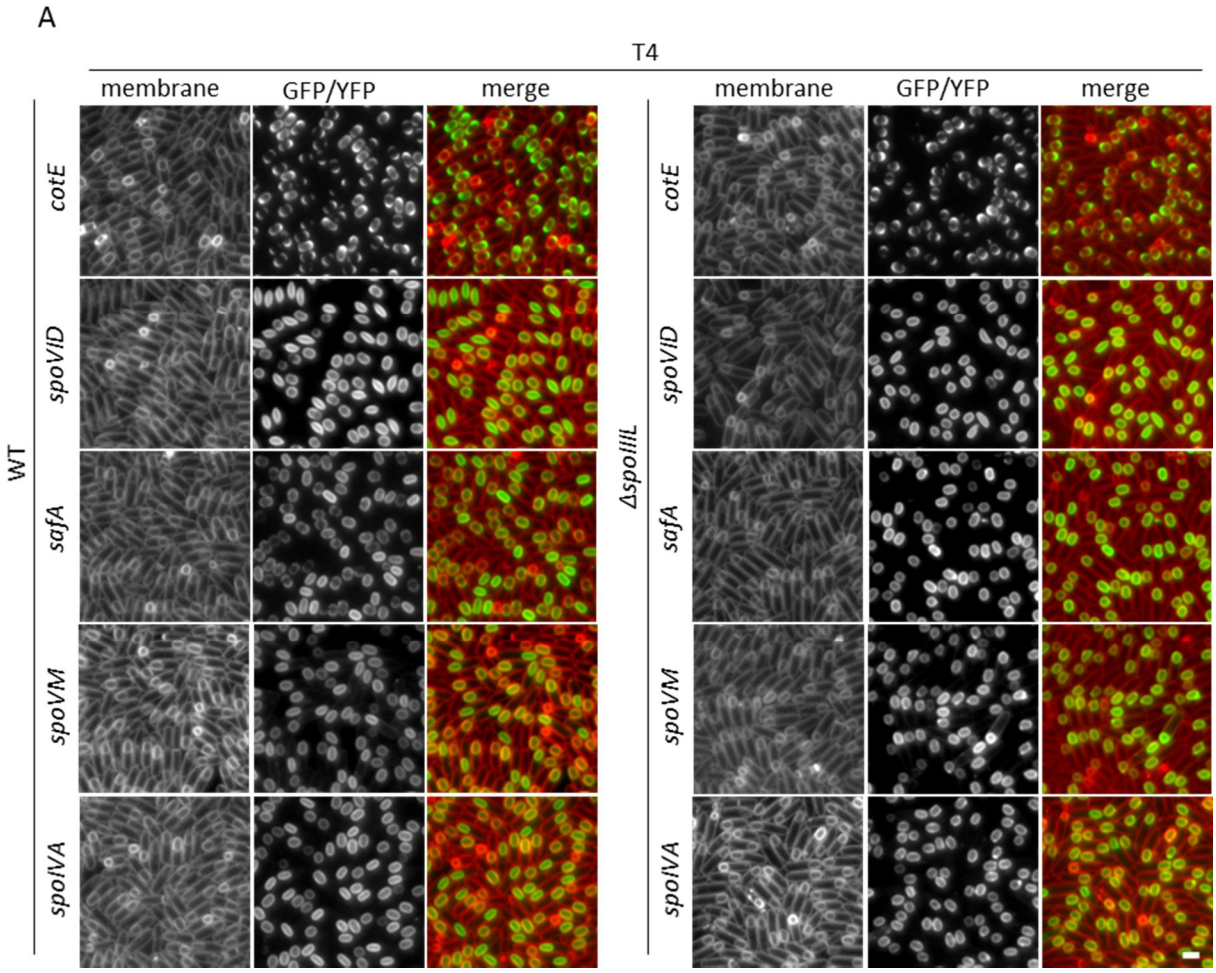

Figure S5.2: **SpoIIIL does not influences the localization of the coat proteins**: Fluorescence localization of the coat proteins in otherwise wild-type cells as well as in the *ΔspoIIIL* single mutant at T4 (A). Fluorescence signal is false-coloured green in the merged images. Cell membranes were visualised using TMA-DPH fluorescent membrane dye and are false-coloured red in the merged images. Scale bar = 2 µm.

Appendix II

Supplementary figures

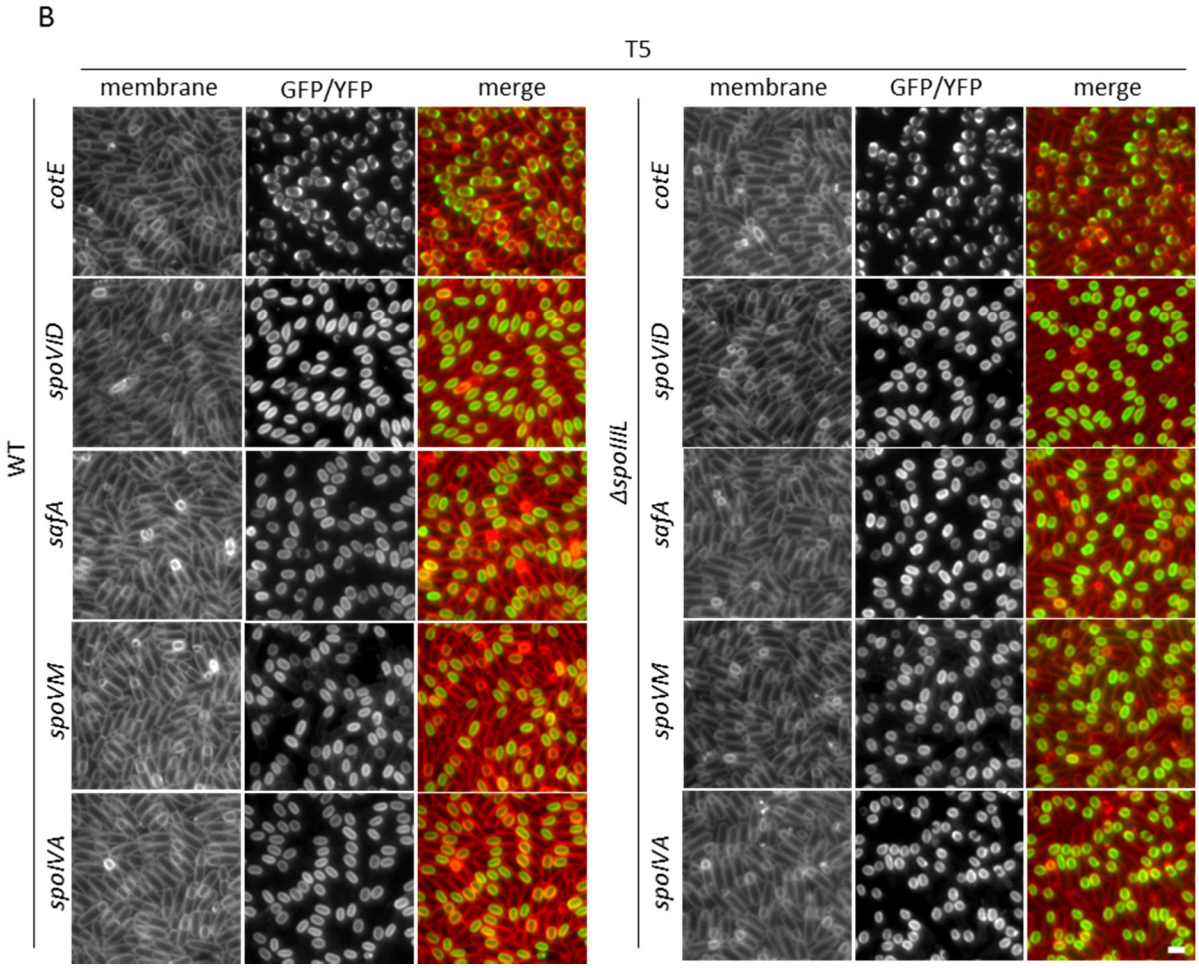

Figure S5.2: **SpoIIIL does not influences the localization of the coat proteins**: Fluorescence localization of the coat proteins in otherwise wild-type cells as well as in the *ΔspoIIIL* single mutant at T5 (B). Fluorescence signal is false-coloured green in the merged images. Cell membranes were visualised using TMA-DPH fluorescent membrane dye and are false-coloured red in the merged images. Scale bar = 2 µm.

Appendix II

Supplementary figures

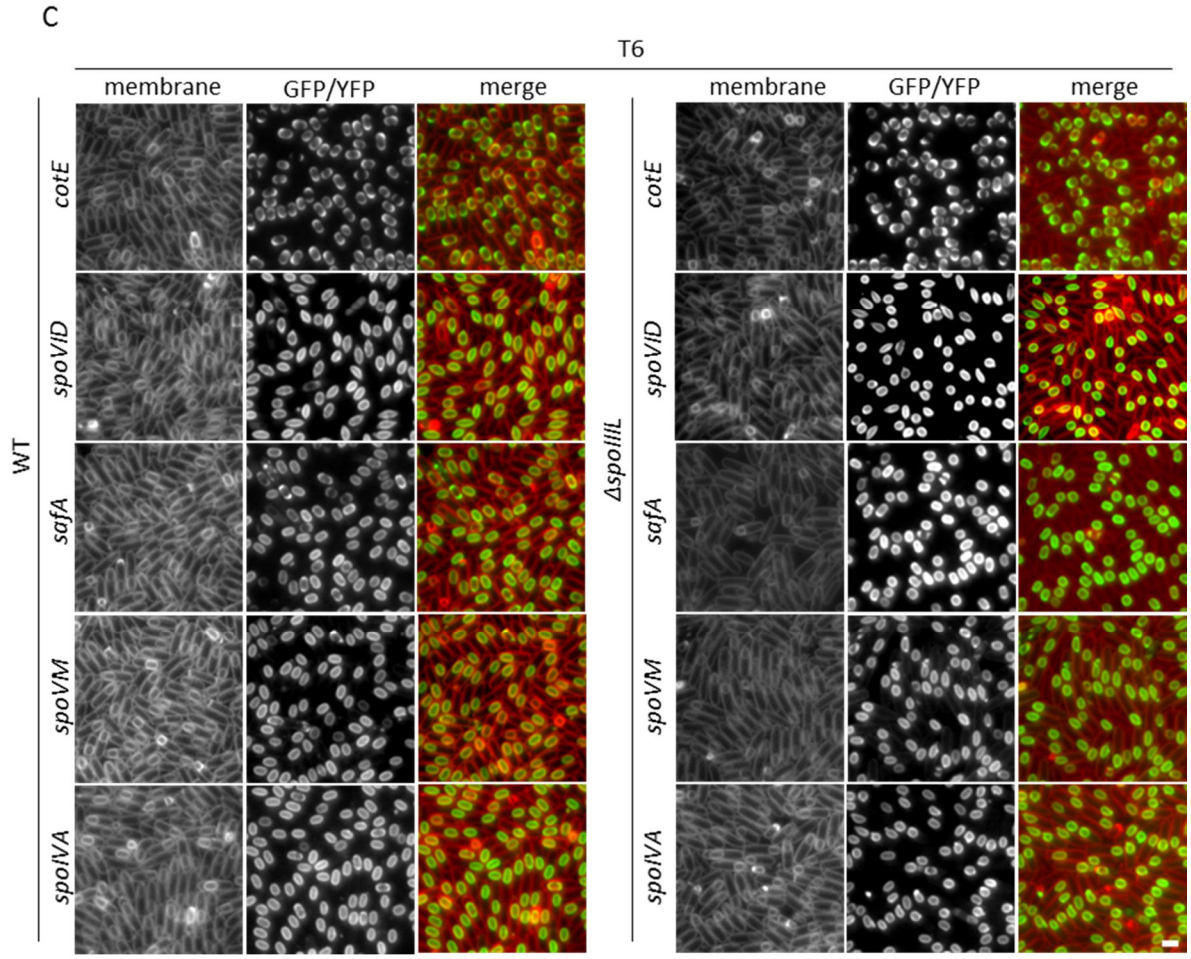

Figure S5.2: **SpoIIIL does not influences the localization of the coat proteins**: Fluorescence localization of the coat proteins in otherwise wild-type cells as well as in the *ΔspoIIIL* single mutant at T6 (C). Fluorescence signal is false-coloured green in the merged images. Cell membranes were visualised using TMA-DPH fluorescent membrane dye and are false-coloured red in the merged images. Scale bar = 2 µm.

Appendix III

Supplementary figures

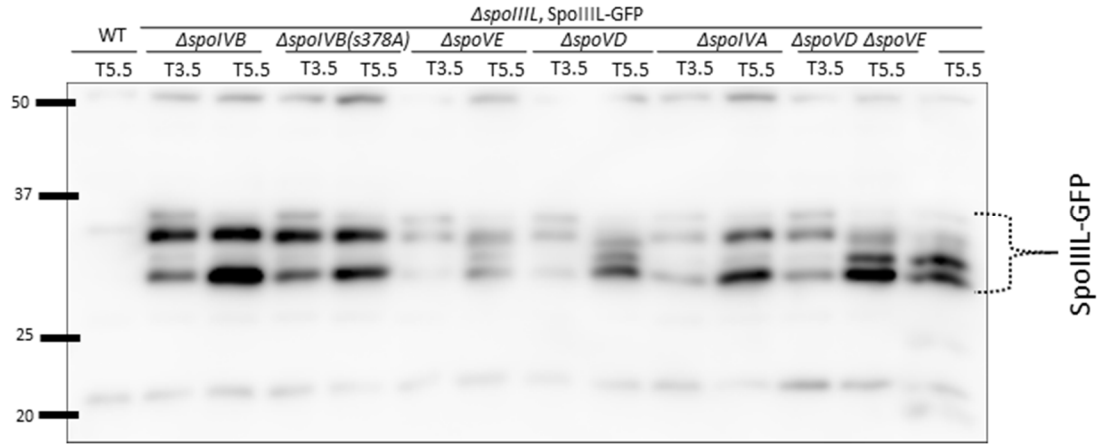

Figure S6.1 SpoVD and SpoVE do not influence SpoIIIL stability. Showing Immunoblot analysis of SpoIIIL-GFP in cell lysates of sporulating *ΔspoIVB*, *ΔspoIVB*(s378A), *ΔspoVE*, *ΔspoVD*, *ΔspoIVA* single mutants, and *ΔspoVD ΔspoVE* double mutant strains collected at T3.5 when SpoIIIL localizes uniformly around the forespore inner membrane, and at T5.5 when SpoIIIL localizes non-uniformly like intriguing patchy-like structures in the forespore cytoplasm. As controls, a cell lysate from sporulating cells collected at T5.5 from a WT strain that does not contain GFP, and an otherwise wild-type strain containing SpoIIIL-GFP at an ectopic locus as its only source of GFP, were included. SpoIIIL-GFP was immunodetected using anti-GFP antibodies. The position of SpoIIIL-GFP is indicated.

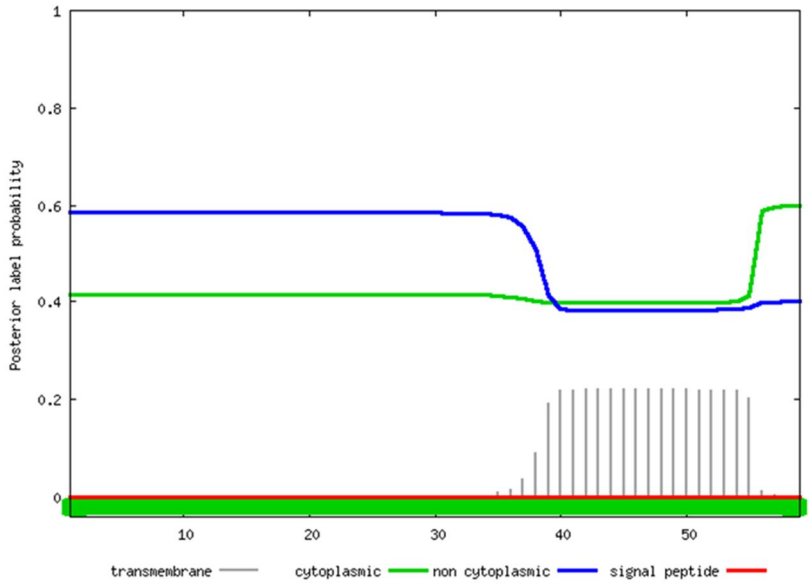

Figure S6.2 Result of SpoIIIL Phobius Analysis. Showing the prediction of transmembrane topology from the amino acid sequence of SpoIIIL.

Appendix III

Supplementary figures

Figure S6.3 Result of SpoIIIL ClustalW Multiple Alignment. Showing the conserved amino acid residues. Red arrow indicates the amino acid sequence for the wild-type *Bacillus subtilis* strain used in this thesis.

8 References

1. F. Kunst, N. Ogasawara, I. Moszer, A. M. Albertini, G. Alloni, V. Azevedo, M. G. Bertero, P. Bessie` res, A. Bolotin, S. Borchert, et al. (1997). The complete genome sequence of the Gram-positive bacterium Bacillus subtilis. NATURE *390*.

2. Westers, L., Westers, H., and Quax, W.J. (2004). Bacillus subtilis as cell factory for pharmaceutical proteins: a biotechnological approach to optimize the host organism. Biochim. Biophys. Acta BBA - Mol. Cell Res. *1694*, 299–310. 10.1016/j.bbamcr.2004.02.011.

3. Amiteye, S. (2020). Highlights of the Genetics and Importance of Bacillus subtilis Spore Formation. J. Adv. Microbiol., 1–11. 10.9734/jamb/2019/v19i330198.

4. Su, Y., Liu, C., Fang, H., and Zhang, D. (2020). Bacillus subtilis: a universal cell factory for industry, agriculture, biomaterials and medicine. Microb. Cell Factories *19*, 173. 10.1186/s12934-020-01436-8.

5. Khodavirdipour, A., Chamanrokh, P., Alikhani, M.Y., and Alikhani, M.S. (2022). Potential of Bacillus subtilis Against SARS-CoV-2 – A Sustainable Drug Development Perspective. Front. Microbiol. *13*, 718786. 10.3389/fmicb.2022.718786.

6. Wu, B., Xiu, J., Yu, L., Huang, L., Yi, L., and Ma, Y. (2022). Biosurfactant production by Bacillus subtilis SL and its potential for enhanced oil recovery in low permeability reservoirs. Sci. Rep. *12*, 7785. 10.1038/s41598-022-12025-7.

7. Vallota-Eastman, A., Bui, C., Williams, P.M., Valentine, D.L., Loftus, D., and Rothschild, L. (2023). *Bacillus subtilis* engineered for aerospace medicine: a platform for off-planet production of pharmaceutical peptides (Pharmacology and Toxicology) 10.1101/2023.02.22.529550.

8. Ihekwaba, A.E., Mura, I., and Barker, G.C. (2014). Computational modelling and analysis of the molecular network regulating sporulation initiation in Bacillus subtilis. BMC Syst. Biol. *8*, 119. 10.1186/s12918-014-0119-x.

9. Lecca, P., Mura, I., Re, A., Barker, G.C., and Ihekwaba, A.E.C. (2016). Time Series Analysis of the Bacillus subtilis Sporulation Network Reveals Low Dimensional Chaotic Dynamics. Front. Microbiol. *7*. 10.3389/fmicb.2016.01760.

10. Vidic, J., Chaix, C., Manzano, M., and Heyndrickx, M. (2020). Food Sensing: Detection of Bacillus cereus Spores in Dairy Products. Biosensors *10*, 15. 10.3390/bios10030015.

11. Oliveira, R.B.A., Margalho, L.P., Nascimento, J.S., Costa, L.E.O., Portela, J.B., Cruz, A.G., and Sant'Ana, A.S. (2016). Processed cheese contamination by spore-forming bacteria: A review of sources, routes, fate during processing and control. Trends Food Sci. Technol. *57*, 11–19. 10.1016/j.tifs.2016.09.008.

12. Baldwin, V.M. (2020). You Can't B. cereus – A Review of Bacillus cereus Strains That Cause Anthrax-Like Disease. Front. Microbiol. *11*, 1731. 10.3389/fmicb.2020.01731.

13. Sharma, N., Kumar, J., Thakur, S., Sharma, S., and Shrivastava, V. (2013). Antibacterial study of silver doped zinc oxide nanoparticles against Staphylococcus aureus and Bacillus subtilis. Drug Invent. Today *5*, 50–54. 10.1016/j.dit.2013.03.007.

14. Meeske, A.J., Rodrigues, C.D.A., Brady, J., Lim, H.C., Bernhardt, T.G., and Rudner, D.Z. (2016). High-Throughput Genetic Screens Identify a Large and Diverse Collection of New Sporulation Genes in Bacillus subtilis. PLOS Biol. *14*, e1002341. 10.1371/journal.pbio.1002341.

15. Zeigler, D.R., Prágai, Z., Rodriguez, S., Chevreux, B., Muffler, A., Albert, T., Bai, R., Wyss, M., and Perkins, J.B. (2008). The Origins of 168, W23, and Other *Bacillus subtilis* Legacy Strains. J. Bacteriol. *190*, 6983–6995. 10.1128/JB.00722-08.

16. Barák, I., Ricca, E., and Cutting, S.M. (2004). From fundamental studies of sporulation to applied spore research: Bacterial sporulation. Mol. Microbiol. *55*, 330–338. 10.1111/j.1365-2958.2004.04445.x.

17. Piggot, P.J., and Hilbert, D.W. (2004). Sporulation of Bacillus subtilis. Curr. Opin. Microbiol. *7*, 579–586. 10.1016/j.mib.2004.10.001.

18. Oren, A., and Garrity, G.M. (2021). Valid publication of the names of forty-two phyla of prokaryotes. Int. J. Syst. Evol. Microbiol. *71*. 10.1099/ijsem.0.005056.

19. Broder, D.H., and Pogliano, K. (2006). Forespore Engulfment Mediated by a Ratchet-Like Mechanism. Cell *126*, 917–928. 10.1016/j.cell.2006.06.053.

20. Sonenshein, A.L. (2000). Control of sporulation initiation in Bacillus subtilis. Curr. Opin. Microbiol. *3*, 561–566. 10.1016/S1369-5274(00)00141-7.

21. Morlot, C., and Rodrigues, C.D.A. (2018). The New Kid on the Block: A Specialized Secretion System during Bacterial Sporulation. Trends Microbiol. *26*, 663–676. 10.1016/j.tim.2018.01.001.

22. Kunst, F., Ogasawara, N., Moszer, I., Albertini, A.M., Alloni, G., Azevedo, V., Bertero, M.G., Bessières, P., Bolotin, A., Borchert, S., et al. (1997). The complete genome sequence of the Gram-positive bacterium Bacillus subtilis. Nature *390*, 249–256. 10.1038/36786.

23. Earl, A.M., Losick, R., and Kolter, R. (2008). Ecology and genomics of Bacillus subtilis. Trends Microbiol. *16*, 269–275. 10.1016/j.tim.2008.03.004.

24. Ramos-Silva, P., Serrano, M., and Henriques, A.O. (2019). From Root to Tips: Sporulation Evolution and Specialization in Bacillus subtilis and the Intestinal Pathogen Clostridioides difficile. Mol. Biol. Evol. *36*, 2714–2736. 10.1093/molbev/msz175.

25. Ramos-Silva, P., Serrano, M., and Henriques, A.O. (2019). From Root to Tips: Sporulation Evolution and Specialization in Bacillus subtilis and the Intestinal Pathogen Clostridioides difficile. Mol. Biol. Evol. *36*, 2714–2736. 10.1093/molbev/msz175.

26. Higgins, D., and Dworkin, J. (2012). Recent progress in *Bacillus subtilis* sporulation. FEMS Microbiol. Rev. *36*, 131–148. 10.1111/j.1574-6976.2011.00310.x.

27. Earl, A.M., Losick, R., and Kolter, R. (2008). Ecology and genomics of Bacillus subtilis. Trends Microbiol. *16*, 269–275. 10.1016/j.tim.2008.03.004.

28. Meeske, A.J., Rodrigues, C.D.A., Brady, J., Lim, H.C., Bernhardt, T.G., and Rudner, D.Z. (2016). High-Throughput Genetic Screens Identify a Large and Diverse Collection of New

Sporulation Genes in Bacillus subtilis. PLOS Biol. *14*, e1002341. 10.1371/journal.pbio.1002341.

29. Lin, P., Yuan, H., Du, J., Liu, K., Liu, H., and Wang, T. (2020). Progress in research and application development of surface display technology using Bacillus subtilis spores. Appl. Microbiol. Biotechnol. *104*, 2319–2331. 10.1007/s00253-020-10348-x.

30. Lecca, P., Mura, I., Re, A., Barker, G.C., and Ihekwaba, A.E.C. (2016). Time Series Analysis of the Bacillus subtilis Sporulation Network Reveals Low Dimensional Chaotic Dynamics. Front. Microbiol. *7*. 10.3389/fmicb.2016.01760.

31. Narula, J., Devi, S.N., Fujita, M., and Igoshin, O.A. (2012). Ultrasensitivity of the Bacillus subtilis sporulation decision. Proc. Natl. Acad. Sci. *109*, E3513–E3522. 10.1073/pnas.1213974109.

32. Mutlu, A., Kaspar, C., Becker, N., and Bischofs, I.B. (2020). A spore quality–quantity tradeoff favors diverse sporulation strategies in Bacillus subtilis. ISME J. *14*, 2703–2714. 10.1038/s41396-020-0721-4.

33. Burbulys, D., Trach, K.A., and Hoch, J.A. (1991). Initiation of sporulation in B. subtilis is controlled by a multicomponent phosphorelay. Cell *64*, 545–552. 10.1016/0092-8674(91)90238-T.

34. Veening, J.-W., Murray, H., and Errington, J. (2009). A mechanism for cell cycle regulation of sporulation initiation in Bacillus subtilis. Genes Dev. *23*, 1959–1970. 10.1101/gad.528209.

35. Errington, J. (2003). Regulation of endospore formation in Bacillus subtilis. Nat. Rev. Microbiol. *1*, 117–126. 10.1038/nrmicro750.

36. Amiteye, S. (2020). Highlights of the Genetics and Importance of Bacillus subtilis Spore Formation. J. Adv. Microbiol., 1–11. 10.9734/jamb/2019/v19i330198.

37. JEFFERY ERRINGTON (1993). Bacillus subtilis Sporulation: Regulation of Gene Expression and Control of Morphogenesis. Microbiol. Rev. *57*, 1–33.

38. Doan, T., Morlot, C., Meisner, J., Serrano, M., Henriques, A.O., Moran, C.P., and Rudner, D.Z. (2009). Novel Secretion Apparatus Maintains Spore Integrity and Developmental Gene Expression in Bacillus subtilis. PLoS Genet. *5*, e1000566. 10.1371/journal.pgen.1000566.

39. Khanna, K., Lopez-Garrido, J., Sugie, J., Pogliano, K., and Villa, E. (2021). Asymmetric localization of the cell division machinery during Bacillus subtilis sporulation. eLife *10*. 10.7554/eLife.62204.

40. Tan, I.S., and Ramamurthi, K.S. (2014). Spore formation in *B acillus subtilis*: *Bacillus subtilis* sporulation. Environ. Microbiol. Rep. *6*, 212–225. 10.1111/1758-2229.12130.

41. Jeffrey Meisner, Xin Wang, Monica Serrano, Adriano O. Henriques, and Charles P. Moran, Jr. (2008). A channel connecting the mother cell and forespore during bacterial endospore formation. PNAS *105*, 15100–15105.

42. Higgins, D., and Dworkin, J. (2012). Recent progress in *Bacillus subtilis* sporulation. FEMS Microbiol. Rev. *36*, 131–148. 10.1111/j.1574-6976.2011.00310.x.

43. Errington, J. (2003). Regulation of endospore formation in Bacillus subtilis. Nat. Rev. Microbiol. *1*, 117–126. 10.1038/nrmicro750.

44. Strauch, M.A., and Hoch, J.A. (1993). Signal transduction in Bacillus subtilis sporulation. Curr. Opin. Genet. Dev. *3*, 203–212. 10.1016/0959-437X(93)90024-J.

45. Khanna, K., Lopez-Garrido, J., Zhao, Z., Watanabe, R., Yuan, Y., and Villa, E. The molecular architecture of engulfment during Bacillus subtilis sporulation. 29.

46. Rubio, A., and Pogliano, K. (2004). Septal localization of forespore membrane proteins during engulfment in Bacillus subtilis. EMBO J. *23*, 1636–1646. 10.1038/sj.emboj.7600171.

47. Doan, T., Morlot, C., Meisner, J., Serrano, M., Henriques, A.O., Moran, C.P., and Rudner, D.Z. (2009). Novel Secretion Apparatus Maintains Spore Integrity and Developmental Gene Expression in Bacillus subtilis. PLoS Genet. *5*, e1000566. 10.1371/journal.pgen.1000566.

48. Khanna, K., López-Garrido, J., Sugie, J., Pogliano, K., and Villa, E. (2020). Asymmetric localization of the cell division machinery during *Bacillus subtilis* sporulation (Microbiology) 10.1101/2020.07.22.216184.

49. Tan, I.S., and Ramamurthi, K.S. (2014). Spore formation in *B acillus subtilis*: *Bacillus subtilis* sporulation. Environ. Microbiol. Rep. *6*, 212–225. 10.1111/1758-2229.12130.

50. Piggot, P.J., and Hilbert, D.W. (2004). Sporulation of Bacillus subtilis. Curr. Opin. Microbiol. *7*, 579–586. 10.1016/j.mib.2004.10.001.

51. Barák, I., Ricca, E., and Cutting, S.M. (2004). From fundamental studies of sporulation to applied spore research: Bacterial sporulation. Mol. Microbiol. *55*, 330–338. 10.1111/j.1365-2958.2004.04445.x.

52. Zhang, L., Higgins, M.L., Piggot, P.J., and Karow, M.L. (1996). Analysis of the role of prespore gene expression in the compartmentalization of mother cell-specific gene expression during sporulation of Bacillus subtilis. J. Bacteriol. *178*, 2813–2817. 10.1128/JB.178.10.2813-2817.1996.

53. Errington, J. (1993). and Control of Morphogenesist. MICROBIOL REV *57*, 33.

54. Fimlaid, K.A., Jensen, O., Donnelly, M.L., Siegrist, M.S., and Shen, A. (2015). Regulation of Clostridium difficile Spore Formation by the SpoIIQ and SpoIIIA Proteins. PLOS Genet. *11*, e1005562. 10.1371/journal.pgen.1005562.

55. Sun, Y.-L., Sharp, M.D., and Pogliano, K. (2000). A dispensable role for forespore-specific gene expression in engulfment of the forespore during sporulation of Bacillus subtilis. J. Bacteriol. *182*, 2919–2927.

56. Zeytuni, N., Hong, C., Flanagan, K.A., Worrall, L.J., Theiltges, K.A., Vuckovic, M., Huang, R.K., Massoni, S.C., Camp, A.H., Yu, Z., et al. (2017). Near-atomic resolution cryoelectron microscopy structure of the 30-fold homooligomeric SpoIIIAG channel essential

to spore formation in *Bacillus subtilis*. Proc. Natl. Acad. Sci. *114*, E7073–E7081. 10.1073/pnas.1704310114.

57. Meisner, J., Maehigashi, T., Andre, I., Dunham, C.M., and Moran, C.P. (2012). Structure of the basal components of a bacterial transporter. Proc. Natl. Acad. Sci. *109*, 5446–5451. 10.1073/pnas.1120113109.

58. Camp, A.H., Wang, A.F., and Losick, R. (2011). A Small Protein Required for the Switch from F to G during Sporulation in Bacillus subtilis. J. Bacteriol. *193*, 116–124. 10.1128/JB.00949-10.

59. Rodrigues, C.D.A., Marquis, K.A., Meisner, J., and Rudner, D.Z. (2013). Peptidoglycan hydrolysis is required for assembly and activity of the transenvelope secretion complex during sporulation in *Bacillus subtilis*: Septal localization of SpoIIQ. Mol. Microbiol. *89*, 1039–1052. 10.1111/mmi.12322.

60. Rodrigues, C.D.A., Ramírez-Guadiana, F.H., Meeske, A.J., Wang, X., and Rudner, D.Z. (2016). GerM is required to assemble the basal platform of the SpoIIIA-SpoIIQ transenvelope complex during sporulation in *Bacillus subtilis*: GerM is required to assemble the SpoIIIA-SpoIIQ complex. Mol. Microbiol. *102*, 260–273. 10.1111/mmi.13457.

61. Crawshaw, A.D., Serrano, M., Stanley, W.A., Henriques, A.O., and Salgado, P.S. (2014). A mother cell-to-forespore channel: current understanding and future challenges. FEMS Microbiol. Lett. *358*, 129–136. 10.1111/1574-6968.12554.

62. Fimlaid, K.A., Jensen, O., Donnelly, M.L., Siegrist, M.S., and Shen, A. (2015). Regulation of Clostridium difficile Spore Formation by the SpoIIQ and SpoIIIA Proteins. PLOS Genet. *11*, e1005562. 10.1371/journal.pgen.1005562.

63. Crawshaw, A.D., Serrano, M., Stanley, W.A., Henriques, A.O., and Salgado, P.S. (2014). A mother cell-to-forespore channel: current understanding and future challenges. FEMS Microbiol. Lett. *358*, 129–136. 10.1111/1574-6968.12554.

64. Tocheva, E.I., López-Garrido, J., Hughes, H.V., Fredlund, J., Kuru, E., VanNieuwenhze, M.S., Brun, Y.V., Pogliano, K., and Jensen, G.J. (2013). Peptidoglycan transformations during *Bacillus subtilis* sporulation: Peptidoglycan remodelling. Mol. Microbiol. *88*, 673–686. 10.1111/mmi.12201.

65. McKenney, P.T., Driks, A., and Eichenberger, P. (2013). The Bacillus subtilis endospore: assembly and functions of the multilayered coat. Nat. Rev. Microbiol. *11*, 33–44. 10.1038/nrmicro2921.

66. Morlot, C., Uehara, T., Marquis, K.A., Bernhardt, T.G., and Rudner, D.Z. (2010). A highly coordinated cell wall degradation machine governs spore morphogenesis in Bacillus subtilis. Genes Dev. *24*, 411–422. 10.1101/gad.1878110.

67. Morlot, C., and Rodrigues, C.D.A. (2018). The New Kid on the Block: A Specialized Secretion System during Bacterial Sporulation. Trends Microbiol. *26*, 663–676. 10.1016/j.tim.2018.01.001.

68. Driks, A. (2002). Overview: development in bacteria: spore formation in Bacillus subtilis. Cell. Mol. Life Sci. CMLS *59*, 389–391.

69. Fujita, M., González-Pastor, J.E., and Losick, R. (2005). High- and Low-Threshold Genes in the Spo0A Regulon of *Bacillus subtilis*. J. Bacteriol. *187*, 1357–1368. 10.1128/JB.187.4.1357-1368.2005.

70. Piggot, P.J. (1996). Spore development in Bacillus subtilis. Curr. Opin. Genet. Dev. *6*, 531–537.

71. Devi, S.N., Kiehler, B., Haggett, L., and Fujita, M. (2015). Evidence that Autophosphorylation of the Major Sporulation Kinase in Bacillus subtilis Is Able To Occur in trans. J. Bacteriol. *197*, 2675–2684. 10.1128/JB.00257-15.

72. Rubio, A., and Pogliano, K. (2004). Septal localization of forespore membrane proteins during engulfment in Bacillus subtilis. EMBO J. *23*, 1636–1646. 10.1038/sj.emboj.7600171.

73. Mohamed, A.M.T., Chan, H., Luhur, J., Bauda, E., Gallet, B., Morlot, C., Cole, L., Awad, M., Crawford, S., Lyras, D., et al. (2021). Chromosome Segregation and Peptidoglycan Remodeling Are Coordinated at a Highly Stabilized Septal Pore to Maintain Bacterial Spore Development. Dev. Cell *56*, 36-51.e5. 10.1016/j.devcel.2020.12.006.

74. Doan, T., and Rudner, D.Z. (2007). Perturbations to engulfment trigger a degradative response that prevents cell-cell signalling during sporulation in Bacillus subtilis: Engulfment defects trigger a degradative response. Mol. Microbiol. *64*, 500–511. 10.1111/j.1365-2958.2007.05677.x.

75. Broder, D.H., and Pogliano, K. (2006). Forespore Engulfment Mediated by a Ratchet-Like Mechanism. Cell *126*, 917–928. 10.1016/j.cell.2006.06.053.

76. Tocheva, E.I., López-Garrido, J., Hughes, H.V., Fredlund, J., Kuru, E., VanNieuwenhze, M.S., Brun, Y.V., Pogliano, K., and Jensen, G.J. (2013). Peptidoglycan transformations during *Bacillus subtilis* sporulation: Peptidoglycan remodelling. Mol. Microbiol. *88*, 673–686. 10.1111/mmi.12201.

77. Serrano, M., Crawshaw, A.D., Dembek, M., Monteiro, J.M., Pereira, F.C., Pinho, M.G., Fairweather, N.F., Salgado, P.S., and Henriques, A.O. (2016). The SpoIIQ-SpoIIIAH complex of *C lostridium difficile* controls forespore engulfment and late stages of gene expression and spore morphogenesis: The SpoIIQ-SpoIIIAH complex of *C. difficile*. Mol. Microbiol. *100*, 204–228. 10.1111/mmi.13311.

78. Khanna, K. (2020). The Molecular Architecture of Spore Morphogenesis in Bacillus subtilis (University of California, San Diego).

79. Chan, H., Taib, N., Gilmore, M.C., Mohamed, A.M.T., Hanna, K., Luhur, J., Nguyen, H., Hafiz, E., Cava, F., Gribaldo, S., et al. (2022). Genetic Screens Identify Additional Genes Implicated in Envelope Remodeling during the Engulfment Stage of Bacillus subtilis Sporulation. mBio *13*, e01732-22. 10.1128/mbio.01732-22.

80. Camp, A.H., and Losick, R. (2009). A feeding tube model for activation of a cell-specific transcription factor during sporulation in Bacillus subtilis. Genes Dev. *23*, 1014–1024. 10.1101/gad.1781709.

81. Bhavsar, A.P., and Brown, E.D. (2006). Cell wall assembly in Bacillus subtilis: how spirals and spaces challenge paradigms. Mol. Microbiol. *60*, 1077–1090. 10.1111/j.1365-2958.2006.05169.x.

82. Hilbert, D.W., and Piggot, P.J. (2004). Compartmentalization of Gene Expression during *Bacillus subtilis* Spore Formation. Microbiol. Mol. Biol. Rev. *68*, 234–262. 10.1128/MMBR.68.2.234-262.2004.

83. McPherson, D.C., Driks, A., and Popham, D.L. (2001). Two Class A High-Molecular-Weight Penicillin-Binding Proteins of *Bacillus subtilis* Play Redundant Roles in Sporulation. J. Bacteriol. *183*, 6046–6053. 10.1128/JB.183.20.6046-6053.2001.

84. Campo, N., and Rudner, D.Z. (2007). SpoIVB and CtpB Are Both Forespore Signals in the Activation of the Sporulation Transcription Factor σ^K in *Bacillus subtilis*. J. Bacteriol. *189*, 6021–6027. 10.1128/JB.00399-07.

85. Doan, T., and Rudner, D.Z. (2007). Perturbations to engulfment trigger a degradative response that prevents cell-cell signalling during sporulation in Bacillus subtilis: Engulfment defects trigger a degradative response. Mol. Microbiol. *64*, 500–511. 10.1111/j.1365-2958.2007.05677.x.

86. Popham, D.L., and Bernhards, C.B. (2015). Spore Peptidoglycan. Microbiol. Spectr. *3*, 3.6.10. 10.1128/microbiolspec.TBS-0005-2012.

87. Delerue, T., Anantharaman, V., Gilmore, M.C., Popham, D.L., Cava, F., Aravind, L., and Ramamurthi, K.S. (2022). Bacterial developmental checkpoint that directly monitors cell surface morphogenesis. Dev. Cell *57*, 344-360.e6. 10.1016/j.devcel.2021.12.021.

88. Meador-Parton, J., and Popham, D.L. (2000). Structural Analysis of *Bacillus subtilis* Spore Peptidoglycan during Sporulation. J. Bacteriol. *182*, 4491–4499. 10.1128/JB.182.16.4491-4499.2000.

89. Vasudevan, P., Weaver, A., Reichert, E.D., Linnstaedt, S.D., and Popham, D.L. (2007). Spore cortex formation in Bacillus subtilis is regulated by accumulation of peptidoglycan precursors under the control of sigma K. Mol. Microbiol. *65*, 1582–1594. 10.1111/j.1365-2958.2007.05896.x.

90. Fay, A., Meyer, P., and Dworkin, J. (2010). Interactions Between Late-Acting Proteins Required for Peptidoglycan Synthesis during Sporulation. J. Mol. Biol. *399*, 547–561. 10.1016/j.jmb.2010.04.036.

91. Luhur, J., Chan, H., Kachappilly, B., Mohamed, A., Morlot, C., Awad, M., Lyras, D., Taib, N., Gribaldo, S., Rudner, D.Z., et al. (2020). A dynamic, ring-forming MucB / RseB-like protein influences spore shape in Bacillus subtilis. PLOS Genet. *16*, e1009246. 10.1371/journal.pgen.1009246.

92. Errington, J. (2003). Regulation of endospore formation in Bacillus subtilis. Nat. Rev. Microbiol. *1*, 117–126. 10.1038/nrmicro750.

93. Macheboeuf, P., Contreras-Martel, C., Job, V., Dideberg, O., and Dessen, A. (2006). Penicillin Binding Proteins: key players in bacterial cell cycle and drug resistance processes. FEMS Microbiol. Rev. *30*, 673–691. 10.1111/j.1574-6976.2006.00024.x.

94. Errington, J. (1993). Bacillus subtilis sporulation: regulation of gene expression and control of morphogenesis. Microbiol. Rev. *57*, 1–33.

95. Green, E.R., and Mecsas, J. (2016). Bacterial Secretion Systems: An Overview. Microbiol. Spectr. *4*, 4.1.13. 10.1128/microbiolspec.VMBF-0012-2015.

96. Gunasinghe, S.D., Webb, C.T., Elgass, K.D., Hay, I.D., and Lithgow, T. (2017). Super-Resolution Imaging of Protein Secretion Systems and the Cell Surface of Gram-Negative Bacteria. Front. Cell. Infect. Microbiol. *7*, 220. 10.3389/fcimb.2017.00220.

97. Rodrigues, C.D.A., Henry, X., Neumann, E., Kurauskas, V., Bellard, L., Fichou, Y., Schanda, P., Schoehn, G., Rudner, D.Z., and Morlot, C. (2016). A ring-shaped conduit connects the mother cell and forespore during sporulation in *Bacillus subtilis*. Proc. Natl. Acad. Sci. *113*, 11585–11590. 10.1073/pnas.1609604113.

98. Meisner, J., Wang, X., Serrano, M., Henriques, A.O., and Moran, C.P. (2008). A channel connecting the mother cell and forespore during bacterial endospore formation. Proc. Natl. Acad. Sci. *105*, 15100–15105. 10.1073/pnas.0806301105.

99. Camp, A.H., and Losick, R. (2009). A feeding tube model for activation of a cell-specific transcription factor during sporulation in Bacillus subtilis. Genes Dev. *23*, 1014–1024. 10.1101/gad.1781709.

100. Rodrigues, C.D.A., Henry, X., Neumann, E., Kurauskas, V., Bellard, L., Fichou, Y., Schanda, P., Schoehn, G., Rudner, D.Z., and Morlot, C. (2016). A ring-shaped conduit connects the mother cell and forespore during sporulation in *Bacillus subtilis*. Proc. Natl. Acad. Sci. *113*, 11585–11590. 10.1073/pnas.1609604113.

101. Chen, I. (2005). The Ins and Outs of DNA Transfer in Bacteria. Science *310*, 1456–1460. 10.1126/science.1114021.

102. Ducret, A., Quardokus, E.M., and Brun, Y.V. (2016). MicrobeJ, a tool for high throughput bacterial cell detection and quantitative analysis. 14.

103. Sterlini, J.M., and Mandelstam, J. (1969). Commitment to Sporulation in Bacillus subtilis and its Relationship to Development of Actinomycin Resistance. *113*, 9.

104. SCHAEFFER, P., MILLET, J., and AUBERT, J.-P. (1965). CATABOLIC REPRESSION OF BACTERIAL SPORULATION.pdf. Proc Natl Acad Sci USA *54*, 704–711.

105. Loo, L.-H., Laksameethanasan, D., and Tung, Y.-L. (2014). Quantitative Protein Localization Signatures Reveal an Association between Spatial and Functional Divergences of Proteins. PLoS Comput. Biol. *10*, e1003504. 10.1371/journal.pcbi.1003504.

106. Bujnicki, J.M., Elofsson, A., Fischer, D., and Rychlewski, L. Structure prediction meta server. 2.

107. Ginalski, K., Elofsson, A., Fischer, D., and Rychlewski, L. (2003). 3D-Jury: a simple approach to improve protein structure predictions. Bioinformatics *19*, 1015–1018. 10.1093/bioinformatics/btg124.

108. Jones, D.T. Protein Secondary Structure Prediction Based on Position-specific Scoring Matrices. 8.

109. Soding, J., Biegert, A., and Lupas, A.N. (2005). The HHpred interactive server for protein homology detection and structure prediction. Nucleic Acids Res. *33*, W244–W248. 10.1093/nar/gki408.

110. Rigden, D.J., and Galperin, M.Y. (2008). Sequence analysis of GerM and SpoVS, uncharacterized bacterial 'sporulation' proteins with widespread phylogenetic distribution. Bioinformatics *24*, 1793–1797. 10.1093/bioinformatics/btn314.

111. Xie, X., Guo, N., Xue, G., Xie, D., Yuan, C., Harrison, J., Li, J., Jiang, L., and Huang, M. (2019). Solution Structure of SpoIVB Reveals Mechanism of PDZ Domain-Regulated Protease Activity. Front. Microbiol. *10*, 1232. 10.3389/fmicb.2019.01232.

112. Yan, X., Yu, H.-J., Hong, Q., and Li, S.-P. (2008). Cre/ *lox* System and PCR-Based Genome Engineering in *Bacillus subtilis*. Appl. Environ. Microbiol. *74*, 5556–5562. 10.1128/AEM.01156-08.

113. Colin R Harwood and Simon M Cutting Molecular Biological Methods for Bacillus (Chichester ; New York : Wiley, ©1990.).

114. Cutting, S., Driks, A., Schmidt, R., Kunkel, B., and Losick, R. (1991). Forespore-specific transcription of a gene in the signal transduction pathway that governs Pro-sigma K processing in Bacillus subtilis. Genes Dev. *5*, 456–466.

115. Anagnostopoulos, C., and Spizizen, J. (1961). REQUIREMENTS FOR TRANSFORMATION IN *BACILLUS SUBTILIS*. J. Bacteriol. *81*, 741–746. 10.1128/jb.81.5.741-746.1961.

116. Loyo, C., and Burton, B. (2018). Quantitative Transformation Efficiency Assay for Bacillus subtilis. BIO-Protoc. *8*. 10.21769/BioProtoc.3109.

117. Konkol, M.A., Blair, K.M., and Kearns, D.B. (2013). Plasmid-Encoded ComI Inhibits Competence in the Ancestral 3610 Strain of Bacillus subtilis. J. Bacteriol. *195*, 4085–4093. 10.1128/JB.00696-13.

118. Koo, B.-M., Kritikos, G., Farelli, J.D., Todor, H., Tong, K., Kimsey, H., Wapinski, I., Galardini, M., Cabal, A., Peters, J.M., et al. (2017). Construction and Analysis of Two Genome-Scale Deletion Libraries for Bacillus subtilis. Cell Syst. *4*, 291-305.e7. 10.1016/j.cels.2016.12.013.

119. Gibson, D.G., Young, L., Chuang, R.-Y., Venter, J.C., Hutchison, C.A., and Smith, H.O. (2009). Enzymatic assembly of DNA molecules up to several hundred kilobases. Nat. Methods *6*, 343–345. 10.1038/nmeth.1318.

120. Van Opijnen, T., Bodi, K.L., and Camilli, A. (2009). Tn-seq: high-throughput parallel sequencing for fitness and genetic interaction studies in microorganisms. Nat. Methods *6*, 767–772. 10.1038/nmeth.1377.

121. Johnson, C.M., and Grossman, A.D. (2014). Identification of host genes that affect acquisition of an integrative and conjugative element in *B acillus subtilis*: Genes in recipients that affect conjugation. Mol. Microbiol., n/a-n/a. 10.1111/mmi.12736.

122. Hajduk, I.V., Mann, R., Rodrigues, C.D.A., and Harry, E.J. (2019). The ParB homologs, Spo0J and Noc, together prevent premature midcell Z ring assembly when the early stages of replication are blocked in *Bacillus subtilis*. Mol. Microbiol. *112*, 766–784. 10.1111/mmi.14319.

123. Rodrigues, C.D.A., Henry, X., Neumann, E., Kurauskas, V., Bellard, L., Fichou, Y., Schanda, P., Schoehn, G., Rudner, D.Z., and Morlot, C. (2016). A ring-shaped conduit connects the mother cell and forespore during sporulation in *Bacillus subtilis*. Proc. Natl. Acad. Sci. *113*, 11585–11590. 10.1073/pnas.1609604113.

124. Schindelin, J., Arganda-Carreras, I., Frise, E., Kaynig, V., Longair, M., Pietzsch, T., Preibisch, S., Rueden, C., Saalfeld, S., Schmid, B., et al. (2012). Fiji: an open-source platform for biological-image analysis. Nat. Methods *9*, 676–682. 10.1038/nmeth.2019.

125. Zdilla, M.J., Hatfield, S.A., McLean, K.A., Cyrus, L.M., Laslo, J.M., and Lambert, H.W. (2016). Circularity, Solidity, Axes of a Best Fit Ellipse, Aspect Ratio, and Roundness of the Foramen Ovale: A Morphometric Analysis With Neurosurgical Considerations. J. Craniofac. Surg. *27*, 222–228. 10.1097/SCS.0000000000002285.

126. Russ, J.C. (1998). The image processing handbook 3rd ed. (CRC Press).

127. Rodrigues, C.D.A., Ramírez-Guadiana, F.H., Meeske, A.J., Wang, X., and Rudner, D.Z. (2016). GerM is required to assemble the basal platform of the SpoIIIA-SpoIIQ transenvelope complex during sporulation in *Bacillus subtilis*: GerM is required to assemble the SpoIIIA-SpoIIQ complex. Mol. Microbiol. *102*, 260–273. 10.1111/mmi.13457.

128. Fredlund, J., Broder, D., Fleming, T., Claussin, C., and Pogliano, K. (2013). The SpoIIQ landmark protein has different requirements for septal localization and immobilization: Localization and immobilization of SpoIIQ. Mol. Microbiol. *89*, 1053–1068. 10.1111/mmi.12333.

129. Rodrigues, C.D.A., Marquis, K.A., Meisner, J., and Rudner, D.Z. (2013). Peptidoglycan hydrolysis is required for assembly and activity of the transenvelope secretion complex during sporulation in *Bacillus subtilis*: Septal localization of SpoIIQ. Mol. Microbiol. *89*, 1039–1052. 10.1111/mmi.12322.

130. Käll, L., Krogh, A., and Sonnhammer, E.L.L. (2004). A Combined Transmembrane Topology and Signal Peptide Prediction Method. J. Mol. Biol. *338*, 1027–1036. 10.1016/j.jmb.2004.03.016.

131. Besingi, R.N., and Clark, P.L. (2015). Extracellular protease digestion to evaluate membrane protein cell surface localization. Nat. Protoc. *10*, 2074–2080. 10.1038/nprot.2015.131.

132. Weiss, G.A., Watanabe, C.K., Zhong, A., Goddard, A., and Sidhu, S.S. (2000). Rapid mapping of protein functional epitopes by combinatorial alanine scanning. Proc. Natl. Acad. Sci. *97*, 8950–8954. 10.1073/pnas.160252097.

133. Thompson, J.D., Higgins, D.G., and Gibson, T.J. CLUSTAL W: improving the sensitivity of progressive multiple sequence alignment through sequence weighting, position-specific gap penalties and weight matrix choice.

134. Röder, K. (2022). The effects of glycine to alanine mutations on the structure of GPO collagen model peptides. Phys. Chem. Chem. Phys. *24*, 1610–1619. 10.1039/D1CP04775B.

135. Gaohui Sun, Moua Yang, Longguang Jiang, and Mingdong Huang (2021). Regulation of pro-σK activation: a key checkpoint in Bacillus subtilis sporulation. Environ. Microbiol. *23*, 2366–2373.

136. Mastny, M., Heuck, A., Kurzbauer, R., Heiduk, A., Boisguerin, P., Volkmer, R., Ehrmann, M., Rodrigues, C.D.A., Rudner, D.Z., and Clausen, T. (2013). CtpB Assembles a Gated Protease Tunnel Regulating Cell-Cell Signaling during Spore Formation in Bacillus subtilis. Cell *155*, 647–658. 10.1016/j.cell.2013.09.050.

137. Serrano, M., Hövel, S., Moran, C.P., Henriques, A.O., and Völker, U. (2001). Forespore-Specific Transcription of the *lonB* Gene during Sporulation in *Bacillus subtilis*. J. Bacteriol. *183*, 2995–3003. 10.1128/JB.183.10.2995-3003.2001.

138. Molière, N., and Turgay, K. (2013). General and Regulatory Proteolysis in Bacillus subtilis. In Regulated Proteolysis in Microorganisms, D. A. Dougan, ed. (Springer Netherlands), pp. 73–103. 10.1007/978-94-007-5940-4_4.

139. Ramírez-Guadiana, F.H., Rodrigues, C.D.A., Marquis, K.A., Campo, N., Barajas-Ornelas, R. del C., Brock, K., Marks, D.S., Kruse, A.C., and Rudner, D.Z. (2018). Evidence that regulation of intramembrane proteolysis is mediated by substrate gating during sporulation in Bacillus subtilis. PLOS Genet. *14*, e1007753. 10.1371/journal.pgen.1007753.

140. McKenney, P.T., and Eichenberger, P. (2012). Dynamics of spore coat morphogenesis in Bacillus subtilis: Kinetics and regulation of spore encasement. Mol. Microbiol. *83*, 245–260. 10.1111/j.1365-2958.2011.07936.x.

141. Rogers, L.D., and Overall, C.M. (2013). Proteolytic post-translational modification of proteins: proteomic tools and methodology. Mol. Cell. Proteomics *12*, 3532–3542.

142. Huang, K.C., Mukhopadhyay, R., Wen, B., Gitai, Z., and Wingreen, N.S. (2008). Cell shape and cell-wall organization in Gram-negative bacteria. Proc. Natl. Acad. Sci. *105*, 19282–19287. 10.1073/pnas.0805309105.

143. Typas, A., Banzhaf, M., Gross, C.A., and Vollmer, W. (2012). From the regulation of peptidoglycan synthesis to bacterial growth and morphology. Nat. Rev. Microbiol. *10*, 123–136. 10.1038/nrmicro2677.

144. Egan, A.J.F., Errington, J., and Vollmer, W. (2020). Regulation of peptidoglycan synthesis and remodelling. Nat. Rev. Microbiol. *18*, 446–460. 10.1038/s41579-020-0366-3.

145. Egan, A.J.F., Cleverley, R.M., Peters, K., Lewis, R.J., and Vollmer, W. (2017). Regulation of bacterial cell wall growth. FEBS J. *284*, 851–867. 10.1111/febs.13959.

146. Munoz-Lopez, M., and Garcia-Perez, J. (2010). DNA Transposons: Nature and Applications in Genomics. Curr. Genomics *11*, 115–128. 10.2174/138920210790886871.

147. Van Opijnen, T., and Camilli, A. (2013). Transposon insertion sequencing: a new tool for systems-level analysis of microorganisms. Nat. Rev. Microbiol. *11*, 435–442.

148. Chao, M.C., Abel, S., Davis, B.M., and Waldor, M.K. (2016). The design and analysis of transposon insertion sequencing experiments. Nat. Rev. Microbiol. *14*, 119–128. 10.1038/nrmicro.2015.7.

149. Jules, M., Le Chat, L., Aymerich, S., and Le Coq, D. (2009). The *Bacillus subtilis ywjI* (*glpX*) Gene Encodes a Class II Fructose-1,6-Bisphosphatase, Functionally Equivalent to the Class III Fbp Enzyme. J. Bacteriol. *191*, 3168–3171. 10.1128/JB.01783-08.

150. Gautam, A., Rishi, P., and Tewari, R. (2011). UDP-N-acetylglucosamine enolpyruvyl transferase as a potential target for antibacterial chemotherapy: recent developments. Appl. Microbiol. Biotechnol. *92*, 211–225. 10.1007/s00253-011-3512-z.

151. Dubois, T., Krzewinski, F., Yamakawa, N., Lemy, C., Hamiot, A., Brunet, L., Lacoste, A.-S., Knirel, Y., Guerardel, Y., and Faille, C. (2020). The *sps* Genes Encode an Original Legionaminic Acid Pathway Required for Crust Assembly in Bacillus subtilis. mBio *11*, e01153-20. 10.1128/mBio.01153-20.

152. Elsholz, A.K.W., Hempel, K., Michalik, S., Gronau, K., Becher, D., Hecker, M., and Gerth, U. (2011). Activity Control of the ClpC Adaptor McsB in Bacillus subtilis. J. Bacteriol. *193*, 3887–3893. 10.1128/JB.00079-11.

153. Battesti, A., and Gottesman, S. (2013). Roles of adaptor proteins in regulation of bacterial proteolysis. Curr. Opin. Microbiol. *16*, 140–147. 10.1016/j.mib.2013.01.002.

154. Zhang, A., Pompeo, F., and Galinier, A. (2021). Overview of protein phosphorylation in bacteria with a main focus on unusual protein kinases in Bacillus subtilis. Res. Microbiol. *172*, 103871. 10.1016/j.resmic.2021.103871.

155. Begley, T.P., Downs, D.M., Ealick, S.E., McLafferty, F.W., Van Loon, A.P.G.M., Taylor, S., Campobasso, N., Chiu, H.-J., Kinsland, C., Reddick, J.J., et al. (1999). Thiamin biosynthesis in prokaryotes. Arch. Microbiol. *171*, 293–300. 10.1007/s002030050713.

156. Park, J.-H., Burns, K., Kinsland, C., and Begley, T.P. (2004). Characterization of Two Kinases Involved in Thiamine Pyrophosphate and Pyridoxal Phosphate Biosynthesis in *Bacillus subtilis* : 4-Amino-5-Hydroxymethyl-2-Methylpyrimidine Kinase and Pyridoxal Kinase. J. Bacteriol. *186*, 1571–1573. 10.1128/JB.186.5.1571-1573.2004.

157. Jurgenson, C.T., Begley, T.P., and Ealick, S.E. (2009). The Structural and Biochemical Foundations of Thiamin Biosynthesis. Annu. Rev. Biochem. *78*, 569–603. 10.1146/annurev.biochem.78.072407.102340.

158. Scheffers, D.-J. (2005). Dynamic localization of penicillin-binding proteins during spore development in Bacillus subtilis. Microbiology *151*, 999–1012. 10.1099/mic.0.27692-0.

159. Straume, D., Piechowiak, K.W., Kjos, M., and Håvarstein, L.S. (2021). Class A PBPs: It is time to rethink traditional paradigms. Mol. Microbiol. *116*, 41–52. 10.1111/mmi.14714.

160. Deller, M.C., Kong, L., and Rupp, B. (2016). Protein stability: a crystallographer's perspective. Acta Crystallogr. Sect. F Struct. Biol. Commun. *72*, 72–95. 10.1107/S2053230X15024619.

161. Lee, J.M., Hammarén, H.M., Savitski, M.M., and Baek, S.H. (2023). Control of protein stability by post-translational modifications. Nat. Commun. *14*, 201. 10.1038/s41467-023-35795-8.

162. Gershenson, A. (2014). Deciphering Protein Stability in Cells. J. Mol. Biol. *426*, 4–6. 10.1016/j.jmb.2013.10.004.

163. Bukowska-Faniband, E., and Hederstedt, L. (2013). Cortex synthesis during *Bacillus subtilis* sporulation depends on the transpeptidase activity of SpoVD. FEMS Microbiol. Lett. *346*, 65–72. 10.1111/1574-6968.12202.

164. Tan, I.S., and Ramamurthi, K.S. (2014). Spore formation in *B acillus subtilis*: *Bacillus subtilis* sporulation. Environ. Microbiol. Rep. *6*, 212–225. 10.1111/1758-2229.12130.

165. Silvaggi, J.M., Popham, D.L., Driks, A., Eichenberger, P., and Losick, R. (2004). Unmasking Novel Sporulation Genes in *Bacillus subtilis*. J. Bacteriol. *186*, 8089–8095. 10.1128/JB.186.23.8089-8095.2004.

166. Fukushima, T., Yamamoto, H., Atrih, A., Foster, S.J., and Sekiguchi, J. (2002). A Polysaccharide Deacetylase Gene (pdaA) Is Required for Germination and for Production of Muramic ʕ-Lactam Residues in the Spore Cortex of Bacillus subtilis. J BACTERIOL *184*.

167. Sekiguchi, J., Akeo, K., Yamamoto, H., Khasanov, F.K., Alonso, J.C., and Kuroda, A. (1995). Nucleotide sequence and regulation of a new putative cell wall hydrolase gene, cwlD, which affects germination in Bacillus subtilis. J. Bacteriol. *177*, 5582–5589. 10.1128/jb.177.19.5582-5589.1995.

168. Catalano, F.A., Meador-Parton, J., Popham, D.L., and Driks, A. (2001). Amino Acids in the *Bacillus subtilis* Morphogenetic Protein SpoIVA with Roles in Spore Coat and Cortex Formation. J. Bacteriol. *183*, 1645–1654. 10.1128/JB.183.5.1645-1654.2001.

169. van Teeseling, M.C.F., de Pedro, M.A., and Cava, F. (2017). Determinants of Bacterial Morphology: From Fundamentals to Possibilities for Antimicrobial Targeting. Front. Microbiol. *8*. 10.3389/fmicb.2017.01264.

170. Caccamo, P.D., and Brun, Y.V. (2018). The Molecular Basis of Noncanonical Bacterial Morphology. Trends Microbiol. *26*, 191–208. 10.1016/j.tim.2017.09.012.

171. Stragier, P., and Losick, R. (1996). MOLECULAR GENETICS OF SPORULATION IN *BACILLUS SUBTILIS*. Annu. Rev. Genet. *30*, 297–341. 10.1146/annurev.genet.30.1.297.